# *I. The Use of Spherosiloxanes as Molecular Building Blocks for Materials and Thin Films*

# *II. A New Method of Using SC-Cut Quartz Oscillators for Chemical Sensing*

Thesis by

*John Frederick Nagel*

*In Partial Fulfillment of the Requirements*

*for the Degree of*

*Doctor of Philosophy*

California Institute of Technology

Pasadena, California

1997

(Submitted November 19, 1996)

*This work is Dedicated to my Grandparents:*

*Fred P. & Norma H. Nagel*
*John F. & Jane K. Ledbetter*

## *Acknowledgments*

Over the years there have been a tremendous number of people who have had an influence over me as both a scientist and a person. Thus, it is only fitting that I take a moment to recognize a few of those here in this culmination of my work to date. It would be impossible to mention everyone that I should in this short note, so please forgive me for any unintentional oversights.

I must begin by recognizing my family, both by blood and marriage. From the earliest age they stressed to me the overriding importance of education and the fact that it is a continuing process, not a simple goal. Without their assistance, encouragement, and love, it would have been impossible to even consider undertaking the course of study which has culminated here. With all my heart I thank you.

I am deeply indebted to my advisor, Dr. Mark E. Davis, not only for taking me on and guiding me through this work, but for sticking by me when my research did not come out as originally planned. Moreover, he created an atmosphere in this research group both stimulating and enjoyable, which allowed me to learn and grow as a scientist.

I wish to acknowledge all the members of the Davis research group, both past and present, for their assistance and camaraderie as we ventured along this journey together. In particular John Lewis, Chris Dartt, and classmate Kelvin Lee have made a lasting impression on me with their friendship and aid over the years.

I want to thank my collaborators, without whom this work could never have been completed. I thank Dr. Don Eigler of IBM and his research group for the opportunity to work in his laboratory studying the behavior of spherosiloxanes on surfaces and for teaching me everything I know about surface science. Dr. John Vohs of U Penn and his research

group carried out the HREELS studies on spherosiloxanes for me. Dr. Bog Kuszta was instrumental in the design and development of the electronics associated with the chemical sensing experiments, and thanks to Tom Dunn for his wealth of knowledge regarding the practical application of electronics. I am also grateful for the assistance of Carlos Maldonado, a SURF student this past summer, who helped carry out many of the sensor experiments.

I graciously acknowledge the financial support for my research from the National Science Foundation with a Graduate Fellowship and the IBM Corporation with an IBM Cooperative Fellowship.

Finally, I would like to express my deepest love and appreciation to my wife Laura. Thank you for sticking by me when things were looking bleak. Without you I would not have made it to this day.

## *Abstract*

The ability to prepare *a priori* ordered materials of a desired structure is a long standing goal in materials research. Recently, there has been great interest in the use of well-defined molecular precursors that can, in principle, be combined in a regular way without degradation to produce ordered materials. This process has been dubbed "lego-chemistry." This work examines the use of spherosiloxanes, a family of polyhedral silicate cage molecules, as molecular building blocks for the synthesis of bulk microporous materials and microporous thin films.

The process for synthesizing and functionalizing the spherosiloxanes with a variety of reactive functional ligands is presented. The reactive molecules are characterized using a suite of analytical and spectroscopic techniques. In order to achieve some degree of control over the condensation process, a binary reaction mechanism utilizing non-hydrolytic reaction conditions is proposed for the production of bulk materials. Experimental results from the non-hydrolytic condensation of spherosiloxanes are presented. The effects of adding various catalysts to the reaction mixture are described. A multinuclear solution NMR study was performed on monomeric silicate analogues of the spherosiloxanes in order to elucidate the non-hydrolytic reaction pathways. It is found that under the conditions of interest ligand exchange predominates over condensation.

A reaction scheme and growth mechanism for the production of a microporous thin film from spherosiloxane precursors is presented and discussed. It is speculated that such an ordered film could function as a framework for the production of a molecular electronic device. The first important steps in this scheme, namely the condensation behavior of spherosiloxanes on the Si (100) - (2x1) reconstructed surface, are explored through a

variety of surface characterization techniques. In particular, low temperature STM is used to record the nature of the species condensed on the surface. An image of a single isolated $(CH_3O)_8Si_8O_{12}$ is recorded and its position and orientation are discussed in the context of the reaction scheme. A HREELS/TPD study of the spherosiloxanes on the same surface is performed and the results discussed.

A new technique for chemical sensing is proposed and is based on the recently developed SC-cut quartz oscillator used in conjunction with the analytical technique known as thermal programmed desorption (TPD). This technique is developed in order to address the need to develop new sensing techniques that are sensitive, selective and cost efficient, for application to the rising threats of terrorism and pollution present today. The technique utilizes two vibrational modes of the crystal, one very sensitive and one relatively insensitive to changes in temperature, that are monitored throughout the experiment. The two mode sensing allows in principle for the simultaneous monitoring of the mass and temperature of the sensor.

A system for evaluating the performance of this sensor is designed and built, and includes an automated data acquisition and control system. The sensor is tested using a variety of chemically selective coatings and analytes. The structure and morphology of the coating used is shown to have a significant effect on the oscillation behavior of the crystal used. TPD experiments are performed with the sensor in order to evaluate its characteristics. In nearly all cases, it is impossible to discern any desorption signal during the TPD experiment. A dual mode analysis that is used to deconvolute the temperature and mass responses of the sensor fails to distinguish any desorption signals except from a very heavily loaded sample, i.e., water on a polyethyleneimine coated crystal where bulk

absorption occurs. A TPD experiment is performed on a hydrated, PEI coated crystal using a Cahn microbalance, and a relationship between the mass loading and frequency change is determined for this system. These values are used to calculate the frequency response for a typical coating where only surface adsorption occurs, and the result is below the minimum detection level of the system. Based on these data, it is determined that the SC-cut sensor fails to show the sensitivity necessary for application as a practical sensor device.

## *Table of Contents*

## *List of Figures*

## *List of Tables*

*Chapter 2 Tables:*



*Chapter 4 Tables:*



*Chapter 6 Tables:*



*Appendix Tables:*

# *Chapter 1:*

## *Preface*

## *1.1 Introduction*

This thesis involves two distinctly different and unrelated projects. The first project involves a family of materials called **spherosiloxanes**, whose unique combination of structure and physical properties makes them well suited as molecular precursors for the synthesis of engineered materials with possible control of the material architecture on a nanoscale level. The objective of this project is to use appropriately functionalized spherosiloxanes as molecular building blocks for the construction of ordered bulk materials and thin films. The portion of the thesis devoted to this topic is organized as follows:

Chapter 2 provides an introduction to spherosiloxanes and general background to the project. The synthetic techniques that are used to prepare and functionalize these molecules with a variety of reactive ligands are described. A thorough characterization of the spherosiloxanes is also presented and involves a variety of techniques including Fourier transform infrared and Raman spectroscopy, multinuclear solution and solid state MAS nuclear magnetic resonance spectroscopy, and powder X-ray diffraction.

Chapter 3 presents results from work aimed at the production of bulk ordered materials via the controlled condensation of spherosiloxanes. After reviewing the work of previous researchers in this area, the primary approach taken for this work is described; that is, the utilization of a binary reaction scheme within a non-hydrolytic condensation mechanism. Experimental results from this work are presented and analyzed, culminating in an NMR study of the condensation behavior of silicate species under non-hydrolytic reaction conditions. Alternative reaction schemes, including the use of catalytic agents, are also investigated.

Chapter 4 gives results from the portion of this project devoted to the production of ordered thin films from spherosiloxane precursors. Work in this area was oriented toward the production of a microporous thin layer that could serve as a framework for the development of molecular electronic devices. A reaction scheme and growth mechanism for such a microporous thin layer, created from spherosiloxanes, is described. The first critical steps in this scheme, namely the condensation behavior of spherosiloxanes on surfaces, are explored through the use of surface characterization techniques including low temperature scanning tunneling microscopy, Auger electron and mass spectroscopy, low energy electron diffraction, and high resolution electron energy loss spectroscopy in conjunction with thermal programmed desorption. The results of this study and the appropriate steps for future work in this area are outlined.

The second project involves the development of a new technique for chemical sensing. In particular, given the recent increase in terrorist threats such as the UNABOMBER, the bombing of the World Trade Center, and the attack on the Federal building in Oklahoma City, as well as other more mundane yet equally dangerous threats, such as leaks and spills from chemical plants and transport vehicles, there is need to develop new techniques for chemical sensing that are sensitive, selective, and economically attractive. To that end, we proposed a technique for chemical sensing based on a new type of quartz crystal oscillator (SC-Cut) that is used in combination with an analytical technique known as thermal programmed desorption (TPD). The goal of the work was to design and build a sensor system based on this TPD/quartz oscillator sensing technique and to evaluate its potential as a chemical sensor.

Chapter 5 presents an introduction to microsensors that are based on quartz oscillators, and includes an introduction to the basic physics that govern these devices. Additionally, the experimental design and setup used in this work are enumerated. Included in this description is an overview of the data acquisition and control program written to operate the sensor system.

Chapter 6 describes the TPD/quartz oscillator technique in detail and presents the results from effects such as the thermal behavior of the oscillator and the nature of the chemically selective coatings. The experimental results from the performance of the sensor are presented and evaluated.

# *Section I:*

## *The Use of Spherosiloxanes as Molecular Building Blocks for Materials and Thin Films*

# *Chapter 2:*

## *Introduction and Synthesis of Spherosiloxanes*

## 2.1. *Introduction and Background*

In many areas of research, the properties of a given material are critically dependent on the details of the structure of the material at the nanoscale level. For example, the physical properties of isotactic polypropylene, in which the methyl groups off the polymer backbone are all ordered in the same way, has dramatically different physical properties and corresponding uses, than atactic polypropylene, in which the methyl groups are randomly oriented along the backbone. An example perhaps more relevant to this work is the case of zeolite-like molecular sieves. It is the completely regular arrangement of pores and channels on the size scale of small molecules that allows for the molecular sieving behavior these materials exhibit as well as the high degree of selectivity possible when they are used in catalytic applications. It was over thirty-five years ago when Richard Feynman first talked of manipulating material structure on the nanoscale to produce new materials and devices. In a speech to the American Physical Society entitled "There's Plenty of Room at the Bottom," Feynman noted that "when we have some *control* of the arrangement of things on a small scale we will get an enormously greater range of possible properties that substances can have, and of different things that we can do." [1] What Feynman was referring to is the ability to control materials structure on a small, local scale by manipulating atoms and molecules one or a few at a time to achieve a desired arrangement.

The ability to control the material structure on the nanometer size scale, one where quantum mechanics play an important role in determining physical properties, will lead to new and better materials with interesting and valuable properties. Some examples include novel electronic, optical, mechanical, electrochemical, photochemical, transport, and cata-

lytic behavior. Many applications are expected to benefit from these new properties including quantum and molecular electronics, nonlinear optics, photonics, chemoselective sensing, and information storage and processing[2].

The ability to make *a priori* materials of a desired structure is clearly one of the long standing goals in many areas of materials research. However, it is often the case that little is known about how the nanoscale structure of a material is formed. Traditional synthetic chemistry allows for some control of material properties; however, it is often limited to control of large scale and bulk material properties. In the last two decades remarkable progress has been made towards nanoscale control of material structure driven by the need to produce ever smaller integrated circuits for computing and communications. Improvements in the traditional semiconductor synthetic techniques, including molecular beam epitaxy (MBE)[3], metal organic chemical vapor deposition (MOCVD) and atomic layer epitaxy (ALE)[4,5], as well as a variety of nanolithographic techniques using x-ray, ion and electron beams, allow for the routine production of submicron structures of a variety of geometries[6,7]. These techniques have been combined successfully to produce quantum confinement effects in one- and zero-dimensional structures, so-called "quantum wires" and "quantum dots"[8]. However, these techniques are still limited to a resolution of around $250 \pm 50$Å, and have not yet been extended into the nanoscale (1 - 10 nm) realm of quantum and molecular electronics.

Perhaps the most important advance towards nanoscale control of material structure came in 1982 with the development of scanning probe microscopy (SPM) by Binnig and Rohrer, researchers at IBM's Zurich research center. The new scanning tunneling microscope (STM) provided the first atomic resolution pictures of conducting surfaces[9-11].

Its direct descendant, the atomic force microscope (AFM) developed by Binnig, Quate, and Gerber in 1986 allowed for similar imaging on insulating surfaces several years later[12]. Since their introduction, new techniques using these microscopes have developed at a blistering pace for surface and molecular imaging[13], surface modification[14], atomic ("single atom") spectroscopy[15], and even for atomic and molecular manipulation[16]. For the first time it is possible to manipulate a single atom or molecule from one position to another[17], or produce a single atom, bi-stable switch[18].

In and of itself, however, scanning probe microscopy does not offer the kind of control over material structure that Feynman spoke of. In order to take advantage of local control of material structure, such as for quantum and molecular electronic devices, it is necessary to make nanoscale structures that can be ordered over "large" surface areas, up to microns and beyond. The semiconductor techniques cannot provide the necessary fine scale control of the features, thus they are essentially "too large"; the current state of scanning probe microscopy can only produce structures that are too irregular or are too small to develop the large scale order needed for most device applications. What is needed is a technique which offers nanoscale structure control, while allowing facile production of the larger scale architecture. As a result, many have suggested returning to the techniques of chemistry to solve this paradox[2].

As noted earlier, the difficulty of using chemical synthetic techniques lies in the fact that they are essentially bulk techniques. Thus, methods must be developed to manipulate and appropriately order the molecules to form the desired nanoscale structures. Two methods that are currently being used to direct the synthesis of these structures are "patterning" and "templating." Patterning involves a marriage of chemistry and semiconduc-

tor techniques, using nanolithography to pattern a surface, followed by site specific synthesis to make nanoscale structures in the patterned areas[19]. Templating utilizes nanoporous host structures as a templates to perform host-guest inclusion chemistry[20]. The problem with host-guest techniques is that the nanoporous host both restricts and dictates the types of large scale architecture that can be produced, thus limiting its utility for many applications. A third suggestion has been to utilize the synthetic and self-assembly properties of biological molecules to form the desired structures[21,22]. The difficulty here results from the tight restrictions the use of biological molecules places on system conditions, including temperature and aqueous environment, which again limits utility for most applications.

One possible way to overcome these problems is to produce a material by assembling in an ordered fashion well-defined molecular precursors. This idea has recently been coined "Lego chemistry"[23]. Our objective with this work is to apply the concept of "Lego chemistry" to the synthesis of inorganic microporous framework oxides, in particular to pure-silica zeolites and related structures, and to the production of microporous thin films for use in molecular electronics. In order to achieve this, a suitable molecular building block must be chosen which can be easily synthesized, and be chemically controlled to have the appropriate functionality for condensation to take place, either by self assembly or another well controlled reaction mechanism.

In particular, we have chosen to start with the $O_h$ -$X_8Si_8O_{12}$ spherosiloxane, shown in Figure 2.1, because its cubic symmetry should help simplify the organization process. Moreover, the polycyclic ring structure of the spherosiloxanes is analogous to secondary structures found in many zeolites. Thus, it seems natural to use them as

building blocks for microporous materials. For example, the structure of $X_8Si_8O_{12}$ is analogous to the "double four ring" found in zeolite A (LTA) (See Figure 2.2.) and many other zeolite and aluminophosphate ($AlPO_4$) materials[24]. This spherosiloxane can now be synthesized in multigram quantities using a recently developed synthetic technique for X = H[25]. Once the $[Si_8O_{12}]$ core has been formed, it can be further functionalized to a variety of reactive ligands including -Cl and $-OCH_3$[26], and $-OSiMe_3$[27]. We have additionally for the first time synthesized multigram quantities of $X_8Si_8O_{12}$ where X = $-OC_2H_5$ and -O(*n* $-C_3H_7$). Structural identification and verification of all these materials has been accomplished by X-ray diffraction, infrared and Raman spectroscopies, mass spectroscopy, and $^1H$, $^{13}C$ and $^{29}Si$ NMR spectroscopy.

## 2.2. *Spherosiloxanes*

Spherosiloxanes are volatile, prismatic members of the family of oligomeric silsesquioxanes with the general formula $(RSiO_{1.5})n$ where n = 6, 8, 10, 12, . . . and R is H, Cl or any of a large number of organic groups[28-32]. (See Figure 2.1.) They were first synthesized in the 1940's[33] and 1950's[34], and first fully characterized by Müller, Köhne, and Sliwinski in 1959[35]. Because of the high degree of symmetry in these molecules, very simple NMR, IR and Raman spectra are obtained. Moreover, the high symmetry of $O_h$-$X_8Si_8O_{12}$ has allowed for the full calculation of its electronic structure[36] as well as a normal coordinate analysis[37]. In addition, these materials are easily sublimable at low temperatures and moderate pressures, something very unusual for materials composed primarily of silicon oxide. Interest in these materials has grown rapidly in the last several years, primarily because of the new synthesis developed by Agaskar[25] which has made them available for the first time in multigram quantities.

Because of their unique properties, spherosiloxanes are promising precursors for many materials applications, most notably ceramics and high quality $SiO_2$ films. Agaskar first reported the synthesis of spherosiloxanes functionalized with polymerizable moieties[31], which are in turn used for the generation of organolithic macromolecular materials (OMMs). These OMMs can then be pyrolyzed and treated with hydrofluoric acid to produce microporous Si-C-O ceramics with high surface area for use as membranes and catalysts[38]. Since that time, spherosiloxanes have been functionalized with a number of organic ligands and used to make a wide variety of organic-inorganic hybrid materials, from dendritic "octopus molecules" with a spherosiloxane core, to spherosiloxane based

liquid-crystalline materials, to photocurable single phase composites for use as dental restoratives[39-41]. Desu *et al* . utilized hydridospherosiloxane precursors for chemical vapor deposition (CVD) to make high quality $SiO_2$ thin films at atmospheric pressure and low substrate temperature[42]. Cagle has used spherosiloxanes for sol-gel polymerization to make silica, studying the molecular growth pathways in the gel and the effect on the resulting silica as compared to other precursors[26]. In an effort to make better ceramic materials, Klemperer and co-workers in the mid-1980s hydrolyzed $(CH_3O)_8Si_8O_{12}$ with water while attempting to make a regular microporous silica[43,44]. The result was a clear gel which dried into a monolithic glass. Although it didn't produce an ordered material, it is notable as the first attempt at using spherosiloxanes as a molecular building block.

Other researchers have looked upon these polyhedral silsesquioxanes as possible models for silica surfaces and silica supported heterogeneous catalysts[45-47]. By using incompletely condensed spherosiloxanes to synthesize metal-substituted spherosiloxanes, it is possible to create isolated metal "active sites" on a silica support. An aluminum silsesquioxanes gel based on spherosiloxanes has been developed as an active catalyst in Diels-Alder reactions of enones[48]. Feher and co-workers have also taken incompletely condensed spherosiloxanes and reacted them with aluminum substituted spherosiloxanes to form dimers that are analogs of aluminosilicate frameworks[49]. (See Figure 2.3.) Although the reaction mechanism for the construction of these dimers is too complex to attempt on a large scale to make 3-dimensional structures, it is an important example of the use of spherosiloxanes as building blocks for the construction of larger structures. Because of their unique resemblance to zeolite subunits, many studies have been made of spherosiloxanes in an attempt to learn more about synthetic process for zeolites[50-54] as

well as investigating the chemical environment inside of zeolites containing these secondary structures[55-59].

## 2.3. *Synthesis of Spherosiloxanes*

As mentioned earlier, the synthesis of the spherosiloxanes used in this work was based on a reaction scheme first developed by Agaskar[25] and later modified by Cagle[26]. The fundamental feature of this reaction is the use of a partially hydrated metal salt to create "scarce water" hydrolysis conditions similar to those obtained in previous spherosiloxane syntheses using sulfuric acid[29]. The reaction scheme starts with the synthesis of $H_8Si_8O_{12}$, which is photochemically chlorinated to $Cl_8Si_8O_{12}$, and finally alkoxylated to $RO_8Si_8O_{12}$ as indicated below:

$$HSiCl_3 + (H_3O)^+ \xrightarrow[C_6H_{14},\ CH_3OH]{FeCl_3\ cat.} H_8Si_8O_{12} + H_{10}Si_{10}O_{15} \quad (1)$$

$$H_8Si_8O_{12} + Cl_2 \xrightarrow[CCl_4]{h\nu} Cl_8Si_8O_{12} \quad (2)$$

$$Cl_8Si_8O_{12} + HC(OR)_3 \xrightarrow[90\text{-}110°C,\ 12hr]{reflux} (RO)_8Si_8O_{12} + RCl + HCOOR \quad (3)$$

where OR = $-OCH_3$, $-OC_2H_5$, $-OC_3H_7$

### 2.3.1. *Synthesis and Characterization of $H_8Si_8O_{12}$*

Hexane (1.0 L) was added to a 5 L round bottom flask equipped with a heavy magnetic stirrer. Ferric chloride (90 g, anhydrous), methanol (80 mL), and concentrated hydrochloric acid (40.0 mL, ~ 1.65 mol) were added in that order with stirring to produce a biphasic mixture with a red-brown bottom layer. Trichlorosilane (40 mL, ~ 0.40 mol) was added to 500 mL hexane in a 1 L round bottom flask and vigorously mixed. An additional 500 mL hexane was then added to bring the total amount of hexane to 1 L. The

trichlorosilane solution was then placed in a 250 mL pressure-equalizing dropping funnel with Teflon stopcocks and added dropwise to the rapidly stirred biphasic mixture over an 8 to 10 hour period, refilling the funnel as necessary. The presence of silicone grease was found to react with the trichlorosilane and lower yields; therefore, all ground glass joints were Teflon coated or wrapped with Teflon tape. After the reaction mixture was stirred for an additional 30 minutes, the upper hexane layer was transferred along with some suspended yellow-green solid to another 5 L round bottom flask, and the black ferric chloride layer was discarded. Calcium chloride (20 g, anhydrous) and potassium carbonate (28 g, anhydrous) were added to the hexane solution and stirred slowly overnight. The mixture was filtered over calcium chloride and concentrated on a rotary evaporator in three batches to ca. 20 mL. The resulting white crystals were isolated on medium fast filter paper (Whatman qualitative, #1) in three crops. The filtrate was collected and washed back into the original flask with ~ 50 mL hexane and the solution concentrated to ca. 10 mL and filtered to produce a fourth crop of product. Total yield of white crystals ranged from 4.5 to 5.8 g of crude product, primarily a mixture of $O_h$-$H_8Si_8O_{12}$ and $D_{5h}$-$H_{10}Si_{10}O_{15}$. (See Figure 2.1.) The four crops of crystals were combined and recrystallized from 125 mL of hot hexane, and slowly cooled overnight. The resulting crystals were filtered and washed with five 10 mL aliquots of cold hexane. Total yield of recrystallized product was 3.2 - 4.0 g (15.2 - 19.0% yield based on $HSiCl_3$).

The synthesized product was characterized using Fourier Transform Infrared spectrometry (FTIR), Raman spectrometry, NMR spectroscopy, and X-ray powder diffraction. The availability of a normal coordinate analysis of $H_8Si_8O_{12}$[37] has allowed calculation of the infrared and Raman active vibrations of the molecule[60], and they are in good agree-

ment with the experimentally determined spectra. Figure 2.4 shows typical IR spectra for $H_8Si_8O_{12}$ as synthesized (top) and after it has been recrystallized and washed (bottom). The $[Si_8O_{12}]$ core of the molecule has characteristic bands at 399 $cm^{-1}$ and 465 $cm^{-1}$ which shift as the ligands at the corners of the molecule are changed. (This confirms the integrity of the core while giving some indication of the attached ligand.) The bands at 868 $cm^{-1}$ and 2270 $cm^{-1}$ are assigned to the Si-H vibrations. (See Table 2.1.) Note that the as synthesized sample (top) has a second Si-H band at 2290 $cm^{-1}$ which results from the $H_{10}Si_{10}O_{15}$ in the sample. The band at 558 $cm^{-1}$ is also assigned to $H_{10}Si_{10}O_{15}$.

Typical Raman spectra for $H_8Si_8O_{12}$ as synthesized (top) and after recrystallization and washing (bottom) are shown in Figure 2.5. The high symmetry of the molecule helps produce the relatively simple spectra shown. See Table 2.2 for the assignment of the vibrational bands. Once again, the as synthesized sample shows an extra band in the region assigned to Si-H vibrations. The two bands at 2302 $cm^{-1}$ and 2286 $cm^{-1}$ are assigned to $H_8Si_8O_{12}$ while the shoulder at 2271 $cm^{-1}$ results from $H_{10}Si_{10}O_{15}$ present in the sample. Additional bands due to $H_{10}Si_{10}O_{15}$ are likely present; however, they are difficult to make out due to their low intensity.

NMR spectroscopy has also been used to characterize these spherosiloxanes. The high symmetry of $O_h$-$H_8Si_8O_{12}$ results in a spectrum which has only a single peak. Figure 2.6 shows a $^1H$ NMR spectrum of recrystallized $H_8Si_8O_{12}$ taken in $CDCl_3$ solution at 300 MHz. The peak at $\delta$ 4.275 ppm corresponds to spherosiloxane, with the peak at $\delta$ 7.285 ppm corresponding to the lock solvent chloroform. The small peaks at $\delta$ 1.595 ppm and $\delta$ 1.270 ppm are assigned to solvent impurities. Solid state $^{29}Si\{^1H\}$ magic angle spin-

ning (MAS) NMR spectra were obtained at 59.6 MHz under gated decoupling conditions to eliminate NOE effects. Typical spectra for the as synthesized and recrystallized $H_8Si_8O_{12}$ samples are shown in Figure 2.7. Figure 2.7.a clearly shows the presence of $H_{10}Si_{10}O_{15}$ as a second peak at d -86.212. After recrystallization and washing, the peak disappears, leaving only the single peak at d -84.186 corresponding to $H_8Si_8O_{12}$, as seen in Figure 2.7.b.

Powder X-ray diffraction (XRD) studies were also performed on these materials. An indexed diffraction pattern for recrystallized and washed $H_8Si_8O_{12}$ is shown in Figure 2.8. The crystal structure for $H_8Si_8O_{12}$ has been solved using single crystal XRD by Auf der Heyde *et al.*, and the powder pattern corresponds well to a simulated pattern based on the Auf der Heyde structure[61]. A full listing of the indexed peaks and the simulated powder pattern for the Auf der Heyde structure can be found in Appendix B.1. All of the spherosiloxanes are moisture sensitive to some extent, depending critically on the attached ligand. Hydridospherosiloxanes are the most robust members of the family; however, they still decompose over time into amorphous material. XRD is a useful tool to follow this process and determine the state of decomposition. The loss of intensity and disappearance of some peaks, as well as the appearance of new peaks due to decomposition products can readily be seen in Figure 2.9.

### *2.3.2. Synthesis and Characterization of $Cl_8Si_8O_{12}$*

$Cl_8Si_8O_{12}$ is synthesized by a photochemical reaction between $H_8Si_8O_{12}$ and chlorine gas in carbon tetrachloride solution (Reaction 2). The experimental procedure used was as follows:

Carefully recrystallized $H_8Si_8O_{12}$ (2 g, 4.7 mmol) was placed into an oven-dried 500 mL 3-neck flask along with a heavy magnetic stirrer. A fritted gas dispersion tube attached to a chlorine source was fitted in one neck, an adapter with stopcock in the second, and a rubber septum sealed the final neck. Again, Teflon tape was used instead of silicone grease. The flask was purged with nitrogen, and 200 mL of anhydrous $CCl_4$ was transferred to the flask by syringe. This suspension was saturated with chlorine by bubbling the gas through the solution for 20 min. in a fume hood. Excess chlorine was vented through an oil bubbler into a saturated solution of aqueous KOH. The gas dispersion tube was removed and the flask was sealed with a glass stopper. The deep yellow-green solution was irradiated with a low pressure mercury lamp (Hanovia Corp., Newark, NJ, 450 W) in a fume hood. The fume hood door was covered in aluminum foil to guard against escape of UV radiation. After 3 hours, all volatile material was removed on a doubly-trapped vacuum line, leaving a fine white powder. Final purification of the $Cl_8Si_8O_{12}$ occurs by sublimation in a large oven-dried sublimator at 150°C and 0.01 Torr onto a water-cooled cold finger.

As mentioned earlier, all of the spherosiloxanes are moisture sensitive. $Cl_8Si_8O_{12}$ is an extreme example of this fact. Cagle recommends transfer of the crude chlorinated product into the sublimator in a glove box[26]. The FTIR spectrum of this material in a KBr pellet, Figure 2.10, shows that the material has already begun to decompose into $Cl_{(8-x)}(OH)_xSi_8O_{12}$ even during the IR experiment. The presence of the sharp band at 712 $cm^{-1}$ combined with the absence of any Si-H bands (2276 $cm^{-1}$, 881 $cm^{-1}$) indicates that the photochlorination was nearly quantitative. The bands at 515 $cm^{-1}$ and 450 $cm^{-1}$

confirm the integrity of the $[Si_8O_{12}]$ core of the molecule. The broad band centered at 3300 $cm^{-1}$ is attributed to Si-OH, a result of the reaction with atmospheric water.

$^{29}Si\{^1H\}$ solid state MAS NMR of this material is consistent with the results described above. The peak corresponding to $H_8Si_8O_{12}$ at δ -84.186 is completely absent, replaced with 2 peaks at δ -90.059 and δ -92.721 respectively, as shown in Figure 2.11. A cross-polarization NMR experiment confirms the identity of the peak at δ -92.721 as (Si-Cl) and the peak at δ -90.059 as (Si-OH). These results indicate that the photochemical chlorination reaction went to completion and that the product decomposed upon exposure to the atmosphere.

### *2.3.3. Synthesis and Characterization of $(RO)_8Si_8O_{12}$*

The synthesis of $(RO)_8Si_8O_{12}$ results from the combination of the highly reactive $Cl_8Si_8O_{12}$ with an alkoxylating agent, trialkyl-orthoformate ($HC(OR_3)_3$) where the alkyl group is methyl, ethyl, or n-propyl. The synthetic procedure used was as follows:

Following photochemical chlorination to produce $Cl_8Si_8O_{12}$, Argon gas was bubbled through the carbon tetrachloride solution ($CCl_4$) until all unreacted chlorine gas was purged as indicated by a return to a milky-white solution from an intensely yellow-green colored solution. The $Cl_8Si_8O_{12}/CCL_4$ solution was transferred in a glove box to a 500 ml 3-necked round bottom flask equipped with a reflux condenser, septum, and a stopcock. The sealed flask was removed from the glove box and the $CCl_4$ was removed on a vacuum line, leaving the $Cl_8Si_8O_{12}$ powder. The flask was again purged with dry argon and neat trimethylorthoformate (35 mL) was added by syringe to the chlorosiloxane with stirring. The mixture was heated to reflux with an oil bath to reflux at 105°C and stirred at this tem-

perature overnight (12 hr) under nitrogen. Product should be a white to light colored solid suspended in a pale yellow/brown solution. For the synthesis of ethoxy- or n-propoxy spherosiloxanes, the reflux was carried out between 95°C and 110°C even though their trialkylorthoformates have much higher boiling points than the methyl. It is important not to overheat the reaction mixture, especially with ($HC(OEt_3)_3$) or ($HC(OPr_3)_3$), as this will lead to a strongly colored solution of very impure and partially decomposed product. After the reaction, all volatile material was removed under vacuum, leaving a lightly colored solid product. Initial purification is accomplished by recrystallizing the product in toluene (ca. 2 g / 10 mL) to remove any chlorinated by-products which give the material a yellowish tinge. A simulated powder X-ray diffraction pattern for $(CH_3O)_8Si_8O_{12}$ and list of indexed peaks based on the crystal structure determined by Day[43] can be found in Appendix B.2. The ethoxy and n-propoxy products are considerably more soluble in toluene than the methoxy product and require correspondingly less solvent for recrystallization. Final purification of the product is achieved by sublimation at 150°C and 0.01 Torr.

FTIR shows that the bands for the $[Si_8O_{12}]$ core are present at 569 $cm^{-1}$ and 470 $cm^{-1}$. (See Figure 2.12.) The absorptions in the region from 2850 $cm^{-1}$ to 3000 $cm^{-1}$ are characteristic of the C-H stretch of the methoxy group. The absence of the strong stretching band for (Si-Cl) at 712 $cm^{-1}$ indicates that all of the chlorinated material has reacted away, although the two small absorptions in the region of 2350 $cm^{-1}$ may indicate that some of the chlorine groups have reacted to form (Si-H) ligands instead of the desired alkoxy groups. $^1H$ NMR spectroscopy of the sample, presented in Figure 2.13, confirms the results from FTIR. The large peak at $\delta$ 3.325 results from the methyl hydrogens on

$(CH_3O)_8Si_8O_{12}$. The peak at δ 7.115 is assigned to benzene. The small peaks ranging from δ 3.20 to δ 3.30 represent impurities in the material.

### *2.3.4. Alternative Strategies to Spherosiloxane Synthesis*

The reaction scheme presented here may at first glance seem unnecessarily complicated in light of the rather extensive and well understood literature on the alcoholysis of hydrosilanes[62-64]. In fact, alcoholysis of hydrosilanes can be accomplished in the presence of a wide variety of acidic, basic, and transition metal catalysts, and in some cases without any catalyst at all. However, the functional group transformation of the $[Si_8O_{12}]$ spherosiloxane core is indeed quite difficult, as it is necessary to convert Si-H bonds to Si-OR without breaking any Si-O bonds in the spherosiloxane core. Little work had been done on functional group transformation of the spherosiloxane core until researchers in Klemperer's group at Illinois began studying them in the mid-1980's[43,44,65]. Their work showed that the Si-H bond in $H_8Si_8O_{12}$ is unusually inert and that attempts to use acidic or basic catalysts result in cleavage of the $[Si_8O_{12}]$ core[44]. As a result, they developed the first multistep syntheses, proceeding through the chlorinated intermediate. Reactions of methoxide salts with $Cl_8Si_8O_{12}$ results in cleavage of the $[Si_8O_{12}]$, as does reaction of $Cl_8Si_8O_{12}$ with methanol under strictly anhydrous conditions using excess triethylamine in order to trap the resultant HCl. Ultimately, they developed several successful routes to $(CH_3O)_8Si_8O_{12}$, the first by reaction of $Cl_8Si_8O_{12}$ with methyl nitrite:

$$\mathbf{Cl_8Si_8O_{12} + CH_3ONO \longrightarrow (CH_3O)_8Si_8O_{12} + NOCl} \quad (4)$$

Methyl nitrite is known to be a mild reagent for the Si-Cl to Si-$OCH_3$ transformation; however, it is unsuitable for general use due to its toxicity and explosive nature[66-68]. The second method to produce $(CH_3O)_8Si_8O_{12}$ is the one presented earlier and used for this work. Recently, work by Cagle in the Klemperer labs has produced a single step route to $(CH_3O)_8Si_8O_{12}$[26]:

$$\mathbf{H_8Si_8O_{12} + (CH_3)_3SnOCH_3 \longrightarrow (CH_3O)_8Si_8O_{12} + (CH_3)_3SnH} \quad (5)$$

Unfortunately, although this reaction proceeds in about 48% yield, it is even more difficult than the multistep route adopted. This is due to the need for strictly anhydrous reaction conditions as well as the need to perform a multistep synthesis of trimethylmethoxytin since it is not commercially available.

One of the most successful catalysts for the alcoholysis of hydrosilanes is triphenylphosphine rhodium(I) chloride, also known as Wilkinson's catalyst[63,69,70]. It has been shown to convert hydrosilanes to their corresponding alkoxide by reacting with alcohols in as little as 10 minutes at 0°C. The primary factor controlling the reaction is the number of hydrides and the degree of steric hindrance at the Si center. Lower reaction temperatures and shorter reaction times were necessary for unhindered multihydrides. However, it is possible to react $Ph_3SiH$, a relatively hindered monohydride, with ethanol to $Ph_3SiOEt$ at 60°C in 30 minutes[69]. On the surface, it would appear that this catalyst should work well for alcoholysis of spherosiloxanes because the Si-H is relatively unhindered and under these conditions the catalyst is unlikely to attack the $[Si_8O_{12}]$ core. Following Ojima *et al.* 0.75 g $H_8Si_8O_{12}$ were dissolved in 50 ml n-hexane in a round bottom flask with a mag-

netic stirrer. 5.7 mg. of $(Ph_3P)_3RhCl$ (0.4 mol %) and 0.54 g anhydrous methanol (a slight stoichiometric excess) were added to the solution and the mixture was heated to reflux. After 20 hours, the mixture was filtered to remove the catalyst and the solvent was removed by rotovap. The resulting white powder was tested by $^1H$ and $^{13}C$ NMR in $C_6D_6$ solution and was found to contain only the $H_8Si_8O_{12}$ starting product with no evidence of any alkoxylation taking place.

An attempt was also made to find a suitable replacement reaction for the photochlorination reaction of $H_8Si_8O_{12}$ to $Cl_8Si_8O_{12}$. $H_8Si_8O_{12}$ was reacted with Eschenmoser's salt while heating in THF according to the following reaction:

$$H_8Si_8O_{12} + (CH_3)_2N^+{=}CH_2Cl \xrightarrow[\Delta]{THF} Cl_8Si_8O_{12} + (CH_3)_3N \uparrow \quad (6)$$

It was believed that the removal of trimethylamine by vaporization from the reaction mixture would provide a sufficient driving force to run the reaction. 0.5 g of $H_8Si_8O_{12}$ and 0.88 g of the salt were added to 100 ml of anhydrous tetrahydrofuran in a 250 ml flask fitted with a condenser, septum, and stopcock. The solution was heated to 75°C with stirring for 8 hours and the solution took on a milky white appearance while refluxing. FTIR spectroscopy proved the reaction to be unsuccessful. Analysis of the reaction products indicated that while the reaction did proceed, the spherosiloxane product was incompletely chlorinated, and moreover, that the $[Si_8O_{12}]$ core had been partially decomposed in the reaction, possibly by the amine.

## 2.4. Experimental Methods

### 2.4.1. Chemical Characterizations

Fourier Transform Infrared (FTIR) spectra were obtained with a Nicolet System 800 Spectrometer using KBr pellets that contained 2 wt% sample. Raman Spectra were recorded on a Nicolet Raman accessory. X-ray powder diffraction (XRD) patterns were collected using Cu-K$\alpha$ radiation on a Scintag XDS-2000 diffractometer that is equipped with a liquid nitrogen cooled Germanium solid-state detector. Data acquisitions were performed using a Digital Instruments MicroVax 3100 system. Solid-state NMR spectra for $^{29}Si$ were obtained using magic angle spinning (MAS) on a Bruker AM 300 system at a frequency of 59.6 MHz. $^{1}H$ and $^{13}C$ NMR solution spectra were obtained on a GE NMR QE PLUS system at 300 MHz and 75.5 MHz respectively. $^{29}Si$ NMR solution spectra were obtained using a Bruker AM 500 system operating at a frequency of 99.3 MHz under gated decoupling conditions to reduce Nuclear Overhauser Effects (NOE) unless otherwise noted. $CDCl_3$, $C_6D_6$, or a 50:50 v/v mixture of $C_6D_6$:$CCl_4$ was used as the solution/lock solvent for the samples. 10 mm quartz NMR tubes were used for the $^{29}Si$ experiments to reduce the signal obtained from sample tube and 0.15-0.20 M $Cr(acac)_3$ was added as a paramagnetic relaxation agent in some cases in an attempt to reduce $T_1$ values and further eliminate NOE effects. All solution spectra were obtained and referenced using TMS as an internal standard.

## *Literature Cited*

(1) Feynman, R. P. In *Miniaturization*; GIlbert, H. D. Ed.; Reinhold Publishing Corp.: New York, 1961; pp 282-296.

(2) Ozin, G. A. *Adv. Mater.* **1992**, *4*, 612-649.

(3) *Silicon Molecular Beam Epitaxy*, Bean, J. C.; Iyer, S. S.; Wang, K. L. Eds.; Materials Research Society: Pittsburgh, PA, 1991; Vol. 220.

(4) *Thin Film Growth Techniques for Low-Dimensional Structures*, Farrow, R. F. C.; Parkin, S. S. P.; Dobson, P. J.; Neave, J. H.; Arrott, A. S. Eds.; Plenum Press: New York, 1987; Vol. 163.

(5) *Atomic Layer Epitaxy*, Suntola, T.; Simpson, M. Eds.; Chapman and Hall: New York, 1990.

(6) *Nanostructures: Fabrication and Physics*, Berger, S. D.; Craighead, H. G.; Kern, D.; Smith III, T. P. Eds.; Materials Research Society: Pittsburgh, PA, 1990.

(7) *Nanostructure Physics and Fabrication, Proceedings of the International Symposium, (College Station, TX)*, Reed, M. A.; Kirk, W. P. Eds.; Academic Press: New York, 1989.

(8) *Science and Engineering of One- and Zero-Dimensional Semiconductors*, Beaumont, S. P.; Sotomayor Torres, C. M. Eds.; Plenum Press: New York, 1990; Vol. 214.

(9) Binnig, G.; Rohrer, H. *Helv. Phys. Acta* **1982**, *55*, 726-735.

(10) Binnig, G.; Rohrer, H.; Gerber, C.; Wiebel, E. *Phys. Rev. Lett.* **1982**, *49*, 57-61.

(11) Binnig, G.; Rohrer, H. *Surf. Sci.* **1983**, *126*, 236-244.

(12) Binnig, G.; Quate, C. F.; Gerber, C. *Phys. Rev. Lett.* **1986**, *56*, 930-933.

(13) Frommer, J. *Angew. Chem. Int. Ed. Engl.* **1992**, *31*, 1298-1328.

(14) Parkinson, B. In *Supramolecular Architecture: Synthetic Control in Thin Films and*

*Solids*; Bein, T. Ed.; American Chemical Society: Washington D. C., 1992; pp 76-85.

(15) Tromp, R. M.; Hamers, R. J.; Demuth, J. E. *Science* **1986**, *234*, 304-309.

(16) Stroscio, J. A.; Eigler, D. M. *Science* **1991**, *254*, 1319-1326.

(17) Eigler, D. M.; Schweizer, E. K. *Nature* **1990**, *344*, 524-526.

(18) Eigler, D. M.; Lutz, C. P.; Rudge, W. E. *Nature* **1991**, *352*, 600-603.

(19) Nishizawa, M.; Shibuya, M.; Sawaguchi, T.; Matsue, T.; Uchida, I. *J. Phys. Chem.* **1991**, *95*, 9042-9044.

(20) Ozin, G. A.; Özkar, S. *Adv. Mater.* **1992**, *4*, 11-22.

(21) Drexler, K. E. *Engines of Creation*; Anchor Press: New York, 1986.

(22) Drexler, K. E. *Nanosystems*; John Wiley & Sons, Inc.: New York, 1992.

(23) Stein, A.; Keller, S. W.; Mallouk, T. E. *Science* **1993**, *259*, 1558-1563.

(24) Meier, W. M.; Olson, D. H.; Baerlocher, C. *Atlas of Zeolite Structure Types*; 4th ed.; Elsevier: London, 1996.

(25) Agaskar, P. A. *Inorganic Chemistry* **1991**, *30*, 2707-2708.

(26) Cagle, P. C. Ph.D. Dissertation; University of Illinois at Champaign-Urbana, 1992.

(27) Agaskar, P. A.; Day, V. W.; Klemperer, W. G. *J. Am. Chem. Soc.* **1987**, *109*, 5554-5556.

(28) Bürgy, H.; Calzaferri, G.; Herren, D.; Zhadanov, A. *Chimia* **1991**, *45*, 3-8.

(29) Frye, C. L.; Collins, W. T. *J. Am. Chem. Soc.* **1970**, *92*, 5586-5588.

(30) Feher, F. J.; Budzichowski, T. A. *J. Organomet. Chem.* **1989**, *379*, 33-40.

(31) Agaskar, P. A. *Inorg. Chem.* **1990**, *29*, 1603.

(32) Agaskar, P. A. *Synth. React. Inorg. Met.-Org. Chem.* **1990**, *20*, 483-492.

(33) Scott, D. W. *J. Am. Chem. Soc.* **1946**, *68*, 356-357.

(34) Barry, A. J.; Daudt, W. H.; Domicone, J. J.; Gilkey, J. W. *J. Am. Chem. Soc.* **1955**, *77*, 4248-4252.

(35) Müller, R.; Köhne, F.; Sliwinski, S. *J. Prakt. Chem.* **1959**, *9*, 71-74.

(36) Calzaferri, G.; Hoffmann, R. *J. Chem. Soc., Dalton Trans.* **1991**, 917-928.

(37) Bornhauser, P.; Calzaferri, G. *Spectrochim. Acta, Part A* **1990**, *46*, 1045-1056.

(38) Agaskar, P. A. *Journal of the Royal Chemical Society, Chemical Communications* **1992**, 1024-1026.

(39) Bassindale, A. R.; Gentle, T. E. *J. Mater. Chem.* **1993**, *3*, 1319-1325.

(40) Sellinger, A.; Laine, R. M. *Abstr. Pap. ACS* **1994**, *208*, Preprint.

(41) Sellinger, A.; Laine, R. M. *Chem. Mater.* **1996**, *8*, 1592-1593.

(42) Desu, S. B.; Peng, C. H.; Agaskar, P. A. *J. Electrochem. Soc.* **1992**, *139*, 2682-2685.

(43) Day, V. W.; Klemperer, W. G.; Mainz, V. V.; Millar, D. M. *J. Am. Chem. Soc.* **1985**, *107*, 8262-8264.

(44) Millar, D. M. Ph.D. Dissertation; University of Illinois at Champaign-Urbana, 1987.

(45) Edelmann, F. T. *Angew. Chem. Int. Ed. Engl.* **1992**, *31*, 586-587.

(46) Feher, F. J.; Budzichowski, T. A.; Rahimian, K.; Ziller, J. W. *J. Am. Chem. Soc.* **1992**, *114*, 3859-3866.

(47) Liu, J.-C. *Chem. Commun.* **1996**, 1109-1110.

(48) Abbenhuis, H. C. L.; van Herwijnen, H. W. G.; van Santen, R. A. *Chem. Commun.* **1996**, 1941-1942.

(49) Feher, F. J.; Weller, K. J. *Organometallics* **1990**, *9*, 2638-2640.

(50) Dutta, P.; Shieh, D.-C. *Appl. Spectrosc.* **1985**, *39*, 343-346.

(51) Dutta, P. K.; Shieh, D. C. *J. Raman Spectrosc.* **1985**, *16*, 312-314.

(52) Dutta, P. K.; Shieh, D. C. *Appl. Spectrosc.* **1985**, *39*, 343-346.

(53) Dutta, P. K.; Shieh, D. C. *J. Phys. Chem.* **1986**, *90*, 2331-2334.

(54) Franklin, K. R.; Lowe, B. M. In *Zeolites: Facts, Figures, Future*; Jacobs, P. A.; van Santen, R. A. Eds.; Elsevier: Amsterdam, 1989; pp 179-188.

(55) Dutta, P. K.; Puri, M. *J. Phys. Chem.* **1987**, *91*, 4329-4333.

(56) Dutta, P. K.; Shieh, D. C.; Puri, M. *J. Phys. Chem.* **1987**, *91*, 2332-2336.

(57) Dutta, P. K.; Shieh, D. C.; Puri, M. *Zeolites* **1988**, *8*, 306-309.

(58) Dutta, P. K.; DelBarco, B. *J. Phys. Chem.* **1988**, *92*, 354-357.

(59) Dutta, P. K.; Rao, K. M.; Park, J. Y. *J. Phys. Chem.* **1991**, *95*, 6654-6656.

(60) Bärtsch, M.; Bornhauser, P.; Bürgy, H.; Calzaferri, G. *Spectrochim. Acta, Part A* **1991**, *47*, 1627-1629.

(61) Auf der Heyde, T. P. E.; Bürgi, H. B.; Bürgy, H.; Törnroos, K. W. *Chimia* **1991**, *45*, 38-40.

(62) Lukevics, E.; Dzintara, M. *J. Organomet. Chem.* **1985**, *295*, 265-315.

(63) Corriu, R. J. P.; Moreau, J. J. E. *Journal of the Royal Chemical Society, Chemical Communications* **1973**, 38-39.

(64) Bedard, T. C.; Corey, J. Y. *J. Organomet. Chem.* **1992**, *428*, 315-333.

(65) Voronkov, M. G.; Zagata, L. *Chem. Abstr.* **1968**, *69*, 1004.

(66) Wilberg, E.; Stecher, O.; Neumaier, A. *Inorg. Nucl. Chem. Lett.* **1965**, *1*, 31.

(67) Slovak, J. M.; Hill, R. N. *J. Occup. Med* **1981**, *23*, 857.

(68) Selle, H. *Z. Electrochem.* **1957**, *61*, 672.

(69) Ojima, I.; Kogure, T.; Nihonyanagi, M.; Kono, H.; Inaba, S. *Chem. Lett.* **1973**, 501-504.

(70) Corriu, R. J. P.; Moreau, J. J. E. *J. Organomet. Chem.* **1976**, *114*, 135-144.

(71) Davis, M. E. *Ind. Eng. Chem.* **1991**, *30*, 1675-1683.

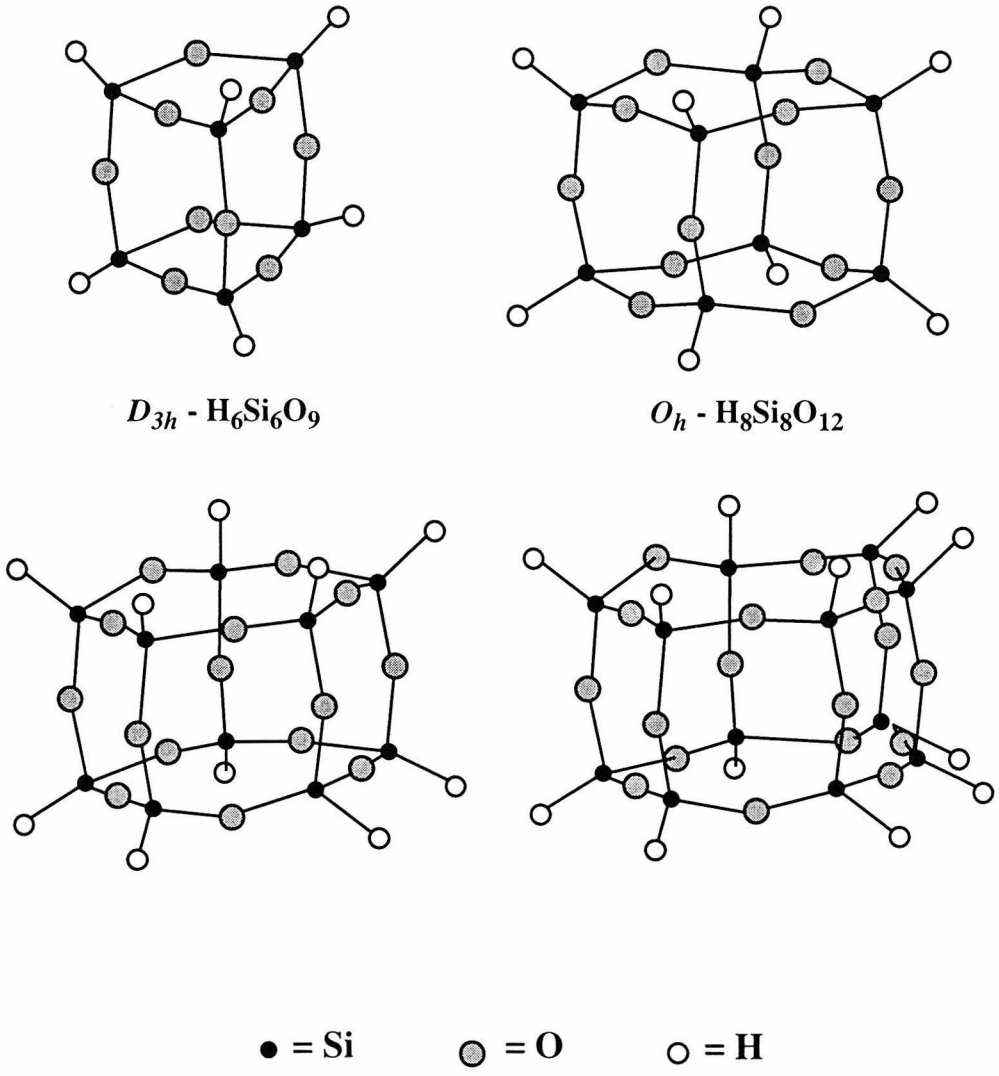


**Figure 2.1:** Structures of the first four members of the family of polyhedral silsesquioxanes with a general formula of $(RSiO_{1.5})_{2n}$, also known as Spherosiloxanes.

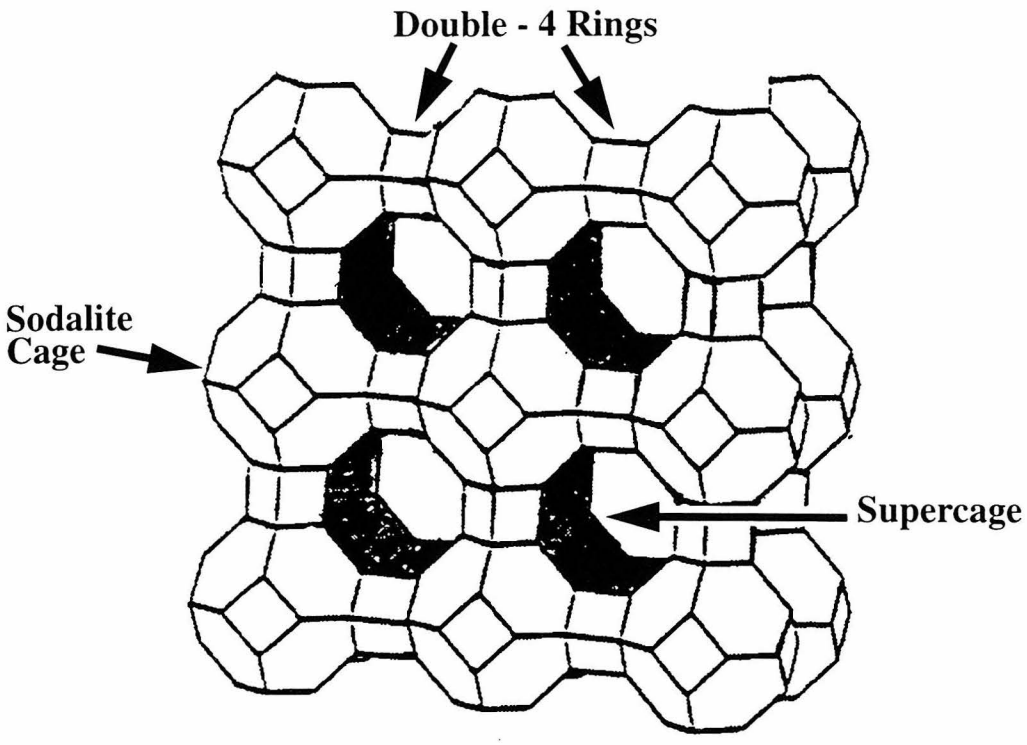


**Figure 2.2:** Structure of Zeolite A (LTA). Zeolite A is composed entirely of double four-ring subunits; six double four rings are connected to form each sodalite cage. Adapted from Davis[71].

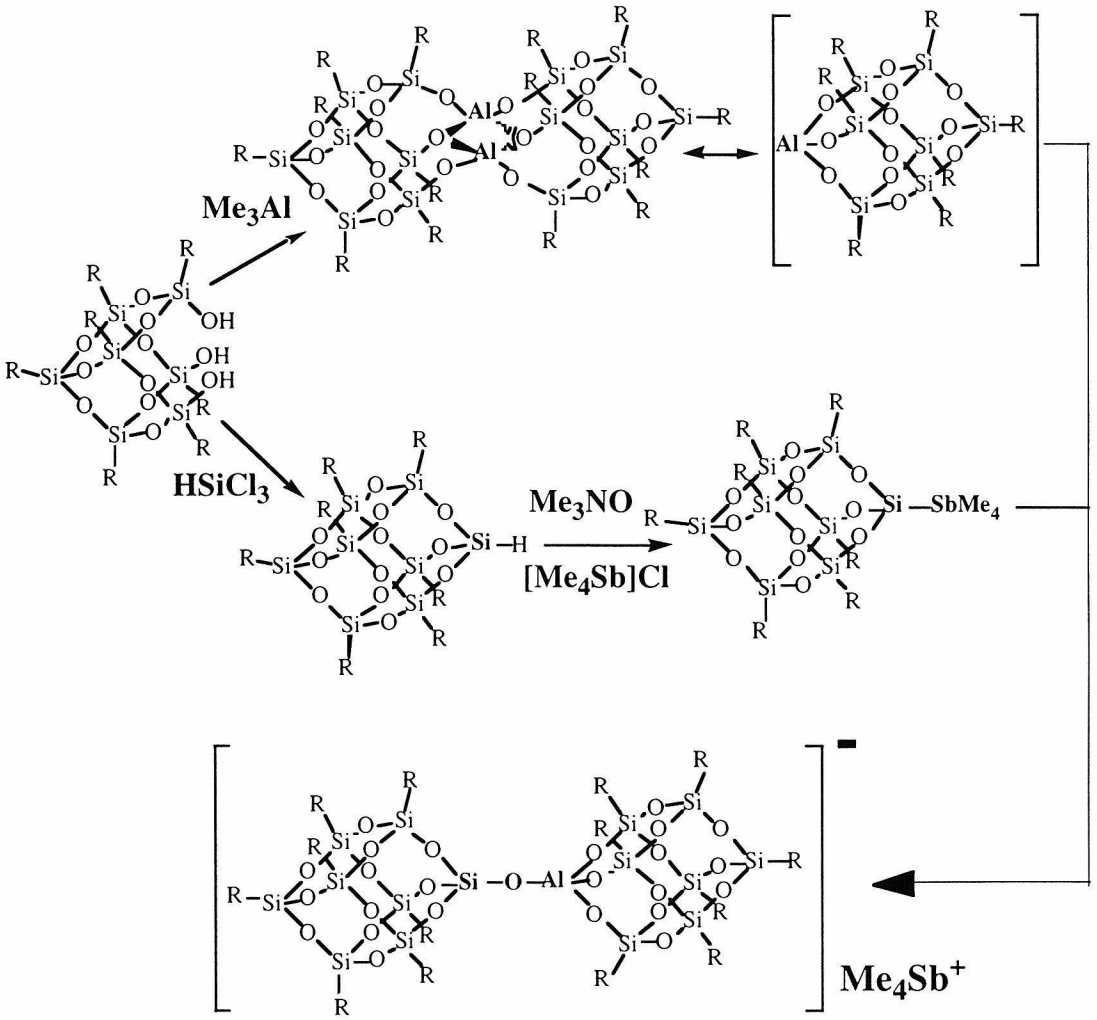


**Figure 2.3:** Reaction scheme for the formation of aluminosilicate linked spherosiloxane dimers. Adapted from Feher[49].

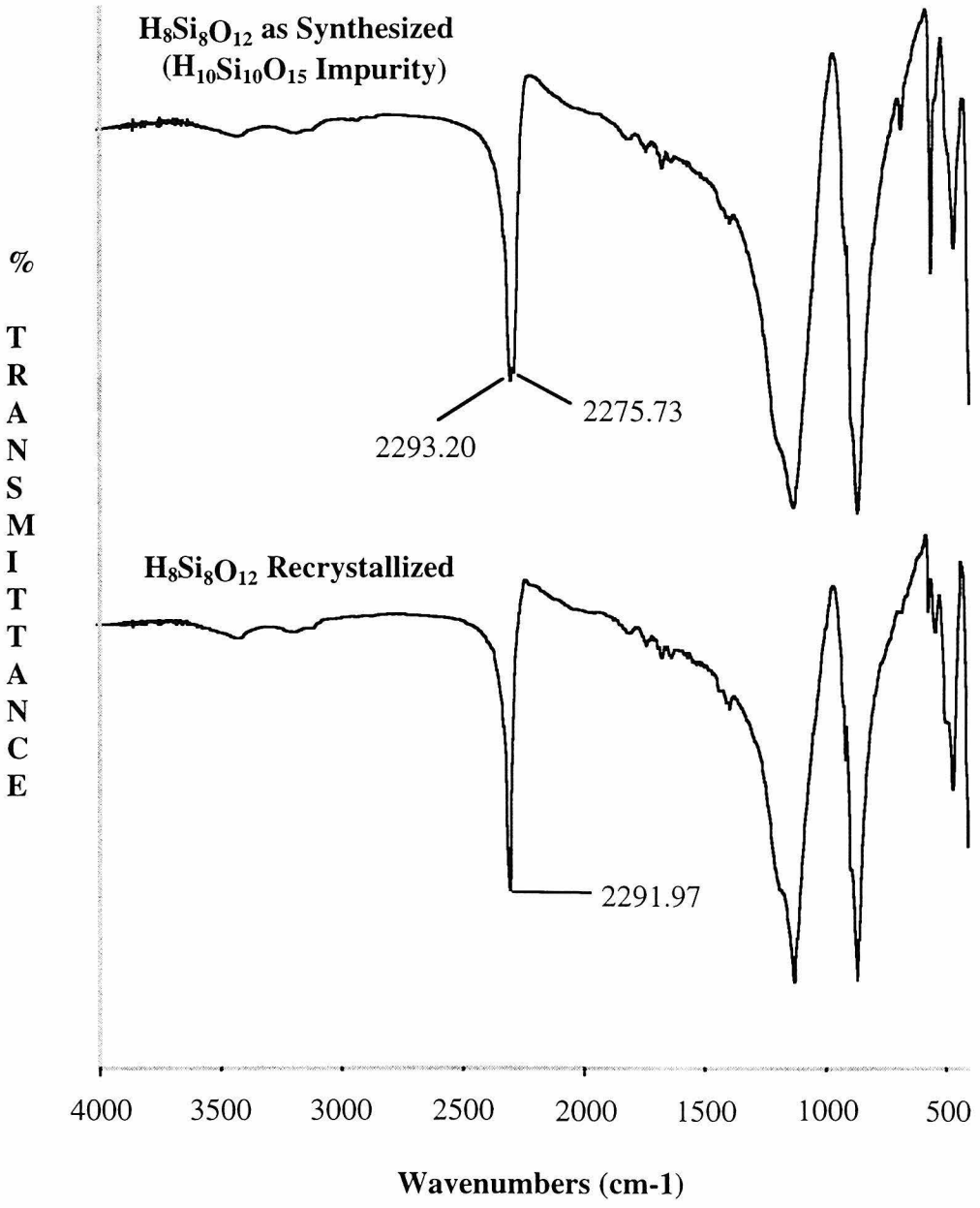


**Figure 2.4:** Characteristic FTIR spectra for $H_8Si_8O_{12}$ as synthesized (top) and after recrystallization from hot/cold hexane followed by washing five times with 10 ml cold hexane (bottom).

| Normal Mode | Wavenumber ($cm^{-1}$) | Type of Vibration |
|---|---|---|
| $T_{1u}$ | | |
| $\nu_{24}$ | 2292 | ν (Si-H) |
| $\nu_{25}$ | 1140 | ν (Si-O) |
| $\nu_{26}$ | 881 | δ (O-Si-H) |
| $\nu_{27}$ | 566 | δ (O-Si-O) |
| $\nu_{28}$ | 465 | ν (Si-O) |
| $\nu_{29}$ | 399 | δ (O-Si-O) |

**Table 2.1:** Observed IR active fundamental modes for $H_8Si_8O_{12}$. Adapted from Bärtsch[60].

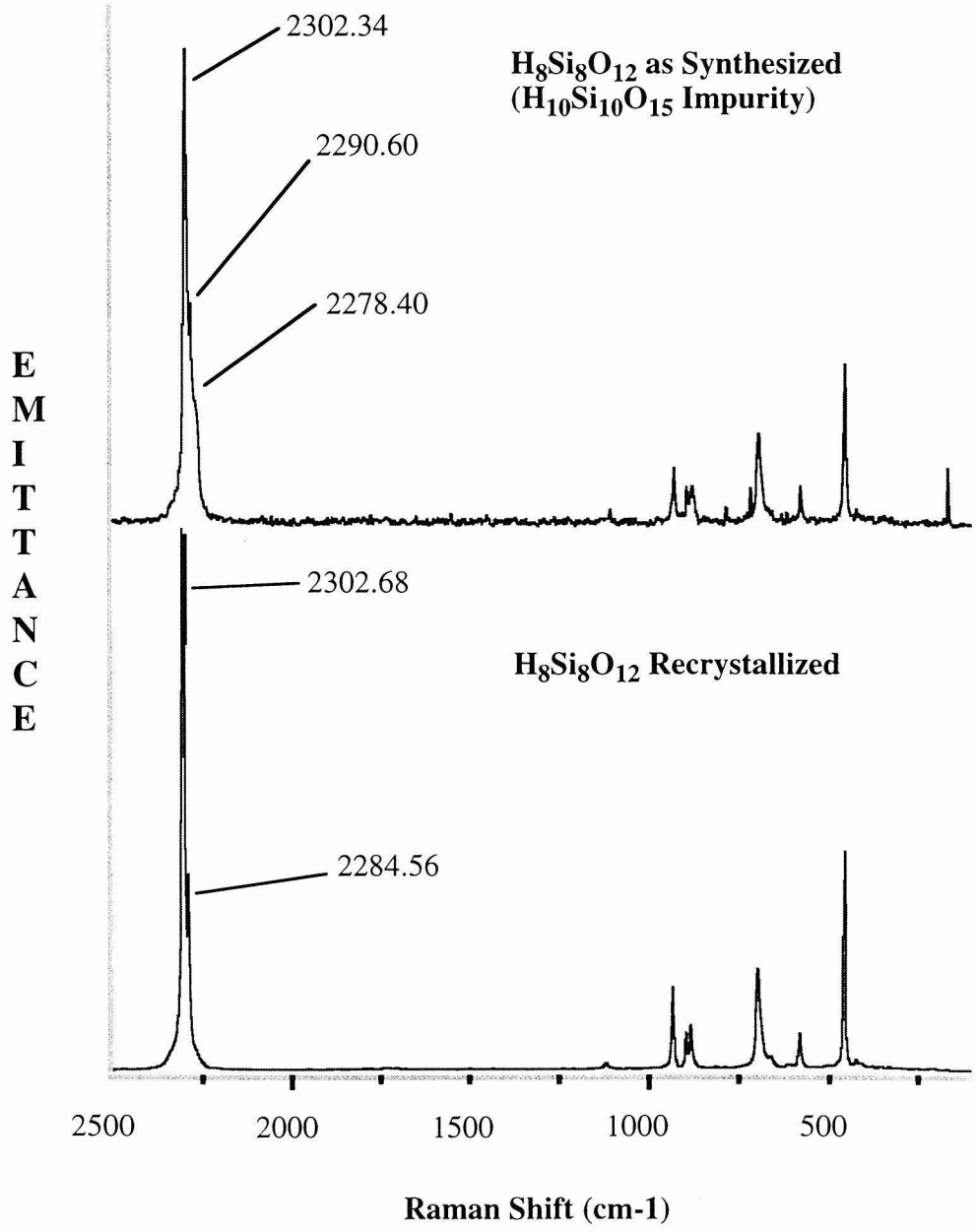


**Figure 2.5:** Characteristic Raman spectra for $H_8Si_8O_{12}$ as synthesized (top) and after recrystallization from hot/cold hexane followed by washing five times with 10 ml cold hexane (bottom).

| Normal Mode | Wavenumber ($cm^{-1}$) | Type of Vibration |
|---|---|---|
| $\mathbf{A_{1g}}$ | | |
| $\nu_1$ | 2302 | ν (Si-H) |
| $\nu_2$ | 579 | δ (O-Si-H) |
| $\nu_3$ | 456 | ν (Si-O) |
| $\mathbf{E_g}$ | | |
| $\nu_5$ | 932 | δ (O-Si-H) |
| $\nu_6$ | 697 | ν (Si-O) |
| $\nu_7$ | 345 | δ (O-Si-O) |
| $\nu_8$ | 84 | δ (Si-O-Si) |
| $\mathbf{T_{2g}}$ | | |
| $\nu_{12}$ | 2286 | ν (Si-H) |
| $\nu_{13}$ | 1118 | ν (Si-O) |
| $\nu_{14}$ | 897, 883 | δ (O-Si-H) |
| $\nu_{15}$ | 609 | ν (Si-O) |
| $\nu_{16}$ | 411 | δ (O-Si-O) |
| $\nu_{17}$ | 171 | δ (O-Si-O) |

**Table 2.2:** Observed Raman active fundamental modes for $H_8Si_8O_{12}$. Adapted from Bärtsch[60].

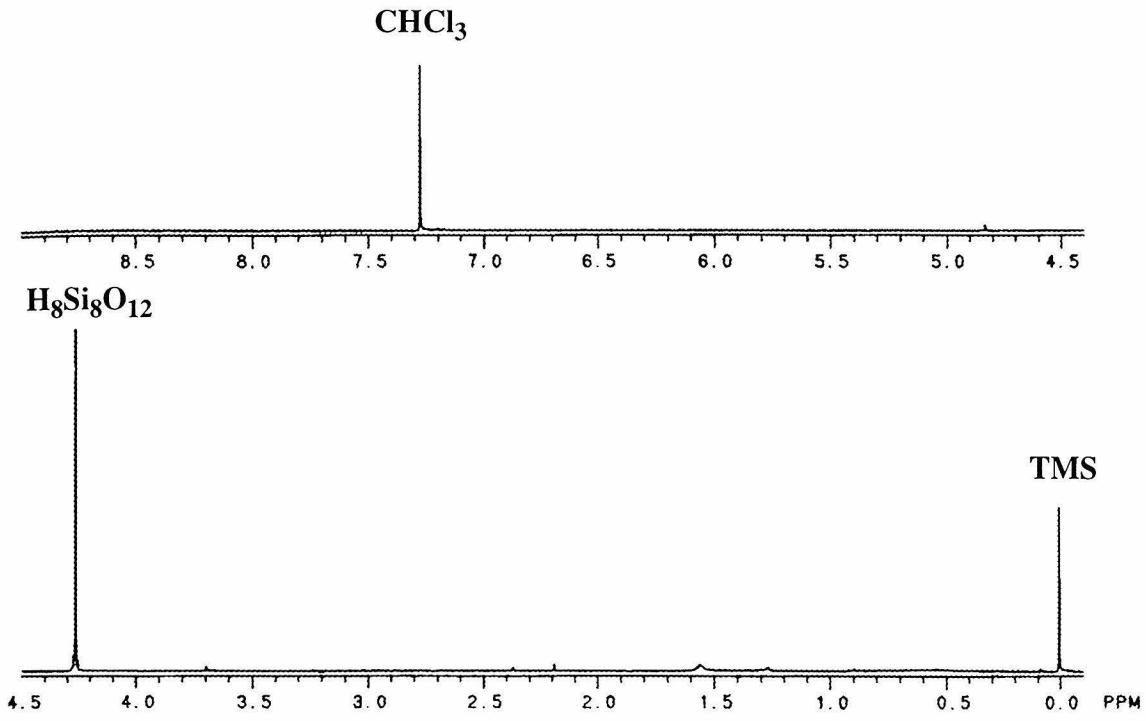


**Figure 2.6:** $^{1}H$ solution NMR of $H_8Si_8O_{12}$ in chloroform-$d_1$. The high degree of symmetry in the molecule results in a single peak in the proton spectrum.

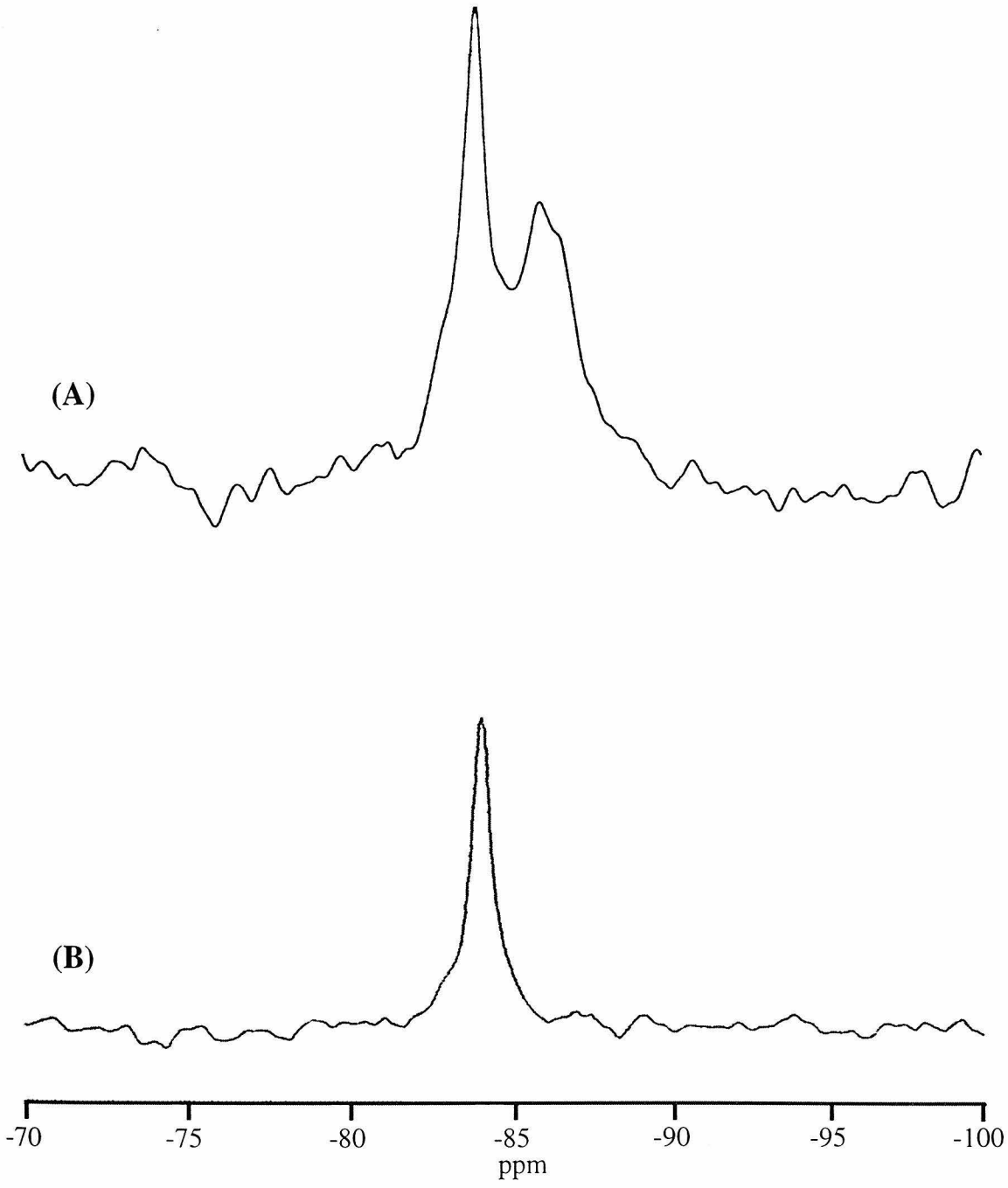


**Figure 2.7:** $^{29}Si$ MAS NMR spectra: (A) Spectrum of as synthesized product, a mixture of $H_8Si_8O_{12}$, δ -84.2 ppm, and $H_{10}Si_{10}O_{15}$, δ -86.2 ppm; (B) Spectrum of recrystallized $H_8Si_8O_{12}$.

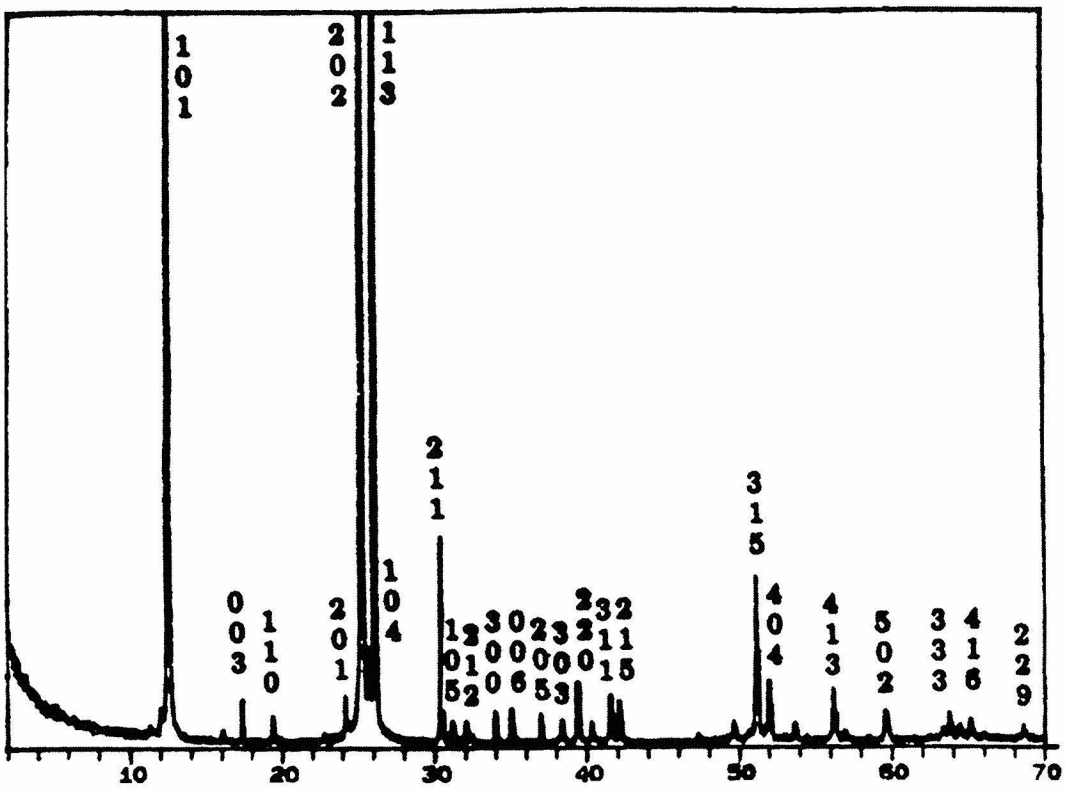


**Figure 2.8:** Indexed powder x-ray diffraction pattern of recrystallized $H_8Si_8O_{12}$.

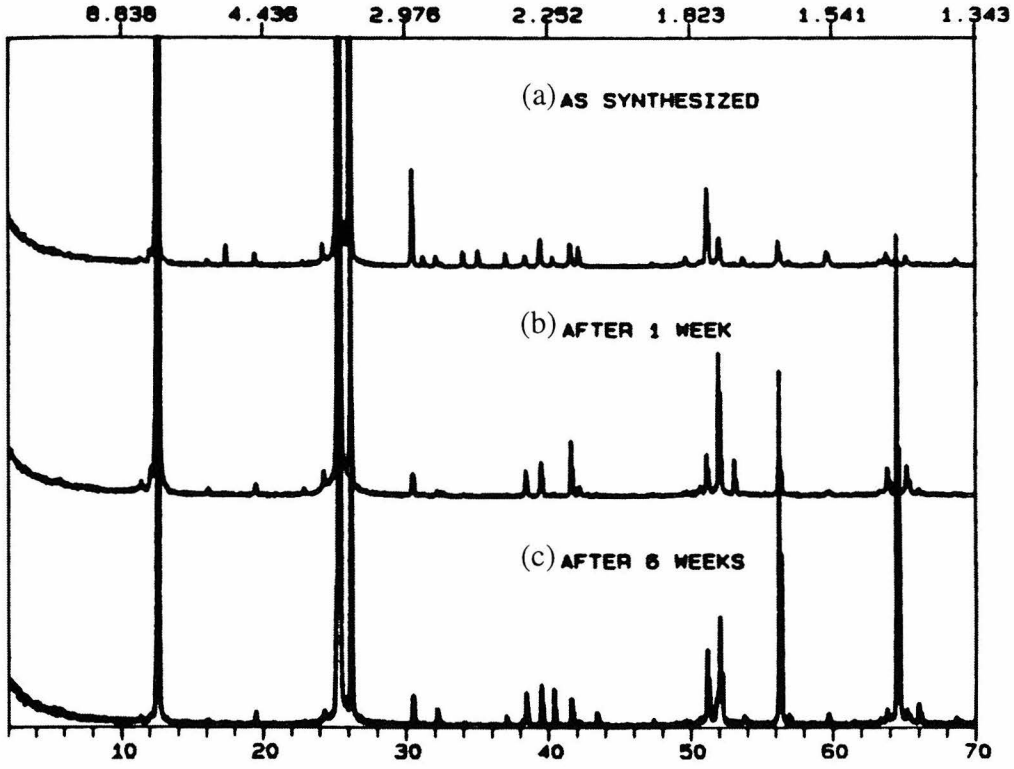


**Figure 2.9:** Powder x-ray diffraction patterns of $H_8Si_8O_{12}$ (a) as synthesized, (b) after 1 week, (c) after 6 weeks.

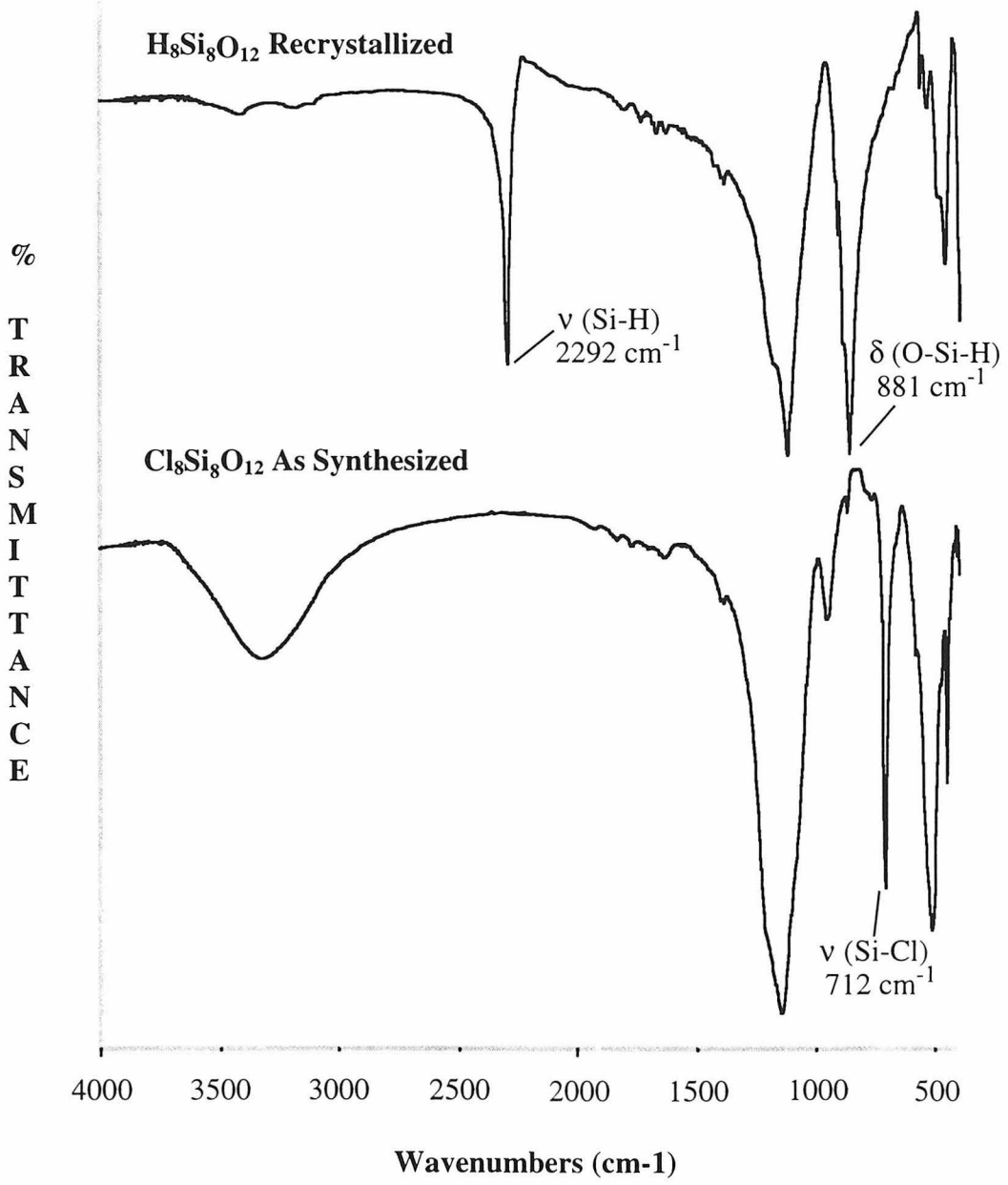


**Figure 2.10:** FTIR spectra of purified $H_8Si_8O_{12}$ (top) and the resulting product of its photochlorination reaction, $Cl_8Si_8O_{12}$ (bottom).

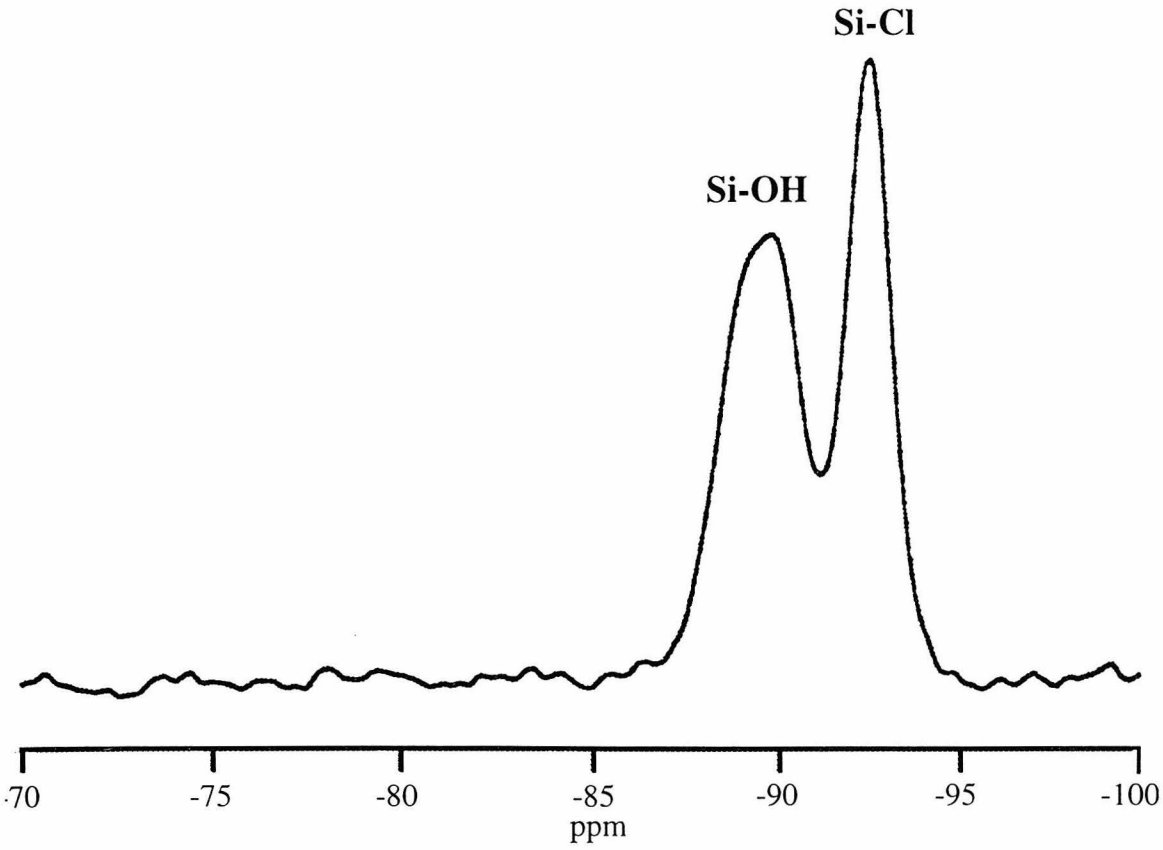


**Figure 2.11:** $^{29}Si$ MAS NMR spectrum of $Cl_8Si_8O_{12}$. Even a brief exposure to water in the atmosphere begins to decompose the material into $Cl_{8-x}(OH)_xSi_8O_{12}$.

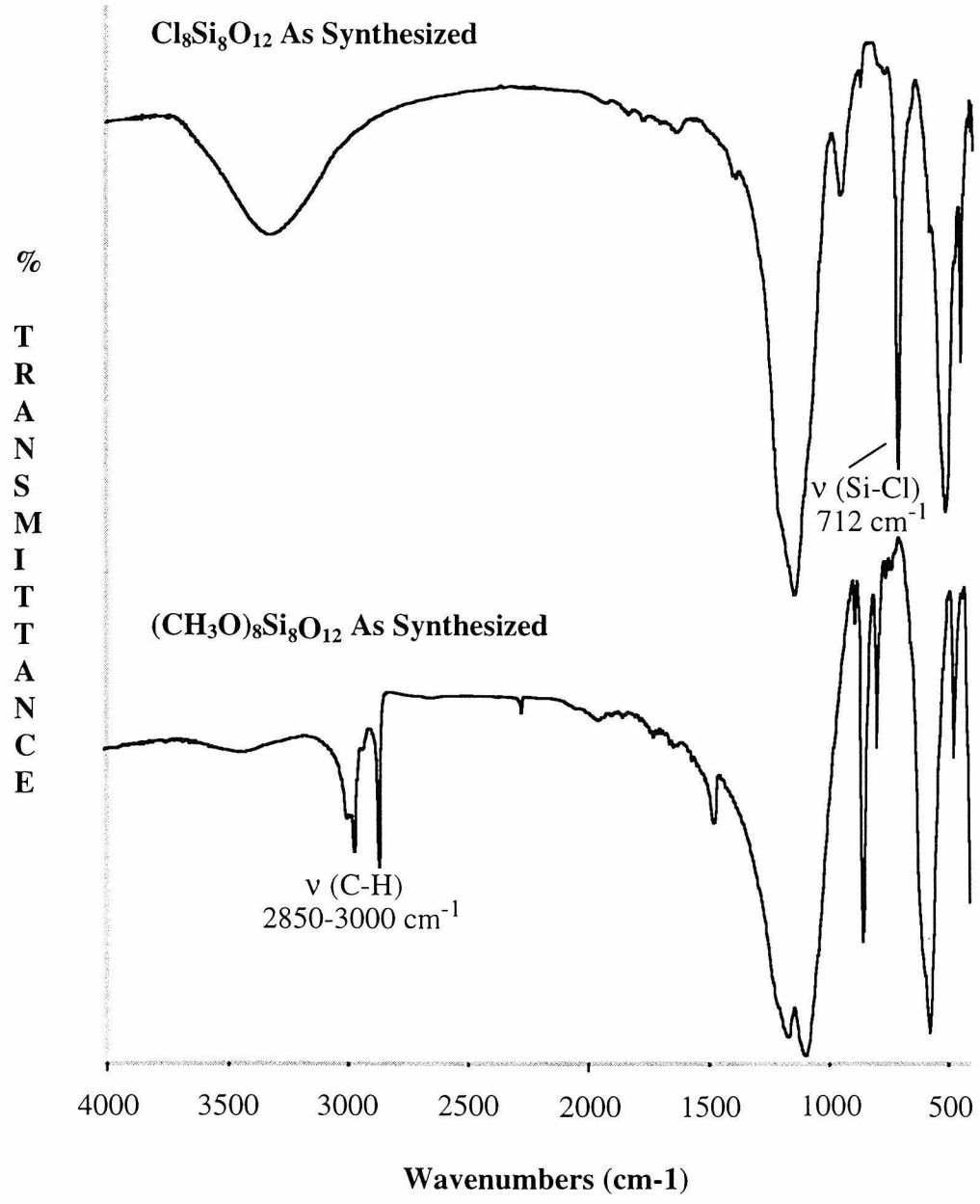


**Figure 2.12:** FTIR spectra of $Cl_8Si_8O_{12}$ (top) and $(CH_3O)_8Si_8O_{12}$ (bottom). The disappearance of the Si-Cl stretch at 712cm$^{-1}$ indicates that all of the chlorine has reacted and appearance of bands in the C-H stretching region from 2850-3000cm$^{-1}$ are characteristic of the methoxy functionality.

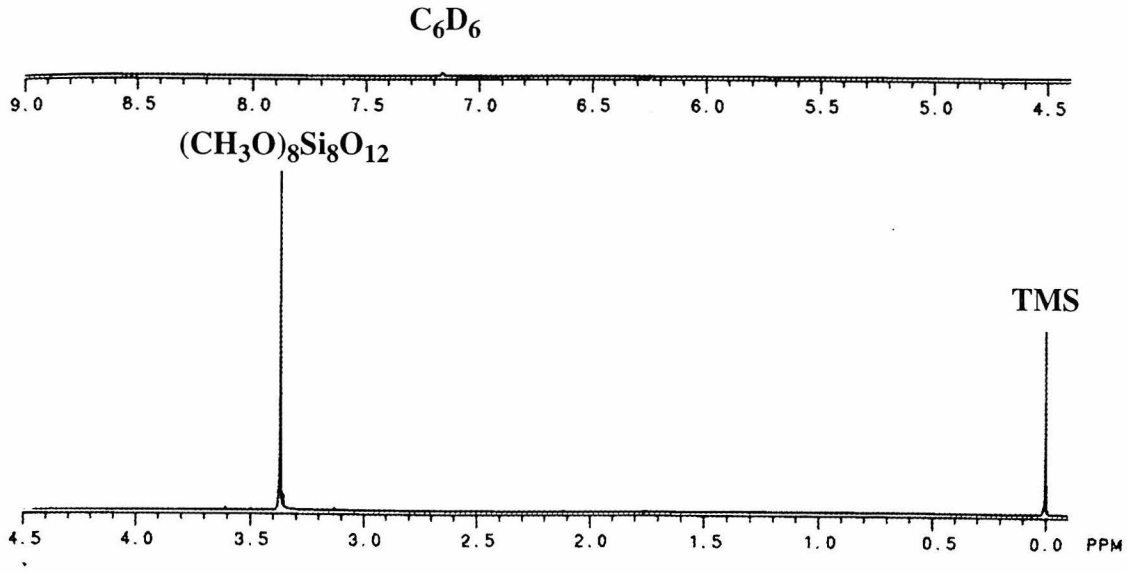


**Figure 2.13:** $^{1}H$ solution NMR of $(CH_3O)_8Si_8O_{12}$ in benzene-$d_6$. The high degree of symmetry in the molecule results in a single peak in the proton spectrum.

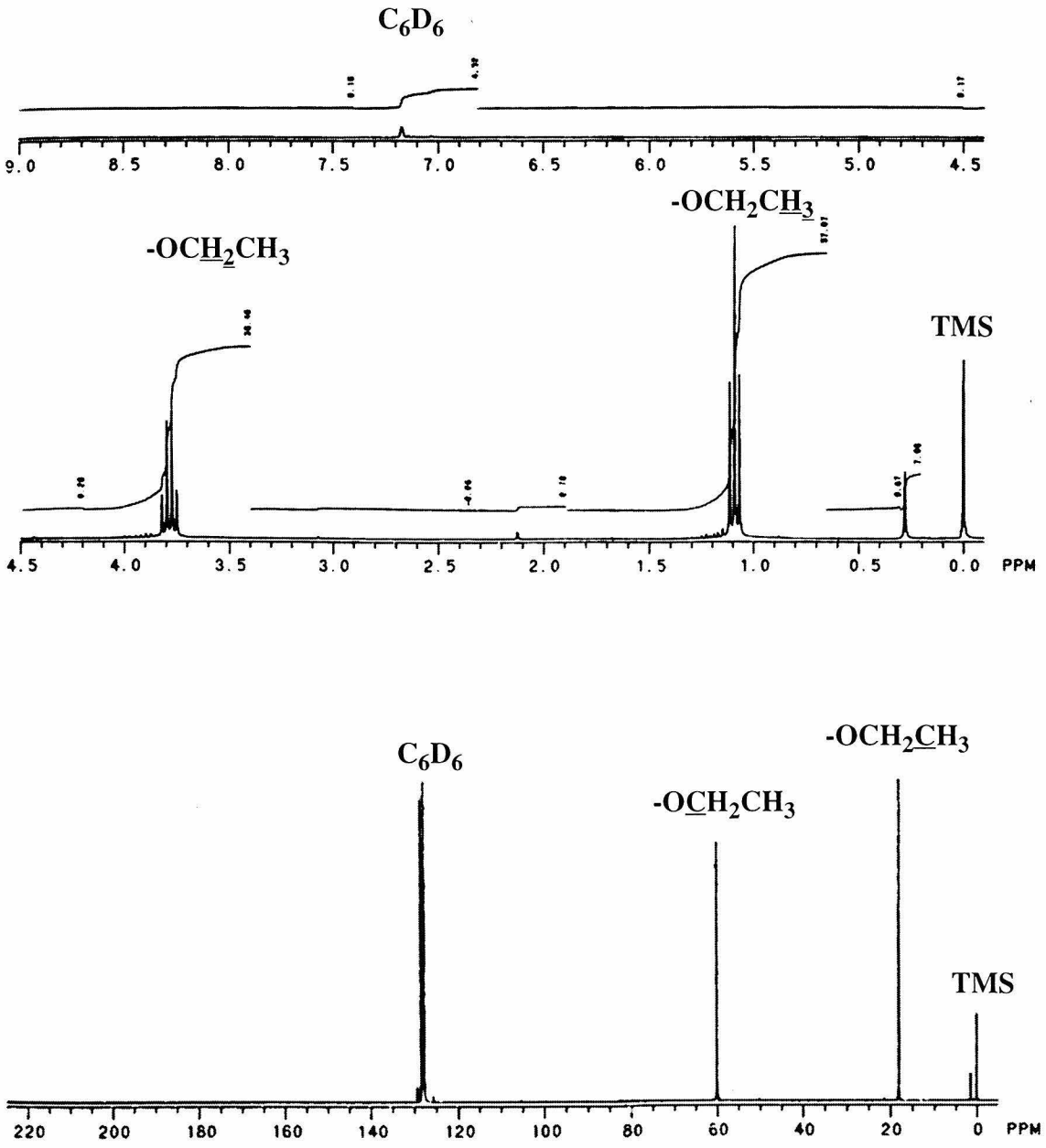


**Figure 2.14:** Solution $^{1}H$ (top) and $^{13}C$ (bottom) spectra of as synthesized $(C_2H_5O)_8Si_8O_{12}$ with peak assignments.

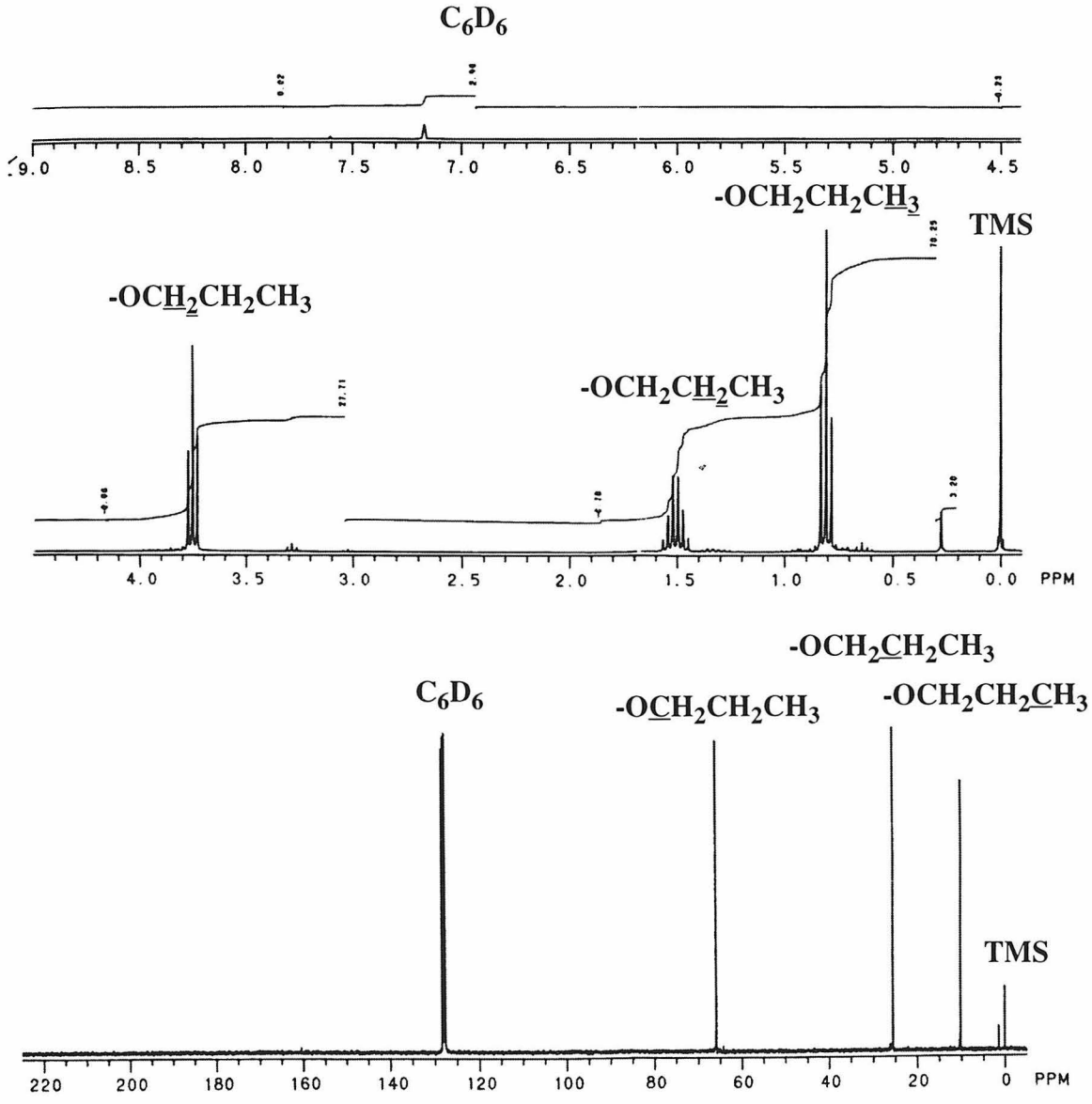


**Figure 2.15:** Solution $^{1}H$ (top) and $^{13}C$ (bottom) spectra of as synthesized $(n\text{-}C_3H_7O)_8Si_8O_{12}$ with peak assignments.

# *Chapter 3:*

## *Reactions of Spherosiloxanes*

## 3.1. *Introduction and Background*

The unique structural and physical properties of spherosiloxanes make them an excellent choice for use as molecular building blocks. Since they are composed primarily of silicon oxide, they are much more thermally stable than organic materials, and are compatible with current electronic materials, particularly silicon. $H_8Si_8O_{12}$ can now be readily synthesized in gram quantities and can be functionalized with a wide variety of reactive groups. Additionally, the $[Si_8O_{12}]$ family of spherosiloxanes has been very well characterized. There is experimental evidence to suggest that spherosiloxanes can be used to create structures with a defined order via controlled condensation[1]. Moreover, the similarity to structural units in zeolites and other ordered materials suggests that it should be possible to condense molecules of the cubic spherosiloxane $X_8Si_8O_{12}$ into a well ordered structure resembling a zeolite. In fact, this possibility was suggested in a recent review of solid-state synthesis by Stein, Keller, and Mallouk[2].

Zeolites are crystalline (alumino)silicate structures with pores and cages on the size scale of small molecules. Because of their unique structure and their stability as inorganic materials, they are widely used as adsorbents and for catalytic and molecular separations applications[3], and indeed are critical to the petrochemical industry because of their role in the catalytic cracking of crude oil. Currently, there are about 100 known forms of zeolites, of which about 40 occur naturally, and most of which have been synthesized in the laboratory[4]. In nature, zeolites form under hydrothermal conditions, that is, at high temperature and pressure in an aqueous environment. These conditions are mimicked in the lab by using autoclave reactors as reaction vessels. A typical synthesis has (1) a silicon (and possibly aluminum) source such as fumed silica, (2) a mineralizing agent such as

$OH^-$ or $F^-$ which serves to depolymerize the silica source and to help nucleate the new product, (3) a structure directing agent, typically a quaternary ammonium cation, and (4) water. The reactants are premixed, possibly forming a "synthesis gel," and then charged into the autoclave reactors to be heated in ovens from 100°C - 250°C for periods from hours to months. Since the nucleation and growth of the zeolite structure takes place inside a sealed reactor, it is extremely difficult to study the mechanisms which govern the formation of zeolites. Moreover, it is possible to produce more than one different type of zeolite structure from the same starting gel composition simply by variations in the reaction temperature and duration. Thus, although significant progress has been made toward understanding the forces governing the synthesis of pure silica zeolites[5-7], and even some progress toward structure synthesis by design[8,9], it is currently not possible to produce *a priori* a zeolite of a given desired structure. As a result a new technique for zeolite synthesis which would allow for the formation of a predictable structure by controlled condensation of known building blocks would be quite desirable. This should be possible by using known building blocks which get incorporated into the final structure without degradation in a "lego chemistry" fashion.

A systematic study of four-connected, three-dimensional nets (crystalline structures containing tetrahedral atoms such as zeolites and spherosiloxanes) has been carried by J.V. Smith over the last 30 years[10]. This study provides a basis for the development of theoretical framework structures that can be derived from spherosiloxane type substructures. A simple structure assuming maximum separation of the condensing spherosiloxanes has been simulated and is presented with its simulated diffraction pattern in Figure 3.1. This structure is one of the most likely candidates for synthesis from condensation of

spherosiloxanes based on bond angles and distances commonly found in zeolites[11]. The structure found in Figure 3.1 corresponds to theoretical net #46 as assigned by Smith[12] and to date has not been found to occur naturally or synthesized in the laboratory. A simulated x-ray diffraction pattern for this material can be found in Figure 3.2 and complete information on the structure parameters can be found in Appendix B.3.

It might seem that there are a limited number of structures that can be synthesized using a single building block such as a $X_8Si_8O_{12}$. However, by the simple expedient of introducing an additional silicon center at each of the eight vertices of $X_8Si_8O_{12}$, it is possible to greatly increase the number of possible structures that can be synthesized. In this way it is possible to synthesize the known $AlPO_4$-16 or (AST) structure, which has been synthesized in pure silica form[13,14]. (See Figure 3.3.) Moreover, if instead of adding another tetrahedral silicon center, a heteroatom such as aluminum, boron, or titanium were added, a structure with acidic or oxidative catalytic centers is created. Perhaps, even more importantly, those heteroatom centers would be in well ordered, specific sites within the zeolite structure, a long standing goal in zeolite research.

The first question that must be addressed in order to realize this objective is how to achieve ordered condensation of the spherosiloxane building blocks. In their attempt to make a regular network of spherosiloxanes for the development of porous silica, Day and Klemperer used $(CH_3O)_8Si_8O_{12}$ in a hydrolytic reaction scheme, as shown below:

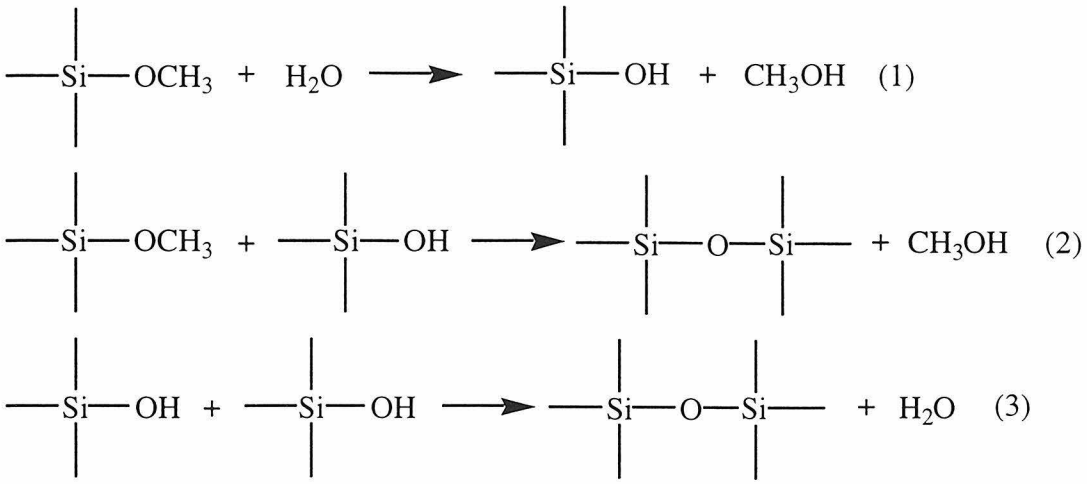

The reaction resulted in an amorphous material, yielding a monolithic glass, probably due to the irreversibility of Si-O-Si bond formation[2]. Since every Si-OR could react with every other Si-OR, there were no restrictions on random Si-O-Si bond formation, and once the bonding network is formed, it cannot be annealed into a crystalline structure. This type of uncontrolled condensation reaction, therefore, will not produce the type of ordered structures desired. In his synthetic scheme for producing an aluminosilicate linked spherosiloxane dimer (See Figure 2.3), Feher addressed this problem by creating a situation where there was only one reactive center on each spherosiloxane. Thus, when they were condensed together, the only possible product was the produced dimeric structure with the Si-O-Al linkage[1].

From the above discussions, it is clear that a reaction scheme that reduces the number of possible condensation pathways is desirable. In a recent paper, Corriu *et al.* suggest just such a scheme for the preparation of binary oxide gels by using a non-hydrolytic sol-gel process[15]. The non-hydrolytic condensation reaction that leads to the formation of M-

O-M' bridges by the release of alkyl halide follows the following reaction scheme:

$$\mathbf{M(OR)_n + M'X_{n'} \rightarrow (RO)_{n-1}M\text{-}O\text{-}M'X_{n'-1} + RX} \quad (4)$$

By using spherosiloxanes as the central group, where M = M' = $[Si_8O_{12}]$, OR = $OCH_3$, and X = Cl, it should be possible to carry out the same type of condensation as with binary oxides. $Cl_8Si_8O_{12}$ and $(CH_3O)_8Si_8O_{12}$ are functionalized spherosiloxanes whose synthesis has been described earlier, and are thus readily available as precursors for this reaction. The advantage this type of condensation has over a more traditional hydrolytic condensation scheme lies in the fact that this is a binary condensation reaction and under truly non-aqueous reaction conditions, the individual reactants will be unable to self-condense. Moreover, it is highly unlikely that any two individual spherosiloxane molecules will make more than one bond between them. This is a consequence of the molecular geometry which would result from such a multiple reaction, the formation of three adjacent four-membered silicate rings. The central four-ring would be highly strained, and as a result, this structure has never been observed in a silica-based zeolite structure to date.

Although we propose to utilize a scheme where the two species must condense in an alternating arrangement, i.e., ABABAB, etc., where A = $Cl_8Si_8O_{12}$ and B = $(CH_3O)_8Si_8O_{12}$, it is still highly unlikely that an ordered structure will result from simply combining the two species and allowing them to react. Some control over the reactants must be maintained to prevent random condensation to form a sol-gel structure. One possible way to overcome this difficulty is to carry out the condensation as a diffusion limited reaction. Diffusion limited control of the reaction can be achieved by using a technique

long known by geologists and mineralogists; that is, carrying out the condensation within a polymeric gel[16,17]. The gel method of crystal growth dates back to the end of the 19th century, regaining popularity in the 1960's and 1970's. This technique has successfully been applied to the growth of large single crystals of zeolites for x-ray structure determination[18]. Reactants are placed at opposite ends of a sealed, gel-filled tube and allowed to diffuse to the center where they nucleate and crystal growth occurs. (See Figure 3.4.) The condensation zone can be within the gel, or simply filled with solvent for ease of crystal recovery. The reaction is then controlled by variables such as concentration, temperature, and solvent size and polarity. By combining the non-hydrolytic condensation reaction with the gel method of crystal growth, it may be possible to produce framework structures with three-dimensional order from condensed spherosiloxanes, thereby opening a new pathway into zeolite synthesis.

## 3.2. *Spherosiloxane Condensation*

### 3.2.1. *Non-Hydrolytic Condensation of Spherosiloxanes*

The first attempt at binary condensation between $Cl_8Si_8O_{12}$ and $(CH_3O)_8Si_8O_{12}$ was carried out in a jacketed glass stirred reactor in carbon tetrachloride. Equimolar amounts ($1.1 \times 10^{-2}$ M) of the two reactants were added to 40 ml $CCl_4$ and the solution was heated at 40°C with stirring for 11 days. During the course of the reaction, additional $CCl_4$ was added to maintain a constant fluid level. The product was then collected by filtration inside a controlled atmosphere glove box. FTIR spectroscopy showed that the characteristic bands for Si-Cl and Si-$OCH_3$ were absent, as well as a very strong band corresponding to a Si-OH stretch around 3350 $cm^{-1}$. In addition, there was a band indicative of adsorbed water. X-ray diffraction (XRD) on the sample showed a single peak at $2\Theta = 17.9$ degrees followed by a broad feature centered about 25 degrees indicating the presence of a largely amorphous material. This type of diffraction pattern was observed on a number of occasions and is thought to correspond to a largely amorphous material, with the single sharp peak resulting from a fractal-type condensation in some portion of the material. These two analytical results suggest that the reaction was not non-hydrolytic in nature, rather that water served as a condensation catalyst in this case leading to the amorphous, fractalized material.

In order to prevent the introduction of water into the reaction mixture, all reactions from this point on were carried out in sealed, Teflon lined, autoclave reactors. In addition to preventing the introduction of water, it was thought that a completely sealed reaction vessel would prevent the loss of methyl chloride, the very volatile by-product of the reac-

tion, thus making the reaction irreversible and reducing the possibility of creating a ordered structure. A typical reaction involved placing an equimolar mixture of $Cl_8Si_8O_{12}$ and $(CH_3O)_8Si_8O_{12}$ ($8.5 \times 10^{-3}$ M) in $CCl_4$ solution, 20 ml in a 23 ml bomb reactor or 40 ml in a 45 ml reactor. The lower concentration was chosen to accommodate the low solubility of $Cl_8Si_8O_{12}$ in an attempt to keep all the reactants in solution. The sealed reactors were placed in ovens ranging from 40°C to 110°C and heated for 6 days to several months. In nearly all cases, there was no evidence of any form of condensed product or precipitate from the reaction mixture. In addition, there was no detectable signal from condensed silica by solution $^{29}Si$ NMR. In order to facilitate the reaction by creating a nucleation center, several attempts were also made to create a "seed crystal" by reacting one of the components in an eight-fold or greater excess of the other, thus in effect growing the crystal layer by layer. These experiments also showed no indication of any condensed product. One exception to this was a reaction carried out for 6.5 days at 60°C. 5.0 mg. of solid product were recovered from the walls of the Teflon liner of the reactor. X-ray diffraction indicated that this material had some degree of crystallinity, as indicated by 5 small peaks among an amorphous baseline. After calcination of the sample in air (10°C/min to 500°C), at least three of the peaks remained. Several attempts to reproduce this experiment failed to yield any condensed product.

The results of a later experiment may provide an explanation of this result, as well as the lack of reproducibility in these experiments. This experiment was one of the "seed crystal" experiments with $(CH_3O)_8Si_8O_{12}$ reacted in an excess of $Cl_8Si_8O_{12}$ at 75°C for six weeks. The product was 40.5 mg. of a large needle like solid (approx. 100 μm by 1 mm) mixed with particles of amorphous solid. This product showed a large degree of

crystallinity and the diffraction pattern was similar to one created from the simulated condensed spherosiloxane structure shown earlier. However, this product collapsed on heating to around 200°C. Ultimately, the crystalline phase was determined to be triethylamine hydrochloride. It is believed to have leached from the Teflon liner of the reactor from previous experiments involving traditional zeolite syntheses. The amorphous phase was found to be condensed silica, catalyzed by the amine. From this point forward, all reactions were carried out in new Teflon liners which had not been exposed to any amines from previous zeolite syntheses. This result suggests that the 5 mg. of condensed product mentioned previously were due to a catalytic effect from amine in the liner of the reactor, especially as it was found to nucleate on the walls of the reactor.

It was clear from the preceding experiments that the condensation of $Cl_8Si_8O_{12}$ and $(CH_3O)_8Si_8O_{12}$ was not occurring as might be expected based on the previous binary condensation studies by Corriu *et al.* As a result, several approaches were attempted to try to achieve condensation between these species. A presentation by Potter at the Materials Research Society Spring Meeting (San Francisco, April 1994) suggested that larger ligands on the condensing species worked best when performing non-hydrolytic condensation reactions[19]. Thus, the synthetic techniques for $(C_2H_5O)_8Si_8O_{12}$ and $(n\text{-}C_3H_7O)_8Si_8O_{12}$ were developed as described previously. When these reactants were used in the condensation reactions, there was no indication of condensation as before. In addition, a variety of catalysts were employed in the reaction to see it they could facilitate condensation. Also, some alternative reaction schemes were attempted to try to arrive at a ordered, condensed structure. Finally, it was decided to try to follow the condensation process by the use of solution NMR, both on the reaction mixture and on reactant analogs,

in an attempt to understand why no condensation was observed under the non-hydrolytic reaction conditions.

### *3.2.2. Catalysts Applied to the Non-Hydrolytic Condensation of Spherosiloxanes*

In an attempt to achieve a condensed spherosiloxane product, a variety of catalysts were used to facilitate the reaction. The first attempts involved the use of acid and base catalysts. Triethylamine ($(C_2H_5)_3N$) and concentrated hydrochloric acid (HCl), 1 mol% based on $Cl_8Si_8O_{12}$, were added to 1:1 mixtures of $Cl_8Si_8O_{12}$ and $(CH_3O)_8Si_8O_{12}$ and heated for 13 days at 75°C. A solid precipitate was formed and found to be amorphous by XRD for both samples. Next, pyridine was employed, using spherosiloxane reactant ratios of 1:1, 1:8, and 8:1 and heating at 75°C to 110°C for 7 days, and once again all samples produced a condensed product which was found to be amorphous by XRD. 2,6-Lutidine, whose structure is that of pyridine with methyl groups on either side of the nitrogen, was used next in an attempt to prevent any possible nucleophillic attack on the spherosiloxane [$Si_8O_{12}$] core because of its steric hindrance around the nucleophillic site. It also resulted in amorphous precipitate products.

Lewis acid catalysts were applied next in attempts to achieve a condensed product while still maintaining sufficient control to give ordered materials. Equimolar mixtures of $Cl_8Si_8O_{12}$ and $(CH_3O)_8Si_8O_{12}$ were reacted in $CCl_4$ solution with 1 mol % $AlCl_3$ and $FeCl_3$ as catalysts. These reactions produced gelatinous solid products. An attempt to produce an aluminum terminated spherosiloxane by reacting $(CH_3O)_8Si_8O_{12}$ with an eight-fold excess of $AlCl_3$ in $CCl_4$ in an autoclave at 110°C for 21 days again produced a clear gelatinous solid product.

### *3.2.3. Alternative Reaction Schemes for Spherosiloxane Condensation*

An examination of the crystal structures of $H_8Si_8O_{12}$[20] and $(CH_3O)_8Si_8O_{12}$[21] reveals that in the molecular crystals the spherosiloxane molecules are oriented and arranged in much the same way as in the simulated condensed spherosiloxane structure presented earlier. There is currently no crystal structure available for $Cl_8Si_8O_{12}$ because of its extreme sensitivity to water. However, it is reasonable to assume that the molecules are oriented much the same as in the other two structures because of the high degree of symmetry in all the spherosiloxanes. Thus, the question arises as to whether it would be possible to anneal the molecular structure into an ordered condensed structure. To that end, a co-precipitate was made of $Cl_8Si_8O_{12}$ and $(CH_3O)_8Si_8O_{12}$ by dissolving 1 g of purified $(CH_3O)_8Si_8O_{12}$ in 105 ml of saturated $Cl_8Si_8O_{12}$ solution which was heated to 75°C for 15 hours and cooled while stirring. The resulting clear solution had the $CCl_4$ slowly removed without heating under vacuum. XRD of the resulting solid appeared to be a physical mixture of the two reactants. Half of the co-precipitate was placed inside an autoclave reactor for heating at 110°C. The other half was steam treated in an autoclave reactor also at 110°C. This steam treatment has been shown effective in the synthesis of zeolites from a pre-mixed synthesis gel and the method is known as vapor-phase synthesis[22]. After eight days of heating, the sample not exposed to steam showed little change by FTIR or XRD from the initial co-precipitate. However, the sample subjected to steaming showed complete conversion to amorphous silica.

Another approach to controlled condensation of spherosiloxanes involved the use of a controlled pre-hydrolysis of $(CH_3O)_8Si_8O_{12}$ before reacting with $Cl_8Si_8O_{12}$. This

approach was suggested by a presentation at the MRS 1994 Fall Meeting by Kim[23,24]. He and co-workers at the Pacific Northwest Laboratory showed that the controlled prehydrolysis of organosilicon and organotitanium precursors in formamide solution could be used for the synthesis of mesoporous materials. Thus, an attempt was made to use prehydrolyzed spherosiloxanes in formamide solution as a reactant in the condensation reactions.

60 mg. of purified $(CH_3O)_8Si_8O_{12}$ were dissolved in 5 ml formamide in a Teflon autoclave liner. The appropriate stoichiometric amount (13 µl) of distilled water was added and the mixture was stirred at room temperature for two hours. To this mixture, an eight-fold excess of either $(CH_3O)_8Si_8O_{12}$ (480 mg. in 10 ml formamide) or $Cl_8Si_8O_{12}$ (505 mg. in 35 ml $CCl_4$) was added and sealed in an autoclave. After three weeks reaction at 110°C, the $(CH_3O)_8Si_8O_{12}$ only reaction had formed an amorphous solid and the mixed spherosiloxane reaction had formed a gelatinous amorphous solid.

### *3.2.4. NMR Studies of Spherosiloxane Non-Hydrolytic Condensation*

In order to understand the reason for the difficulties encountered in the non-hydrolytic condensation of spherosiloxanes and the reason behind the lack of condensation observed in this system, a series of experiments using $^{29}Si$, $^{1}H$ and $^{13}C$ solution NMR on the reaction mixture and products of the nonhydrolytic condensations was undertaken. Unfortunately, due to low concentrations in the reaction mixture (due to solubility limitations) and extremely long relaxation times (even utilizing a paramagnetic relaxation agent, $Cr(acac)_3$), it was in some cases impossible to obtain a $^{29}Si$ NMR signal from $Cl_8Si_8O_{12}$. As a result, a series of analogs were used to try to understand the condensation behavior under conditions identical to those for the spherosiloxanes, with the exception that higher

concentrations were used to facilitate NMR analysis.

In the first set of analog experiments, silicon tetrachloride ($SiCl_4$) and tetramethyl orthosilicate (TMOS) were used as the analogs for $Cl_8Si_8O_{12}$ and $(CH_3O)_8Si_8O_{12}$ respectively and they were reacted together using 4:1 and 1:4 molar ratios in $CCl_4$ in autoclave reactors at 110°C for 10 days. In addition, 4:1 and 1:4 molar mixtures of silicon tetrachloride with tetramethylorthogermanate (TMOG) and tetramethyl orthosilicate with germanium tetrachloride ($GeCl_4$) were used to distinguish between self and binary condensation should any condensation occur during the reaction. The results are quite clear and are reflected in all three nuclei studied ($^{29}Si$, $^{13}C$, and $^{1}H$): the silicate species in $CCl_4$ solution under these conditions are undergoing a ligand exchange reaction rather than condensing in a non-hydrolytic fashion. Figure 3.5 shows the $^{29}Si$ solution spectrum of the reaction of $SiCl_4$ to TMOS in a four to one molar ratio. Initially, there are peaks for $SiCl_4$ ($\delta$ -18.7 ppm) and TMOS ($\delta$ -78.6 ppm) in the appropriate four to one ratio. After the reaction, the peak for TMOS has disappeared and has been replaced by new peaks at $\delta$ -36.3, $\delta$ -52.6, and $\delta$ -66.7 ppm corresponding to the ligand exchanged species $Cl_3Si(OCH_3)$, $Cl_2Si(OCH_3)_2$, and $ClSi(OCH_3)_3$ respectively. This is confirmed by the similar appearance of new peaks in the $^{13}C$ and $^{1}H$ spectra found in Figures 3.6 and 3.7. Figure 3.8 shows the $^{29}Si$ solution spectrum of the reaction of TMOS to $SiCl_4$ in a four to one molar ratio. Once again, the initial peaks for $SiCl_4$ ($\delta$ -18.7 ppm) and TMOS ($\delta$ -78.6 ppm) are present in the appropriate four to one ratio. After the reaction, the peak for $SiCl_4$ has disappeared and has been replaced this time by a single new peak, at $\delta$ -66.7 ppm, corresponding to the ligand exchanged species $ClSi(OCH_3)_3$. Again these results are

reflected in the $^{13}C$ and $^{1}H$ spectra found in Figures 3.9 and 3.10.

The experiments involving germanium based reactants showed similar results except that the ligand exchange had already begun at room temperature, and thus exchanged peaks were visible even in the before heating spectra. In order to compare these results with a known system from the sol-gel literature where condensation was known to occur, $SiCl_4$ was reacted with $Ti(iPrO)_4$ in a 1:1 ratio in $CCl_4$ for 10 days at 110°C. The product was a dark brown solid mass which was x-ray amorphous. $^{29}Si$ NMR of the supernatant showed a single peak at $\delta$ -119.9 ppm corresponding to fully condensed ($Q^4$, Si-O-Ti) silicon. (See Figure 3.11.) Thus, it is apparent that for the silica based system, the relative rates of exchange and condensation are such that without some type of catalyst, water or acid/base, condensation of the silica species is unlikely. However, non-hydrolytic condensation occurs quite readily for the more reactive system involving mixed metal oxides, particularly if the reaction involves one or more transition metal species.

## *3.3. Discussion and Final Results*

Concerning the work of Corriu *et al.*[15,25-28], it is clear that the non-hydrolytic condensation technique works quite well on a mixed metal oxide system, or on a transition metal oxide. However, in the case where a pure silica system was used, those workers did not use the standard non-hydrolytic condensation route presented earlier. Instead, they used a variation on the mechanism where an alcohol or aldehyde was reacted with two equivalents of silicon tetrachloride[26]:

$$\mathbf{2\ {\equiv}Si\text{-}X\ +\ ROH\ \rightarrow\ {\equiv}Si\text{-}O\text{-}Si{\equiv}\ +\ HX\ +\ RX} \quad \mathbf{(5)}$$

Under these conditions, not only is an acid by-product produced, which can serve to auto-catalyze the reaction, but some water is also likely created in the process which should aid in the condensation process as well. While this may not be a problem when making amorphous oxides, it clearly will not work for the condensation of spherosiloxanes to make any kind of ordered material. A slight variation on this reaction uses an ether rather than aldehyde or alcohol as the oxygen source for the condensation reaction:

$$\mathbf{2\ {\equiv}Si\text{-}X\ +\ ROR\ \rightarrow\ {\equiv}Si\text{-}O\text{-}Si{\equiv}\ +2\ RX} \quad \mathbf{(6)}$$

In this case, it might be possible to control the reaction for spherosiloxane condensation. Thus, two equivalents of $Cl_8Si_8O_{12}$ were reacted with diisopropyl ether in $CCl_4$ solution in an autoclave reactor with heating at 110°C for 18 days. In this case a solid condensate was produced. Solution and solid state $^{29}Si$ NMR spectra did show peaks at $\delta$ -90 ppm and a smaller set of peaks at around $\delta$ -108 to -110 ppm; however, XRD showed this sample to be amorphous as well.

Because of the many problems with the spherosiloxane condensation, it was deemed unwise to attempt the gel controlled condensation experiments to get diffusion controlled reaction. Although no experiments were actually carried out in a gel matrix, early in the process of testing the condensation, an experiment was carried out where $SiCl_4$ and TMOS were added from opposite sides of a U-shaped glass tube and allowed to diffuse through $CCl_4$ solution to react and condense. As with the results presented previously, no condensation took place.

## *Literature Cited*

(1) Feher, F. J.; Weller, K. J. *Organometallics* **1990**, *9*, 2638-2640.

(2) Stein, A.; Keller, S. W.; Mallouk, T. E. *Science* **1993**, *259*, 1558-1563.

(3) Davis, M. E. *Ind. Eng. Chem.* **1991**, *30*, 1675-1683.

(4) Meier, W. M.; Olson, D. H.; Baerlocher, C. *Atlas of Zeolite Structure Types*; 4th ed.; Elsevier: London, 1996.

(5) Burkett, S. L.; Davis, M. E. *J. Phys. Chem.* **1994**, *98*, 4647-4653.

(6) Burkett, S. L.; Davis, M. E. *Chem. Mater.* **1995**, *7*, 920-928.

(7) Burkett, S. L.; Davis, M. E. *Chem. Mater.* **1995**, *7*, 1453.

(8) Zones, S. I.; Olmstead, M. M.; Santilli, D. S. *J. Am. Chem. Soc.* **1992**, *164*, 4195-4201.

(9) Lobo, R. F.; Pan, M.; Chan, I.; Medrud, R. C.; Zones, S. I.; Crozier, P. A.; Davis, M. E. *J. Phys. Chem.* **1994**, *98*, 12040.

(10) Smith, J. V.; Rinaldi, F. *Mineralogy Mag.* **1962**, *33*, 202-212.

(11) Liebau, F. *Structural Chemistry of Silicates*; Springer-Verlag: Berlin, 1985.

(12) Smith, J. V. *Am. Mineralogist* **1978**, *63*, 960-969.

(13) Bennett, J. M.; Kirchner, R. M. *Zeolites* **1991**, *11*, 502-506.

(14) Caullet, P.; Guth, J. L.; Hazm, J.; Lamblin, J. M.; Gies, H. *Eur. J. Solid State Inorg. Chem.* **1991**, *28*, 345-361.

(15) Corriu, R. J. P.; Leclercq, D.; Lefèvre, P.; Mutin, P. H.; Vioux, A. *Chem. Mater.* **1992**, *4*, 961-963.

(16) Henish, H. K. *Crystal Growth in Gels*; Penn State University Press: University Park, PA, 1970.

(17) Henisch, H. K. *Crystals in Gels and Liesegang Rings*; Cambridge University Press: Cambridge, 1988.

(18) Ciric, J. *Science* **1967**, *155*, 689.

(19) Potter, B. G.; Tuttle, B. A.; Voigt, J. A.; Garino, T. J.; Headley, T. J., *Structure Property Relationships of Highly Textured, Chemically Prepared, Pb(Zr, Ti)$O_3$ Thin Films*, Materials Research Society Spring Meeting, San Francisco, CA, 1994.

(20) Auf der Heyde, T. P. E.; Bürgi, H. B.; Bürgy, H.; Törnroos, K. W. *Chimia* **1991**, *45*, 38-40.

(21) Day, V. W.; Klemperer, W. G.; Mainz, V. V.; Millar, D. M. *J. Am. Chem. Soc.* **1985**, *107*, 8262-8264.

(22) Matsukata, M.; Nishiyama, N.; Ueyama, K. *Microporous Mater.* **1996**, *7*, 109-117.

(23) Kim, A. Y. In *Advances in Porous Materials*; Kmomarneni, S.; Smith, D. M.; Beck, J. S. Eds.; Materials Research Society: Pittsburgh, PA, 1995.

(24) Liu, J.; Kim, A. Y.; Virden, J. W.; Bunker, B. C. *Langmuir* **1995**, *11*, 689-692.

(25) Acosta, S.; Arnal, P.; Corriu, R. J. P.; LeClerq, D.; Mutin, P. H.; Vioux, A. In *Better Ceramics Through Chemistry VI*; Cheetham, A. K.; Brinker, C. J.; Mecartney, M. L.; Sanchez, C. Eds.; Materials Research Society: Pittsburgh, PA, 1994; pp 43-54.

(26) Corriu, R. J. P.; Leclercq, D.; Lefèvre, P.; Mutin, P. H.; Vioux, A. *J. Non-Cryst. Solids* **1992**, *146*, 301-303.

(27) Corriu, R. J. P.; Leclercq, D.; Lefèvre, P.; Mutin, P. H.; Vioux, A. *J. Mater. Chem.* **1992**, *2*, 673-674.

(28) Acosta, S.; Corriu, R. J. P.; LeClerq, D.; Mutin, P. H.; Vioux, A. In *Better Ceramics Through Chemistry VI*; Cheetham, A. K.; Brinker, C. J.; Mecartney, M. L.; Sanchez, C.

Eds.; Materials Research Society: Pittsburgh, PA, 1994; pp 345-350.

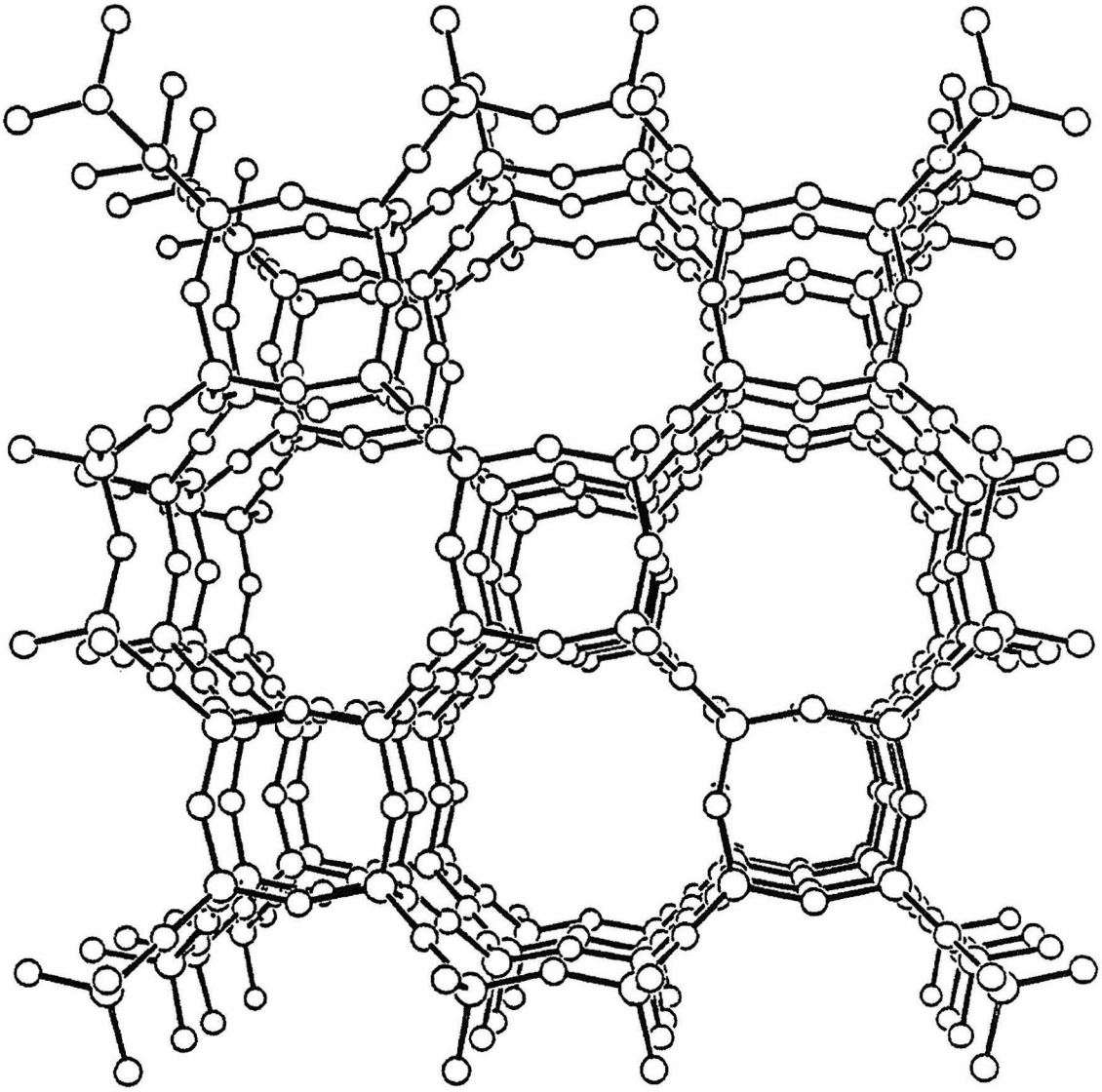

**Figure 3.1:** Simulation of a likely structure formed by the controlled condensation of spherosiloxanes. Structure simulation was performed using Cerius modeling software.

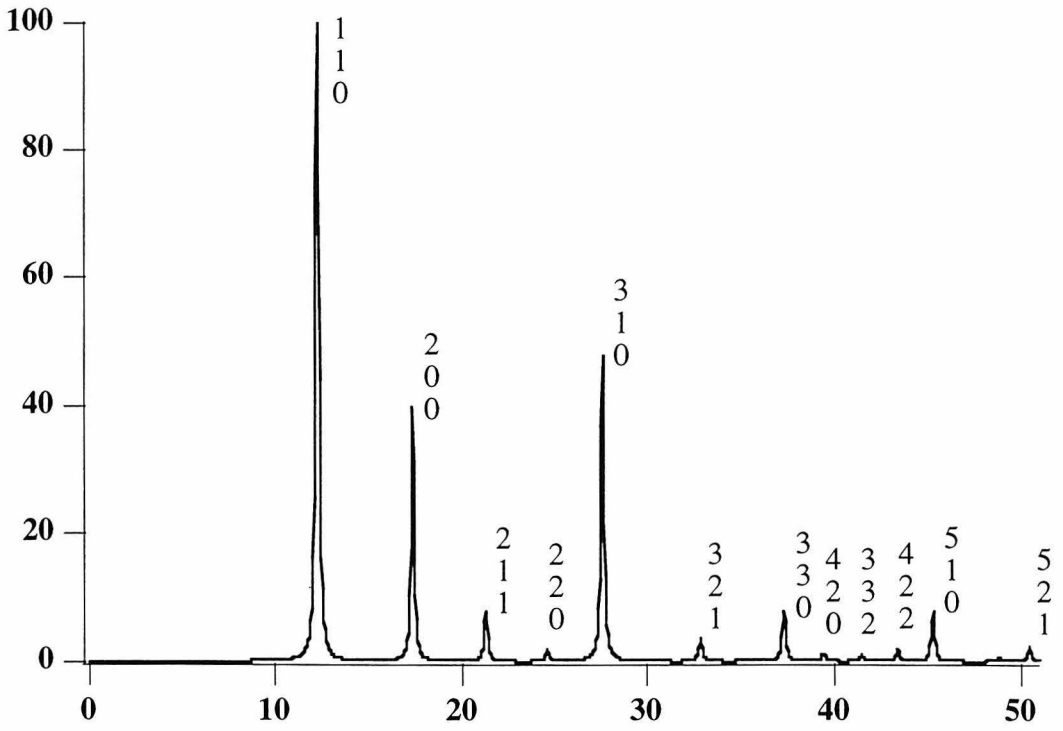


**Figure 3.2:** Simulated powder x-ray diffraction pattern for the model structure presented in Figure 3.1. Diffraction simulation performed using Cerius modeling software.

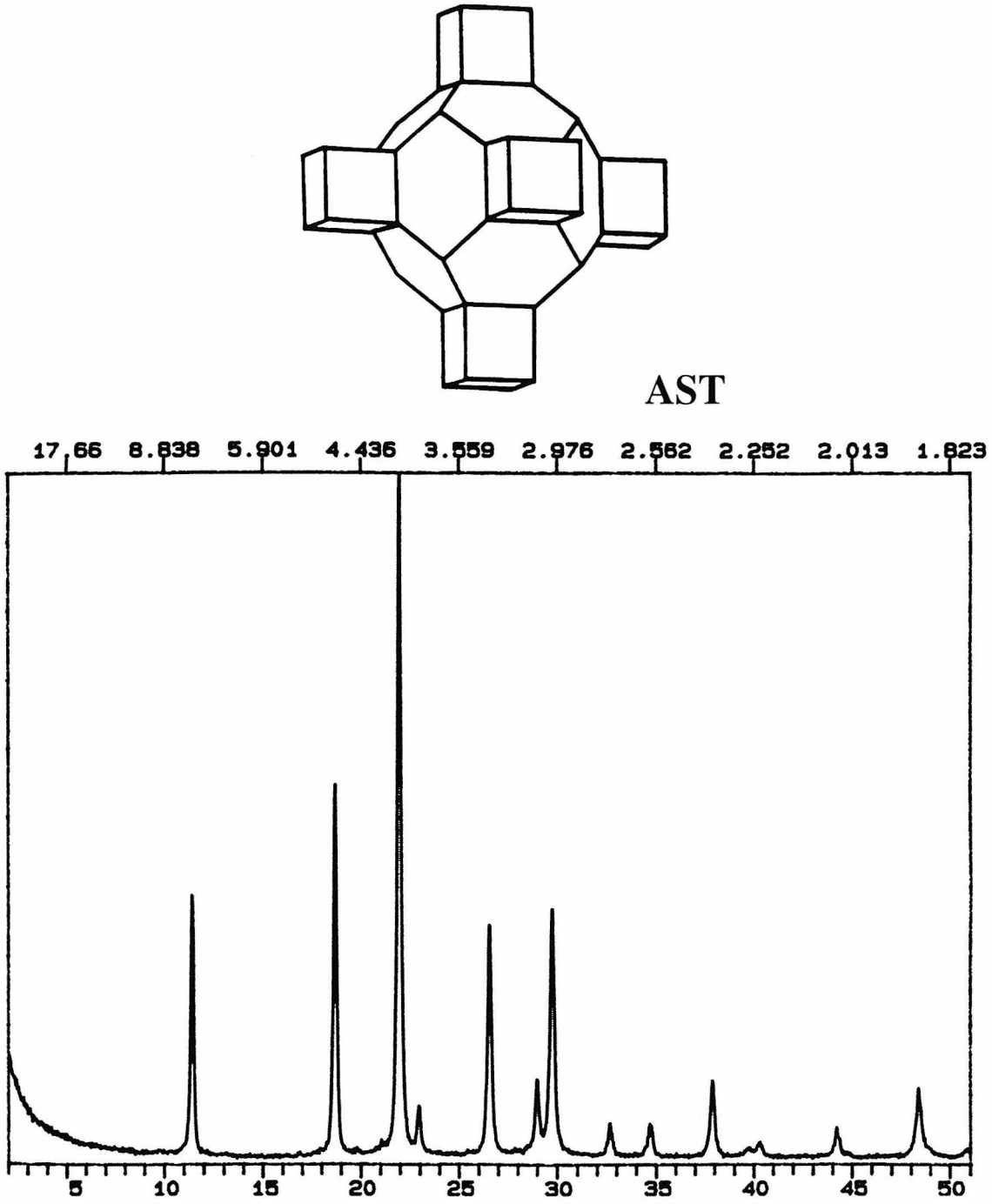


**Figure 3.3:** (Top) Idealized framework topology for the AlPO4-16 (AST) structure showing the double four-ring secondary building unit, as well as the additional tetrahedral atom site. (Bottom) Powder x-ray diffraction pattern for SSZ-40, a pure silica material with the AST crystal structure.

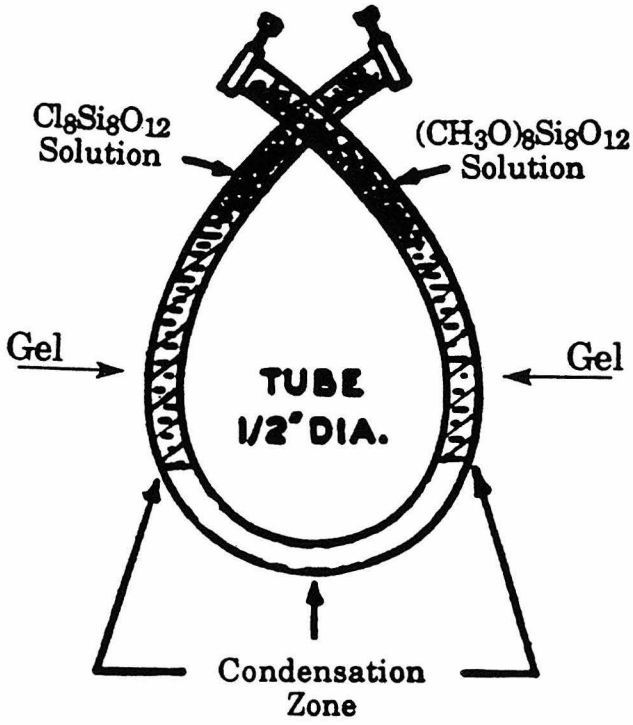


**Figure 3.4:** Schematic diagram showing the reaction geometry for the gel method of condensation of spherosiloxanes to achieve a diffusion limited reaction.

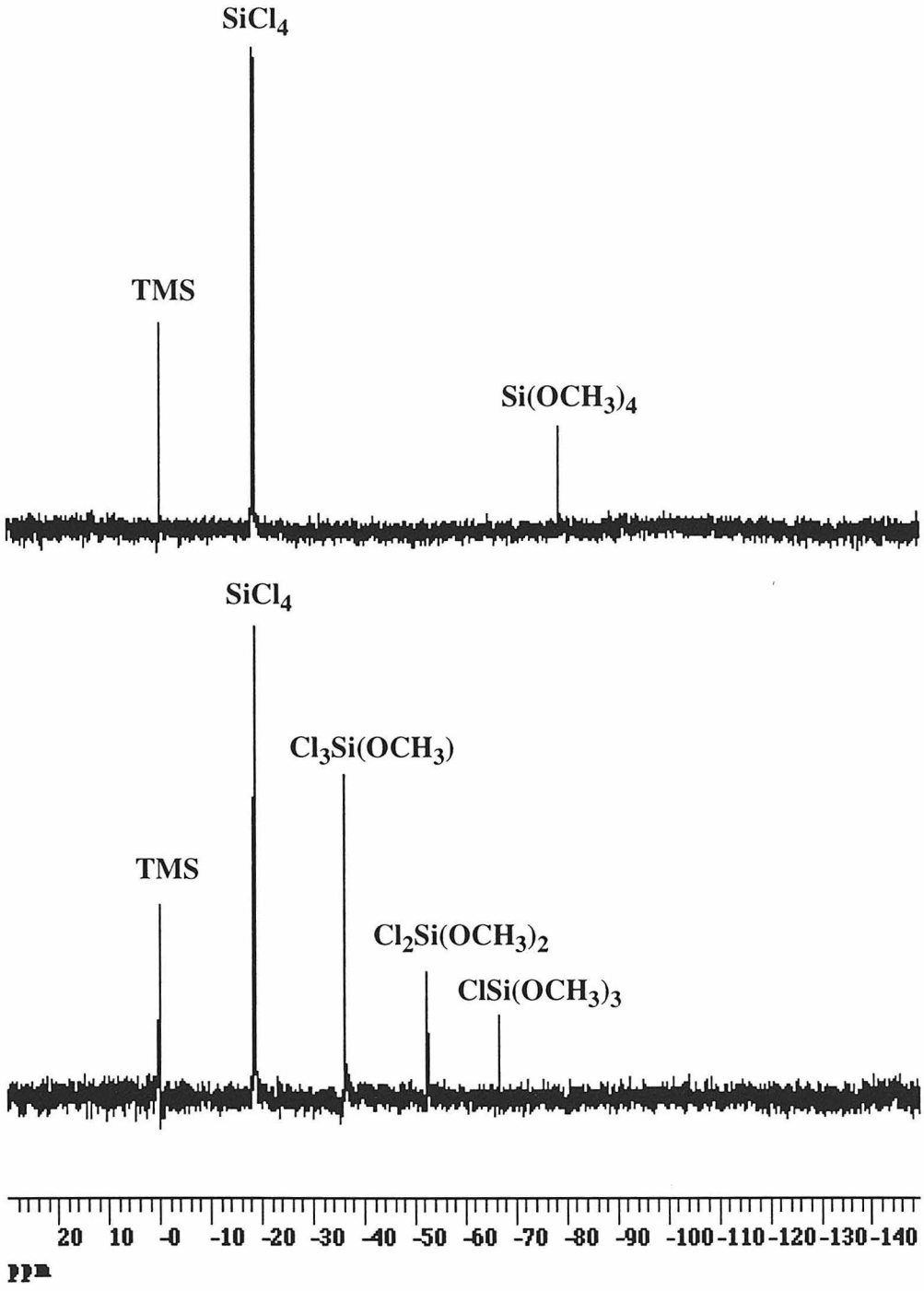


**Figure 3.5:** $^{29}Si$ solution NMR of reaction between $SiCl_4$ and TMOS (4:1 ratio) in $CCl_4$ before (top) and after (bottom) heating at 110°C for 10 days. Notice sample has undergone a ligand exchange reaction, resulting in the new mixed ligand peaks at δ -36.3, δ -52.6, and δ -66.7 ppm and the absence of the peak for TMOS at δ - 78.6 ppm.

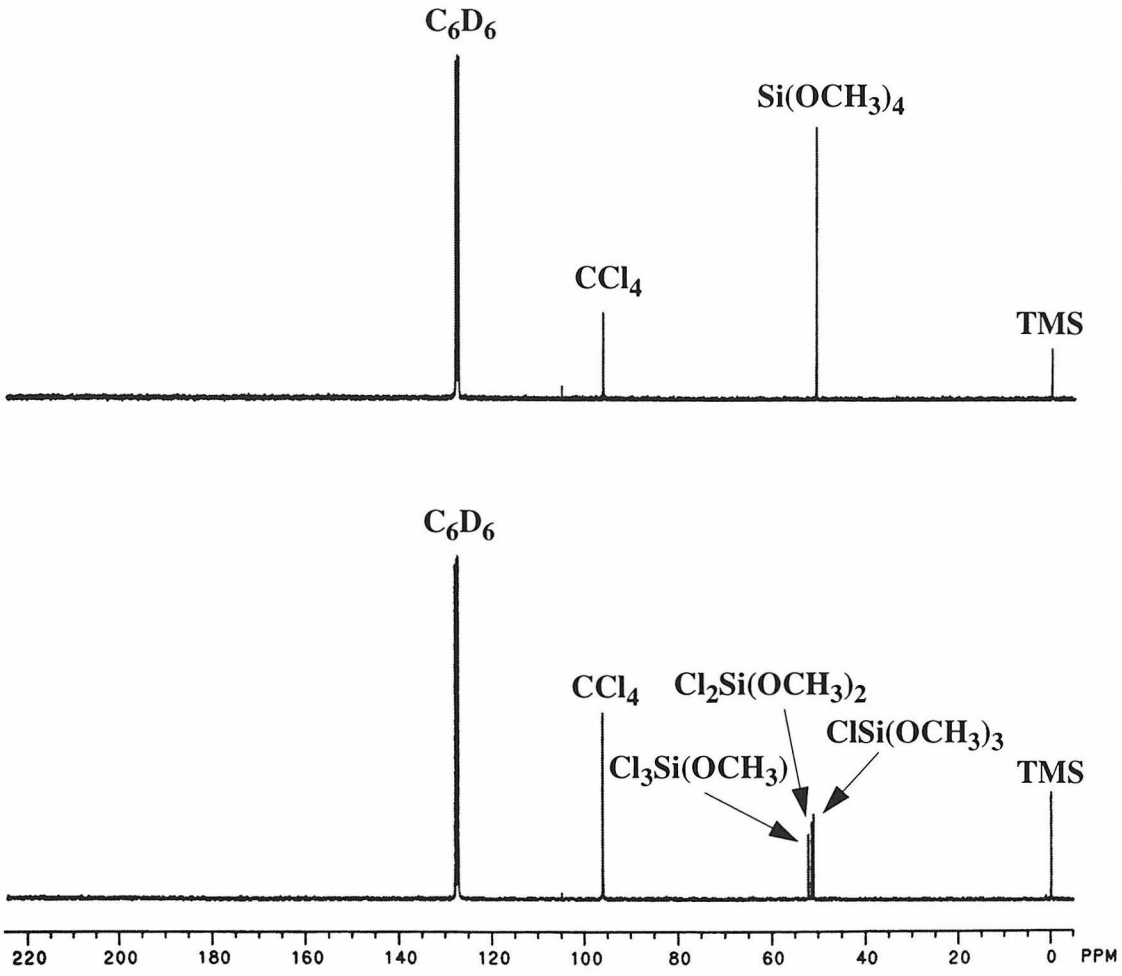


**Figure 3.6:** $^{13}C$ solution NMR of reaction between $SiCl_4$ and TMOS (4:1 ratio) in $CCl_4$ before (top) and after (bottom) heating at 110°C for 10 days. Notice sample has undergone a ligand exchange reaction as indicated by the new peaks at δ 51.22, δ 51.66, and δ 52.35 ppm, shifted downfield and replacing the peak for $Si(OCH_3)_4$ at δ 50.82 ppm.

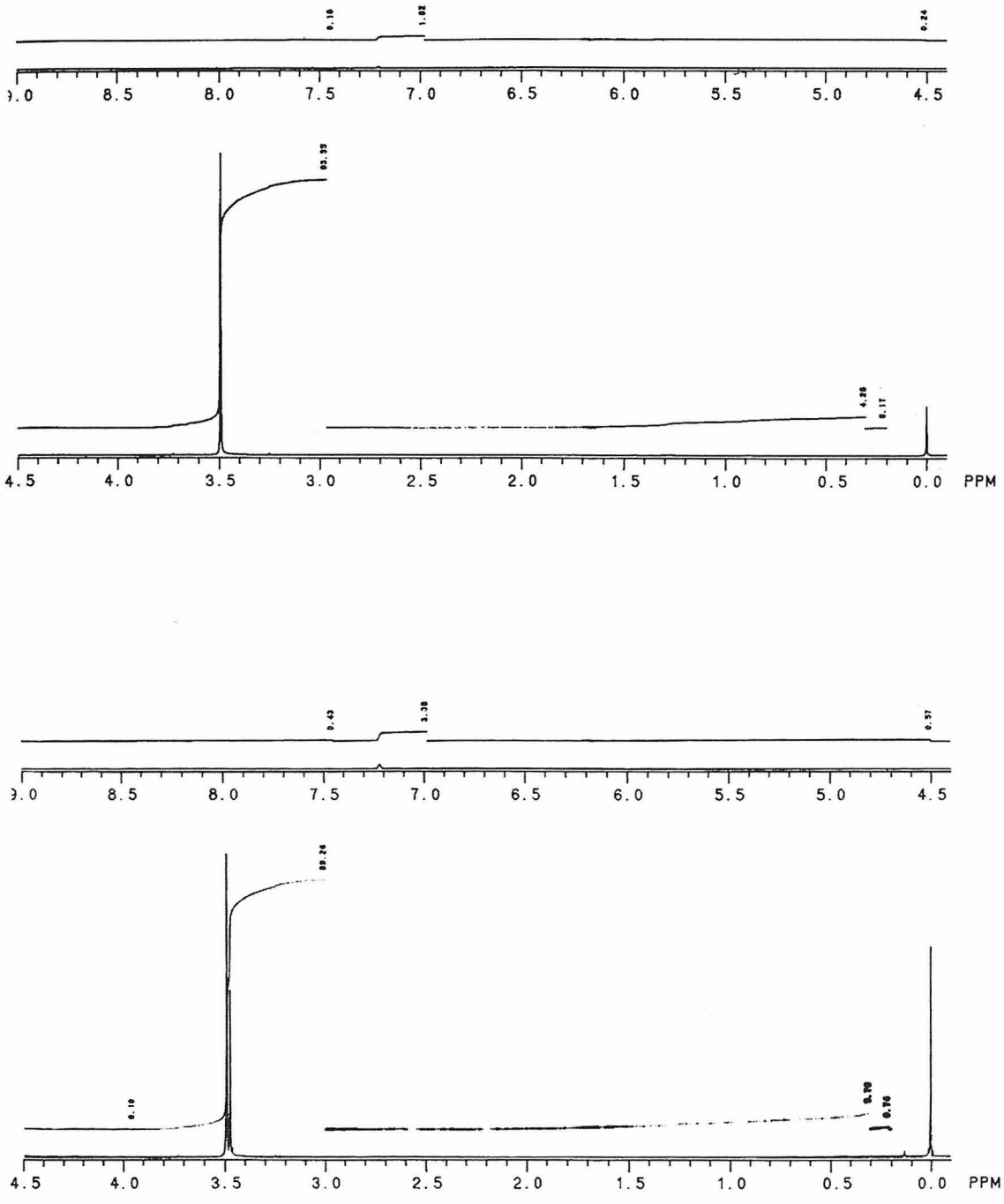


**Figure 3.7:** $^{1}H$ solution NMR of reaction $SiCl_4$ and TMOS (4:1 ratio) in $CCl_4$ before (top) and after (bottom) heating at 110°C for 10 days. Notice sample has undergone a ligand exchange reaction as indicated by the multiplet of peaks near δ 3.5 ppm.

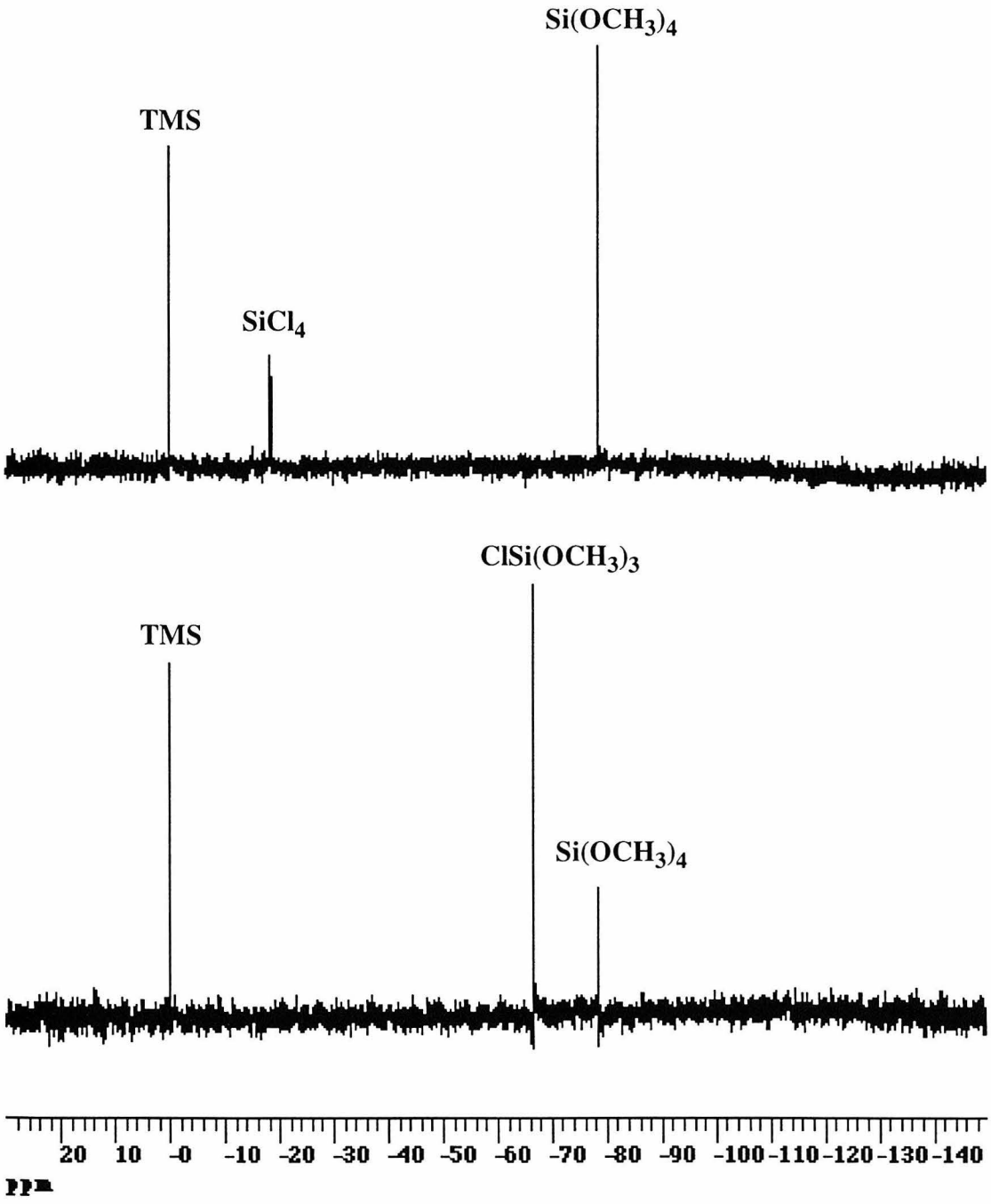


**Figure 3.8:** $^{29}Si$ solution NMR of reaction between TMOS and $SiCl_4$ (4:1 ratio) in $CCl_4$ before (top) and after (bottom) heating at 110°C for 10 days. Notice sample has undergone a ligand exchange reaction resulting in a new mixed ligand peak at δ -66.7ppm and the absence of the peak for $SiCl_4$ at δ -18.7 ppm.

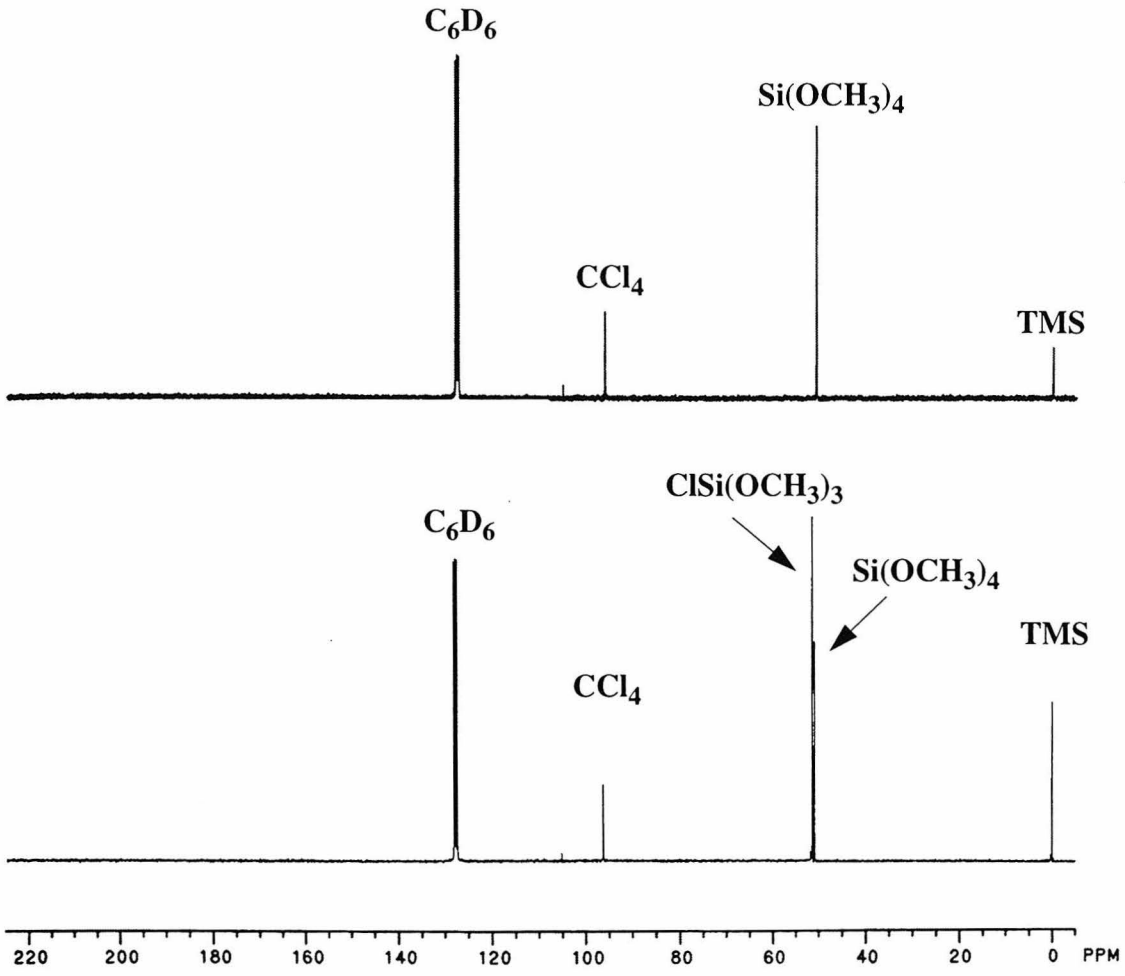


**Figure 3.9:** $^{13}C$ solution NMR of reaction between TMOS and $SiCl_4$ (4:1 ratio) in $CCl_4$ before (top) and after (bottom) heating at 110°C for 10 days. Notice sample has undergone a ligand exchange reaction as indicated by the new peak at δ 51.28 ppm, shifted downfield and the peak for $Si(OCH_3)_4$ at δ 50.82 ppm.

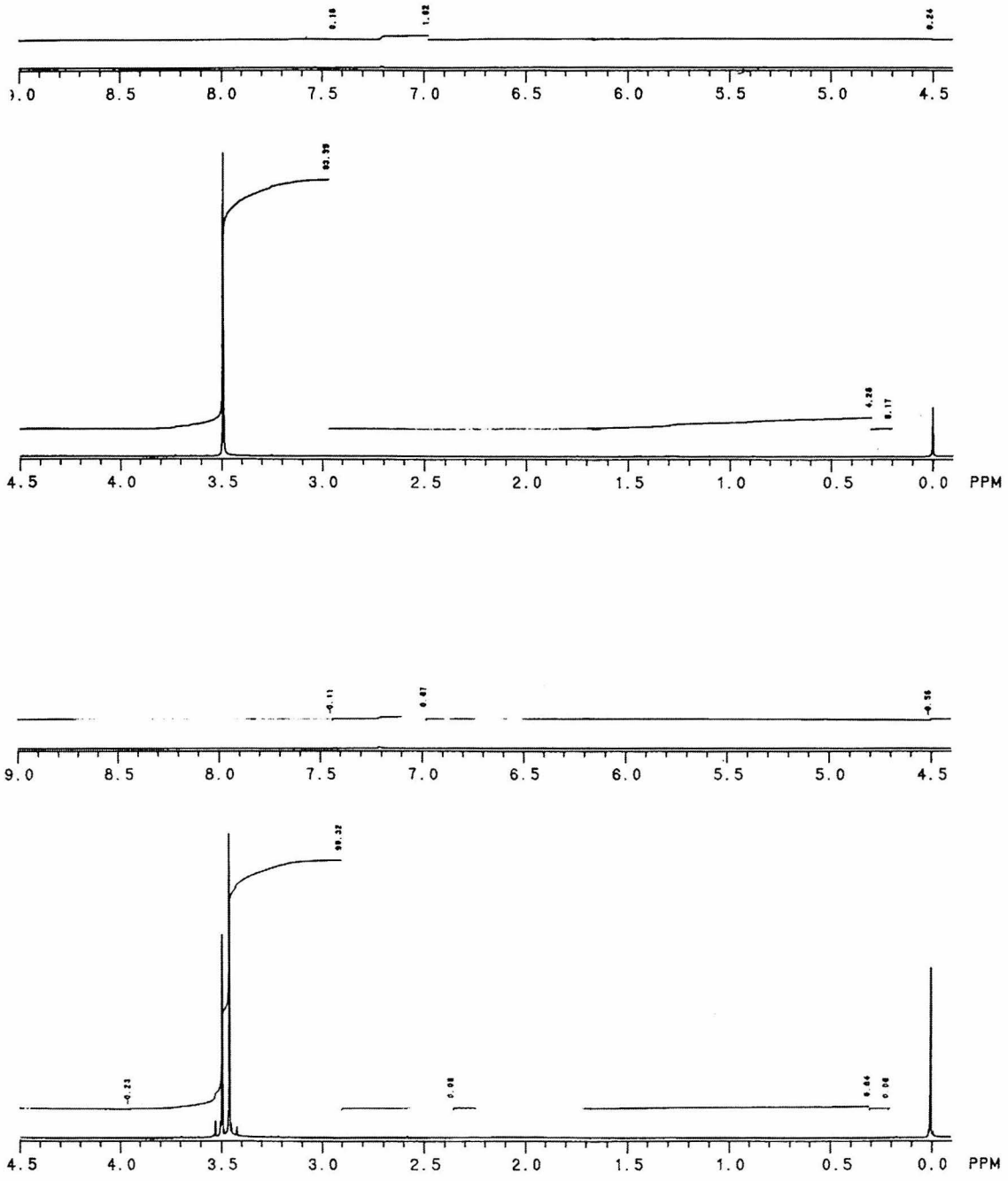


**Figure 3.10:** $^{1}H$ solution NMR of reaction between TMOS and $SiCl_4$ (4:1 ratio) in $CCl_4$ before (top) and after (bottom) heating at 110°C for 10 days. Notice sample has undergone a ligand exchange reaction as indicated by the multiplet of peaks near δ 3.5 ppm.

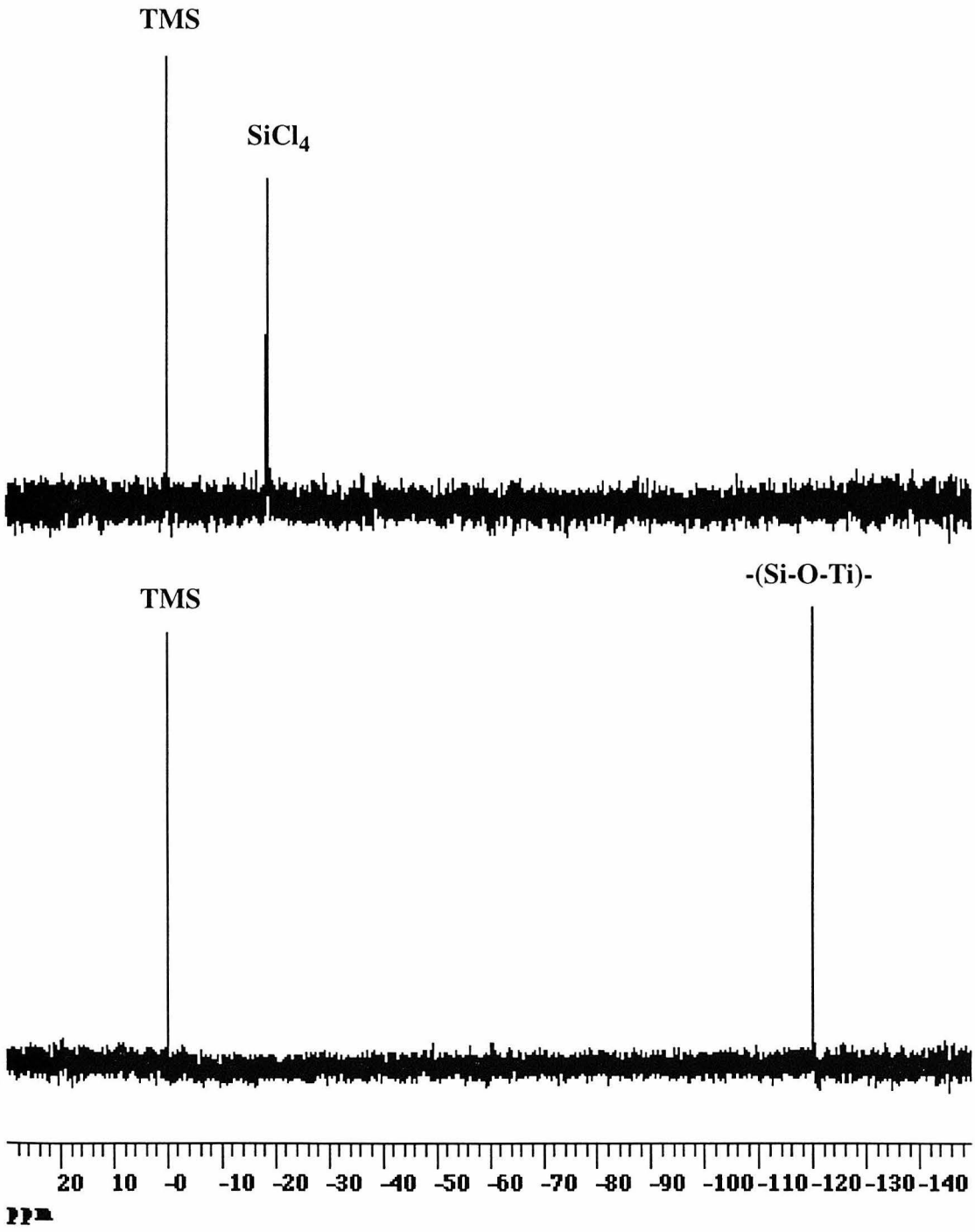


**Figure 3.11:** Solution $^{29}Si$ NMR of a 1:1 molar ratio of $SiCl_4$ to $Ti(iPrO)_4$ in $CCl_4$ before heating for 10 days at 110°C (top) and of the supernatant after heating (bottom.)

# *Chapter 4:*

## *Condensation Behavior of Spherosiloxanes on Surfaces*

## *4.1. Introduction and Background*

In recent years, there has been a growing interest in developing techniques which would lead to microporous thin films for a variety of applications, including molecular electronics for ultra high density information storage, artificial photosynthesis, chemical separations and membrane technology. The desire for ultra high density information storage goes back many years and has become ever increasingly important as computers get faster and computer programs and data storage requirements get increasingly larger. In fact, Feynman, in his famous essay, talked of "writing the entire 24 volumes of the Encyclopedia Britannica on the head of a pin," and even postulated that each letter could consist of 1000 metal atoms and still have sufficient room for the entire work[1]. Moreover, as the demands for ever faster computers and ever larger memory chips continue to accelerate, ever smaller integrated circuits are needed. However, many of the current techniques (Si-CMOS technology) on which these devices are based will begin to encounter severe physical limitations as feature sizes in these devices approach 100 nm, likely to occur in the first decade of the next century[2]. (See Figure 4.1.) Thus, there is a tremendous impetus to develop new ideas and techniques to meet this challenge and explore the possibilities inherent within. This goes to the heart of the matter discussed in Chapter 1, being able to control the structure of materials on the nanoscale regime.

The advent of scanning probe microscopy[3-5] and its application to the manipulation of matter down to the realm of individual atoms[6,7] has opened up new possibilities for developing new types of structures and devices for molecular electronics. In 1991 Don Eigler demonstrated the first example of molecular electronic device with his creation of a single-atom, two-state switch[8]. While clearly it would be impossible to produce a useful

device in this way as a single STM would prove too slow, Eigler postulated that it might be possible to use similar techniques to migrate individual atoms between discrete cages or binding sites within a microporous thin layer, and thus create a useful device based on atomic switches[9]. Quate and co-workers have been studying the problem of increasing the data rates possible using scanning probe microscopy by increasing the data acquisition rates of individual SPM devices[10,11], as well making significant progress on independently controllable arrays of scanning probe microscope tips[12]. However, in order to make a functional device from an array of atomic switches a viable possibility, it is necessary that the pores within the layer be organized in a regular way, to facilitate the addressing and accessing of the information contained in the atomic switches. An ideal way to satisfy these needs would be with the creation of a zeolite-like thin film on a conducting surface. Given the work already underway using spherosiloxanes as building blocks for bulk microporous materials, it seemed natural to apply the idea to the synthesis of microporous thin films as well.

Another aspect of the spherosiloxanes that make them unique is their surprisingly high volatility for molecules composed primarily of silicon oxide. Because of this, it is possible to sublime and transport spherosiloxane molecules through the vapor phase without degradation. Correspondingly, interest has grown in using spherosiloxanes for a variety of applications in the area of semiconductors. In 1992, Desu *et al.* first demonstrated the use of hydridospherosiloxanes in the chemical vapor deposition (CVD) growth of amorphous silica films[13]. By utilizing lower temperature reaction conditions, Holl and McFeely have shown that $H_8Si_8O_{12}$ can be chemisorbed onto the reconstructed Si(100) - (2x1) surface without damaging the $[Si_8O_{12}]$ core structure[14,15]. Calzaferri *et al.* reacted

$Cl_8Si_8O_{12}$ onto crystals of germanium in order to perform ATR-FTIR spectroscopic studies of this spherosiloxane[16]. The chlorosiloxanes were shown to condense with hydroxyl groups on the Ge surface and the $[Si_8O_{12}]$ core was shown to remain intact while the chlorine atoms were exchanged for hydroxyl groups by washing the surface with water. These results demonstrate the potential of using spherosiloxanes to produce a microporous thin film. Thus our motivation in this work is to explore the potential of using spherosiloxanes for making a microporous layer as a possible housing for an array of atomic switches for high density information storage.

There are three basic questions which must be answered, and correspondingly three steps which must be understood, in order to achieve a microporous thin layer from spherosiloxanes: (1) How do spherosiloxanes react onto the surface of interest? (2) How can spherosiloxanes be reacted onto a surface in a controlled way to give an ordered structure? and (3) How can the subsequent layers be added to the first in order to "grow" a microporous layer. In order to answer these questions, a target surface must first be chosen. We have chosen to use the (2x1) reconstructed surface of silicon (see Figure 4.2) as our substrate surface for several reasons: (1) it has been studied for many years and has been well characterized with regard to structure and surface reactivity[17-21]; (2) any molecular electronic device based on a silicon substrate should be readily integrable with other current semiconductor processing techniques; (3) it may be possible to use the structure of the underlying surface to organize the spherosiloxanes on the surface in the desired fashion to begin growth of a microporous layer.

It turns out that the spacing between the dimer rows of the Si(100) - (2x1) surface is correct for bridging of the dimer rows by an adsorbed $(CH_3O)_8Si_8O_{12}$ molecule. (See

Figure 4.3.) Because the orientation and spacing of the dimers along a given terrace on the surface is completely regular, spherosiloxanes that react onto the surface in this way will be forced into a specific orientation and periodic arrangement on the surface. Moreover, this periodic arrangement is very close to that of a single layer of the simulated microporous structure based on spherosiloxanes presented in Chapter 2. (See Figure 2.1.) Thus, it may be possible to use the structure of the underlying Si(100) - (2x1) surface to organize condensed $(CH_3O)_8Si_8O_{12}$ properly for layer by layer growth of a microporous film.

Once the first layer of spherosiloxane building blocks is condensed and correctly organized, the principles of atomic layer epitaxy[22] (ALE) can be applied to grow a controlled microporous film. ALE takes advantage of a self-limiting binary reaction scheme whereby only a single layer of the adsorbing material can react with the surface. All additional layers are merely physisorbed and can be easily removed. By alternating reactants, single atomic layer control of the reaction is achieved[23-26]. In this way, growth can be controlled over several hundred cycles.

There is significant evidence available in the literature to suggest that $(CH_3O)_8Si_8O_{12}$ will react with the silicon surface dimers in the necessary way. It has been well documented that when molecules react with the Si surface dimer, they tend to dissociate across the dimer thereby satisfying the high energy dangling bonds[19]. Holl and McFeeley, in their studies of the $Si/SiO_2$ interface, demonstrated through the use of Si 2*p* core level photoemission spectroscopy that hydridospherosiloxanes ($H_8Si_8O_{12}$, $H_{12}Si_{12}O_{18}$, and $H_{14}Si_{14}O_{21}$) chemisorb across the surface dimer of Si(100) splitting the Si-H bond and leaving the intact cluster attached to the surface[14,15]. (See Figure 4.4.) In

addition, a study of the reaction of tetraethoxysilane (TEOS) on this surface by thermal programmed desorption (TPD) and high resolution electron energy loss spectroscopy (HREELS), carried out by Danner and Vohs[27], suggests that TEOS adsorbs dissociatively across the surface dimer via cleavage of the C-O bonds in the ethoxy ligands. Since TEOS is an analog of the alkoxy terminated spherosiloxanes, it is reasonable to believe that $(CH_3O)_8Si_8O_{12}$ will also react dissociatively across the surface dimer via cleavage of the C-O bonds of the methoxy ligands.

Based on the aforementioned information, I propose the reaction scheme presented in Figures 4.5.a and b for the synthesis of a thin microporous layer from spherosiloxanes: a clean, reconstructed Si(100) - (2x1) surface is prepared and characterized. Purified $(CH_3O)_8Si_8O_{12}$ is then adsorbed onto the surface from the vapor phase and reacts across the surface dimers to bridge between the dimer rows on the surface. Thus, the underlying surface positions and orients the spherosiloxanes in a periodic arrangement that is appropriate for layer by layer growth of the microporous film. Since the spherosiloxanes cannot self condense, a self-limiting reaction is achieved and the growth can be controlled layer by layer. Once the first layer is chemisorbed onto the surface, the physisorbed layers are flushed away and water is introduced to hydrolyze the $-OCH_3$ groups on top of the adsorbed layer to -OH. Based on the work by Calzaferri *et al.*, this should have no effect on the $[Si_8O_{12}]$ core of the adsorbed molecule[16]. The top of the adsorbed layer is once again reactive toward chemisorption with more $(CH_3O)_8Si_8O_{12}$, and the process is cycled to thus grow the microporous film in a very controlled fashion. In reality, it should only take a very few cycles (4 or 5) to get the multiple cages needed as binding sites for an adsorbed molecule. The most critical step in this process is the organization of the first

layer on the surface because once it is organized appropriately, the layer by layer growth of the microporous film should be straightforward.

## *4.2. Surface Condensation Behavior of $H_8Si_8O_{12}$ & $(CH_3O)_8Si_8O_{12}$*

The first step in the production of microporous thin films from spherosiloxanes is to understand the condensation behavior of spherosiloxanes on the Si(100) -(2x1) surface.

### *4.2.1. Experimental*

Purified spherosiloxane samples were prepared in our laboratory by the synthetic procedures presented in Chapter 2 and placed in sealed vessels under argon atmosphere. The samples then were transported to Dr. Eigler's laboratory at the IBM Almaden Research Center and attached to the ultra-high vacuum (UHV) system there where all of the experiments were carried out. The system is built around a low temperature (operated at 4 K) scanning tunneling microscope (STM). The room temperature sample preparation and analysis system was equipped with two Balzers quadrupolar mass spectrometers, an Auger electron spectrometer (Auger) low energy electron diffraction optics (LEED), and an ion gun for sputtering. The silicon samples used were prepared from 2-inch n-type As-doped Si (100) wafers. Arsenic doping was chosen because Dr. Eigler's previous experience showed that As does not segregate to the surface during thermal processing. This was particularly important because the doping level required was unusually high ($1.4 \times 10^{20}/cm^3$, max resistance 0.004 ohm•cm) in order to maintain sample conductivity at 4 K. The silicon wafers were then mounted on sapphire sample holders and held in place with tungsten clips. The spherosiloxane samples were introduced into the vacuum system through the use of either a leak valve or by attaching a heated sample bulb to the system behind a gate valve. During sample dosing, the Si wafer was held and oriented in such a way as to achieve line of sight to the dosing aperture.

### *4.2.2. Preparation of Reconstructed Si(100) - (2x1) Surfaces*

In order to prepare a clean, reconstructed Si(100) - (2x1) surface, the silicon wafer was flashed from room temperature to 1200°C under vacuum at $10^{-10}$ Torr by applying 15 A direct current for 5 seconds. A rapid heating and cooling rate is desirable to minimize the time the sample is in the 800°C to 1150°C temperature regime where the sample is not hot enough to desorb carbon. This prevents the production of pyramids of carbon which form on the surface in this temperature regime. After the current was removed, the sample rapidly cooled to 400°C (several seconds) and then more slowly to room temperature. If the sample had previously been dosed with spherosiloxane, the sample was first cleaned by argon ion sputtering at 1 kV, 20 mA emission at 1 x $10^{-5}$ Torr for several minutes before flash annealing and reuse for spherosiloxane deposition.

In order to verify that this treatment had produced a clean Si (100) surface with the desired (2x1) reconstruction at the surface, the prepared samples were studied by Auger and LEED. Typical Auger spectra of a Si (100) surface before and after sputtering and high temperature annealing is presented in Figure 4.6. Before annealing, clear signals indicating the presence of carbon and oxygen in addition to silicon are present; however, after annealing, only the peak corresponding to silicon at 92 eV is present. A special effort was made to detect any arsenic present on the surface due to surface segregation because of its high dopant concentration level. However, at no time was any signal detected at its characteristic Auger peak at 1228 eV.

Once the surface was shown to be free of any chemical impurities, it was necessary to verify that the surface had annealed to the desired (2x1) reconstruction. A characteristic LEED pattern obtained after the sputtering and annealing process is shown in Figure 4.7.

The absence of any diffraction spots in a LEED pattern is indicative of a disordered surface, whereas the LEED pattern presented in Figure 4.7, a box-like pattern with no diffraction spot at the center of the box, is clearly indicative of the (2x1) reconstructed surface.

A final verification of the surface structure was obtained by directly imaging the surface using the low temperature (4 K) scanning tunneling microscope (STM). Figure 4.8.a and 4.8.b show characteristic images of a Si (100) surface. Both images clearly show the pattern of dimer rows across a terrace. Notice how the orientation of the dimer rows changes by 90 degrees at a step edge corresponding to a single atomic height step. The images also show some examples of surface defects, both point defects or vacancies which may be attributable to the As dopant, as well as some examples of surface adsorbed atoms.

### *4.2.3. Condensation Behavior of $H_8Si_8O_{12}$ on the Si (100) - (2x1) surface*

The first step to producing an epitaxially grown layer from spherosiloxanes involves understanding how they react with the surface. Thus, the initial goal of this work was to find single adsorbed spherosiloxane molecules on the surface by STM in order to verify the picture of spherosiloxane surface reactivity developed in the introduction.

A source of $H_8Si_8O_{12}$ was mounted onto the load lock chamber of the UHV system behind a gate valve. The load lock was equipped with a mass spectrometer which was used to characterize the spherosiloxane source before dosing onto the surface. The source was opened to the load lock and without heating the source produced a vapor pressure of $H_8Si_8O_{12}$ of $1.54 \times 10^{-8}$ Torr. While the spherosiloxane source was equilibrating, a clean Si (100) wafer was annealed in the main chamber of the UHV system. Prior to dosing, the

mass spectrometer and ion gauge in the load lock were turned off so as not to create any contamination on the surface. The reconstructed sample was then oriented to face the spherosiloxane source and the gate valve to the load lock was opened. The Si sample was moved into the load lock for exposure to the $H_8Si_8O_{12}$ source and immediately pulled back out, for a total direct exposure of approximately 1 second. The distance from the sample to source was approximately 6 inches. The sample was then immediately lowered into the low temperature STM chamber at 4 K for imaging.

A characteristic picture of a $H_8Si_8O_{12}$ dosed Si (100) surface is shown in Figure 4.9. This 250 Å x 200 Å image was obtained at imaging conditions of +4.0 V and 1.0 nA. It is possible to make out the dimer rows along the surface as well as the step edge running across the bottom third of the image. In addition, there are a large number of additional adsorbed features on the surface. The picture of $H_8Si_8O_{12}$ bonding presented by Holl and McFeeley is such that it is likely that an adsorbed spherosiloxane molecule would appear in an STM image as a single rounded hump because of the high symmetry of the molecule and its orientation. Moreover, because an adsorbed $H_8Si_8O_{12}$ molecule is insulating on the surface, it will likely appear to have a lower image height than a conducting molecule of the same size and shape. For these reasons, it is impossible to definitively identify any of the particular adsorbates on the surface as spherosiloxanes. Several attempts were made to dose $H_8Si_8O_{12}$ onto the surface and the results in each case were substantially the same. It is safe to conclude, however, that the silicon surface is highly reactive, as indicated by the large number of adsorbates on the surface even with the very short exposure times used in the dosing experiment. In addition, there is nothing in this image which contradicts or invalidates the picture of $H_8Si_8O_{12}$ previously presented. Because $H_8Si_8O_{12}$ is

unlikely to be a suitable precursor for a microporous film, a decision was made at this point to concentrate instead on $(CH_3O)_8Si_8O_{12}$ and its surface condensation behavior due to the very limited time available at IBM.

### *4.2.4. Condensation Behavior of $(CH_3O)_8Si_8O_{12}$ on the Si (100) - (2x1) surface*

The first set of dosing experiments for $(CH_3O)_8Si_8O_{12}$ were carried out with the spherosiloxane introduced into the UHV system by way of a leak valve. The spherosiloxane sample bulb and leak valve were heated to 140°C for dosing. A clean reconstructed Si (100) surface was prepared as described earlier. With the Si sample rotated away from the valve, the leak valve was opened and after an initial pressure burst to $7 \times 10^{-8}$, the pressure recovered to a steady value of $3 \times 10^{-9}$, at which time the Si sample was rotated back into the line of sight position and dosed for 100 seconds after which the valve was closed. The LEED pattern of this dosed surface still showed the (2x1) pattern; however, the intensity had decreased. This dosing procedure was repeated twice more with dosing times of 10 minutes each. The results showed a continued degradation of the LEED pattern with each successive dose until it was virtually non-existent after the final dose. (See Figure 4.10.) STM showed the surface almost completely covered with material to the point that it was nearly impossible to find any areas where the (2x1) reconstruction was still visible. Auger spectra taken of the surface after each successive dosing showed increasing amounts of carbon and oxygen on the surface as expected; however, it also indicated the presence of a significant amount of chlorine on the surface. The presence of chlorine was confirmed after taking a mass spectrum of the dosing beam which showed the characteristic signature of HCl present in the beam. (See Figure 4.11.)

We were initially surprised by the presence of HCl in the sample. However, this result can be explained by the fact that the sample used for this dosing experiment had been heated and stored under vacuum behind the leak valve for approximately 5 months before use. The chlorine likely results from some incompletely methoxylated spherosiloxane product ($Cl_x(CH_3O)_{7-x}Si_8O_{12}$) which although undetectable in the sample by NMR or IR spectroscopy, was present in the sample. A small amount of the chlorine was liberated on the earlier heating and reacted with hydrogen present in the steel of the leak valve over the course of time to make HCl, which in turn reacted on the remaining spherosiloxane to produce some condensation and in turn liberate more of the Cl impurity. As a result of this result, the purification procedure for the $(CH_3O)_8Si_8O_{12}$ to be used in dosing experiments was modified to use a multicycle purification process (three cycles of recrystallization and sublimation) in order to eliminate the residual Cl impurities. In addition, the samples were used as soon as possible after their preparation to reduce the time available for decomposition.

Once a new sample of $(CH_3O)_8Si_8O_{12}$ was prepared, the dosing experiments continued. However, instead of using a leak valve, the sample source arrangement described for the $H_8Si_8O_{12}$ experiments was employed. In order to ascertain what type of dosing conditions to use (duration and source temperature), a quartz crystal microbalance (QCM) was mounted onto the load lock in a line of sight position approximately 12 inches from the spherosiloxane source. We decided to find dosing conditions which would correspond to approximately 3 spherosiloxane molecules per 100 Å by 100 Å area in 10 seconds. The appropriate flux to achieve this corresponded to a frequency change rate of $6.5 \times 10^{-3}$ Hz/sec for the QCM. The spherosiloxane source temperature was varied until this sample flux

was achieved, corresponding to a spherosiloxane source temperature of 110°C. The pressure corresponding to these conditions was approximately 2 x $10^{-8}$ Torr.

A clean, reconstructed Si (100) surface was prepared and dosed with $(CH_3O)_8Si_8O_{12}$ as described for 10 seconds at a spherosiloxane source temperature of 110°C. The sample was immediately lowered into the STM chamber for imaging. Once again, the sample surface was so completely covered with adsorbates that it was again difficult to make out the reconstructed surface in most places. After imaging, an Auger spectrum was obtained which indicated the presence of carbon and oxygen on the surface, but there was no further indication of chlorine contamination. The heavily covered surface was somewhat surprising in light of the QCM experiments. One likely explanation is that the Si (100) surface is much more reactive, and thus has a much higher sticking coefficient (perhaps approaching 1) than the surface of the QCM.

Additional $(CH_3O)_8Si_8O_{12}$ dosing experiments were carried out with successively shorter dosing times and lower source temperatures in order to produce a lightly dosed surface with isolated adsorbate molecules. Source temperatures of 100°C, 70°C, 40°C and 25°C were used with corresponding dosing times of 6 seconds, 4 seconds, 5 seconds, and 2 seconds. The first three of these experiments had qualitatively the same results as the first experiment. For the sample prepared by dosing for 2 seconds at 25°C, again most of the surface showed the same heavy coverage as before. However, several patches of surface were imaged which were essentially free of adsorbates and clearly showed the underlying surface reconstruction. On one of these patches a single adsorbate was imaged which showed the expected characteristics for an adsorbed $(CH_3O)_8Si_8O_{12}$ molecule. (See Figures 4.12 and 4.13.) The adsorbate shows the expected four-fold symmetry of the

cubic spherosiloxane and it seems to be aligned in the direction of the dimer rows. In addition, it is situated such that it appears to be bridging between two of the dimer rows. Line scans taken parallel and perpendicular to the dimer rows (See Figure 4.14) indicate that the adsorbate is bound level across the rows, suggesting that it has made four bonds to the surface. The relatively short apparent image height can be explained because $(CH_3O)_8Si_8O_{12}$ is an insulator, not a conductor. Unfortunately, I was unable to obtain any additional images to confirm this analysis, as this image was obtained on my last day of experiments at IBM and I was unable to arrange any additional time for more experiments. However, we attempted to obtain some additional evidence supporting this picture of spherosiloxane binding from HREELS/TPD studies in collaboration with Dr. John Vohs and his research group at the University of Pennsylvania.

### *4.2.5. HREELS/ TPD Studies of Spherosiloxane Condensation Behavior*

In order to further elucidate the mechanism for spherosiloxane behavior on the Si (100) - (2x1) surface, we initiated a collaboration with Dr. John Vohs and his research group at the University of Pennsylvania. These researchers have developed an experimental technique which combines high resolution electron energy loss spectroscopy (HREELS) with thermal programmed desorption (TPD) which provides useful information about the reaction behavior of molecules on surfaces[28-30]. In particular, they recently carried out a very nice study elucidating the pathways and intermediates in the reaction of tetraethoxysilane on the Si (100) - (2x1) surface[27].

Purified samples of $H_8Si_8O_{12}$ and $(CH_3O)_8Si_8O_{12}$ were prepared in our laboratory and sent to Dr. Vohs in sealed glass ampoules under argon atmosphere. At the University

of Pennsylvania HREELS/TPD experiments were performed under UHV conditions using a McAllister high resolution electron energy loss spectrometer. The first set of experiments performed investigated at the behavior of $H_8Si_8O_{12}$. $H_8Si_8O_{12}$ was dosed onto a Si (100) reconstructed surface with a surface coverage of 0.3 L and 2.0 L, respectively, at 90 K. Data in Figure 4.15 shows that the spectrum of the adsorbed species is very similar to that of the bulk molecule for temperatures below about 400 K. A comparison of the vibrational modes of free and adsorbed $H_8Si_8O_{12}$ can be found in Table 4.1. Initial experiments suggested that $H_8Si_8O_{12}$ adsorbed dissociatively on the surface, as indicated by the presence of the strong peak at about 2030 $cm^{-1}$ which is in the region of Si-H stretching vibrations. (See Figure 4.15 (A).) However, deconvolution of the spectrum indicated that the 2030 $cm^{-1}$ peak is due to a sequential excitation of the modes at 886 $cm^{-1}$ and 1153 $cm^{-1}$. (See Figure 4.15 (B).) The TPD experiment (Figure 4.16) showed a lack of any peaks in the Si-H stretching region below 400 K, when a peak begins to form at 2065 $cm^{-1}$. This result suggests that $H_8Si_8O_{12}$ adsorbs molecularly rather than dissociatively on the surface, in contradiction with the results of Holl and McFeely, as well as the dosing and STM results we obtained at IBM. A possible explanation for this is the fact that in the HREELS study dosing was carried out at low temperature, whereas in the XPS and STM studies, the dosing was performed on a room temperature substrate which may have allowed for higher reactivity of the spherosiloxane with the surface.

$(CH_3O)_8Si_8O_{12}$ experiments were carried out in essentially the same fashion as for $H_8Si_8O_{12}$, except that the adsorption was performed at 120 K on the Si (100) surface and the doses were 6 L and 12 L, respectively. In addition, the sample lines had to be heat

traced to prevent adsorption of the spherosiloxane on the walls which introduced a small amount of water into the sample chamber. The largest peaks in the low temperature HREEL spectra (i.e., those at 1025, 1145, 1455, 2845, and 2970) are characteristic of methoxy groups. (See Figure 4.17.) A comparison of the vibrational modes of free and adsorbed $(CH_3O)_8Si_8O_{12}$ can be found in Table 4.2. Comparison of the HREEL spectrum of $CH_3O$ on Si (111) with the spectrum from $(CH_3O)_8Si_8O_{12}$ suggests that the presence of oxygen in the coordination sphere of the Si atom does not significantly alter the vibrational properties of the methoxy group. As a result, it was not possible to distinguish between methoxy groups bound to the surface and those still on the spherosiloxane, and hence if any dissociative adsorption had taken place. The TPD experiment shows a large drop in intensity as the sample is warmed to room temperature and beyond. (See Figure 4.18.) This result suggests that at 120 K, the spherosiloxane is molecularly adsorbed onto the surface and begins to desorb near room temperature. Once again, this is in direct conflict with our dosing results at IBM and can possibly be attributed to the differences in substrate temperature during dosing.

## *4.3. Conclusions and Future Work*

Based on the work presented here, we have begun to gain some understanding of the condensation behavior of the spherosiloxanes on the Si (100) surface. Clearly, significantly more work must be performed before proceeding to the epitaxial growth of a microporous film. Foremost, the contradiction between the STM and XPS results with the HREELS data needs to be clarified. If the spherosiloxanes are molecularly adsorbed on the surface, it may be possible to test this by using the STM to move the molecules across the surface. However, if the spherosiloxanes are indeed chemisorbed, then it will be impossible to move the adsorbed molecules on the surface. In addition, some additional information about the sorbed species may be obtained by performing molecular spectroscopy on a single spherosiloxane molecule using the STM[31]. Finally, more dosing experiments should be performed to locate more individual spherosiloxanes adsorbed on the surface to confirm the previous results.

Once more is known about the exact nature of the interaction of the spherosiloxane molecules with the surface, this information can be applied to aid in the organization of the first ordered layer on the surface. It is this step which will prove crucial for epitaxial growth of a microporous layer. If it turns out that the molecules are molecularly adsorbed on the Si (100) surface at low temperature, it may be possible to take advantage of this fact to allow packing or ordering of the molecules in the first layer, possibly under the influence of an electric field or moved via the STM using techniques developed by Eigler[6], before locking this ordered structure in place by heating or perhaps with the use of an excimer laser to induce reaction. If, on the other hand, the spherosiloxanes are chemically adsorbed on the surface, a much more controlled dosing technique must be developed,

perhaps even a molecular beam source of spherosiloxanes, to significantly reduce the flux of material to the surface and thereby allow the underlying silicon surface to orient the incoming molecules and organize the first layer of the film. Once an ordered first layer is achieved, the growth of the microporous layer should be readily achieved by the well developed techniques of atomic layer epitaxy presented earlier.

## *Literature Cited*

(1) Feynman, R. P. In *Miniaturization*; GIlbert, H. D. Ed.; Reinhold Publishing Corp.: New York, 1961; pp 282-296.

(2) Lüth, H. *Phys. Stat. Sol. B* **1995**, *192*, 287-299.

(3) Binnig, G.; Rohrer, H. *Helv. Phys. Acta* **1982**, *55*, 726-735.

(4) Binnig, G.; Rohrer, H.; Gerber, C.; Wiebel, E. *Phys. Rev. Lett.* **1982**, *49*, 57-61.

(5) Binnig, G.; Rohrer, H. *Surf. Sci.* **1983**, *126*, 236-244.

(6) Eigler, D. M.; Schweizer, E. K. *Nature* **1990**, *344*, 524-526.

(7) Eigler, D. M.; Weiss, P. S.; Schweizer, E. K.; Lang, N. D. *Phys. Rev. Lett.* **1991**, *66*, 1189-1192.

(8) Eigler, D. M.; Lutz, C. P.; Rudge, W. E. *Nature* **1991**, *352*, 600-603.

(9) Eigler, D. M., Personal Communication, 1992.

(10) Manalis, S. R.; Minne, S. C.; Atalar, A.; Quate, C. F. *Rev. Sci. Instrum.* **1996**, *67*, 3294-3297.

(11) Manalis, S. R.; Minne, S. C.; Quate, C. F. *Appl. Phys. Lett.* **1996**, *68*, 871-873.

(12) Minne, S. C.; Manalis, S. R.; Atalar, A.; Quate, C. F. *J. Vac. Sci. Technol. B* **1996**, *14*, 2456-2461.

(13) Desu, S. B.; Peng, C. H.; Agaskar, P. A. *J. Electrochem. Soc.* **1992**, *139*, 2682-2685.

(14) Holl, M. M. B.; McFeely, F. R. *Phys. Rev. Lett.* **1993**, *71*, 2441-2444.

(15) Holl, M. M. B.; Lee, S.; McFeely, R. F. *Appl. Phys. Lett.* **1994**, *65*, 1097-1099.

(16) Beer, R.; Bürgy, H.; Calzaferri, G.; Kamber, I. *J. Elec. Spec.* **1987**, *44*, 121-130.

(17) Jayaram, G.; Xu, P.; Marks, L. D. *Phys. Rev. Lett.* **1993**, *71*, 3489-3492.

(18) Pollman, J.; Kalla, R.; Krüger, P.; Mazur, A.; Wolfgarten, G. *Appl. Phys. A* **1986**, *41*,

21-38.

(19) Jing, Z.; Whitten, J. L. *Phys. Rev. B* **1992**, *46*, 9544-9550.

(20) Ihara, S.; Ho, S. L.; Uda, T.; Hirao, M. *Phys. Rev. Lett.* **1990**, *65*, 1909-1912.

(21) Hamers, R. J.; Tromp, R. M.; Demuth, J. E. *Phys. Rev. B* **1986**, *34*, 5343-5357.

(22) *Atomic Layer Epitaxy*, Suntola, T.; Simpson, M. Eds.; Chapman and Hall: New York, 1990.

(23) Leskelä, M.; Niinistö, L. In *Atomic Layer Epitaxy*; Suntola, T.; Simpson, M. Eds.; Chapman and Hall: New York, 1990; pp 1-39.

(24) Ritala, M.; Leskelä, M.; Niinistö, L.; Haussalo, P. *Chem. Mater.* **1993**, *5*, 1174-1181.

(25) Ritala, M.; Leskela, M.; Rauhala, E. *Chem. Mater.* **1994**, *6*, 556-561.

(26) Sneh, O.; Wise, M. L.; Okada, L. A.; Ott, A. W.; George, S. M. In; Materials Research Society: Pittsburgh, PA, 1994; Preprint.

(27) Danner, J. B.; Reuter, M. A.; Vohs, J. M. *Langmuir* **1993**, *9*, 455-459.

(28) Danner, J. B. *Appl. Surf. Sci.* **1992**, *62*, 255-262.

(29) Reuter, M. A.; Vohs, J. M. *J. Vac. Sci. Technol. A* **1991**, *9*, 2916-2922.

(30) Reuter, M. A.; Vohs, J. M. *Surf. Sci.* **1992**, *262*, 42-50.

(31) Smith, D. P. E.; Kirk, M. D.; Quate, C. F. *J. Chem. Phys.* **1987**, *86*, 6034-6038.

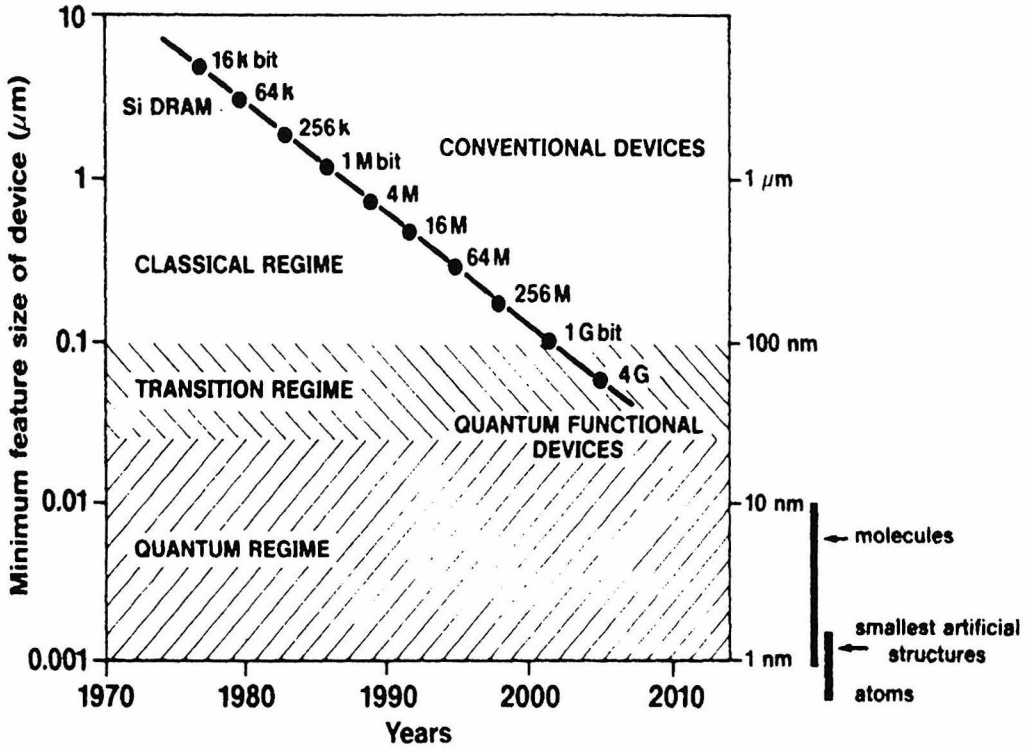


**Figure 4.1:** Extrapolation of the development of Si DRAM feature sized vs. time. Conventional devices fabricated in CMOS ULSI technology reach a critical period between the years 2005 and 2010, where quantum effects determine the possibility of future development. Adapted from Lüth[2].

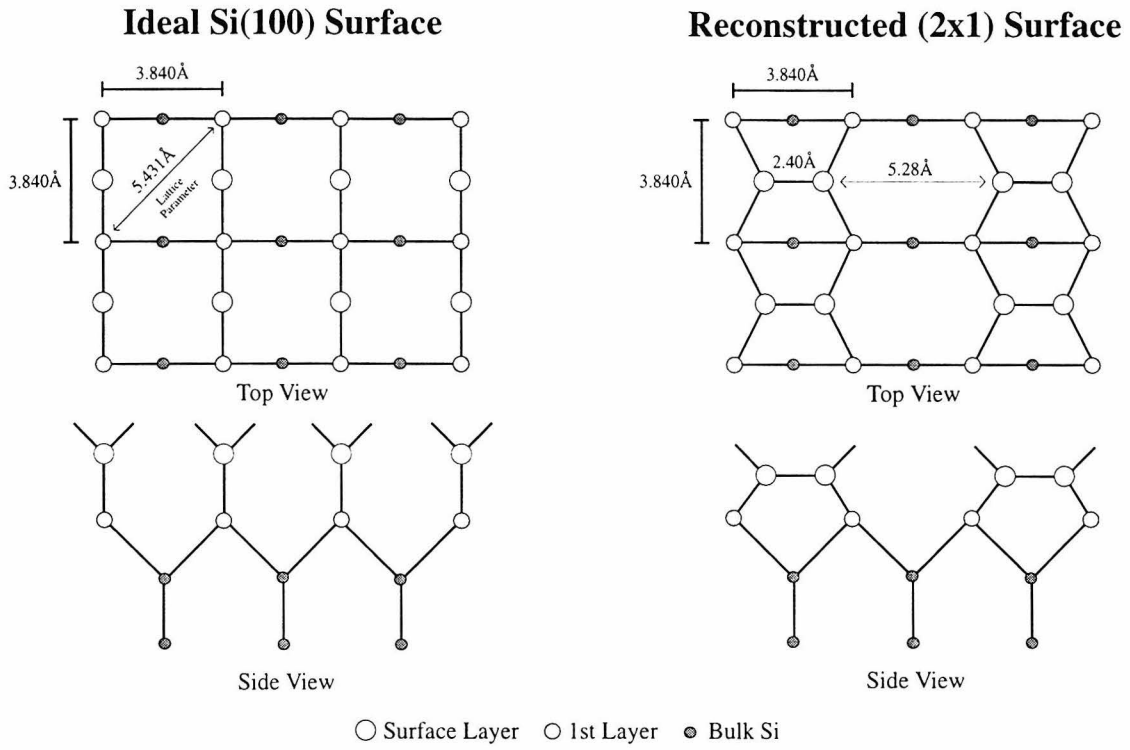


**Figure 4.2:** Schematic diagram of the ideal Si (100) surface and the reconstructed (2x1) surface. Pairs of atoms or "surface dimers" distort from their ideal positions in order to make an additional bond, thereby reducing the number of unattached, or "dangling" bonds, at the surface and correspondingly the surface free energy. The name (2x1) reconstruction comes from the unit cell of the new surface structure which is twice as wide as the ideal surface unit cell, while retaining the same length.

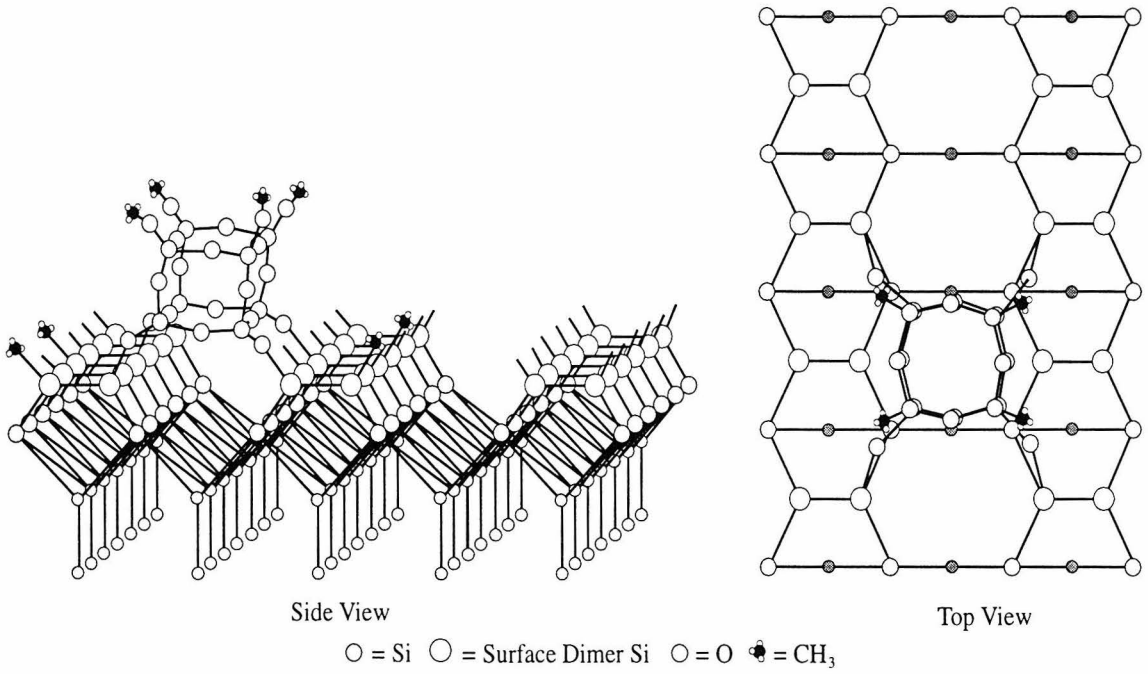


**Figure 4.3:** Schematic diagram of a $(CH_3O)_8Si_8O_{12}$ molecule condensed onto the Si(100) - (2x1) reconstructed surface. The spacing between the dimer rows of the reconstructed surface is correct for bridging by $(CH_3O)_8Si_8O_{12}$. In addition, the surface structure can provide organization of the first layer for crystal growth using an epitaxial growth mechanism.

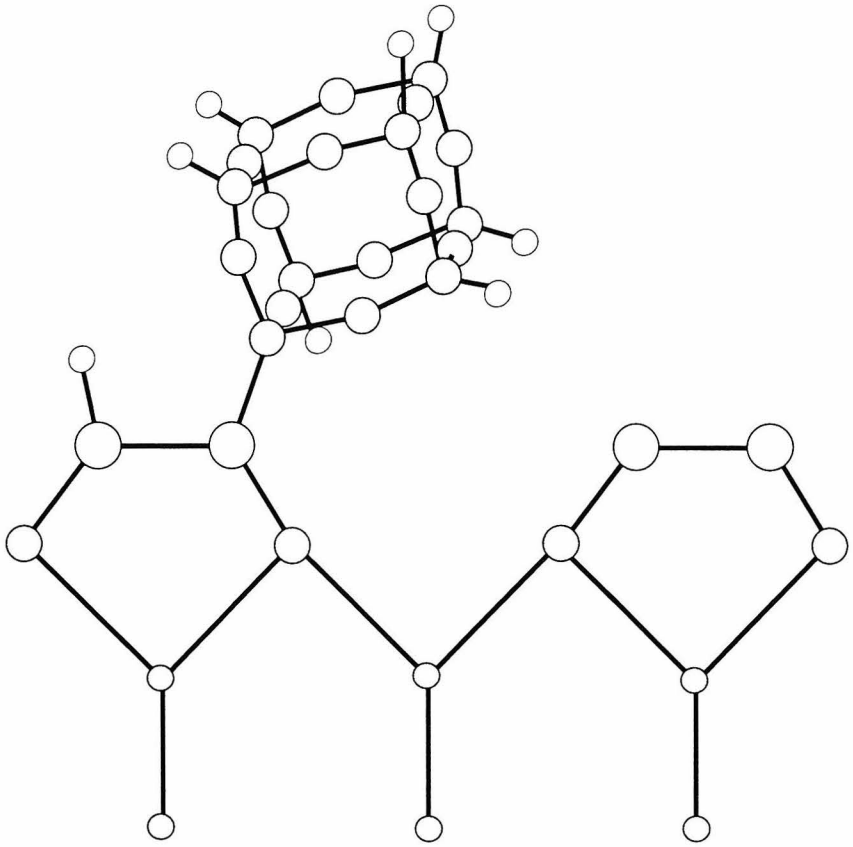

Side View

= Si = Surface Dimer Si = O = H

**Figure 4.4:** Schematic diagram of $H_8Si_8O_{12}$ chemisorbed onto Si(100) - (2x1) as suggested by Holl and McFeeley from X-ray Photoemission Spectroscopy (XPS) results. Adapted from [14].

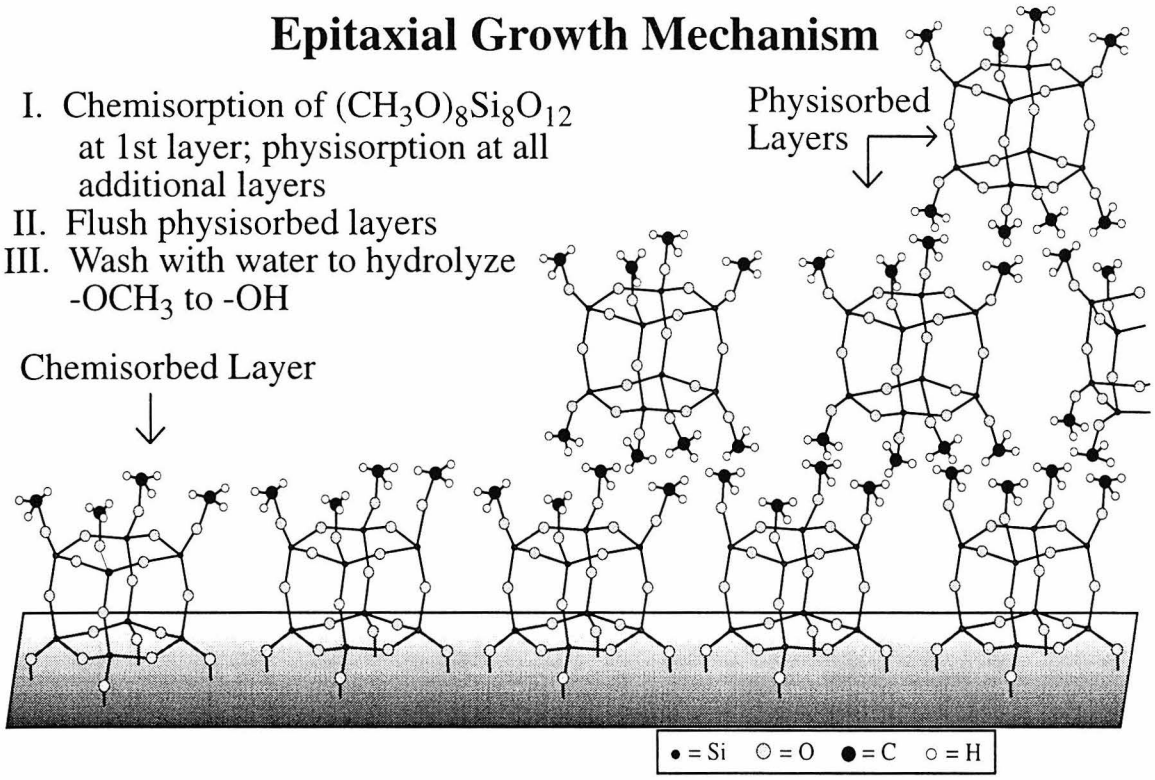


**Figure 4.5.a:** Schematic diagram of proposed epitaxial growth mechanism for the production of microporous thin films from spherosiloxanes. The process begins with chemisorption of $(CH_3O)_8Si_8O_{12}$ molecules onto the desired surface with physisorption at all additional layers. The physisorbed layers are pumped or flushed away and water is introduced to hydrolyze the $-OCH_3$ groups on the top of the first layer to -OH, thereby making them once again reactive toward $(CH_3O)_8Si_8O_{12}$.

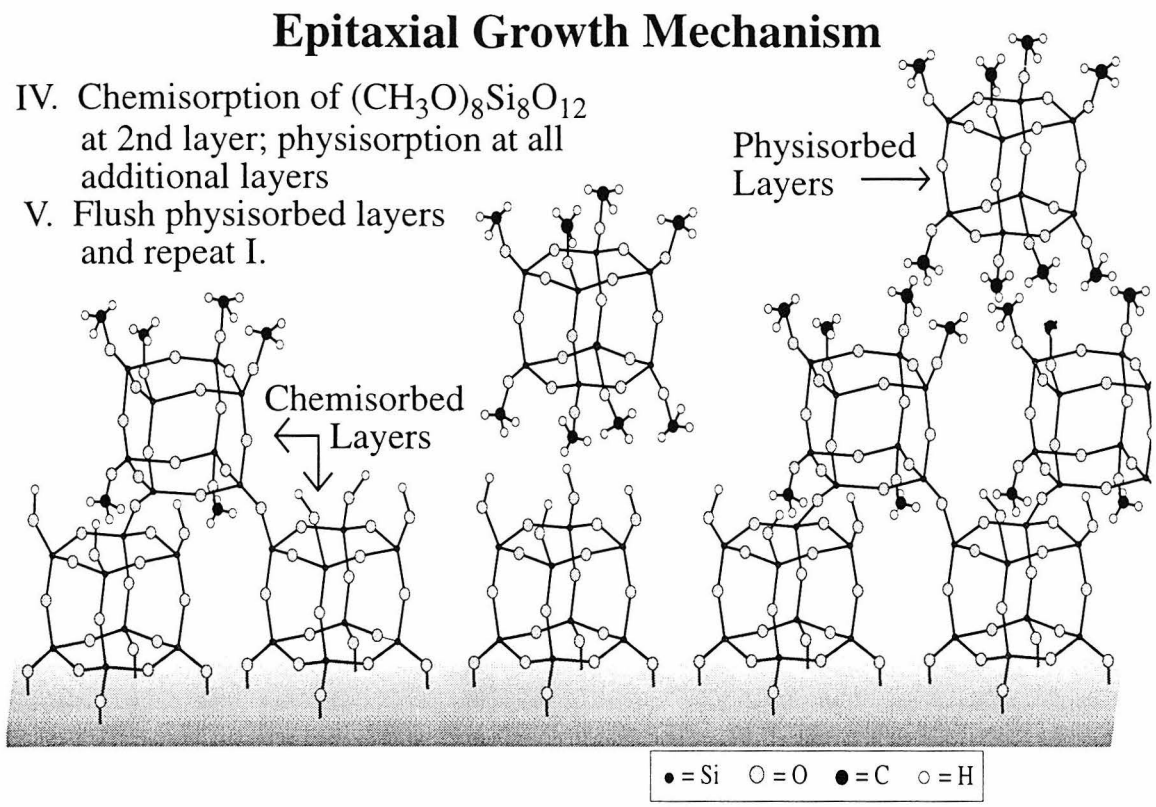


**Figure 4.5.b:** Schematic diagram of proposed epitaxial growth mechanism for the production of microporous thin films from spherosiloxanes. The reaction now continues with chemisorption of $(CH_3O)_8Si_8O_{12}$ molecules onto the second layer with physisorption at all additional layers. The physisorbed layers are pumped or flushed away and the process repeats itself, growing the microporous film layer by layer in a fashion analogous to atomic layer epitaxy (ALE).

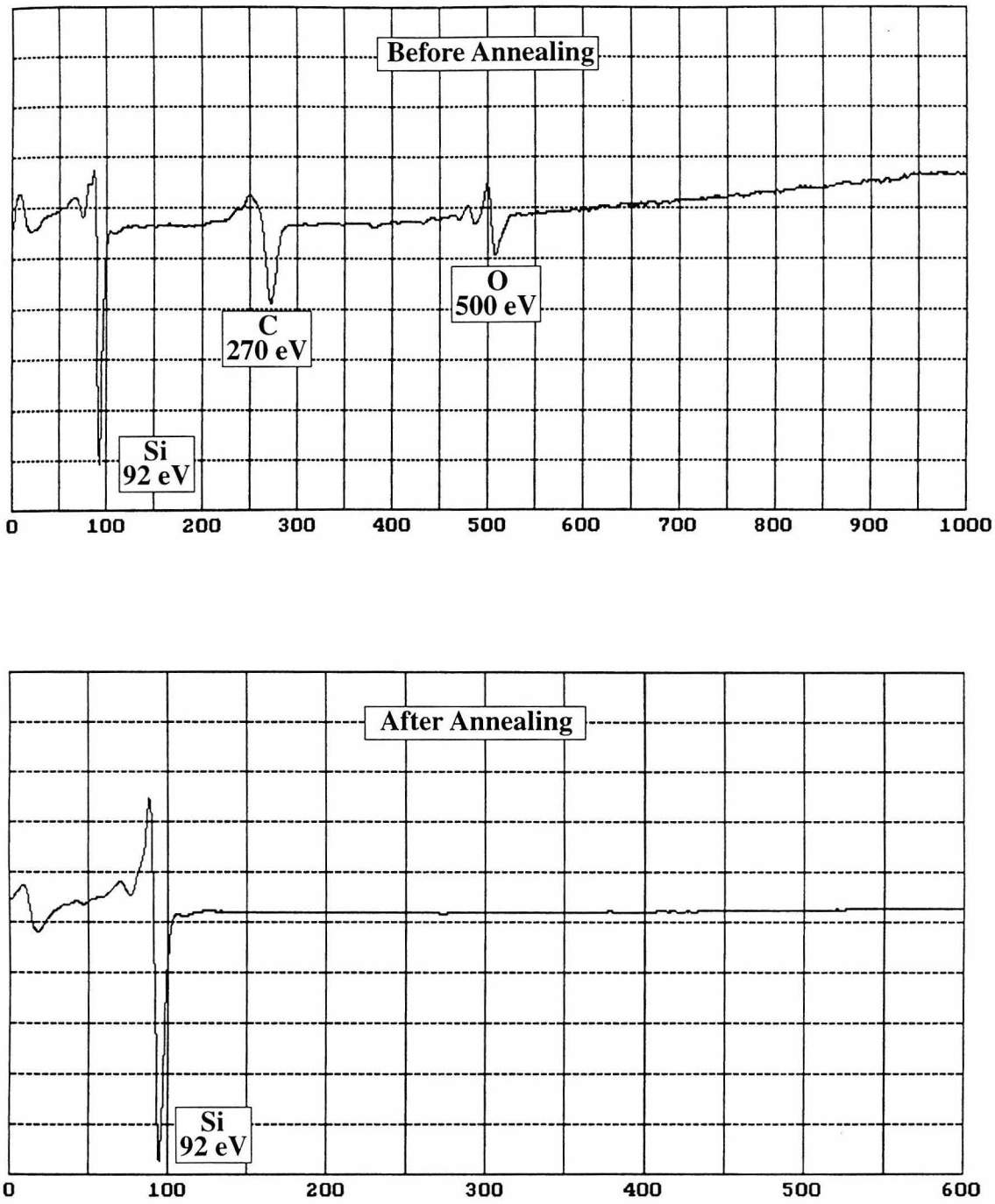


**Figure 4.6:** Auger electron spectra of Si (100) before and after annealing to 1180°C at $10^{-10}$ torr. Note the peaks for Si, C, and O before annealing and the presence of only Si after annealing. Spectra obtained at 3 kV with 1.0 mA emission at a scan rate of 7 eV/sec.

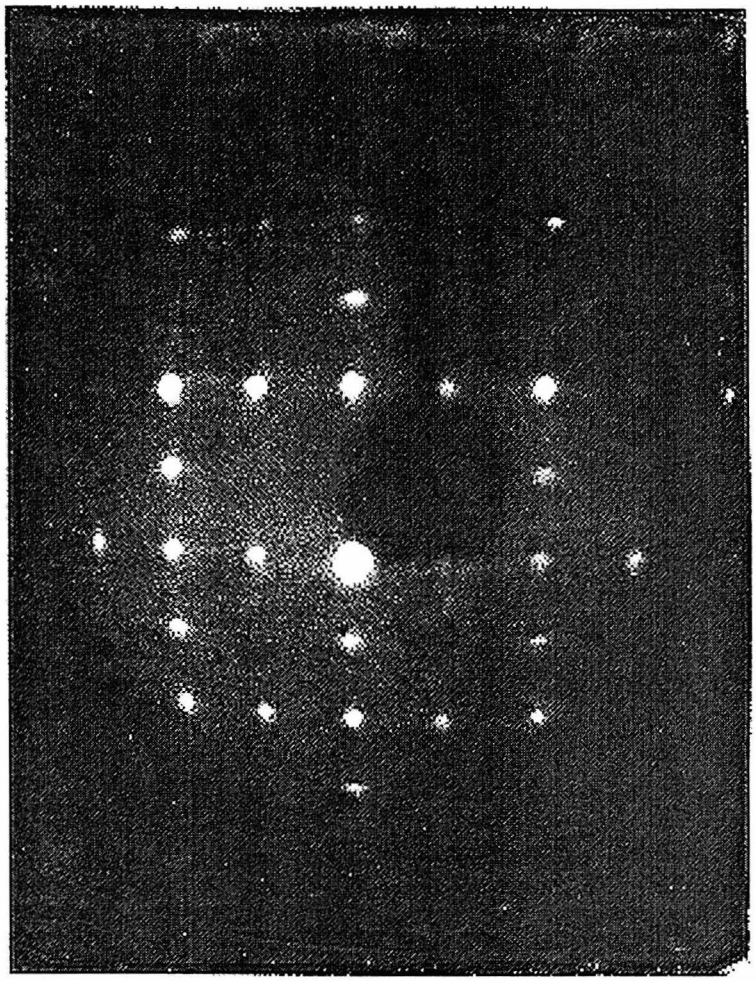

**Figure 4.7:** Low energy electron diffraction (LEED) pattern of a clean, annealed Si(100) - (2x1) reconstructed surface. The box-like pattern without a LEED spot in the center is characteristic of the (2x1) reconstructed surface. LEED pattern obtained at a beam energy of 98.2 eV, using a screen voltage of 5 kV and 0.5 mA emission.

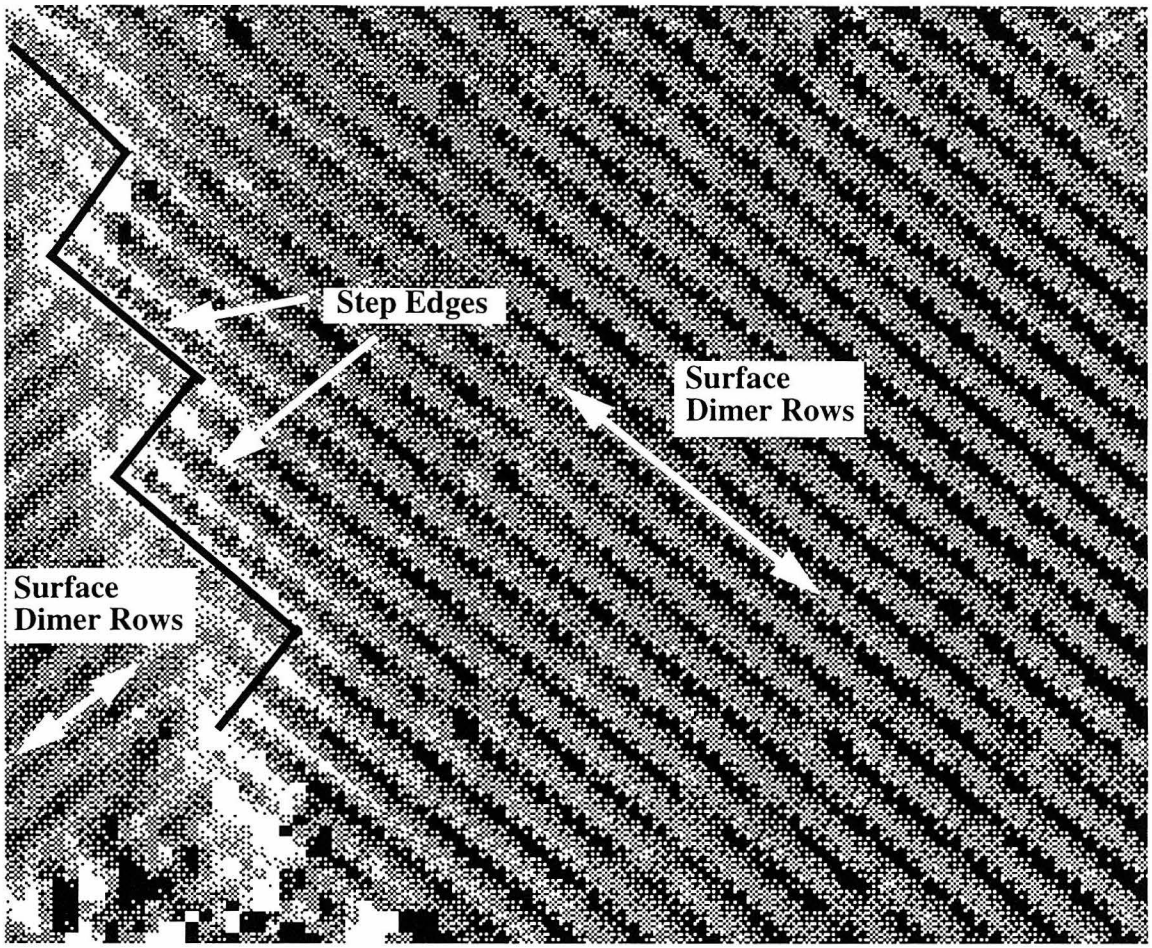


**Figure 4.8.a:** Low temperature STM image of a Si (100) - (2x1) reconstructed surface (175 Å by 200 Å). Note that the surface dimer rows change orientation by 90 degrees at a single atomic height step. Imaging conditions: -4.0 V, 1.0 nA

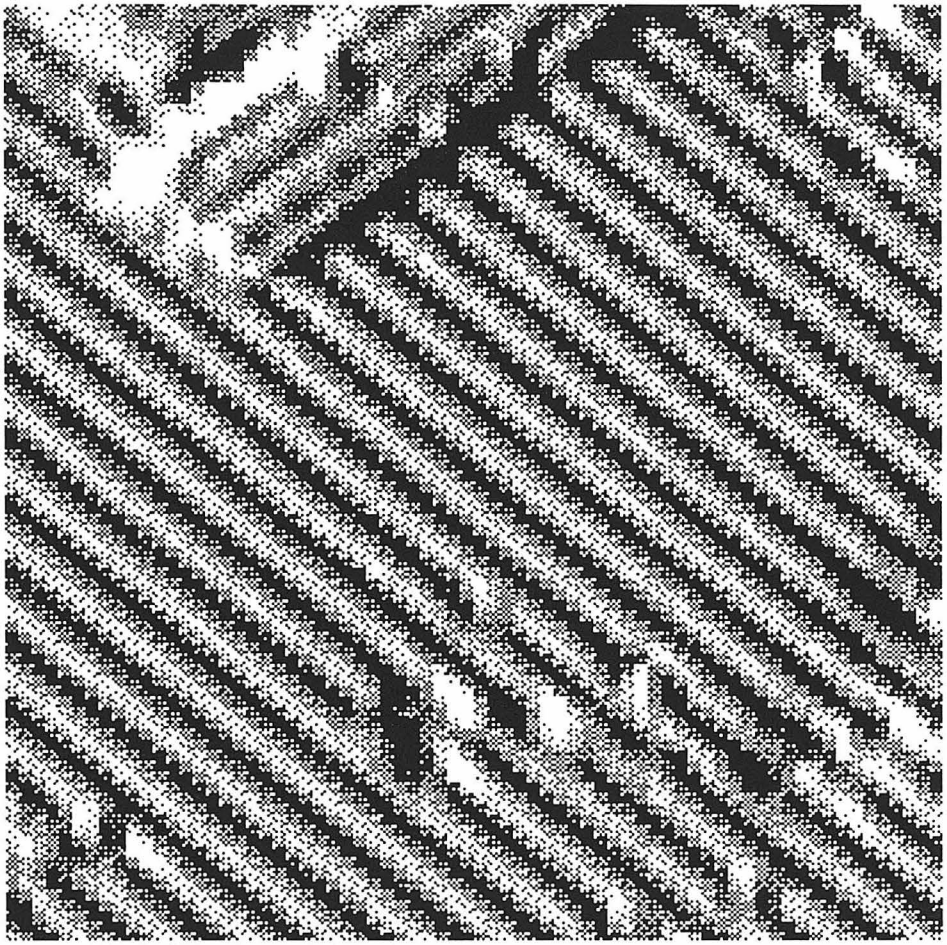

**Figure 4.8.b:** Low temperature STM image of a Si (100) - (2x1) reconstructed surface (140 Å by 140 Å). Note that the surface dimer rows change orientation by 90 degrees at a single atomic height step. Imaging conditions: -4.0 V, 1.0 nA

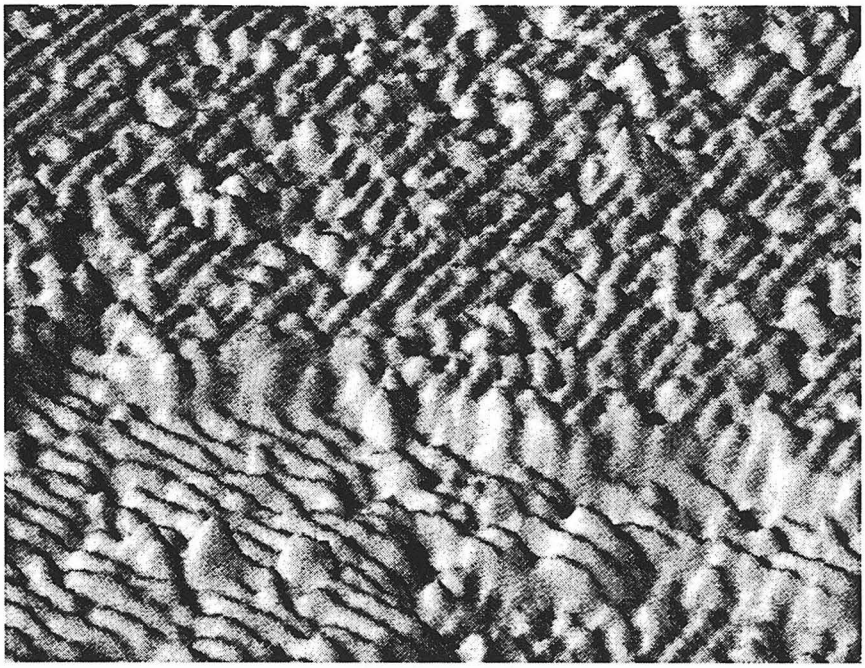

**Figure 4.9:** A low temperature STM image of a Si (100) - (2x1) surface dosed with $H_8Si_8O_{12}$ (200 Å x 250 Å). There is a large number of adsorbates on the surface, but it is impossible to definitively identify any of them as $H_8Si_8O_{12}$. Imaging conditions: +4.0 V, 1.0 nA

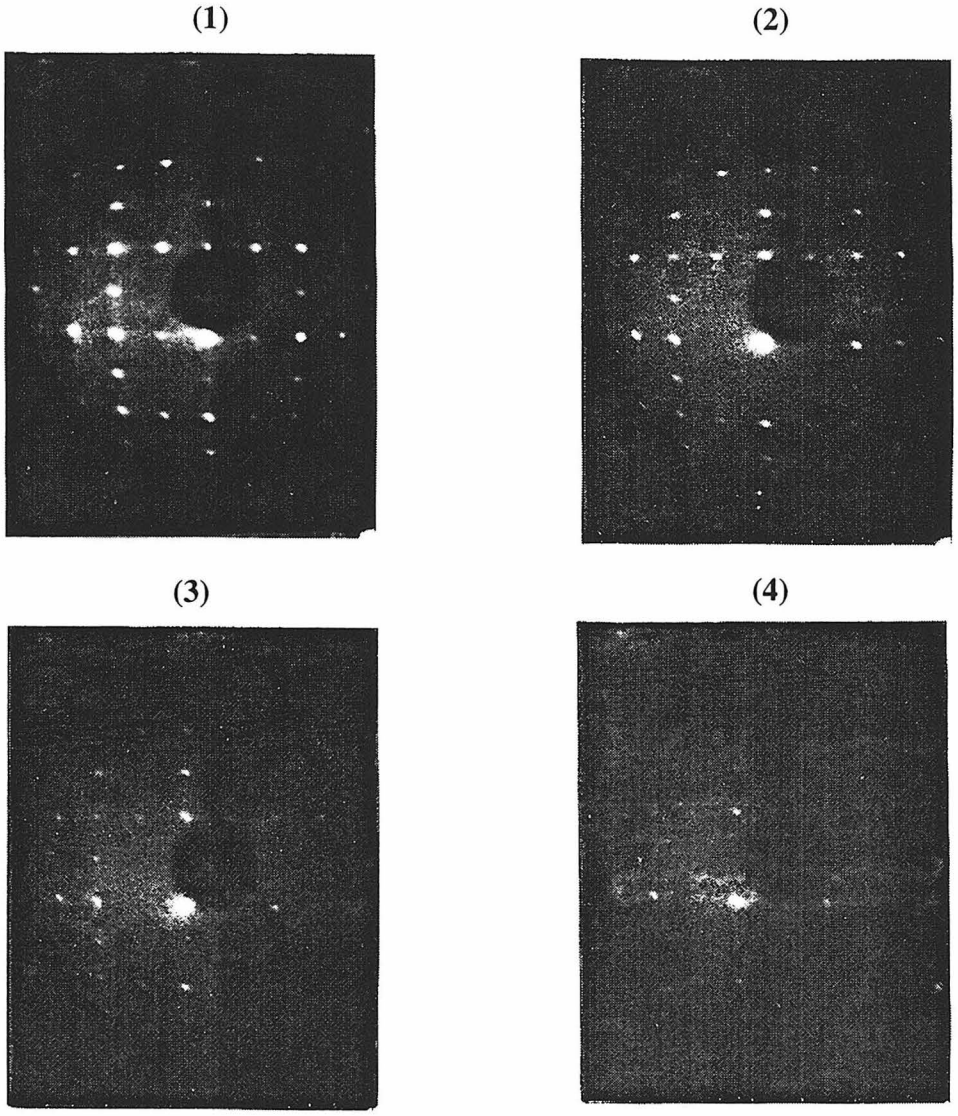


**Figure 4.10:** LEED Patterns for $(CH_3O)_8Si_8O_{12}$ dosing experiments taken (1) before dosing; (2) after a 100 second dose; (3) after a 10 min dose; and (4) after a second 10 minute dose. Notice that the pattern for the (2x1) surface is lost as the amount of $(CH_3O)_8Si_8O_{12}$ on the surface increases. LEED Patterns were obtained at a beam energy of 98.2 eV, using a screen voltage of 5 kV and emission of 0.5 mA.

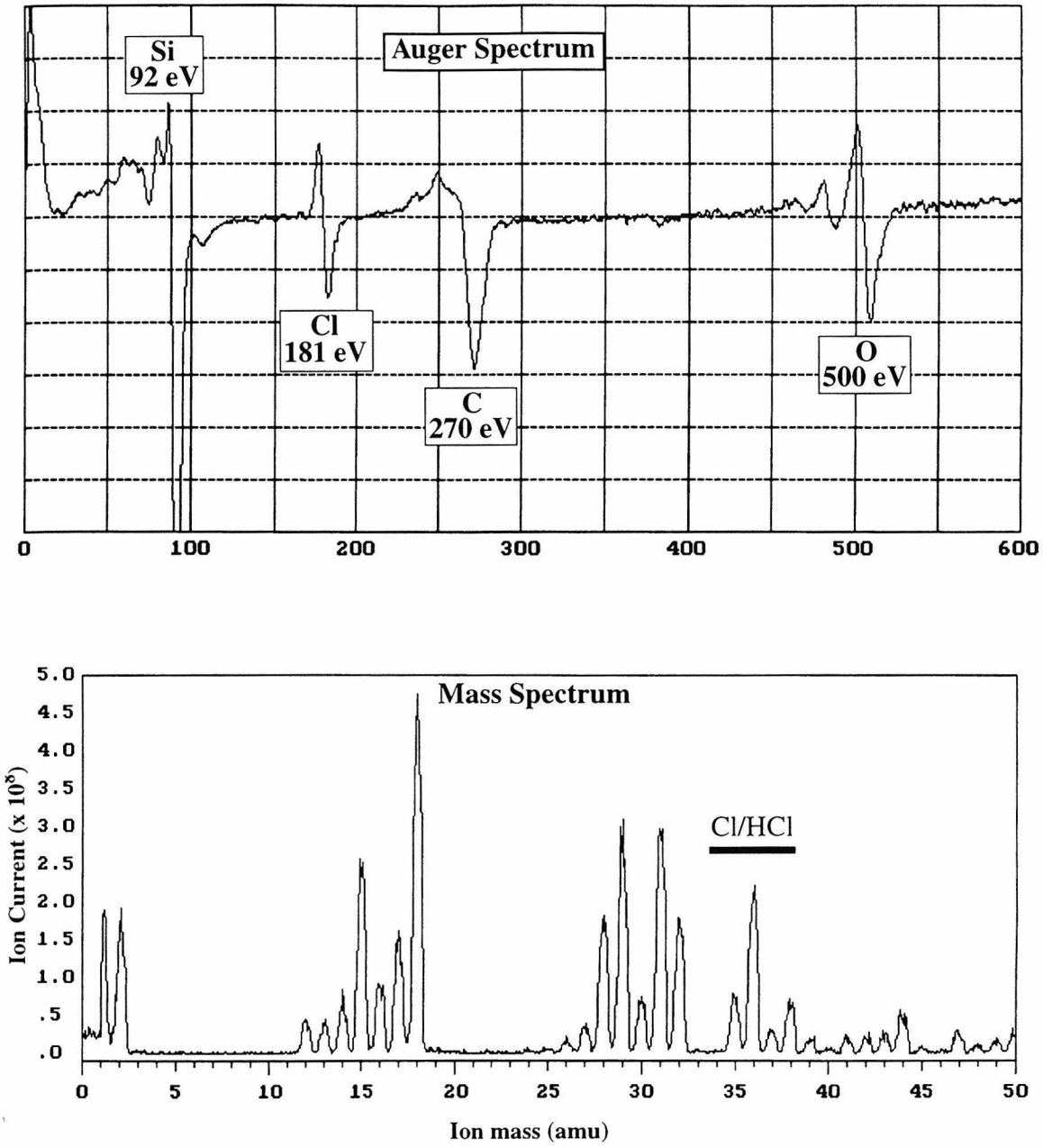


**Figure 4.11:** Auger and mass spectra showing the presence of a chlorine/hydrochloric acid contaminant present in the $(CH_3O)_8Si_8O_{12}$ sample used for dosing. Auger spectrum collected using a scan rate of 7 eV/sec at 3 kV, 1.0 mA emission.

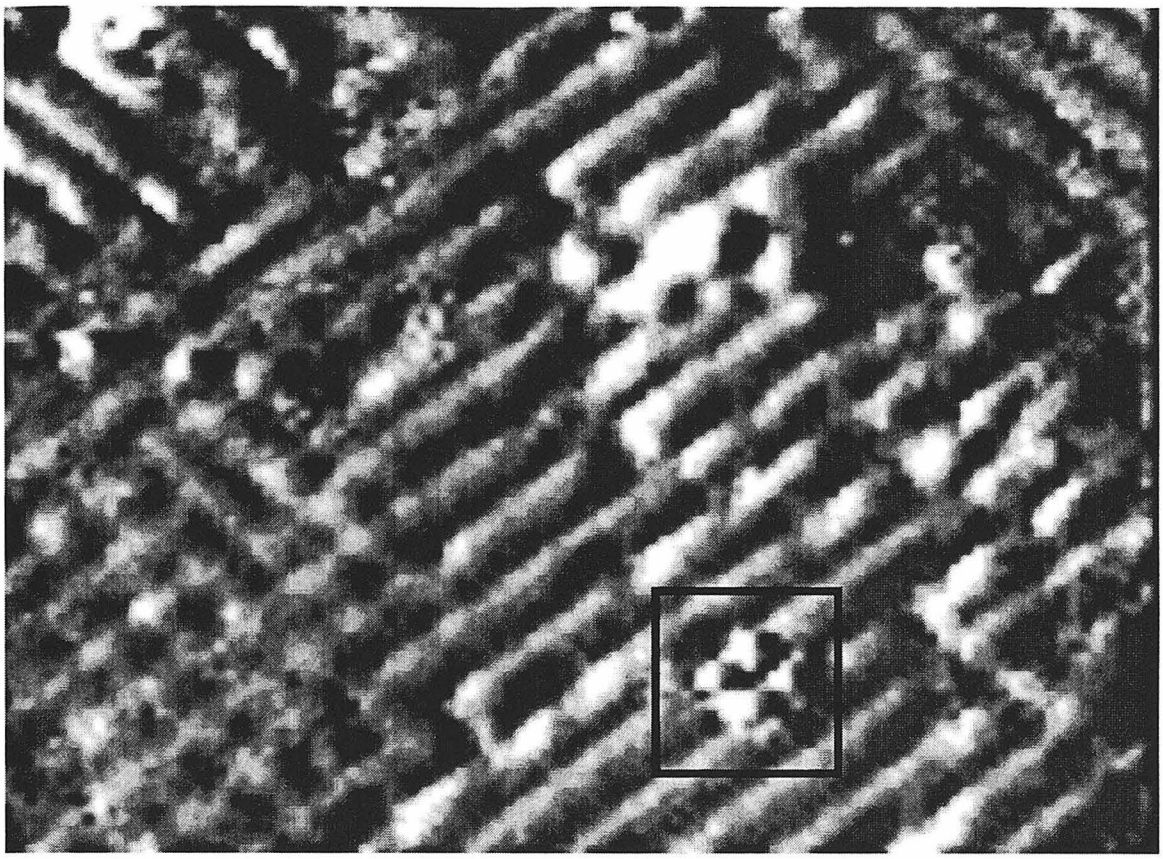

**Figure 4.12:** Low temperature STM image of a $(CH_3O)_8Si_8O_{12}$ dosed surface. Highlighted area is believed to be an isolated $(CH_3O)_8Si_8O_{12}$ molecule adsorbed onto the surface.

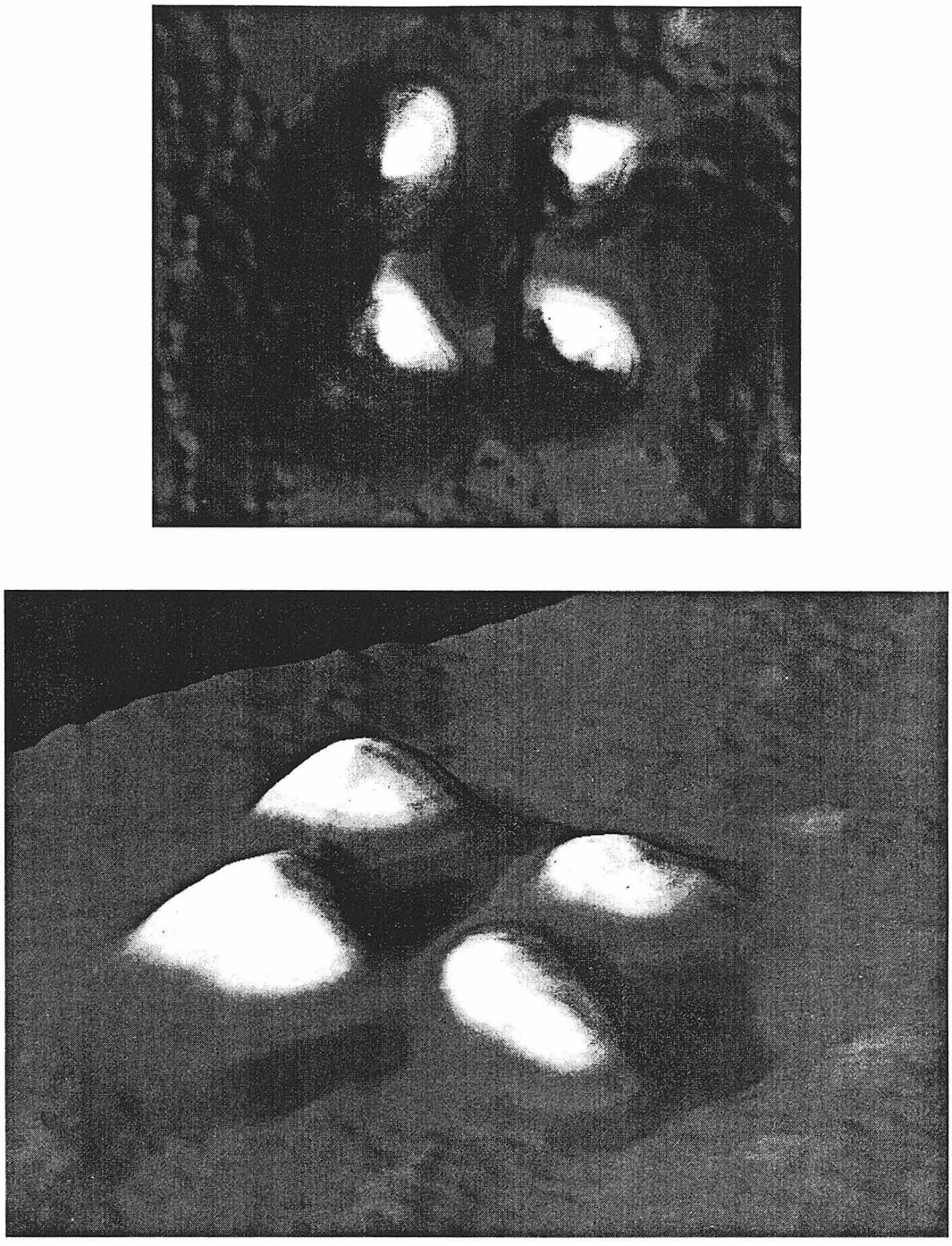

**Figure 4.13:** Close-up top and side views of adsorbed $(CH_3O)_8Si_8O_{12}$ on Si (100) -(2x1).

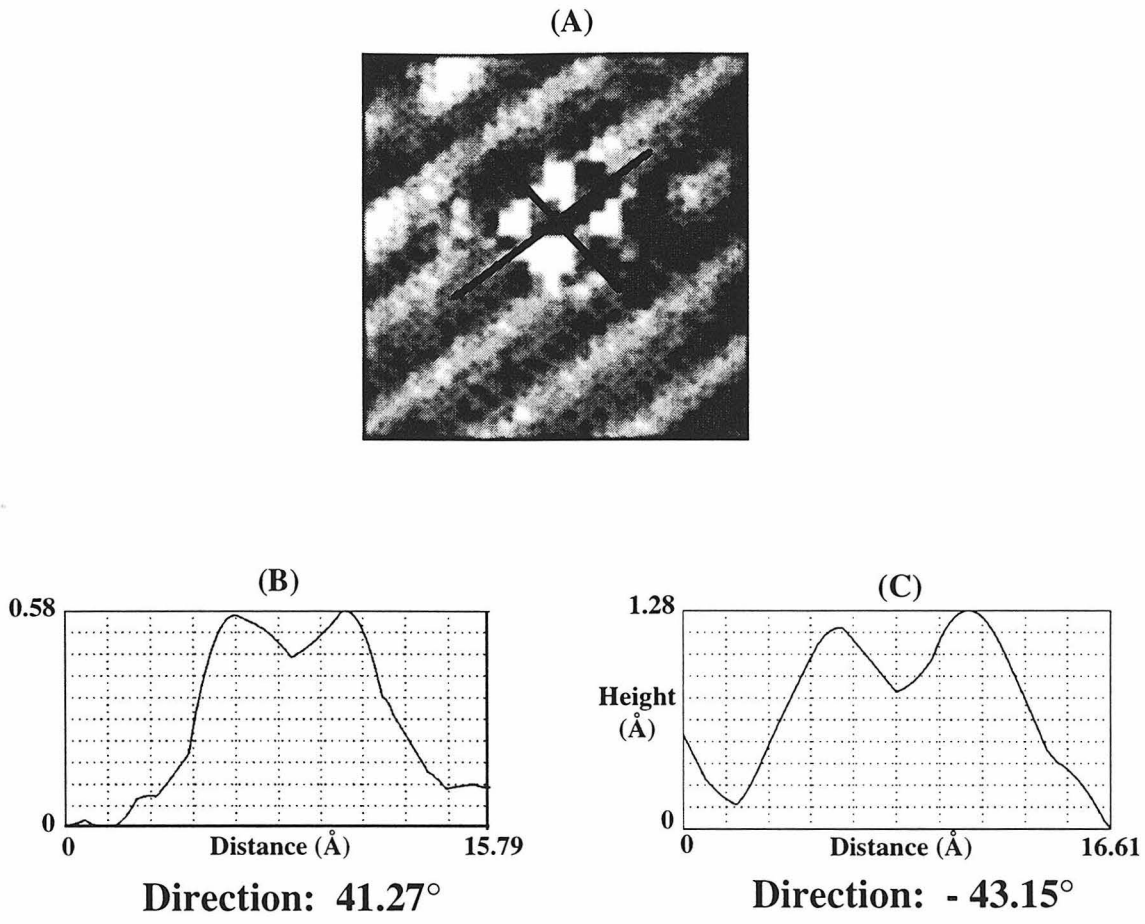


**Figure 4.14:** (A) A close-up image of an individual $(CH_3O)_8Si_8O_{12}$ and the surrounding Si (100) surface. The molecule has the expected four-fold symmetry, is aligned along the direction of the dimer rows, and appears to be bridging two of the rows. (B) and (C) are line scans taken parallel and perpendicular to the dimer rows as indicated on figure (A). The relatively short apparent height of the molecule is likely because $(CH_3O)_8Si_8O_{12}$ is an insulating molecule.

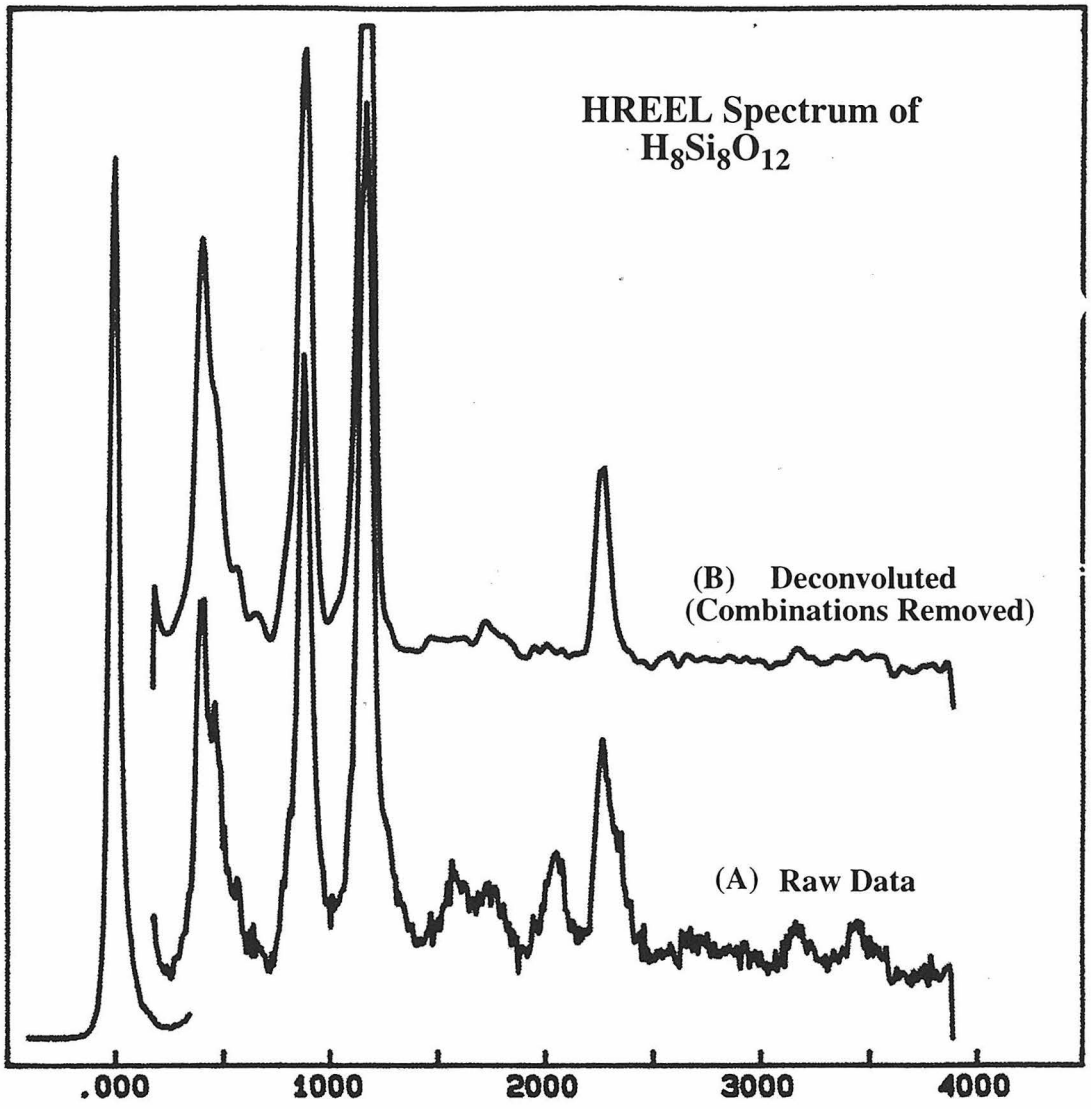


**Figure 4.15:** HREEL Spectrum from a 2 L dose of $H_8Si_8O_{12}$ onto Si (100) - (2x1) surface at 90K. See Table 4.1 for an assignment and listing of the vibrational modes.

| $H_8Si_8O_{12}$/Si(100) | $H_8Si_8O_{12}$/Si(100) | $H_8Si_8O_{12}$ | |
|---|---|---|---|
| Low Coverage | High Coverage | | |
| HREELS | HREELS | FTIR | Vibrational Mode |
| 404 | 404 | 399 | δ (O-Si-O) |
| 465 | 464 | 465 | ν (Si-O) |
| 576 | 568 | 566 | δ (O-Si-O) |
| 675 | 679 | | ν (Si-O)[a] |
| 886 | 877 | 881 | δ (O-Si-H) |
| 1153 | 1170 | 1140 | ν (Si-O) |
| 2263 | 2271 | 2276 | ν (Si-H) |
| 2917 | | | ν (C-H)[b] |

a. For the bulk compound this mode is not IR active. There is, however, a Raman ν (Si-O) active mode at 697 $cm^{-1}$.

b. The C-H stretch is due to hydrocarbon contamination.

**Table 4.1:** Comparison of the vibrational modes of $H_8Si_8O_{12}$ adsorbed on the Si (100) - (2x1) reconstructed surface obtained by high resolution electron energy loss spectroscopy (HREELS) with the vibrational modes of the molecular solid obtained by FTIR. Low and high coverage refer to 0.3 L and 2.0 L doses respectively.

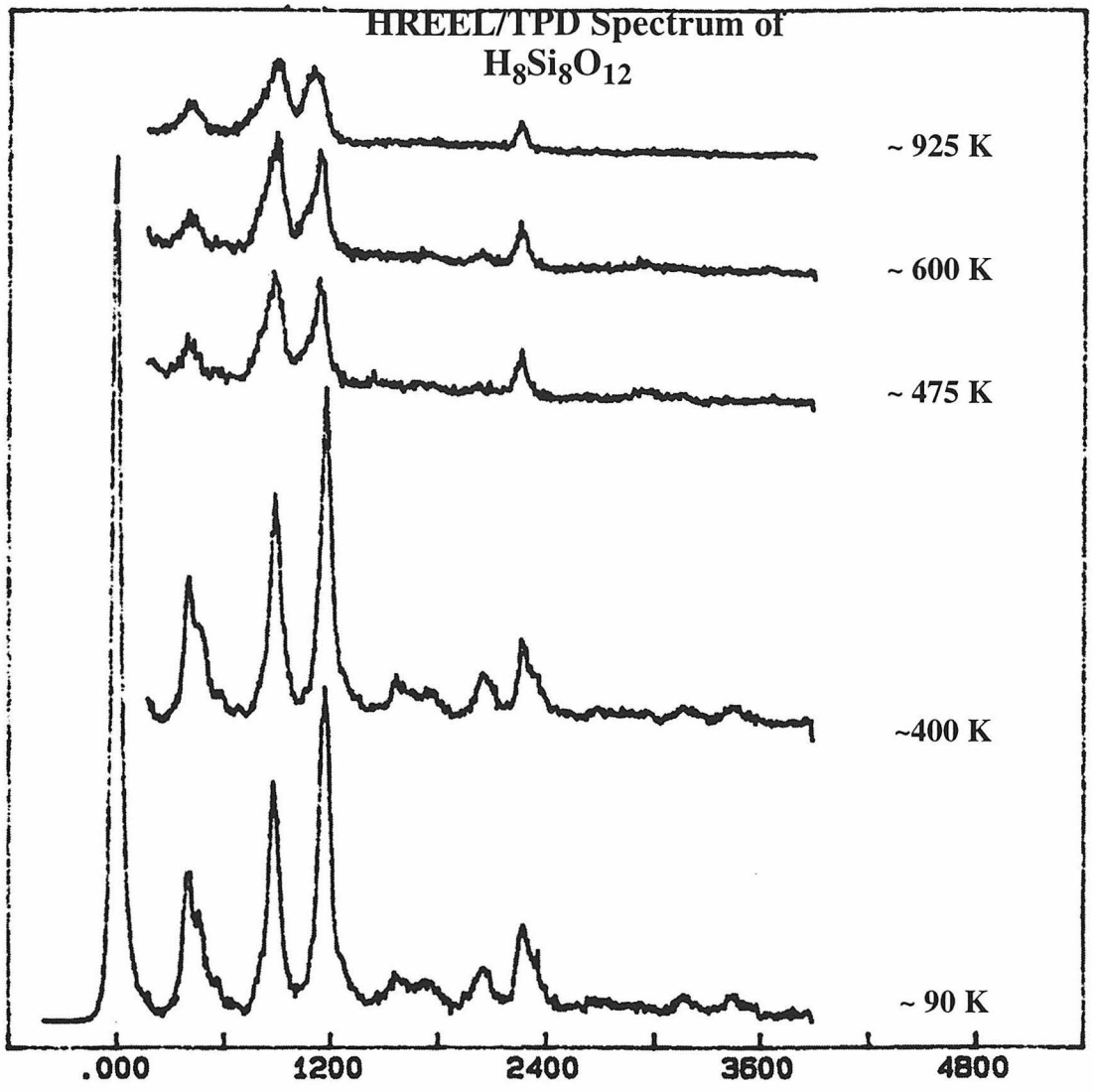


**Figure 4.16:** HREELS/TPD experiment for a 2 L dose of $H_8Si_8O_{12}$ onto Si (100) - (2x1) surface.

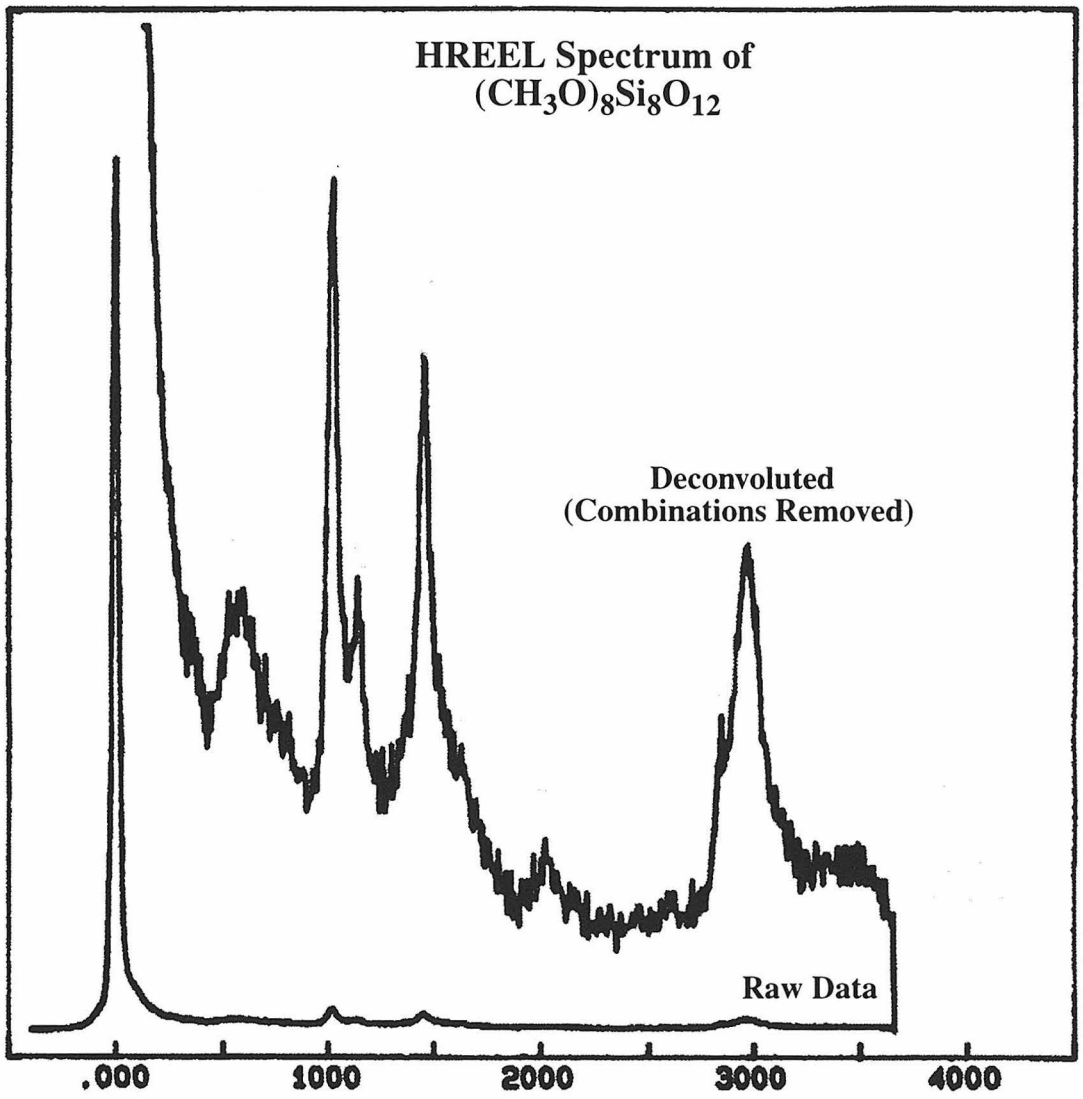


**Figure 4.17:** HREEL Spectrum from a 6 L dose of $(CH_3O)_8Si_8O_{12}$ on Si (100) - (2x1) at 120 K. See Table 4.2 for an assignment and listing of the vibrational modes.

| $(CH_3O)Si_8O_{12}$ (Low Coverage) | $(CH_3O)Si_8O_{12}$ (High Coverage) | $(CH_3O)Si_8O_{12}$ FTIR | $(CH_3O)$/ Si(111) (HREELS) | Vibrational Mode |
|---|---|---|---|---|
| 280 | | | | δ (O-Si-O) |
| | | 464 | | ν (Si-O) |
| 540 | 575 | 569 | | δ (O-Si-O) |
| | | 731,752 | | δ (Si-O-$CH_3$) |
| | | 788 | 775 | ν (Si-$OCH_3$) |
| | | 844 | | δ (O-Si-$OCH_3$) |
| | | 886 | | δ (O-Si-H) |
| 1025 | 1020 | 1084 | 1070 | ν (C-O) |
| 1145 | 1180 | 1154 | 1170 | $CH_3$ Rock |
| 1455 | 1460 | 1471 | 1452 | δ $CH_3$ |
| (1630) | 1605 | | | ??? |
| 2025 | 2050 | 2260 | | ν (Si-H) |
| 2845 | 2850 | 2858 | 2883 | ν ($CH_3$) sym. |
| 2970 | 2955 | 2957 | 2950 | ν ($CH_3$) asym. |

**Table 4.2:** Assignment of HREEL Spectra of $(CH_3O)_8Si_8O_{12}$ on Si (100) reconstructed surface. Low and high coverage refer to 6 L and 12 L doses respectively.

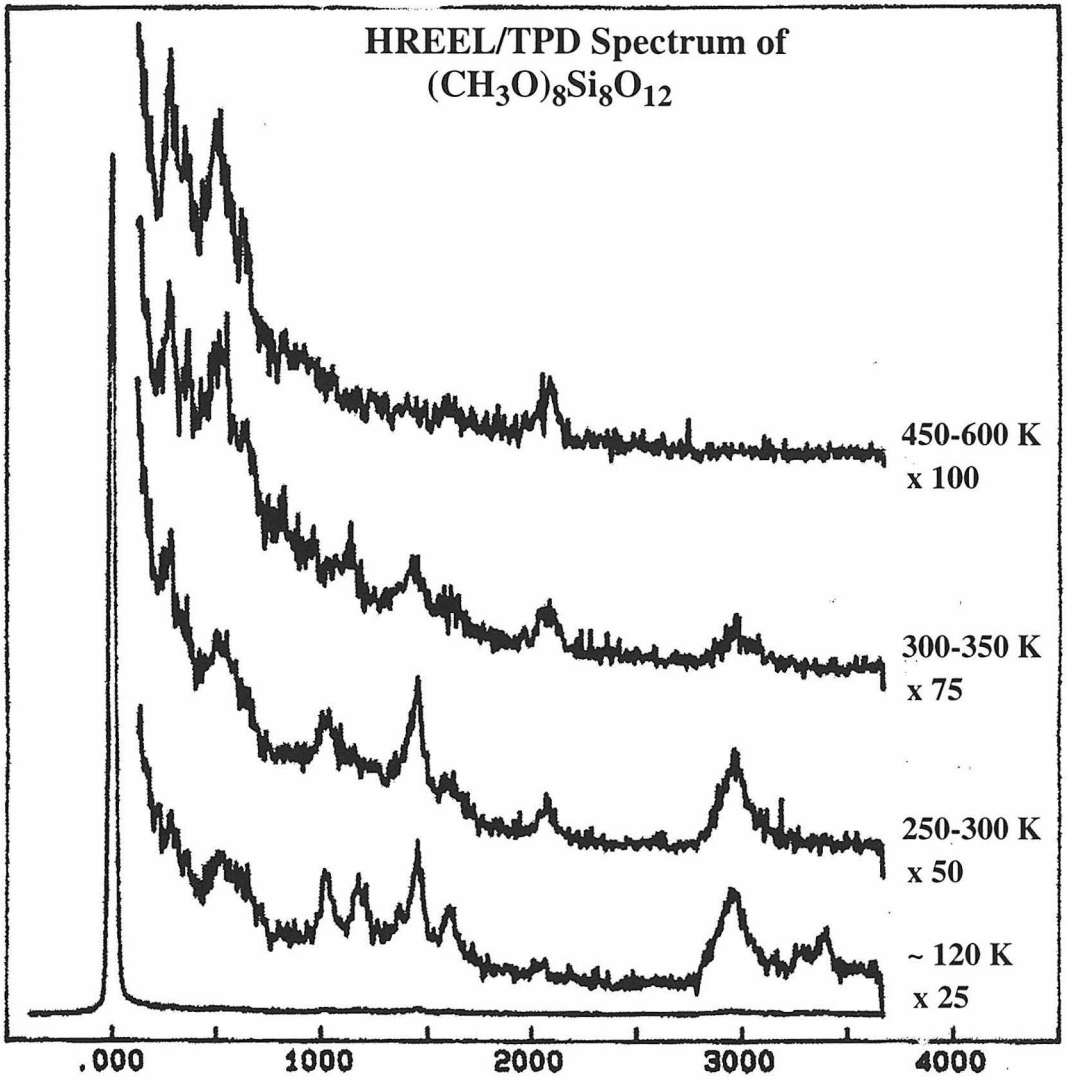


**Figure 4.18:** HREELS/TPD experiment for a 6 L dose of $(CH_3O)_8Si_8O_{12}$ onto a Si (100) - (2x1) surface.

# *Section II:*

## *A New Method of Using SC-Cut Quartz Oscillators for Chemical Sensing*

# *Chapter 5:*

# *Quartz Oscillator Based Sensors: Introduction and Background*

## *5.1. Introduction and Background*

There is much current interest in developing new techniques for chemical sensing, both in continuous monitoring of chemical environments, as well as for the detection of hazardous or illegal substances such as explosives or illegal drugs. If anything, the motivation to pursue new avenues of research in this field is growing in the aftermath of the downing of Pan Am Flight 103, the bombing of the federal building in Oklahoma City, and the legacy of the UNABOMBER. There are a number of techniques currently available for chemical sensing, both for environmental sensing and explosive/drug detection; however, these techniques tend to involve large, cumbersome equipment which has very high power consumption, and a correspondingly high price tag. As a result, they are typically used only when there is an overriding factor, such as airline safety, and even then many of the most powerful detection techniques are not yet in use because of their high cost, low throughput, and/or inconvenient size. For this reason, there has been a movement toward the use of microsensors, such as those based on quartz resonators, as possible alternatives to traditional sensor techniques. A few of the properties one might envision for an ideal sensor include a small, light weight, low power device that is robust, highly sensitive, highly selective, with a fast response and no hysteresis effects. Quartz resonator based microsensors have become popular not only because of their small size and high sensitivity, but other characteristics such as their ruggedness, fast response, and low power consumption. Moreover, new fabrication techniques have made quartz resonator microsensors extremely cost effective compared to traditional techniques. The primary limitation to their widespread application lies in their generally low selectivity in most applications.

The history of quartz resonator based sensors can be traced back to the discovery of piezoelectricity by Pierre and Jacques Curie in 1880[1]. They noted that certain crystals, including quartz, rochelle salt and tourmaline, afford an electric potential difference when a mechanical stress is applied to them. Shortly thereafter, they verified that the converse also holds true, that application of an electric field produces a corresponding mechanical strain in the material. It is this coupling of electrical and mechanical responses of piezoelectric materials which make them useful in sensor applications. Quartz has become the material of choice for resonator applications because of its high chemical and mechanical stability, high quality factor, and relatively high electromechanical coupling factor. In fact, because they vibrate with minimal energy dissipation, quartz crystals are nearly ideal oscillators and have found wide spread use in frequency control, filter circuits, and chemical sensing[2-4].

In the 1920's, Cady first demonstrated that the converse piezoelectric effect could be exploited to produce very stable oscillator circuits[5]. By applying an alternating electric field across a piezoelectric substrate, the alternating strain induces the crystal to oscillate at a particular resonant frequency and generates acoustic standing waves. Any changes in the properties of the crystal, due to its chemical or physical environment, perturb the acoustic waves and a new resonant frequency is established. For example, changes in the temperature or pressure (stress) of the crystal can lead to strong changes in the resonant frequency, and applications have been developed which use resonating crystals as temperature sensors[6]. For chemical sensing applications, the actual perturbation of the acoustic wave is usually the result of the sorption of an analyte on the resonator surface. In 1959, Sauerbrey developed the first quartz resonator-based sensors, postulating that the mass of

a foreign material deposited on an AT-cut or BT-cut quartz resonator is directly proportional to the change in the resonant frequency of the plate[2-4]. Moreover, he developed the heuristic whereby the mass of the deposited material can be treated as an extension of the quartz plate itself and used it to resolve mass changes as small as $10^{-10}$ g. Behrendt later demonstrated that it is the change in the period of the oscillation, rather than the frequency, which is proportional to the mass loading, thereby extending the upper limit on mass loading from two to ten percent of the quartz plate mass[7]. Because of their ability to detect such small changes in mass loading, quartz crystal resonators are commonly referred to as Quartz Crystal Microbalances (QCM).

Since it is the sorption of an analyte on the crystal surface which induces a perturbation of the acoustic wave and thereby induces the change in resonant frequency, the interaction of the surface with adsorbates will have a critical effect on the selectivity of the sensor. Thus, it is the fact that the surface of quartz is rather inert chemically that is primarily responsible for the rather low degree of selectivity displayed by most quartz based microsensors. For this reason, quartz resonators used in sensor applications typically have a chemically selective coating applied to the crystal surface. In 1964, King was the first to use a selective coating to improve the selectivity of a chemical sensor[8]. Since that time, a tremendous amount of research has been conducted on selectively coated quartz resonators, both on the traditional Bulk Acoustic Wave (BAW) oscillators, as well as the higher frequency Surface Acoustic Wave (SAW) based devices. However, to date, even the coated quartz resonators have failed to show a high degree of selectivity necessary for many important applications, such as explosives detection. Thus, there is still a need to find new methods to further improve the selectivity of these sensor devices.

Recently, a new class of BAW quartz resonators has been developed based on the New Linear and Stress Compensated Cut (NLSC or SC-cut) crystals. This new resonator was originally designed for use in temperature sensing applications[9]. As a result, it has ultralinear frequency temperature characteristics and is compensated against the effects of electrode induced stresses, as well as thermal transients and hysteresis effects. It turns out that the SC-cut crystals have several strong vibrational modes, one of which, the B-mode, shows the ultralinear temperature response and a strong, negative thermal response coefficient. However, another strong mode, the C-mode, is relatively insensitive to temperature changes over a temperature region from room temperature up to approximately 225°C. By contrast, the most common type of BAW oscillators, the AT-cut crystals, are optimized for use at or near room temperature (0°C to 60°C) and show strong nonlinear responses or "activity dips" outside this region. (See Figure 5.1.) For the first time, the SC-cut based resonators provide the opportunity for highly sensitive mass detection at temperatures above room temperature.

One possible way to improve the selectivity of a quartz based chemical sensor which takes advantage of the ability of SC-cut oscillators to detect small mass changes above room temperature is by applying the experimental technique known as Thermal Programmed Desorption (TPD)[10]. When an adsorbed layer of atoms or molecules is heated, the surface species may desorb. This is because their surface residence time depends exponentially on temperature ($\tau = \tau_0 \exp(\Delta E/RT)$). If the adsorbate is not resupplied from the gas phase, its surface concentration diminishes rapidly with increasing temperature until the surface becomes clean. The desorption temperature (temperature of the maximum in the desorption peak) is a function of the binding energy of the adsorbed spe-

cies. This energy is a characteristic function of the adsorbate and the surface on which it is adsorbed, thus for a given surface, the desorption temperature provides unique information about a given adsorbate and can be used to differentiate between different adsorbates. Thus by combining the TPD technique with an SC-cut resonator based chemical sensor, it should be possible to improve the selectivity of the sensor system. The desorption event can be monitored by the SC-cut oscillator with a high degree of sensitivity, and the temperature of the desorption event will provide unique chemical information about the nature of the desorbing species. Moreover, by using an array of these sensors, each with a different selective coating which should give different desorption temperatures, a unique fingerprint of a given analyte can be produced.

The goal of this project is to design and build an SC-cut quartz crystal-based sensor system and evaluate it as a chemical sensor using the thermal programmed desorption technique. The motivation for this work is to develop a new chemical sensor that shows higher selectivity than traditional microsensor based detection systems while still providing a sensor design that is small, light weight, and sensitive at a lower cost than traditional sensing techniques. The first experiments were aimed at testing the thermal behavior of the SC-cut crystals, coated and uncoated. Next, a variety of chemically selective coating/analyte pairs were studied using the TPD sensor technique to evaluate the performance of the sensing technique.

### *5.1.1. Basic Physics of Quartz Resonators*

One of the most commonly used materials for sensor applications is quartz. The low temperature form of quartz (see Figure 5.2), $\alpha$-quartz which is stable up to 573°C, crystallizes in the trigonal trapezoidal class, thus it has a three-fold axis of symmetry along

its optic axis, and as a result is non-centro-symmetric[11]. Because of this, a simple model[12] can be employed to characterize this material as a series of small dipoles that have a net positive dipole moment, as shown in Figure 5.3.a. The application of an electric field to these dipoles creates a torque on them, as shown in Figure 5.3.b, inducing a re-orientation of the material resulting in lattice strain and a shear deformation of the material. The direction of the shear depends on the applied potential and the extent of the shear strain depends on the magnitude of the applied potential. By carefully controlling the orientation of the cut of the crystal with respect to its optic axis, and hence, the orientation of the dipole moment, crystal oscillators can be produced which give a preferred mode of displacement, such as flexural, face-shear, thickness shear, torsional, or extensional[6].

The most common form of quartz crystal oscillators, the AT-cut crystal, is made by cutting a quartz rod at an angle of 35.25 degrees with respect to its optic axis. The resulting crystal moves in a thickness shear displacement mode. The resonator used in most of this work is the more recently developed NLSC or SC-cut crystal. It is made by cutting a quartz rod along the plane described in the IEEE doubly rotated plane notation as (ZYtl) $\phi = 9.96° / \theta = 112.70°$. This results in an oscillator which has three primary thickness-vibrational modes. Of these three, two are significantly stronger, the B and C modes mentioned earlier, with the B mode having the sensitive, ultralinear response to temperature changes, and the C-mode being relatively insensitive to temperature changes up to 225°C.

By applying an alternating field across the face of one of these crystals, a shear displacement is induced that has a frequency of oscillation which is equal to that of the applied electric field. The resulting shear wave can be described as an acoustic wave which propagates perpendicular to the direction of motion. Since the oscillatory wave

propagates across the body of the crystals, this class of quartz oscillators is commonly referred to as *bulk acoustic wave* (BAW) oscillators. There is another class of quartz based resonators commonly used in sensor applications, where the oscillation is confined almost entirely to the surface layer of the crystal, the *surface acoustic wave* (SAW) oscillators.

The resonance behavior (harmonic motion) of a quartz resonator is mathematically very similar to the case of a vibrating string, swinging pendulum, or mass on a spring. The amplitude of the oscillation is defined by the energy initially imparted to the system, whereas the resonant frequencies are determined by physical characteristics of the system, such as mass and length. If we model the oscillator as a damped spring which has an inertial mass M, mechanical energy damping r, and spring compliance $C_m$, where $C_m$ is the reciprocal of Hooke's constant, we produce a system which accounts for the dissipation and storage of mechanical energy in a resonator. (See Figure 5.4.a.) The constitutive equation for this system is:

$$\mathbf{M}\left(\frac{\mathbf{d}^2\mathbf{x}}{\mathbf{dt}^2}\right) + \mathbf{r}\left(\frac{\mathbf{dx}}{\mathbf{dt}}\right) + \left(\frac{1}{\mathbf{C_m}}\right)\mathbf{x} = \mathbf{F} \qquad (1)$$

Inspection of this system reveals the correspondence between resistance and the mechanical damping constant r, mass and electrical inductance L, and $1/C_m$ with the reciprocal of capacitance, 1/C. By replacing displacement, x, with electric charge, q, and the applied force, F, with an applied voltage, V, the corresponding equation for the electrical system becomes:

$$L_1\left(\frac{d^2q}{dt^2}\right) + R_1\left(\frac{dx}{dt}\right) + \left(\frac{q}{C_1}\right) = V \qquad (2)$$

This equation represents the equivalent circuit of a quartz resonator with no external connections. Because of the similarity of this circuit to that of the mechanical oscillator shown in Figure 5.4.a, it is commonly referred to as the *motional branch* of the complete equivalent circuit. By including an additional capacitance in a parallel configuration with respect to the motional branch, the static capacitance, $C_0$, of the electrodes and wires can be taken into account. The resulting complete equivalent circuit is known as the Butterworth-Van Dyke equivalent circuit and is shown in Figure 5.4.b.

The ability to express the mechanical properties of a quartz oscillator in electrical equivalents greatly facilitates their characterization because the values of the equivalent circuit components can be easily determined using network analysis. Thus, a common experiment performed with a quartz resonator is to use an impedance (admittance) analyzer to elucidate the properties of a resonator as well as the interaction of the crystal with any coatings or contacting medium. The result is a Nyquist plot[13], whereby the analyzer varies the frequency of the alternating electric field and measures the real and imaginary parts of the admittance at each frequency. The mathematical form of this plot can be derived by applying Kirchoff's rules to the Butterworth-Van-Dyke equivalent circuit:

$$G + i\beta = \frac{R_1}{R_1^2 + \left(\omega L_1 + \frac{1}{\omega C_1}\right)^2} + i\left[\omega C_0 - \frac{\omega L_1 + \frac{1}{\omega C_1}}{R_1^2 + \left(\omega L_1 + \frac{1}{\omega C_1}\right)^2}\right] \qquad (3)$$

where G represents the conductance, the real part of the admittance, β represents the susceptance, the imaginary part of the admittance, and ω represents the angular frequency of the alternating voltage. Rearranging and simplifying this equation gives:

$$\left(\mathbf{G} - \frac{1}{2\mathbf{R}_1}\right)^2 + \left(\beta - \omega\mathbf{C}_0\right)^2 = \left(\frac{1}{2\mathbf{R}_1}\right)^2 \qquad (4)$$

A plot of this equation in conductance-susceptance space (see Figure 5.5) is a circle, and is referred to as the admittance circle.

There are several important features of the admittance circle which are labeled in Figure 5.5. The frequency labeled $f_{Ymax}$ corresponds to the frequency where the amplitude of the oscillation is at a maximum. $f_{Gmax}$ corresponds to the intrinsic oscillatory properties of the crystal since it corresponds to the motional branch of the equivalent circuit. At a higher frequency than $f_{Gmax}$, the susceptance vanishes at a frequency of $f_s$. This is the frequency many resonator drivers operate at, hence it has been called the "series" resonant frequency. At an even higher frequency, the susceptance again vanishes at $f_p$, or the "parallel" resonant frequency. This is very close to the frequency of absolute minimum admittance or $f_{Ymin}$. Because the resonant frequency derived from a mechanical model most closely corresponds to the frequency of minimum absolute admittance, $f_{Ymin}$ is very important in the evaluation of such models[14].

## 5.2. *Experimental Design and Setup*

In order to test the validity of the TPD sensor technique, a suitable test and data acquisition system is needed to be developed to carry out the experiments. At the heart of the experiments was the SC-cut quartz resonator. SC-cut crystals were obtained from Colorado Crystal Corporation, 0.425 in. blank diameter with a HC27/u holder designed to withstand up to 500°C. In order to heat the crystal for the TPD experiment, a stainless steel chamber was manufactured to fit over the crystal. (See Figure 5.6.) Ni-Cr (80-20) resistance wire was wrapped around the chamber to serve as a heating element. The wire was imbedded in a high temperature cement (Omegabond 600) in order to provide more uniform heating of the chamber as well as to insulate the heater. Gas inlet and outlet tubes were incorporated into the chamber to allow introduction of the analyte in a suitable carrier gas as well as removal of the desorbed species during the TPD experiments.

The crystal/heating chamber along with a suitable electronic driver circuit, described in detail in Section 5.2.1., were incorporated into a test system controlled by a Macintosh Quadra 950 using a control and data acquisition system written using the LabVIEW program development system. This system will be described in Section 5.3. Heating of the test chamber was accomplished by the application of a DC voltage supplied by a Variac variable transformer. The Variac was in turn controlled by an Omega CN 3202 temperature controller which controlled the heating ramp during the TPD experiments using a PID control algorithm. Power was supplied to the oscillating crystal and circuit using a Hewlett Packard 3620A dual output DC power supply. The frequencies of the two vibrational modes of interest were monitored using a Hewlett Packard 5685A frequency counter which was interfaced to the macintosh and LabVIEW over a GPIB interface. A

visual display of the behavior of the two modes was obtained using a Tektronix 2246 100MHz dual mode oscilloscope.

Non-gaseous analytes were introduced to the vapor phase using a jacketed glass saturator packed with Chromosorb 102 (80/100 mesh) and the analyte of interest. The partial pressure of the analyte was controlled via the saturator temperature as well as the introduction of a dilution gas flow. Carrier gas flows through the saturator as well as the dilution gas flow were controlled using Brooks 5850E mass flow controllers. Instantaneous introduction of the analyte flow was achieved by the use of a VICI style six-way valve which initiated or terminated gas flow through the saturator loop while maintaining constant total flow of the carrier gas through the system. Once the carrier gas has passed through the crystal chamber, delivering the analyte for adsorption or sweeping away the desorbed species during a TPD experiment, the gas was introduced into a VTI AV-2900 magnetic sector mass spectrometer system. This provided a second method to monitor the amount of analyte introduced for adsorption as well as a way to verify the identity of species as they desorbed. The VTI mass spectrometer was controlled using a Dell computing PC with a pentium processor and Aero Vac software.

Data acquisition and control output signals were accomplished using National Instruments equipment designed for use with the LabVIEW system. The Quadra 950 was equipped with NB-MIO-16X and NB-AO6 analog to digital conversion boards. Signals to and from these boards were passed through a SCXI 1000 signal conditioning unit equipped with two SCXI 1120 multichannel modules and a SCXI 1180 digital passthrough module. Via this system, data acquisition and control signals were used with the Brooks mass flow controllers, the VICI valve, thermocouples monitoring the saturator

and crystal chamber temperatures, and a dipolar junction used to change the vibrational mode monitored by the oscillator circuit. A schematic diagram of the entire test system can be found in Figure 5.7.

### *5.2.1. Design of the Dual-Mode Oscillator*

One of the more critical aspects of the test system is the design of the dual-mode oscillator for use with the SC-cut crystal. Traditional oscillator circuit design has focused almost exclusively on designs to stabilize oscillation in a quartz resonator at a single desired mode to the exclusion of all others. For this work, however, we need not only to stabilize two different modes of oscillation of the crystal, but to be able to switch between the modes quickly and often without a large delay as the resonator stabilizes on the new mode. Thus, the sustained amplifiers used in the oscillator system must provide regeneration conditions for their respective modes only, while rejecting all other modes and anharmonic tones. In order to assist in the prevention of crosstalk and aid in maintaining oscillation at the desired modes, it was decided to use the first harmonic (fundamental) of one of the modes and to use the third harmonic of the other mode. Because they are separated by a much wider region of frequency space, this helps reduce the chances of oscillation at the wrong mode.

A diagram of the oscillator circuit used for this work can be seen in Figure 5.8. For the third overtone oscillator, the Mecham bridge oscillator was used. This oscillator was chosen because it provides good balance in phase. The partially balanced amplitude can then be corrected by an automatic level control (ALC) circuit. For the fundamental mode oscillator, a Colpitts generator was chosen and preceded by a lumped quarter-wave line. This line inverts the low series resonant impedance of the vibrating crystal to a high

impedance seen by the sustaining amplifier. The motivation for this was once again to help prevent crosstalk between the two circuits. In order to allow computer controlled switching between the two modes, a dipolar relay was incorporated into the circuit and controlled by a digital signal from the control software.

At the time of circuit design and construction, it was unclear exactly what frequency crystal (8 or 10 MHz) and which harmonics combination (1st harmonic of B-mode with 3rd harmonic of C-mode or vice versa) would be the most desirable. As a result, the circuit was assembled to be as flexible as possible with regard to selection of the mode frequencies. Correspondingly, a certain amount of mode stability was sacrificed. In future iterations of the oscillator circuit design, it should be possible to further improve the circuit stability for a given choice of crystal frequency and harmonic pair.

## 5.3. *Data Acquisition and Control System*

The data acquisition and experimental control for all the experiments was accomplished through the use of programs written in the LabVIEW program development system. LabVIEW is different from most program development environments (such as C or UNIX) in that programming is accomplished using a graphical programming language, G, which is used to create programs in a block diagram form, rather than through written lines of code. The programs are called virtual instruments (or VIs) because their appearance and operation mimic actual instruments. However, they are analogous to functions in conventional programming languages in that they have both an active user interface (front panel) and a source code equivalent (block diagram) which can accept input from higher level VIs. Moreover, a VI or program written to control a single instrument can be included as a subroutine within another VI as part of a complete control system. Another major difference between LabVIEW and other programming environments is that it takes advantage of *data flow processing*. In a traditional programming environment, the timing of the execution of a particular instruction or line of code is determined by its particular location in the overall instruction set of the program. In LabVIEW, it makes no difference where a particular instruction is in the program or block diagram or in what order it was added to the program. Instead, the instruction executes when all the input data requirements for that particular instruction have been satisfied. Thus, when examining a program written in LabVIEW, the most important thing to understanding the operation of the program is to study the interconnections (wires) between the individual instructions rather than looking right to left and top to bottom.

There are two primary programs which were used in these experiments, one for

monitoring the crystal during the coating process and another one for use during the TPD experiments. The program used while coating the crystal was called Dual Frequency Switch. It allowed for monitoring the frequency change of both modes during the coating process. It had a manual control for switching between the modes because while the coating was carried out while monitoring the 1st harmonic of the C-mode, it was important to check on the 3rd harmonic of the B-mode to prevent loss of signal. This is explained in detail in Chapter 5. In addition, the front panel allowed control of the input parameters of the 5385A frequency counter. (See Figure 5.9.) The block diagram of the program can be seen in Figure 5.10. The boxes which resemble frames of film are called sequence structures and are used to arrange the order of execution of various commands in the program. The boxes with true/false labels are case structures and are used for conditional commands and instructions. The boxes with an arrow in the lower right corner are while loops and commands inside are carried out as long as the input condition is true. Data from each iteration of the program is concatenated into an array which is written into a file which can be read by a spreadsheet program for further data analysis.

The other program used to carry out the TPD experiments was called Sensor Test 7. The front panel interface for this program provided a real-time display of temperature data from the thermocouples on the crystal heating chamber and in the analyte saturator, and it monitored the frequency response of the two vibrational modes of the crystal. (See Figure 5.11.) Also included were controls for the mass flow controllers and VICI valve to control the flow of the analyte to the crystal. This program was set up to automatically switch between monitoring the two different vibrational modes of interest at a user input switching interval. For the experiments presented here, the switching interval used was

either 5 or 10 data points. The length of time for each interval was also determined by the gate time set for the frequency counter. For a majority of the experiments, a gate time of 0.1 sec was used, which corresponded to a switching time of approximately four or eight seconds.

The block diagram for this program has four major subroutines, as shown in Figure 5.12, labeled as the thermocouple read loop, oscillator circuit switch and frequency loop, MFC (mass flow controller) control loop, and VICI control loop. Examination of the oscillator circuit and frequency loop shows it to be very similar in structure to the Dual Frequency Switch Program shown previously, modified to allow for the automatic switching between the modes. Once again, data is concatenated into an array which is then written to a file for post experimental data analysis.

## *Literature Cited*

(1) Curie, P.; Curie, J. *C. R. Acad. Sci.* **1880**, *91*, 294.

(2) Bottom, V. E. *Introduction to Quartz Crystal Unit Design*; Van Nostrand Reinhold: New York, 1982.

(3) Bahadur, H.; Parshad, R. In *Physical Acoustics*; Mason, W. P.; Thurston, R. N. Eds.; Academic Press: New York, 1982; pp 37-171.

(4) Sauerbrey, G. *Z. Phys.* **1959**, *155*, 206.

(5) Ward, M. D.; Buttry, D. A. *Science* **1990**, *249*, 1000-1007.

(6) Benes, E.; Gröschl, M.; Burger, W.; Schmid, M. *Sensors and Actuators, A* **1995**, *48*, 1-21.

(7) Behrendt, K. H. *J. Vac. Sci. Technol.* **1971**, *8*, 622.

(8) King, W. H. *Anal. Chem.* **1964**, *36*, 1735-1739.

(9) Nakazawa, M.; Ballato, A.; Lukaszek, T. *J. Appl. Phys.* **1986**, *60*, 3765-3771.

(10) Somorjai, G. A. *Introduction to Surface Chemistry and Catalysis*; John Wiley and Sons: New York, 1994.

(11) Mason, W. P. *Piezoelectric Crystals and Their Application to Ultrasonics*; Van Nostrand: New York, 1950.

(12) Buttry, D. A.; Ward, M. D. *Chem. Rev.* **1992**, *92*, 1355-1379.

(13) Stephanopoulos, G. *Chemical Process Control*; Prentice-Hall: Englewood Cliffs, 1984.

(14) Benes, E. *J. Appl. Phys.* **1984**, *56*, 608.

(15) Katz, A. M.S. Thesis; University of Minnesota, 1994.

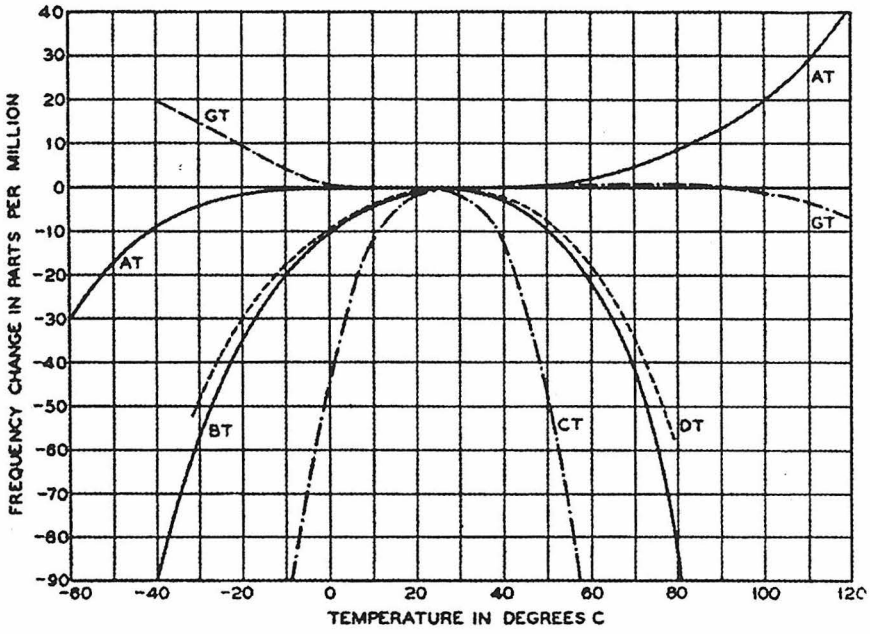


**Figure 5.1:** Temperature frequency characteristics of zero temperature coefficient quartz crystals. Adapted from Mason[11].

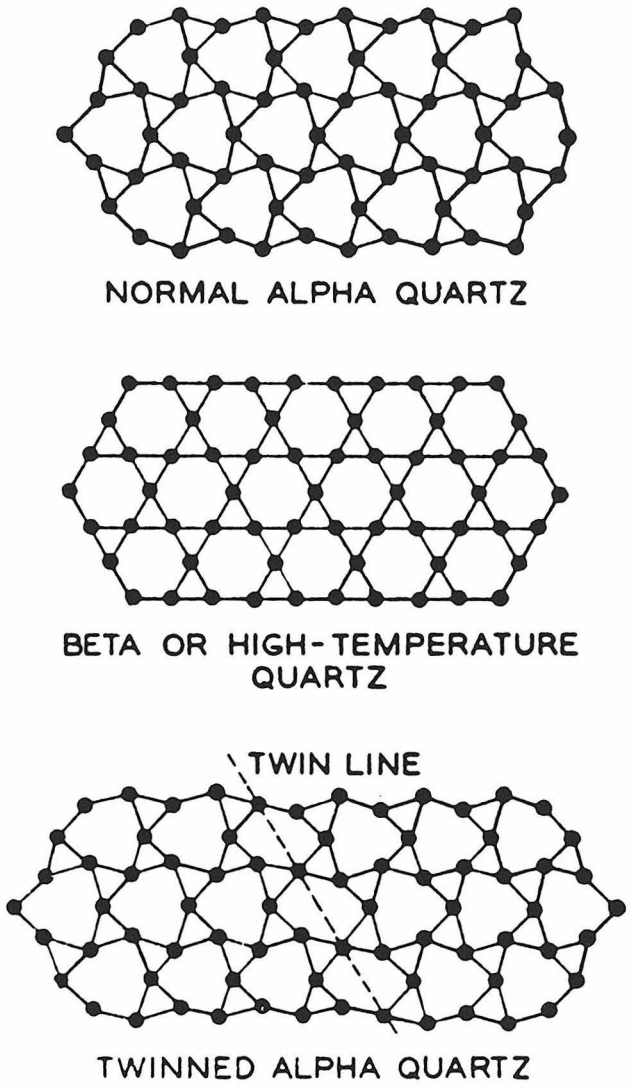


**Figure 5.2:** Schematic diagram of the arrangement of silicon atoms along the optical axis in the most common forms of quartz. α-Quartz is the low temperature phase and is stable up to 573°C; above 573°C, a rearrangement occurs to the hexagonal arrangement shown, known as β-Quartz; if there is a defect or intergrowth of the two forms, the quartz is said to be "twinned." Adapted from Mason[11].

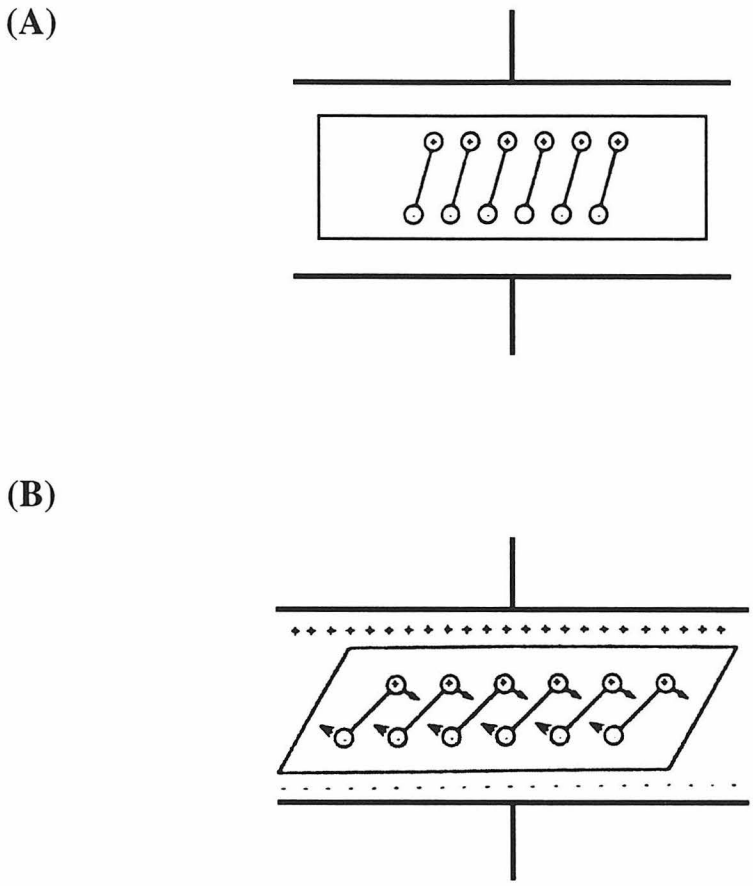


**Figure 5.3:** Schematic representation of a quartz crystal undergoing the converse piezoelectric effect. Application of an electric field causes a reorientation of the dipoles in the material, resulting in lattice strain and a shear deformation of the material. Adapted from Buttry[12].

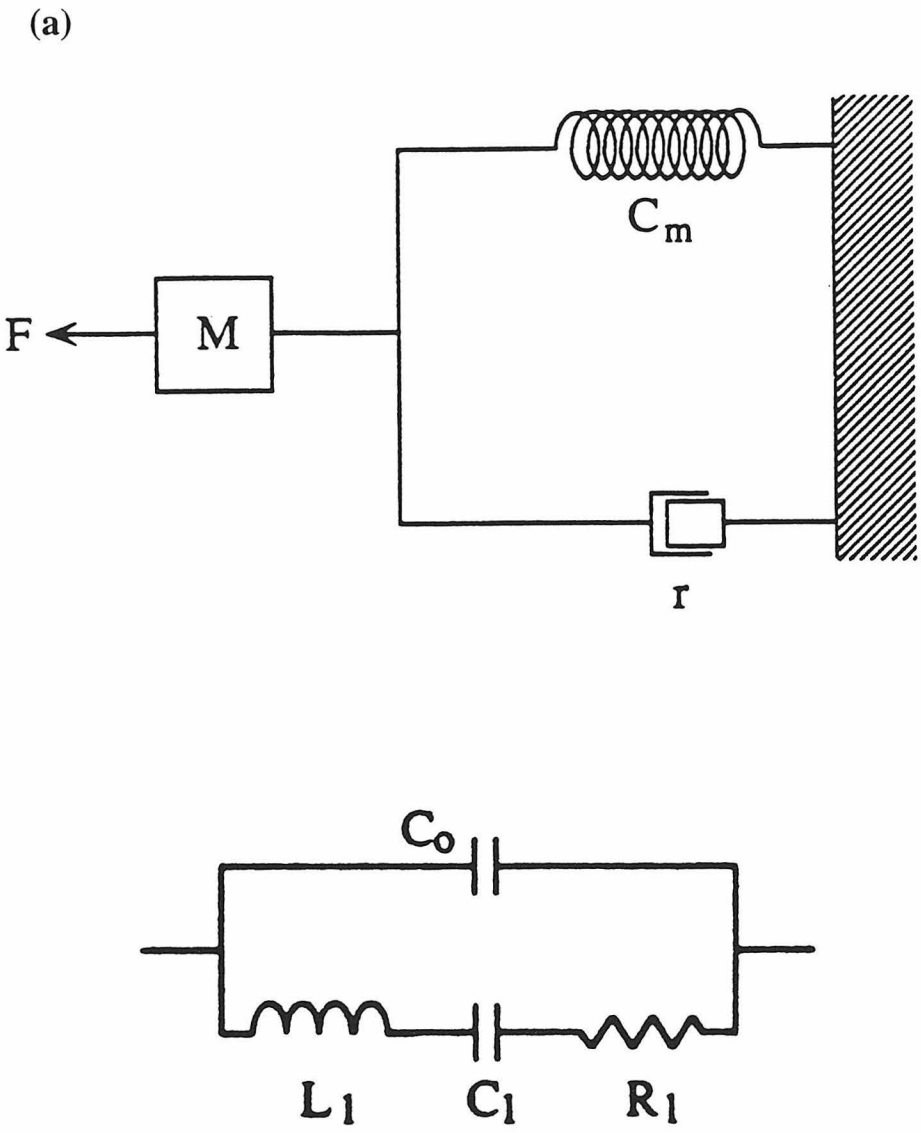


**Figure 5.4:** (a) The mechanical model of an electroacoustical system; (b) the corresponding electrical equivalent, a Butterworth-Van Dyke equivalent circuit. Adapted from Katz[15].

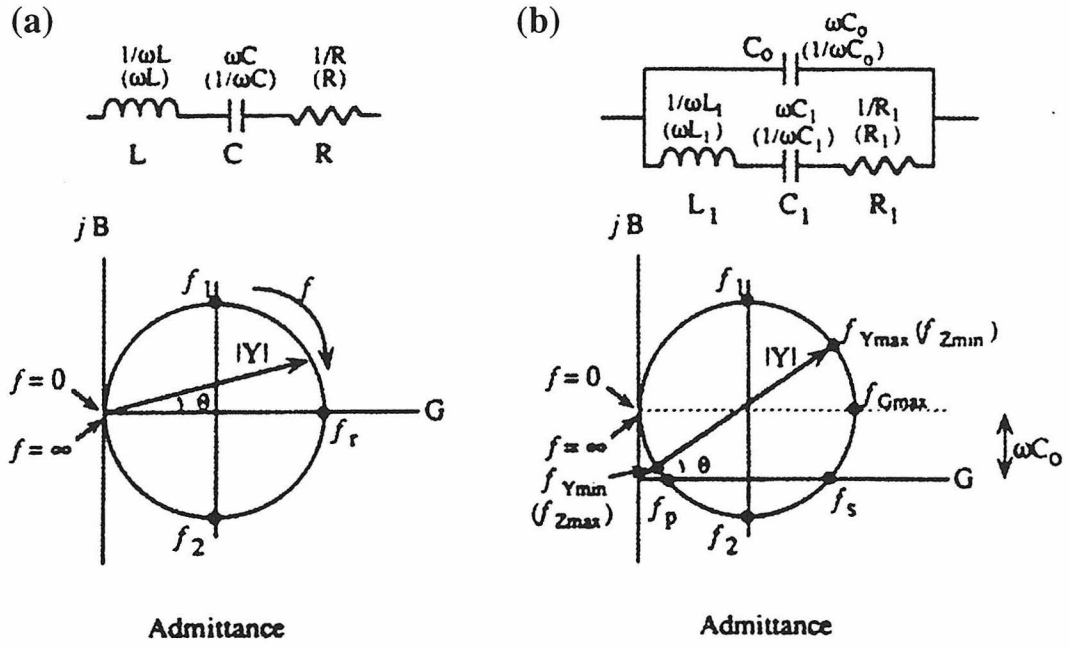


**Figure 5.5:** Nyquist plots showing the admittance circle for (a) the motional branch of an electroacoustic circuit and (b) the Butterworth-Van Dyke equivalent circuit. The significant frequencies are labeled: $f_1$ and $f_2$ are the frequencies of maximum and minimum susceptance, $f_{Ymax}$ and $f_{Ymin}$ are the frequencies of maximum and minimum admittance, $f_{Gmax}$ is the frequency of maximum conductance. The admittance circle for the Butterworth-Van Dyke equivalent circuit is raised above the x axis by $\omega C_0$ compared to that for the motional branch because of the dielectric capacitance of the quartz crystal. This results in two resonant frequencies, $f_s$ (series resonance) and $f_p$ (parallel resonance). Adapted from Buttry[12].

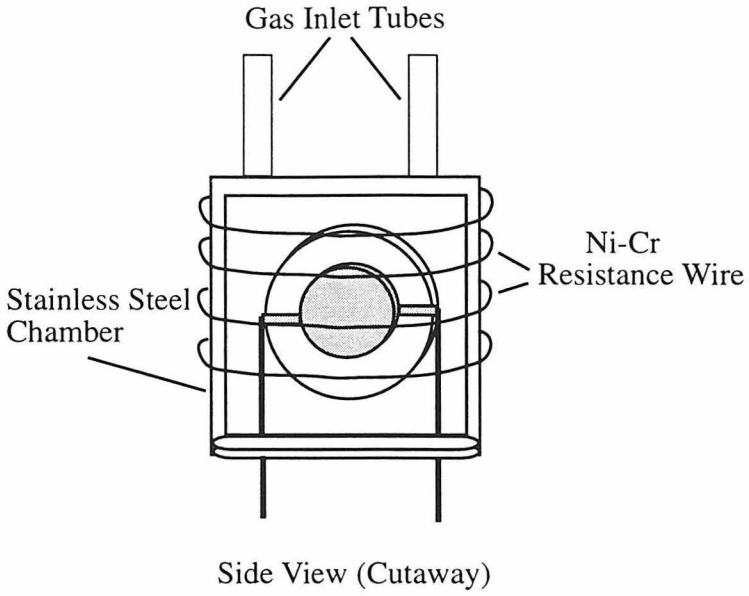


**Figure 5.6:** Schematic diagram of the heating chamber used for the TPD sensor experiments. The heating element was a piece of Ni-Cr (80-20) resistance wire wrapped around the body of the chamber and to which a DC voltage was applied. The resistance wire was imbedded in a high temperature cement (Omegabond 600) to help produce more uniform heating and to insulate the heater wire.

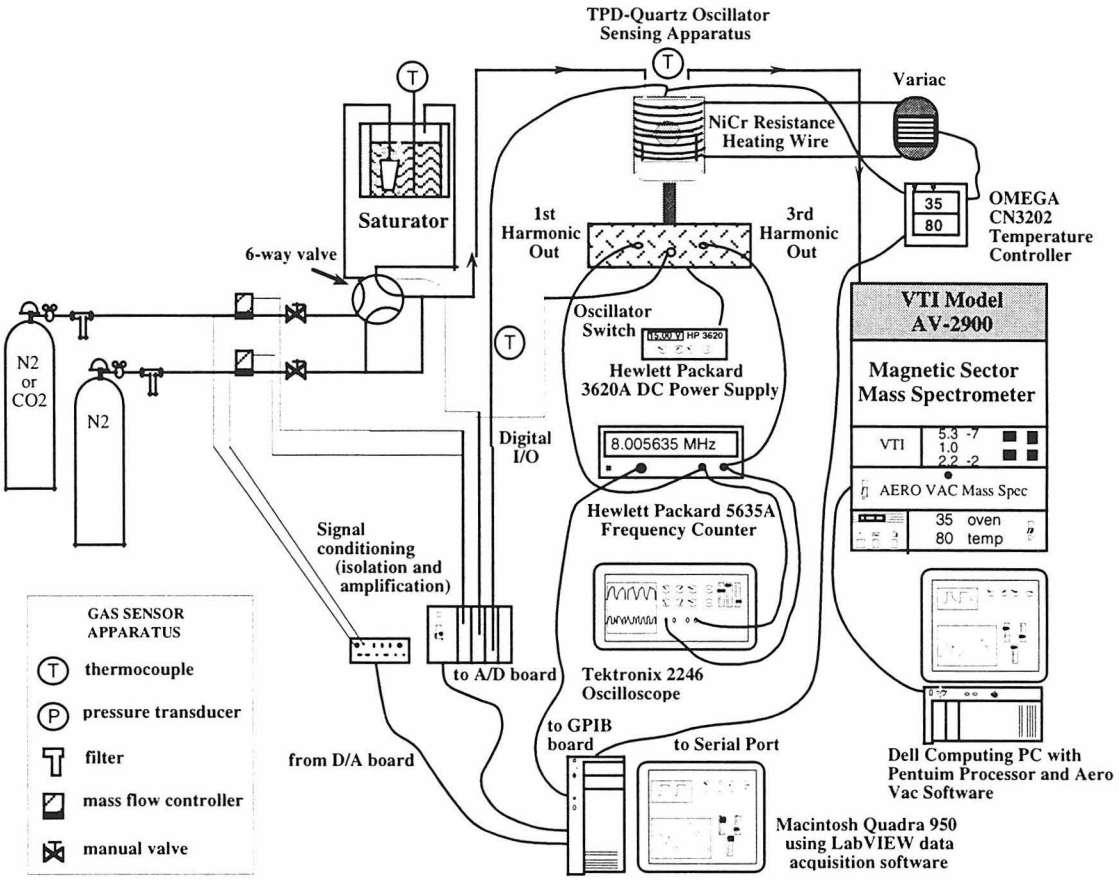


**Figure 5.7:** Schematic diagram of the test system for the TPD/Quartz oscillator based chemical sensor.

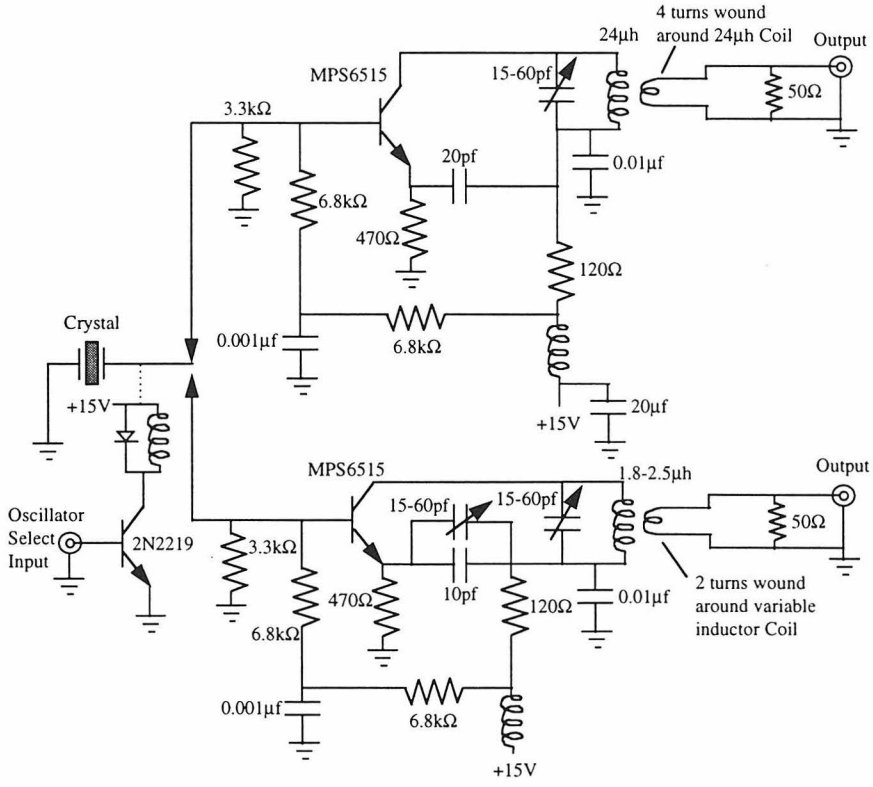


**Figure 5.8:** Diagram of the circuit used with the quartz crystal oscillator. The circuit is designed for monitoring two modes of the crystal, the first harmonic, or fundamental, of the C-mode, and the third harmonic of the B-mode. Which branch of the circuit is operational, and correspondingly, which of the modes is being monitored is determined through the use of a dipolar junction, which is controlled by a digital signal from the LABVIEW control program.

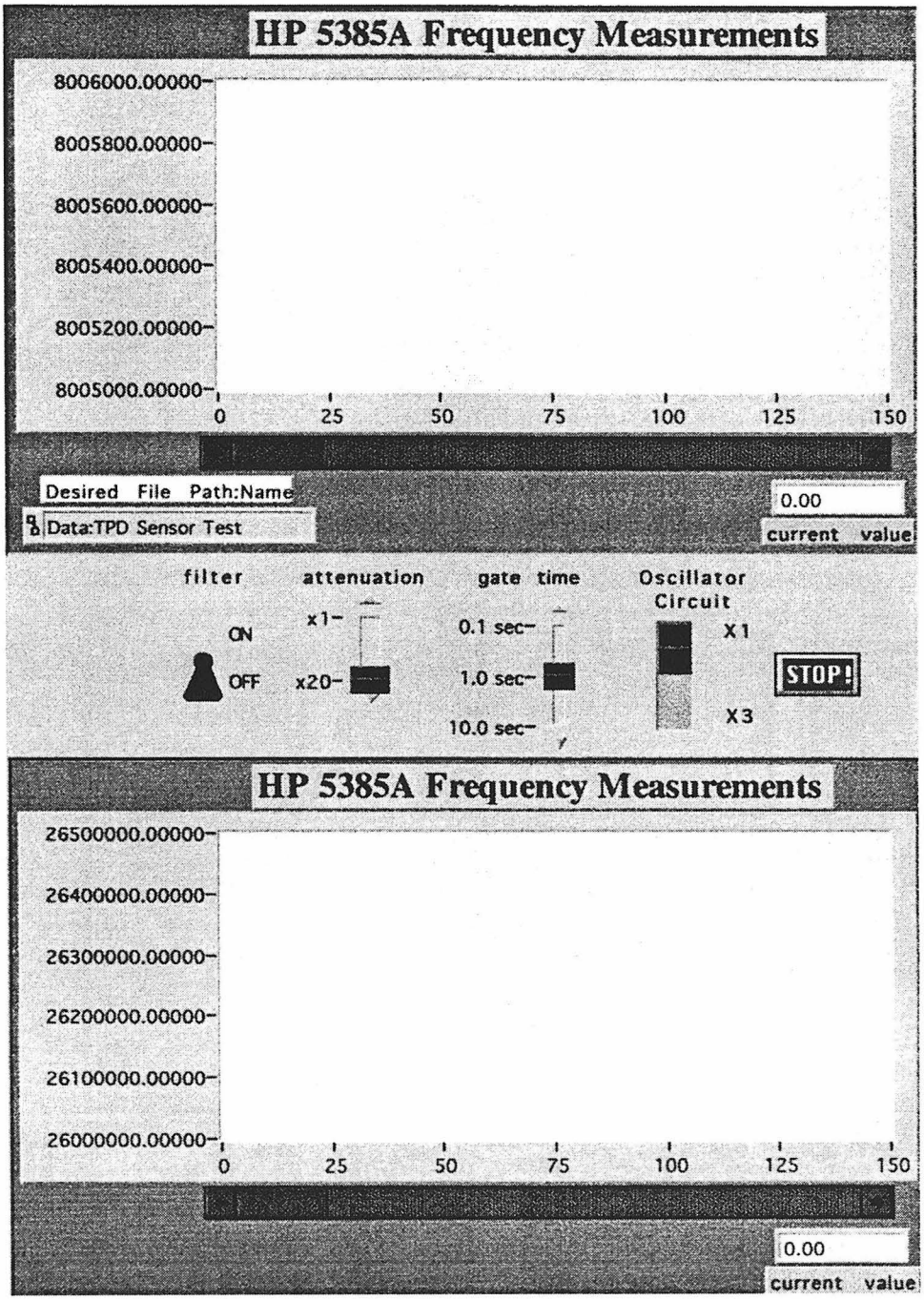


**Figure 5.9:** Front panel of the LabVIEW program Dual Frequency Switch. This program is used to monitor the crystal while the chemically selective coating is applied. Monitoring of the two modes is accomplished by manually switching between the modes.

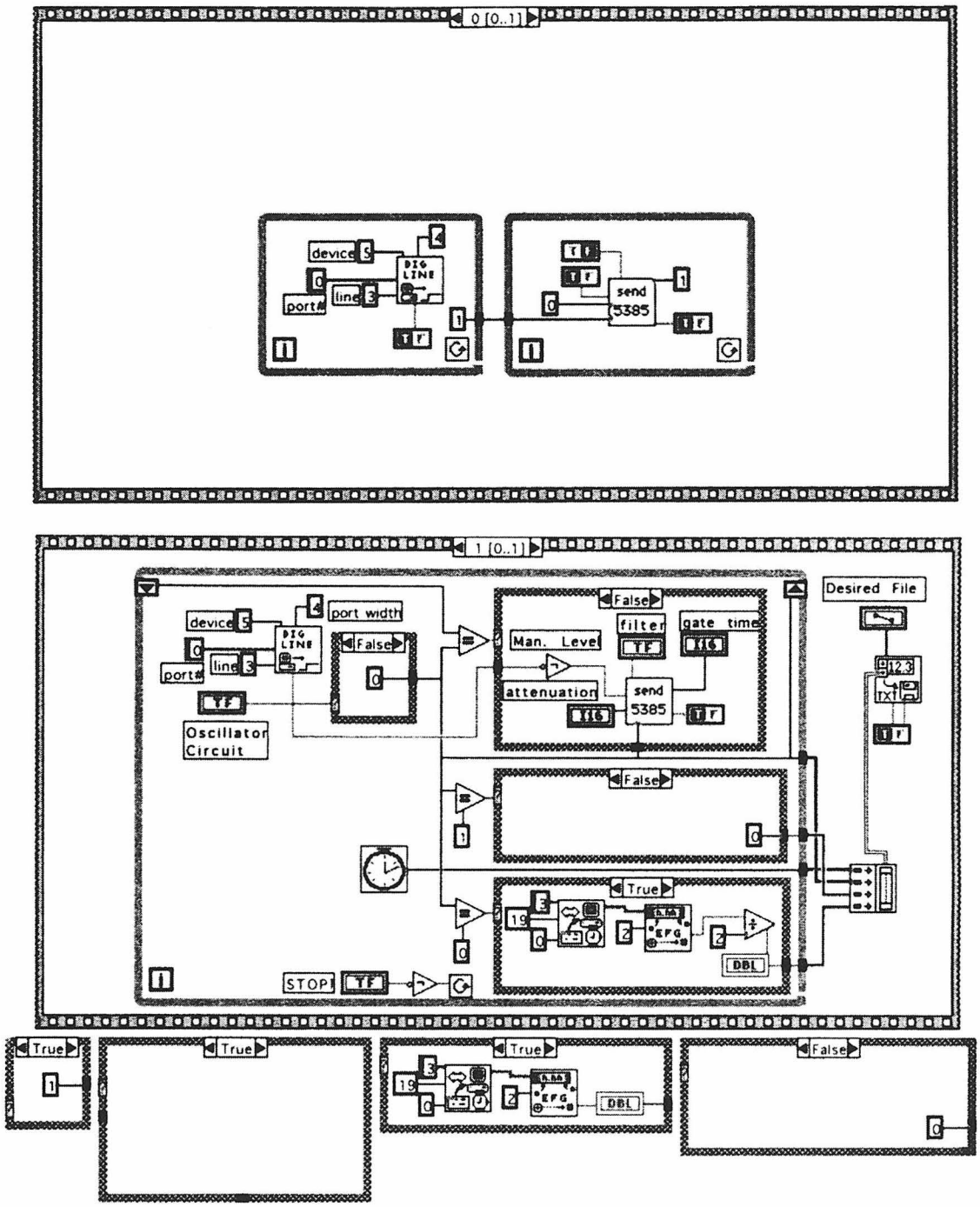


**Figure 5.10:** Block diagram for the LabVIEW program Dual Frequency Switch.

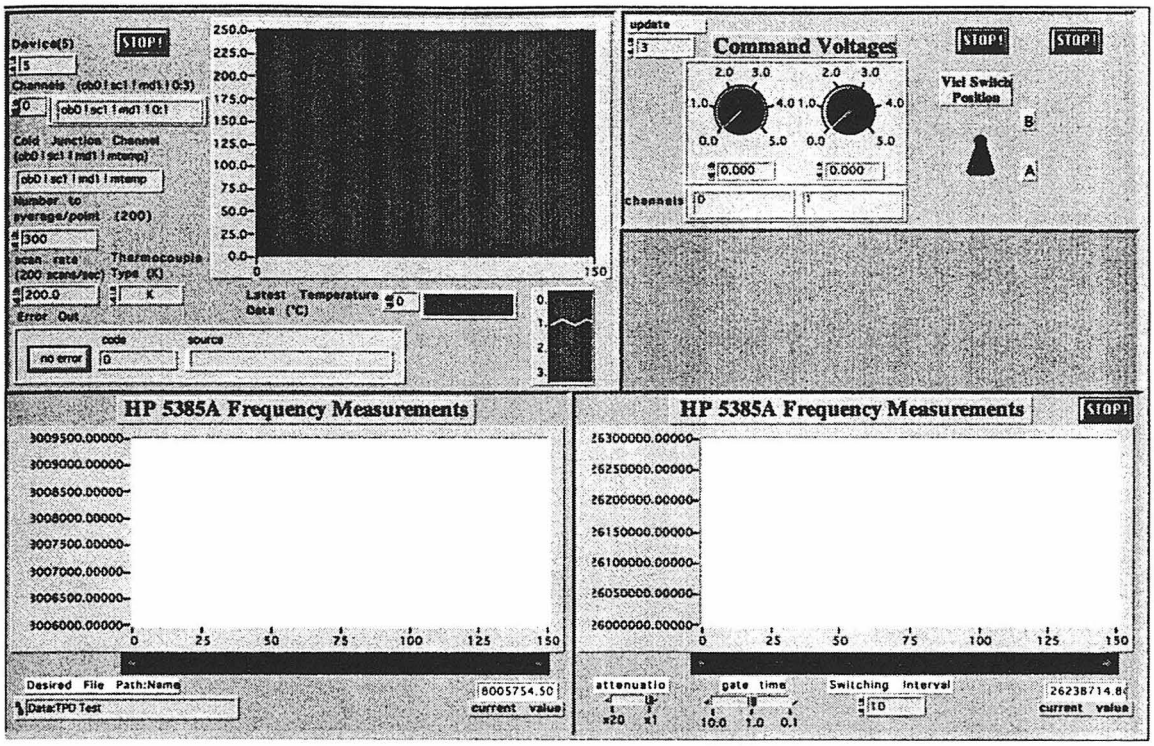


**Figure 5.11:** Front panel for the LabVIEW program Sensor Test 7, used for the TPD experiments in this work. This program has real-time display windows which monitor the temperature of the crystal chamber and analyte saturator and frequency displays for the two modes of interest. Controls values for the mass flow controllers and VICI valve are also input in this window.

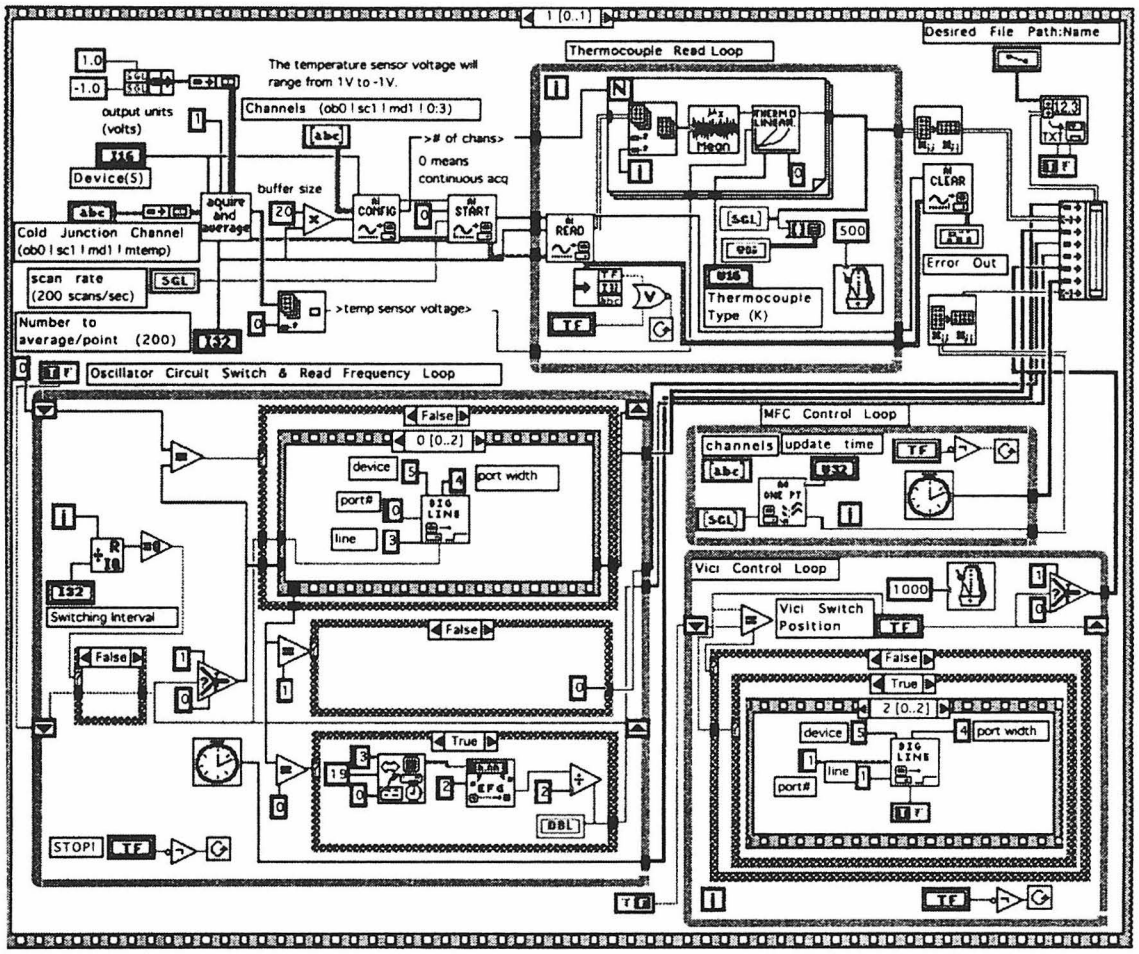


**Figure 5.12:** Partial block diagram for the LabVIEW Program Sensor Test 7. There are four major subroutines in this program: the thermocouple read loop, the oscillator switch and read frequency loop, the mass flow controller control loop, and the VICI valve control loop.

# *Chapter 6:*

# *Chemical Sensing Using Thermal Programmed Desorption*

## 6.1. Introduction

The objective of this work was to develop a new chemical sensor that shows higher selectivity than traditional microsensor-based detection systems, while still providing a sensor design that is small, lightweight, and sensitive at a lower cost than traditional sensing techniques. Such a device could have many applications; e.g., plastic explosives detection. The idea is to provide detectors for explosives which are inexpensive and small enough that they could be used in places currently without such protection, including post offices and company mail rooms for the detection of parcel bombs. Thus, the goal of this project was to design and build a SC-cut quartz crystal based sensor system and evaluate it for chemical sensing when using the thermal programmed desorption technique. Initial design and construction of such a sensor system was presented in the previous chapter. The evaluation of the TPD/quartz oscillator sensing technique involves several steps. The first step is to characterize the behavior of the vibrational modes of the SC-cut crystal, including the temperature response of the uncoated as well as selectively coated crystals. The second step is to coat the SC-cut quartz oscillators with a variety of chemically selective coatings and try to understand the effects the coatings have on the vibrational properties of the crystal modes. The final step is to test the thermal programmed desorption technique on the crystals in a series of single component adsorption/desorption experiments in order to explore the methodology for real chemical sensing.

## *6.2. Evaluation of SC-cut Quartz Oscillator Behavior*

### *6.2.1. Verification of SC-cut Crystal Behavior*

In order to confirm the theoretical behavior of the SC-cut crystals and to determine the frequencies of the B and C vibrational modes, an impedance analyzer was used to characterize the crystal's frequency spectrum. A 10 MHz SC-Cut crystal obtained from Colorado Crystal Corporation was attached to a Schlumberger SI 1260 Impedance Analyzer using the 4 point probe technique. The spectrum was obtained at a constant bias and control voltage while the frequency was swept through the desired range of values. At each point, the real and imaginary parts of the impedance (conductance and susceptance) and total impedance were recorded. The measurement integral used for each data point was one second. Figure 6.1 shows typical results from this analysis, displayed in the "triple plot" format. The three displays include total impedance vs. frequency, phase angle vs. frequency, and the impedance circle or Nyquist plot. Definitions for these values are as follows:

$$\textbf{Total Impedance} \quad |Z| = \sqrt{R^2 + X^2} \qquad (1)$$

$$\textbf{Phase Angle} \quad = \tan^{-1}\left(\frac{X}{R}\right) \qquad (2)$$

where X = susceptance and R = conductance. The impedance plot shows two strong peaks in the spectrum corresponding to the first harmonics of the C- and B-modes. The resonance for the C-mode, corresponding to the minimum impedance which occurs at the leading edge of the peak, is at 10.007669 MHz, with the anti-resonance or maximum

impedance at 10.014053 MHz. The corresponding resonance and anti-resonance values for the B-mode are at 10.960872 MHz and 10.967710 MHz respectively for this crystal. The strength of the peaks in the impedance plot are indicative of the strength of the vibrational modes. Notice that there are some smaller anharmonic peaks in the spectrum as well. The plot of the phase angle versus frequency provides information on the location of $f_{series}$ and $f_{parallel}$ which occur when the phase angle equals zero. The impedance circles in the Nyquist plot are not entirely round because of the step size used in the experiment.

Once the frequency spectrum was characterized and the location of the two modes of interest ascertained, verification of the thermal response behavior of the modes of interest was necessary. A 10 MHz SC-cut crystal was subjected to several cycles of heating and cooling using a manually controlled Variac, and a composite of the results is presented in Figure 6.2. From the graph it is clear that the temperature response of the C-mode and its 3rd harmonic is very small up to around 225°C, whereas the B-mode shows a strong, negative, linear response to temperature as expected. A similar thermal profile was obtained for a 8 MHz SC-cut crystal which had been coated with polystyrene. (See Figure 6.3.) In this case, the crystal was heated from room temperature to 200°C in 45 minutes under a flow of 90 ml/min dry nitrogen. The crystal was allowed to cool naturally in flowing nitrogen to room temperature. Higher temperatures were not explored in order to preserve the integrity of the polymer coating. These profiles show behavior that is qualitatively similar to the uncoated SC-cut crystal. The hysteresis in the 3rd harmonic of the B-mode is due to the fact that the temperature reading was obtained from a thermocouple attached to the heating chamber. This hysteresis was significantly reduced in later experiments by achieving better thermal contact with the stainless steel core of the heating

chamber.

### *6.2.2. Application of Chemically Selective Coatings*

In order for a particular analyte to result in signal that can be discriminated in a TPD experiment, it must be sufficiently strongly adsorbed onto the quartz resonator such that it does not desorb until the crystal has been heated above room temperature. Because of this, combinations of selective coatings and analytes that result in only van der Waals interactions or physical adsorption are unlikely to provide desorption signals that can be discriminated. Rather, coating/analyte pairs resulting in chemical adsorption or hydrogen bonding interactions are necessary for molecular discrimination on the basis of desorption temperature. Since the nature of the chemically selective coating is the primary factor determining the strength of the adsorption interaction, it is the critical factor in determining the success of the TPD sensor experiment.

In this work, a variety of different chemically selective coatings were employed in order to probe the efficacy of the TPD technique. Because one of the primary target applications for this work is for use in plastic explosives detection, a number of the coatings studied were polymers with basic functionalities, primarily amines. The reasoning behind this is the fact that many explosive compounds contain large concentrations of nitrogen, and in particular large numbers of nitro groups. (See Figure 6.4.) Since nitro groups are acidic, they can be expected to adsorb strongly onto coatings with basic functional groups. In addition, selective coatings based on sodium exchanged zeolite Y (NaY) have been explored, using both a silica sol-gel and a colloidal Teflon solution as binders for the zeolite crystals on the surface.

The procedure for the deposition of the chemically selective coating was as fol-

lows: the crystal to be coated was first cleaned by washing with acetone and then sonicating the crystal in an ethanol bath for 10 minutes. While the crystal was being cleaned, a solution or colloidal suspension of the coating of interest was prepared. For the polymers, a 0.2 - 0.5 wt% solution of the polymer in the appropriate solvent, typically methanol or methlyene chloride, was used. For the zeolite Y coating using a Teflon binder, 1 gram of a 1% colloidal Teflon solution was added to 8.96 g of perfluorodecane. After mixing, 0.04 g of sodium exchanged zeolite Y (NaY) heated at 250°C for 8 hours were added to the Teflon solution. The suspension was then ultrasonicated until ready for use. For the silica sol-gel binder, the zeolite-silica suspensions were based on a technique developed by Bein *et al.*[1] A stock solution of tetraethylorthosilicate (TEOS) was made from a mixture of 61 ml of TEOS, 61 ml of ethanol, and 5 ml of 0.04 M hydrochloric acid (HCl). 10 ml of this stock solution were then mixed with 1.0 ml of 0.05 M ammonium hydroxide ($NH_4OH$) to form a silica sol. A 2.5 ml aliquot of this silica sol was added to 5 ml of ethanol to form the final suspension medium. 0.3 g of NaY were added to form the suspension, which was ultrasonicated for 5 minutes before using immediately.

The crystal was then inserted into the oscillator circuit and frequency monitoring of the two modes of interest was begun using the LabVIEW program Dual Frequency Switch. Deposition of the chemically selective coating occurred from an aerosol produced from the previously prepared solution or suspension. An airbrush was used to create the aerosol. An example of the frequency changes that occurred in a typical coating experiment is shown in Figure 6.5. For this experiment, a polyethyleneimine (PEI) coating was applied to an 8 MHz SC-cut crystal. During the deposition, the airbrush was situated approximately 6 inches from the oscillating crystal in order to minimize any effects

on the crystal vibration due to the impact of the aerosol onto the crystal. It was observed that it was possible to cause the crystal to change vibrational modes, for example from the 3rd harmonic of the B-mode at 26.25 MHz to the 3rd harmonic of the C-mode at 23.98 MHz, simply due to the impact of the aerosol on the crystal. The original mode can usually be recovered by switching the oscillator to the 1st harmonic mode and then returning to the third harmonic. The first harmonic modes were considerably more stable with respect to this type of mode change, thus all aerosol deposition took place while monitoring the 1st harmonic mode, with frequent switching to the 3rd harmonic mode to check that oscillation continued at this frequency.

The large transients seen in Figure 6.5 are the result of evaporation of the carrier solvent. The positive transients seen in the 3rd Harmonic of the B-mode are the result of the negative thermal response coefficient of the B-mode. Since evaporation results in cooling of the crystal, the transient change in the frequency of the B-mode is a temporary increase in frequency of the mode, which dominates over the decrease in frequency resulting from the deposited mass. An overall decrease in frequency in the third harmonic mode resulting from the mass of the deposited coating is observed as the crystal returns to equilibrium at room temperature. Deposition continued until the desired amount of selective coating had been deposited.

As indicated earlier, a variety of selective coatings were applied to the crystals. However, there were large differences in the amounts of the particular coatings that could be deposited without causing loss of vibration in one or more of the vibrational modes. For example, coatings such as polyethyleneimine or poly(4-vinylpyridine) could be applied to the crystal up to a frequency change of as much as 10,000 Hz, as measured by

the change in frequency of the C-mode of an 8 MHz crystal, whereas the deposition of a polystyrene coating would cause oscillation to cease after only a 250 Hz change in frequency. In an attempt to understand this result, silicon wafers with gold coated surfaces were prepared by sputtering a layer of gold onto the silicon oxide surface. Selective coatings were then deposited on the gold coated wafers using the airbrush technique. The coated wafers were then dried at 110°C for 10 hours to remove any residual solvent. The polymer coated wafers were studied by scanning electron microscopy (SEM). (See Figure 6.6.) The reason for the gold coating on the substrate was because the electrode material used for the quartz oscillators was gold. The results show that for the PEI coating, a smooth, even coating was achieved on the surface. However, in the case of polystyrene, the coating surface was rippled and rough, and for the zeolite coating, the large particulate nature of the coating was evident. These results suggest that the reason for the very limited amounts of the polystyrene and zeolite coatings that could be used resulted from the morphology of the coating on the surface which scatters, and thus disrupts the acoustic wave of the crystal.

Another important issue with regard to the selective coatings results from the fact that the coatings must withstand the temperature changes that occur during the TPD experiment. Some of the coated crystals experienced a loss of oscillation, primarily in the 3rd harmonic of the B-mode, during heating for the TPD experiment. In most cases, the oscillation resumed when the crystal was again cooled through the temperature where oscillation was lost. An example of this behavior is demonstrated in Figure 6.7. This effect was more pronounced in the cases where the heaviest coatings were used. Initially, it was thought that this effect might be due to a glass transition within the polymer film. How-

ever, an examination of the viscoelastic properties of most polymers suggests that if this were the case, the lower frequency mode would likely be effected first. (See Figure 6.8.) Even though this plot of the dynamic moduli is for a single temperature, the principle of time-temperature superposition suggests that increasing temperature shifts the viscoelastic functions to higher frequency without changing the shape of the curves[2]. In light of the facts that the effect was more pronounced in heavier coatings, and that the morphological structure of the film was shown to effect the oscillation of this mode, the most likely explanation for this phenomenon is that there was some temperature induced structural change in the film which caused the damping of this mode.

### *6.3. Experimental Results*

In order to establish a baseline for future TPD experiments, the first sensor experiment performed used an uncoated quartz oscillator as the sensor, with n-hexane chosen as the analyte. (See Figure 6.9.) The hexane was introduced to the crystal in a 90 ml/min flow of dry nitrogen which passed over the crystal and into the mass spectrometer. Concentration of the hexane was controlled by the saturator temperature, held initially at -18°C, and through the course of the experiment increased to 15°C, resulting in a $P_{Hexane}$ ranging from about 15 to 80 Torr. Characteristic mass peaks for nitrogen (mass 28), oxygen (mass 32), and hexane (mass 43 and 86) were monitored throughout the experiment. The frequency response curve for the 1st harmonic of the C-mode indicates that adsorption did occur on the crystal when hexane was introduced to the crystal. However, when the flow of the hexane was cut off, the frequency returned to the original baseline value, indicating that the adsorption which occurred was physical adsorption only. This is confirmed by the fact that as the concentration of the hexane in the feed was increased, the

corresponding frequency response increased as well. No heating of the crystal occurred since there was no adsorbed analyte to thermally desorb.

The 8 MHz crystal was then coated with polystyrene as described previously. The coating produced a 250 Hz frequency drop in the 1st harmonic of the C-mode. Before each experiment on a selectively coated crystal sensor, the sensor was heated under flowing nitrogen using the same temperature program to be used for the TPD experiment. This was done in order to eliminate any extraneous adsorbates that may have deposited on the crystal as well as to create a known, reproducible condition for the start of the TPD experiment. An experiment was now performed using hexane on the polystyrene coated crystal using the same experimental parameters as for the uncoated quartz crystal. The results of this experiment can be seen in Figure 6.10. The system shows a much larger response to the hexane, indicating more adsorption onto the coated crystal than onto the blank crystal. This logically results from the higher affinity of the hexane for the hydrocarbon coating, than for the bare quartz surface. However, as with the uncoated crystal, only physical adsorption is occurring in this system, indicated by the return to the baseline frequency as soon as the hexane was removed from the gas stream. Once again, no heating of the crystal was carried out since there was no chemically adsorbed analyte to detect.

In order to improve the chances of having an analyte species chemisorbed onto the surface of coated crystal, next coatings studied were chosen with an eye toward having more functionality than hydrocarbon polymers. A good example of this is poly(4-vinylpyridine) (4-PVP) which was used as the selective coating in a TPD experiment for sensing for 2-nitrotoluene, an impurity found in 2,4,6-trinitrotoluene based explosives. Figure 6.11 parts (A) and (B) show frequency response profiles for the two modes of interest as a func-

tion of time for the entire TPD experiment. The profiles are typical of all the sensing experiments conducted. The experimental procedure used was as follows: data collection was begun on the (4-PVP) coated, preheated crystal which had been allowed to re-equilibrate at room temperature. After about 10 minutes (to establish baseline values for the frequencies), the 2-nitrotoluene analyte was introduced in a carrier flow of dry nitrogen at a partial pressure of approximately 0.2 Torr. The mass spectrometer was inoperable at this time, so no mass spectral characterization of the experiment was possible. However, the graph in Figure 6.11 part (C) shows the state of the VICI valve so as to demonstrate the period for which the 2-nitrotoluene analyte was exposed to the sensor. 2-nitrotoluene was allowed to adsorb onto the sensor for a period of approximately 25 minutes before the analyte flow was replaced with dry nitrogen gas at the same flowrate. The adsorption period of the experiment is shown in detail in Figure 6.12. The graph in Figure 6.12 part (A) of the frequency response of the 1st harmonic, C-mode, shows clearly an adsorption onto the sensor, as indicated by the drop in the frequency. This signal represents both chemical and physical adsorption onto the sensor. After the flow of the 2-nitrotoluene was removed, the physisorbed material desorbed almost immediately. However, after allowing the signal to equilibrate under flowing nitrogen, there was still adsorbed 2-nitrotoluene on the sensor. This effect was also seen in the 3rd harmonic of the B-mode, (See Figure 6.12 (B)) although less clearly because there is a slight temperature decrease during the dosing period which causes the strong thermal response of this mode to partially obscure the adsorption response.

Heating of the crystal for the desorption phase of the test began after the 15 minute equilibration period which was allowed following the dosing of the 2-nitrotoluene. For

this experiment, a heating program raised the sensor temperature to 175°C in 20 minutes and held it there for an additional 5 minutes before allowing it to cool to room temperature via natural cooling. The earliest experiments used an even longer heating ramp, up to an hour, and later experiments reduced the temperature ramp to as little as 10 minutes, producing a heating rate of 20°C/minute from room temperature to 225°C. The motivation for this evolution was to reduce the cycle time to levels closer to those necessary for a practical device, as well as to try to enhance the desorption signal by compressing the time coordinate of the experiment.

Figure 6.13 shows the frequency-temperature response curves for the two vibrational modes as well as a profile of the heating program used for the experiment. Qualitatively, the responses strongly resemble the responses seen from the coated crystal when subjected to the same temperature program. It is very difficult from this data to determine the point at which desorption occurs during the experiment. This problem was encountered throughout these experiments. That is, that the sensitivity and response of the sensor to mass changes was insufficient to allow deconvolution of the mass response from the temperature response. The next example will demonstrate this more clearly.

Figure 6.14 shows the results from an experiment for sensing the presence of isopropanol using a poly(4-vinylpyridine) coated crystal and, again, they show the same behavior as seen for nearly all combinations of selective coatings/analytes. This experiment was chosen for illustration because it shows one of the strongest signals seen during the adsorption period throughout these experiments. (See Figure 6.15.) Several attempts were made to try to separate the mass response of the crystal from the thermal response. The first of which takes advantage of the fact that we are monitoring two vibrational

modes of the crystal. The frequency response of the two modes can be modeled as:

$$\Delta F_{1C} = M_1\Delta m + T_1(T)\Delta T \quad (3)$$

$$\Delta F_{3B} = M_3\Delta m + T_3(T)\Delta T \quad (4)$$

resulting in a system of 2 equations in two unknowns. By utilizing the frequency response behavior or the two modes during a heating experiment with no desorption taking place as well as the response to changes during adsorption, the unknowns in this system can be determined and the results used to try to separate the temperature and mass responses of the sensor. Figure 6.15 shows the adsorption of isopropanol onto the poly(4-vinylpyridine) coated sensor, with graphs (A) and (B) showing the responses as recorded and graphs (C) and (D) showing the responses after deconvolution and removal of the temperature response. The good agreement of the shape and features of the two modes after deconvolution suggests that the deconvolution was successful.

This same deconvolution technique was applied to the desorption portion of the TPD experiment, and the results are presented in Figure 6.16 (A) and (B). These graphs show no clear evidence of a desorption event. In fact, the curves are dominated by noise in the experiment. The apparent periodicity in the graphs can be traced to slight oscillations in the heating ramp caused by the temperature controller. Another attempt to deconvolute the mass and temperature signals can be found in Figure 6.16 (C) and (D). These mass response curves were generated by subtracting the frequency response curves during the heating portion of the TPD experiment, which should contain both temperature and mass components, from the frequency response obtained during the cooling portion of the experiment, which should contain only temperature responses if desorption has occurred. Again, the results are very similar to the dual mode analysis, with no clear desorption sig-

nal evident in the data. These results point to the fact that the mass response sensitivity of this sensor based on the SC-cut crystal may not be adequate to provide the resolution required for this application.

There is some evidence that the technique may still be valid even though the mass sensitivity of the SC-cut crystal is low. In the sensor experiments involving polyethyleneimine (PEI) as the chemically selective coating, there was some clear evidence of a desorption signal during the TPD heating experiment. This occurred for two analytes, water and carbon dioxide. Frequency response profiles for the thermal desorption of water from a PEI coated sensor can be seen in Figure 6.17. Even though there was a loss of oscillation in the 3rd harmonic, B-mode on heating, there is clearly a large desorption signal beginning at around 35 degrees C that can be seen ending just above 50 degrees in both frequency response curves. This is even more clear in the graphs showing the frequency response as a function of temperature shown in Figure 6.18. Graph (C) on this figure shows the desorption peak clearly by subtracting the heating response curve from the cooling curve. The reason there was such a strong signal in this case, whereas in all other experiments there was insufficient mass sensitivity to detect any desorption signal, is because PEI is an extremely hydrophilic polymer, that can adsorb up to its weight and more in water. In fact, the polymer comes as a 50% solution in water. For this case, the mass sensitivity was not a problem, because the mass loading signal was so large it overwhelmed the temperature response. It was possible to get a desorption signal from carbon dioxide off this coating as well, by introducing pure $CO_2$ gas during the adsorption period. The desorption signal was much smaller than for water. However, it exactly overlaid the water desorption with regard to both temperature and duration. This result can be

explained by the high affinity for carbon dioxide by water, causing a cooperative adsorption with water on the polymer, with a corresponding desorption under the same conditions as water.

In order to quantify the mass change that occurs for a given frequency change during a TPD analysis, the following experiment was performed: a clean, dry, quartz oscillator was coated with polyethyleneimine as described previously. Under flowing dry nitrogen, the coated crystal was heated to 175°C in 30 minutes, held at 175°C for 10 minutes, then cooled to room temperature in order to desorb any residual methanol or water from the coating process so that the frequency change resulting from the addition of the dehydrated polymer alone could be determined. The coated crystal was then allowed to absorb water from the ambient atmosphere for 12 hours and the frequency change for the water absorption determined.

The hydrated, polyethyleneimine coated crystal was placed in a Cahn D200 microbalance in order to determine the mass changes. The crystal was first heated to 175°C in flowing dry nitrogen to desorb the water from the coated crystal and cooled to room temperature in order to determine the mass change resulting from the water desorption. In order to remove the polymer coating, the crystal was then heated in a 50:50 mixture of nitrogen and oxygen to 300°C in 60 minutes, held at 300°C for 20 minutes, and cooled to room temperature in order to determine the mass of the polymer coating. This procedure removes the PEI by combustion with dioxygen. Table 6.2 contains the mass response values for addition of polyethyleneimine onto an uncoated crystal, and for water onto a polyethyleneimine coated crystal, determined by correlating the mass changes observed in the microbalance experiment with the frequency changes recorded from the

coating and adsorption experiments.

Examination of the values reported in Table 6.2 reveals several important points that must be addressed. First, the results show a significantly lower sensitivity for water on the polymer coated crystal than for placing the polymer coating on a clean crystal; that is, it takes approximately 1.8 times more sorbed mass of water to provide a given response on a PEI coated crystal than polymer mass on a clean crystal. Second, although the numbers appear to be sufficiently small to provide the desired sensitivity at first glance, a quick calculation shows that to be untrue. The microbalance experiment determined that the hydrated, PEI coated crystal contained 66.9 μg of polymer and 49.9 μg (43 wt%) of water. In order to have that high of a sorption level, the water molecules must be absorbing into the bulk of the polymer, rather than simply adsorbing onto the surface of the coating. (See Figure 6.19.) The much more common situation is that of adsorption, where a typical analyte will adsorb at a level of approximately 1 wt% or less. Such a loading would produce a frequency response of less than 2 Hz in the C-mode of an 8 MHz crystal. This value is below the mimimum detection level in this system of approximately 5-10 Hz and well below levels necessary to produce a reliable response for chemical sensing.

Comparing the sensitivity of this system to other oscillator based sensor systems, AT-cut quartz oscillators have been shown to respond to mass changes on the order of $10^{-10}$g, and surface acoustic wave (SAW) based sensor devices, because of their very high resonant frequencies, can have detection limits on the order of 100 picograms, based on a frequency response of approximately 400 Hz/ng commonly achievable by these devices[3]. However, the AT-cut bulk resonators have problems previously mentioned which make them unsuitable choices for use in a TPD detection technique, including the lack of a sec-

ond strong vibrational mode which can be used to deconvolute the temperature and mass responses, as well as strong non-linearities and activity dips when heated above 50°C. The surface acoustic wave resonators, however, provide a possible candidate for the resonating device in the TPD technique which merits further study. The SAW resonators currently in use today for chemical sensing utilize Rayleigh waves as their primary mode of oscillation. However, there are other types of surface waves, including shear horizontal waves, which might be used to provide a second vibrational mode to deconvolute the temperature effects in a TPD experiment. The shear horizontal waves are not currently well understood and are an active area of research, thus I cannot make any suggestions about how such a dual mode SAW device sould be prepared.

## *6.4 Conclusions*

From the results presented in this work, a chemical sensing device based on thermal programmed desorption using a SC-cut quartz oscillator can be fabricated and a functioning device shown to be able to monitor water vapor using a polyethyleneimine film. However, these sensors based on SC-cut quartz oscillators fail to show the high degree of mass sensitivity necessary from a microsensor in order for it to show practical utility. When testing devices that used a variety of analytes and selective coatings, the sensor fails to produce an identifiable desorption peaks in all cases, except for the case of a polyethyleneimine coating with water, or carbon dioxide cooperatively absorbed with water. Practical application of the sensing technique developed here will require the use of another type of oscillator with a higher mass sensitivity, while still having two different oscillation modes with different temperature dependencies.

## *Literature Cited*

(1) Bein, T.; Brown, K.; Frye, G. C.; Brinker, C. J. *J. Chem. Soc.* **1989**, *111*, 7640-7641.

(2) Graessley, W. W. In *Physical Properties of Polymers*; Mark, J. E.; Eisenberg, A.; Graessley, W. W.; Mandelkern, L.; Samulski, E. T.; Koenig, J. L.; Wignall, G. D. Eds.; American Chemical Society: Washington, DC, 1993.

(3) Sun, J.T. M.S. Thesis; California Institute of Technology, 1993.

(4) Rouhi, A. M. *Chemical & Engineering News* July 24, **1995**, 10-19.

(5) Langmuir, I. *J. Chem. Soc.* **1918**, *40*, 1361.

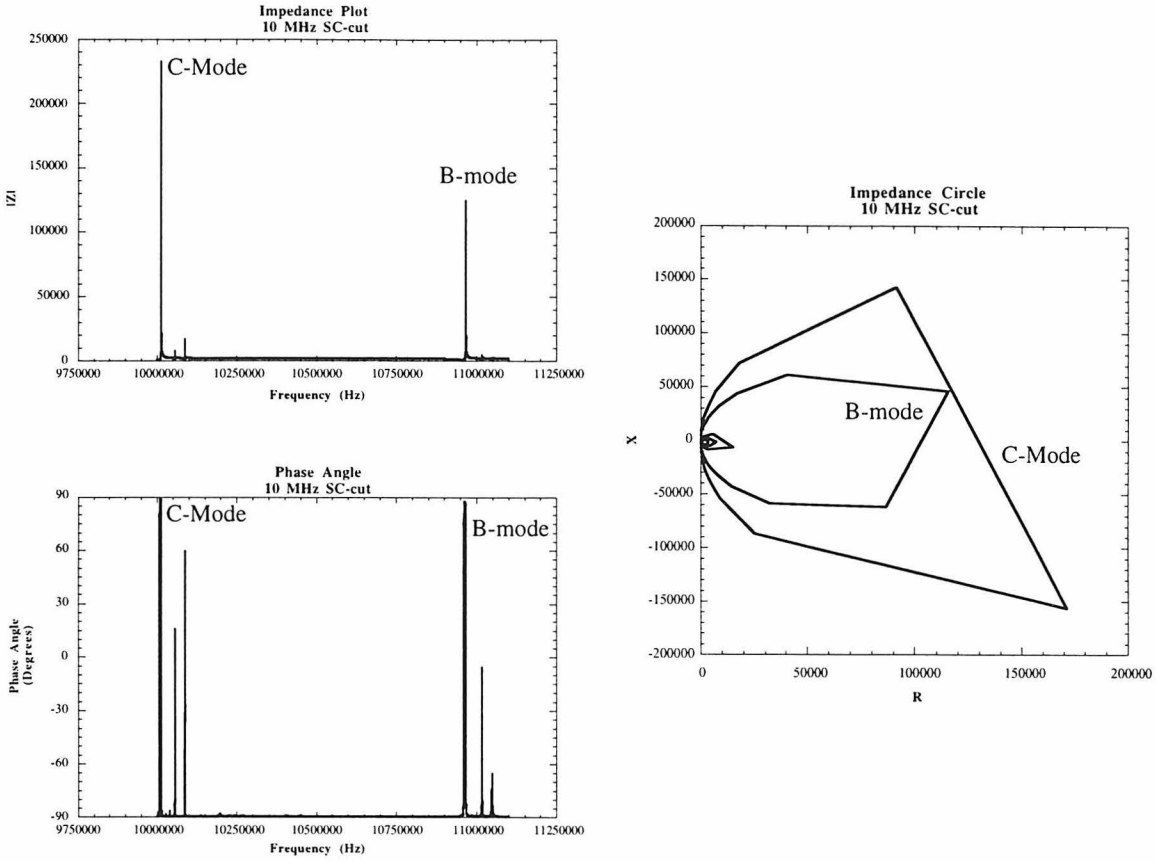


**Figure 6.1:** Impedance analyzer characterization of the 1st harmonic region of a 10 MHz SC-cut crystal. The triple plot display shows impedance vs. frequency, phase angle vs. frequency, and the impedance circle or Nyquist plot.

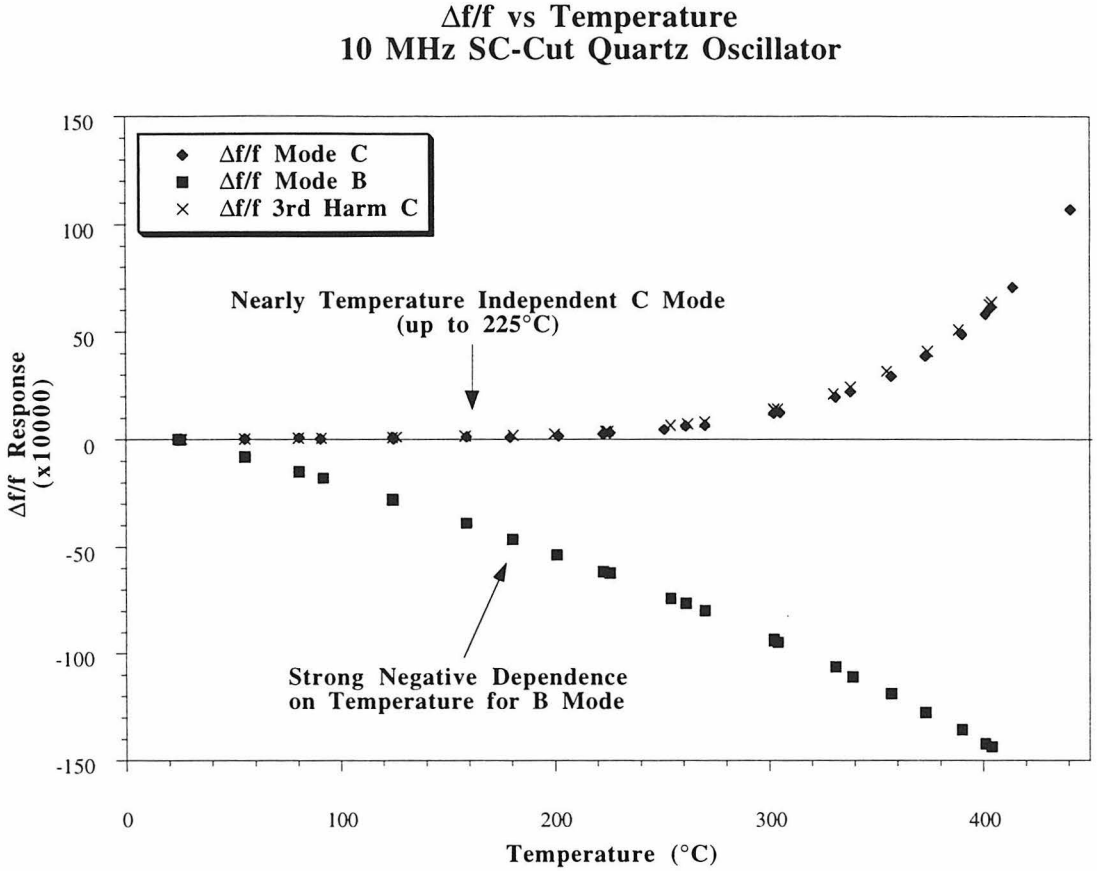


**Figure 6.2**: Temperature response profiles for uncoated 10 MHz SC-cut crystals.

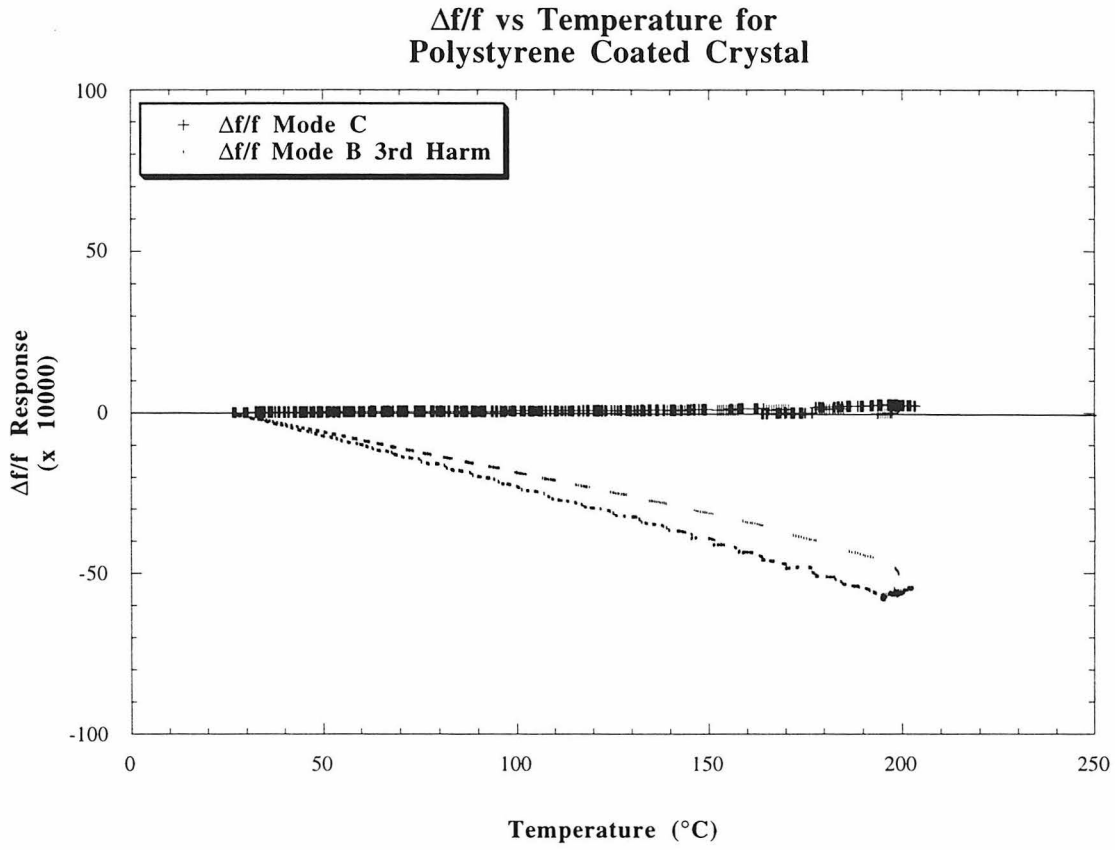


**Figure 6.3:** Temperature response profiles for a polystyrene coated 8 MHz SC-cut crystal. The hysteresis seen in the 3rd harmonic of the B-mode on cooling is primarily due to the fact that the thermocouple used to record the temperature was measuring the chamber temperature, not the actual crystal. This problem was significantly reduced in later experiments by achieving better thermal contact to the stainless steel core of the heater chamber.

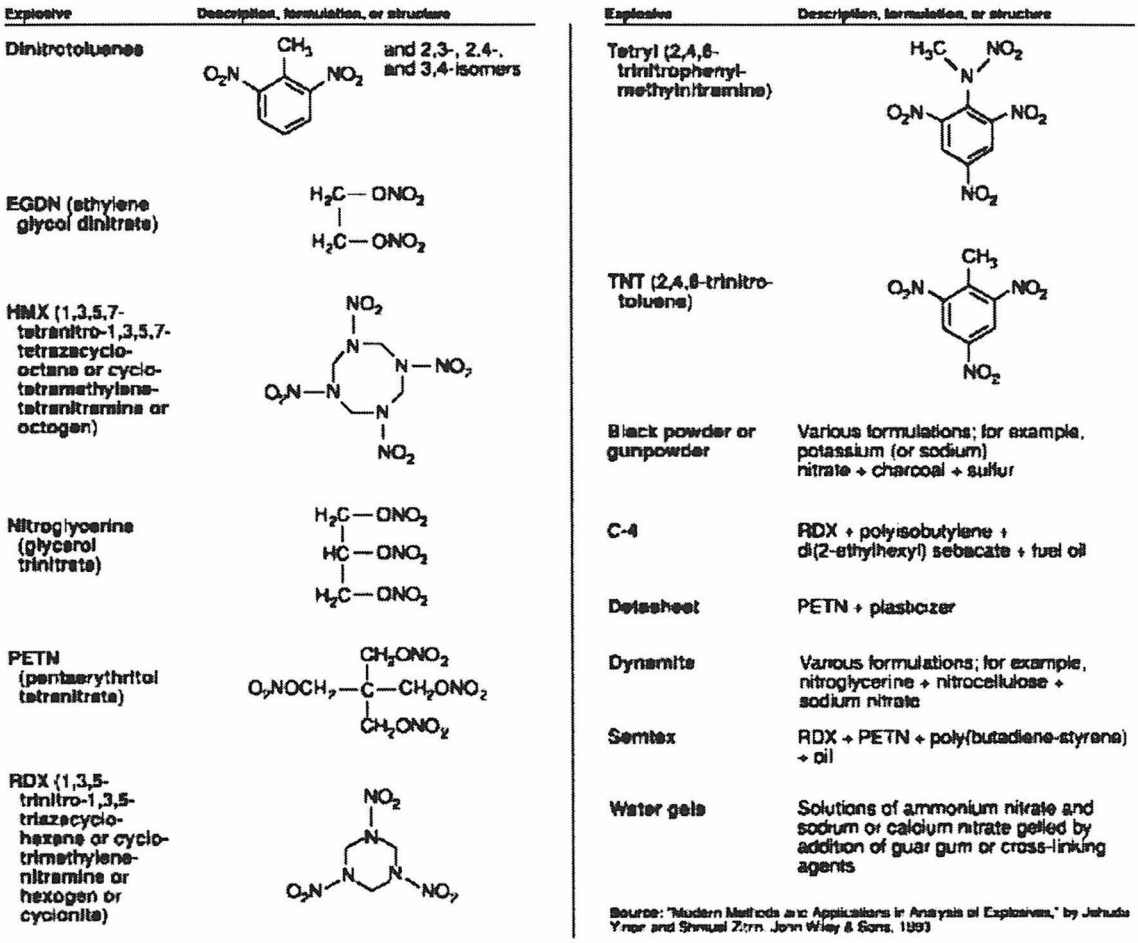


**Figure 6.4:** Examples of common constituents found in plastic explosives. The common features to this class of compounds include high density and high nitrogen content, typically including large numbers of nitro-functional groups. Adapted from Rouhi[4].

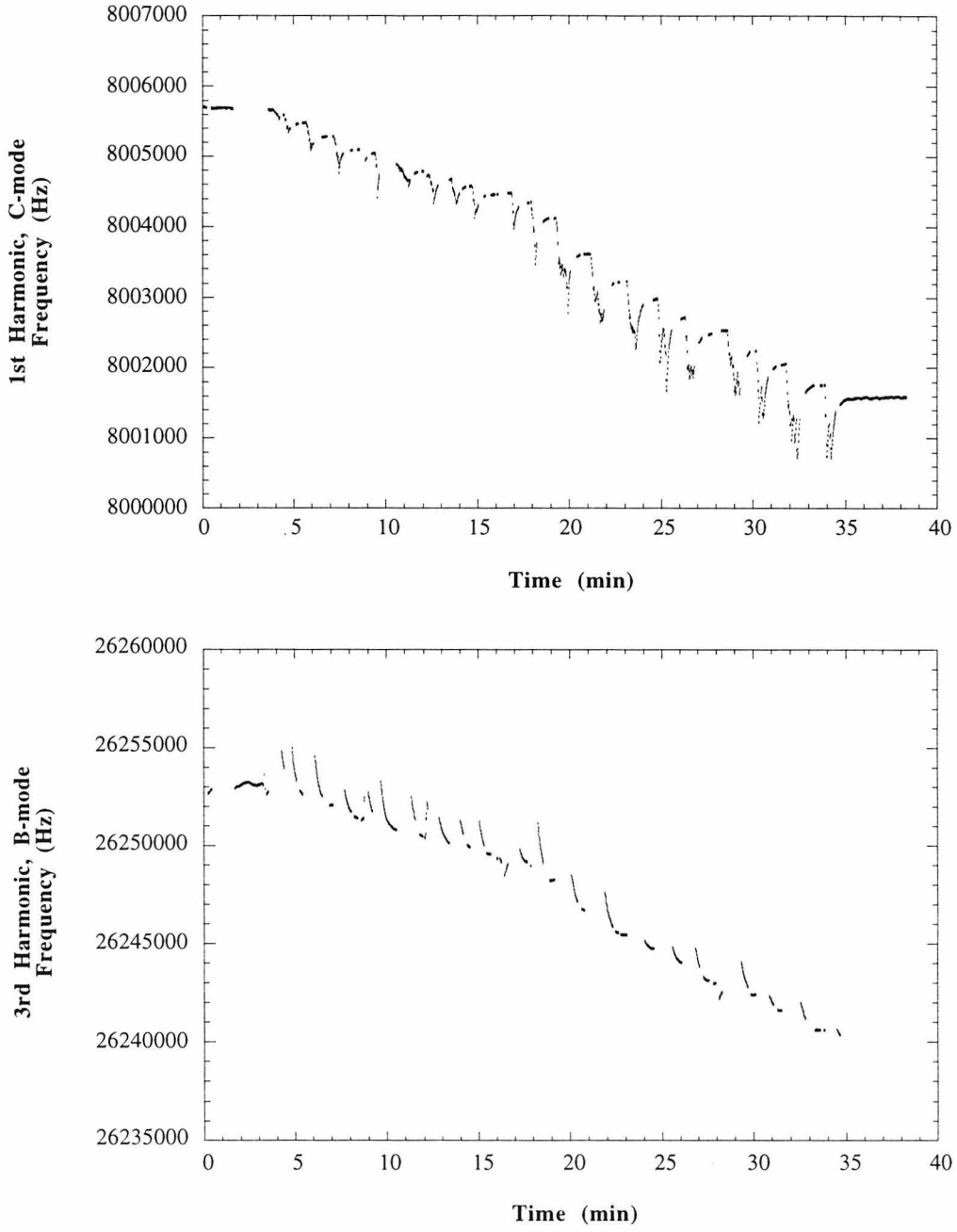


**Figure 6.5:** Results from the application of a PEI to an 8 MHz SC-cut quartz oscillator. The large transients in the signal result from the evaporation of the carrier solvent. The transients are negative for the 3rd harmonic of the B-mode because of the cooling effects of the evaporation.

| Selective Coating | Solution/Suspension Medium | Maximum Coating Achieved* |
|---|---|---|
| Polyethyleneimine | 0.3% in methanol | 9000 Hz |
| Polystyrene | 0.2% in methylene chloride | 250 Hz |
| Poly-4-vinylpyridine | 0.4% in methanol | 9500 Hz |
| Polyaniline | 0.2% in methylene chloride | 0 Hz† |
| NaY | colloidal Teflon | 250 Hz |
| NaY | silica sol-gel | 250 Hz |

* As measured by the frequency change in the 1st harmonic, C-mode of an 8 MHz SC-cut Crystal

† Application of polyaniline to the crystal caused immediate loss of oscillation. A possible explanation is that since polyaniline is a conductive polymer, it caused a short circuit across the crystal.

**Table 6.1:** Listing of chemically selective coatings used in this work, along with the solution/suspension from which it was deposited and the maximum coating achieved.

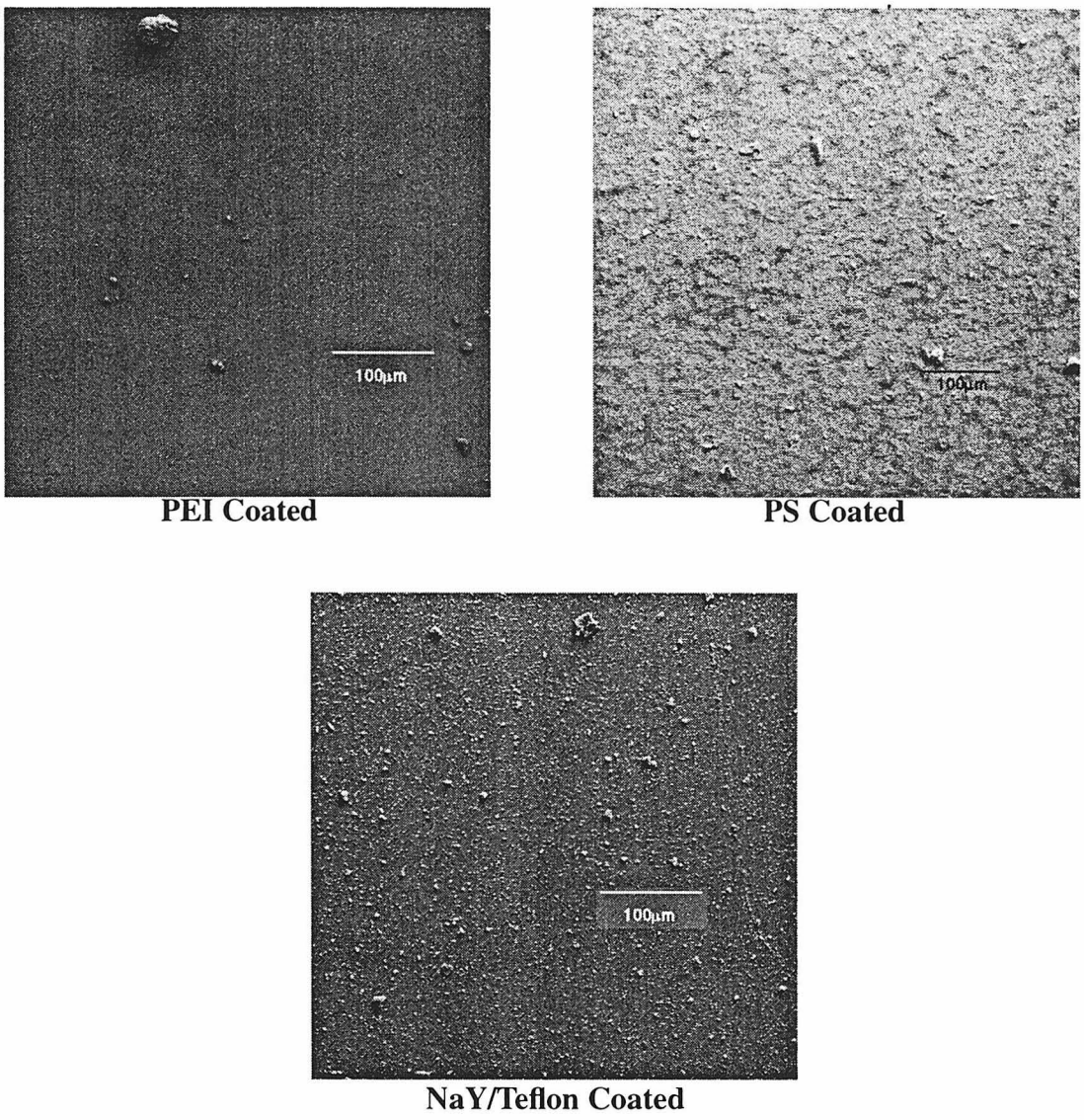


**Figure 6.6**: Scanning electron micrographs (SEM) of three of the coatings used in this study. Notice how the surface of the PEI coated sample is smooth whereas the PS coated sample is rough and wavy and the NaY coated sample shows the particulate nature of the zeolite coating.

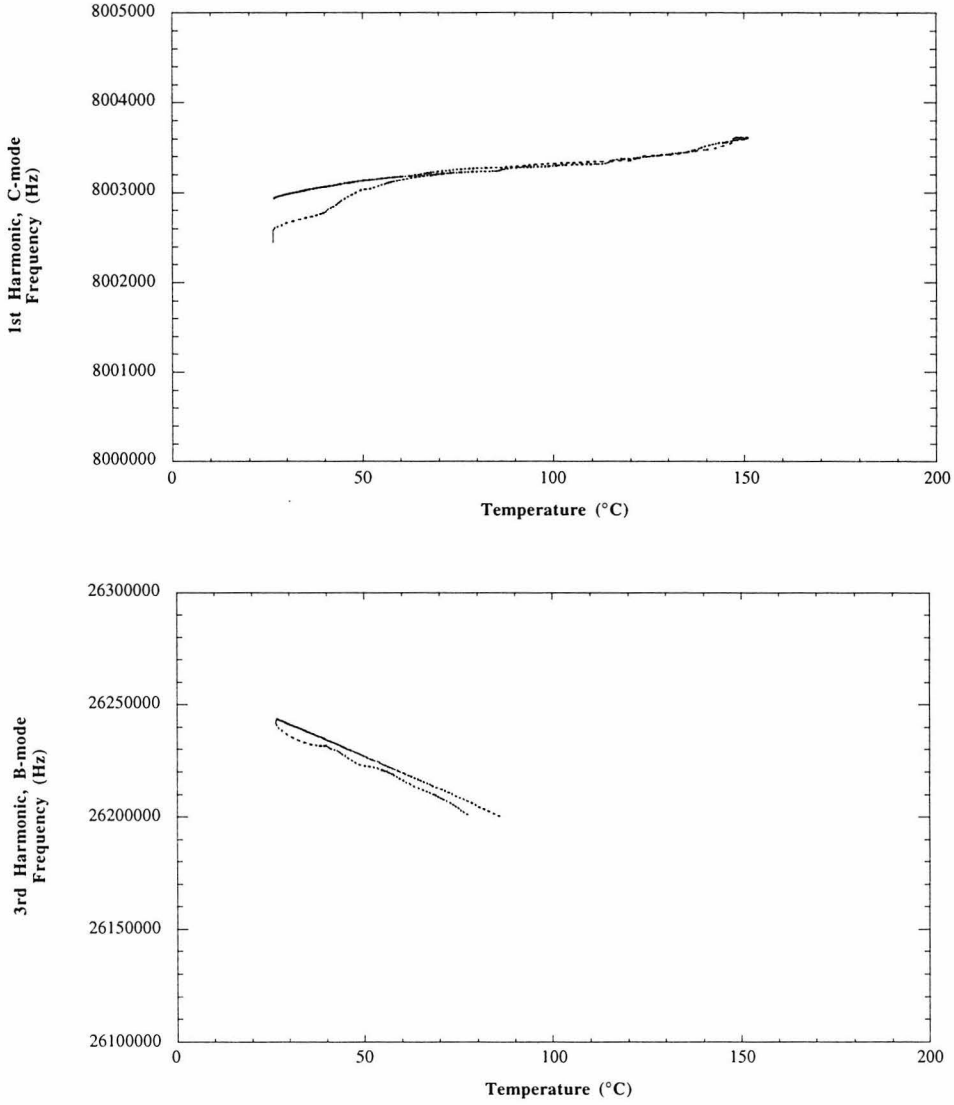


**Figure 6.7:** TPD experiment on a PEI coated crystal showing the loss of oscillation in the 3rd harmonic, B-mode during heating. The loss is likely attributable to a thermally induced structural change in the coating which disrupts the acoustic waves.

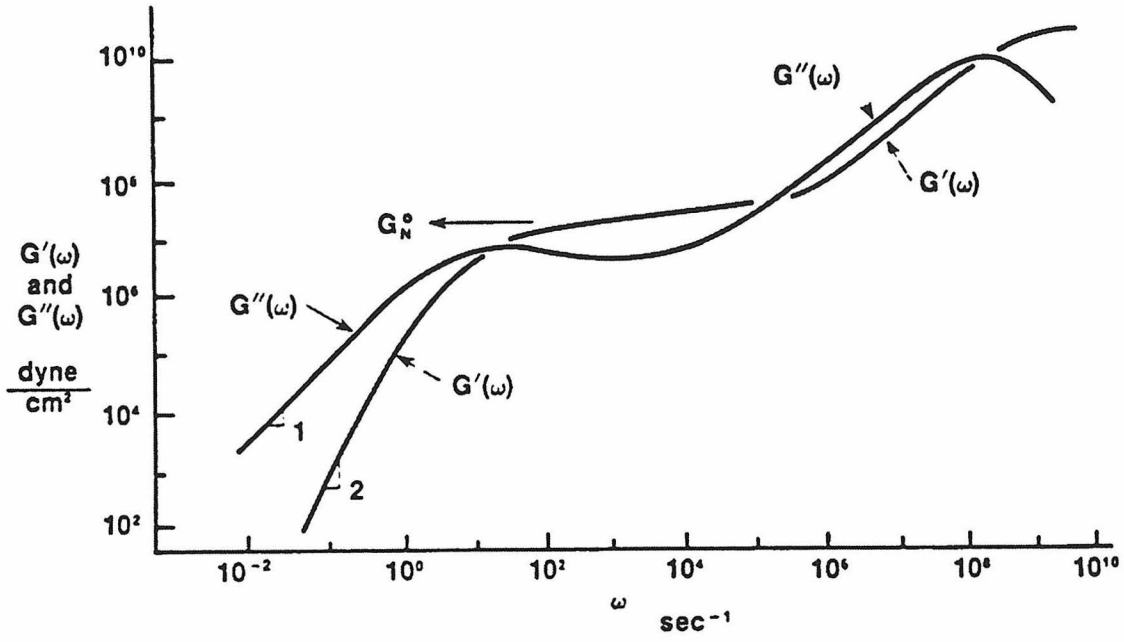


**Figure 6.8:** Dynamic moduli as functions of frequency for a typical polymer melt. Adapted from Graessley[2].

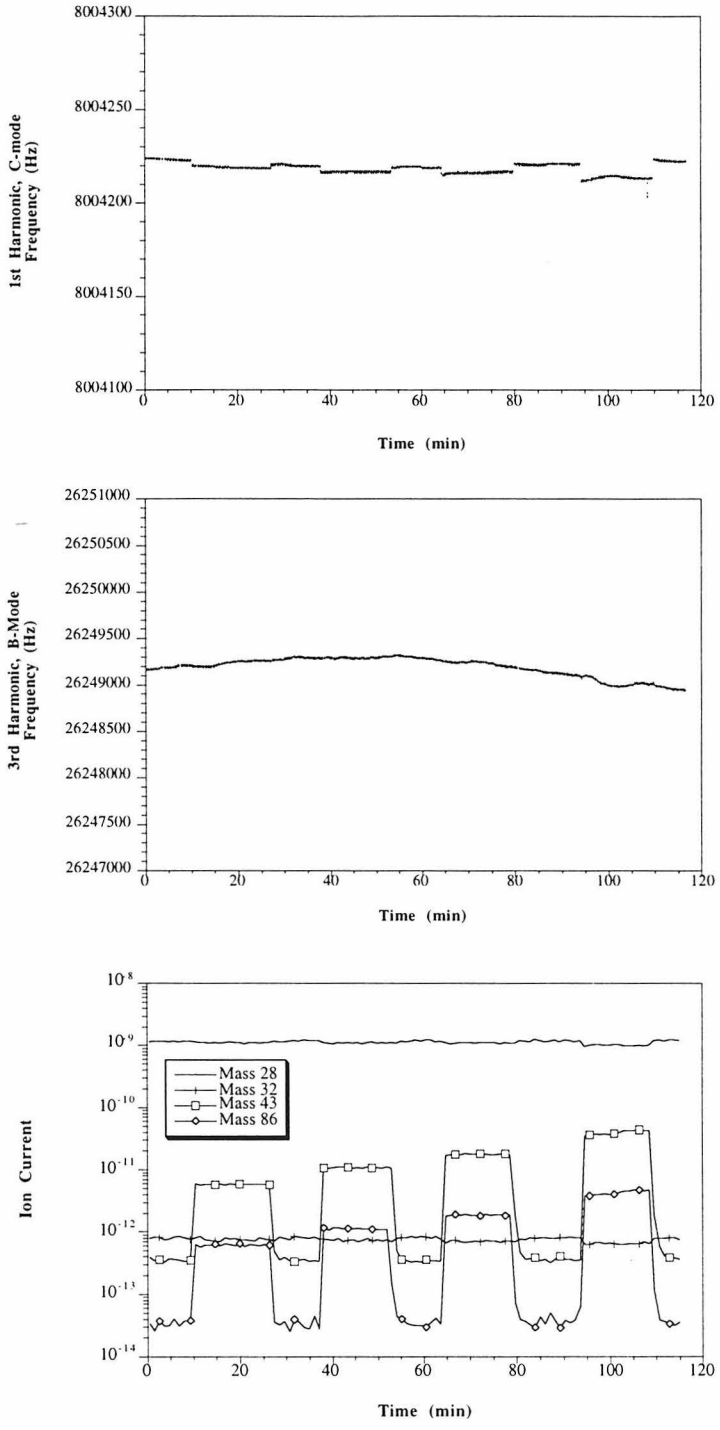


**Figure 6.9:** Results of a TPD experiment testing for n-hexane with an uncoated SC-cut oscillator. Only physical adsorption of the hexane takes place, hence desorption occurs without heating when the analyte source is removed.

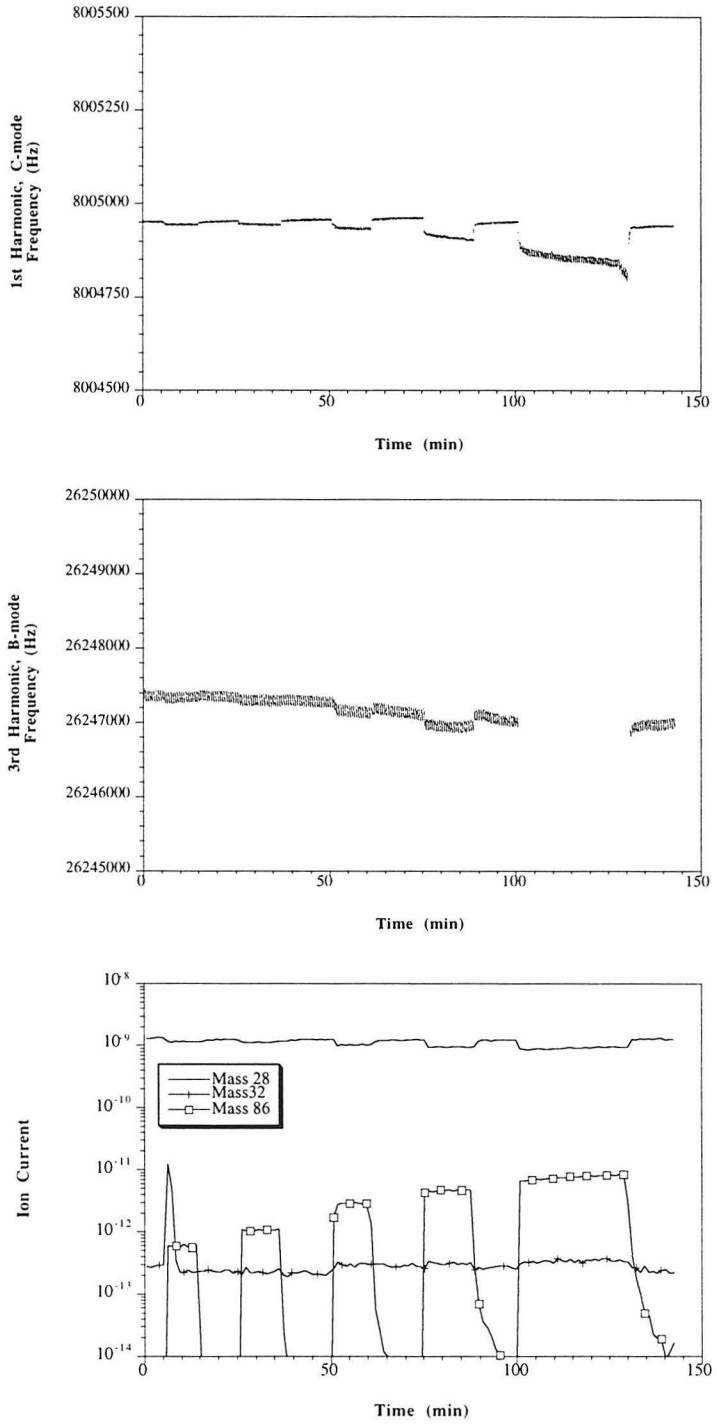


**Figure 6.10:** Results of a TPD experiment testing for hexane on a polystyrene coated crystal. Only physical adsorption is observed for this system.

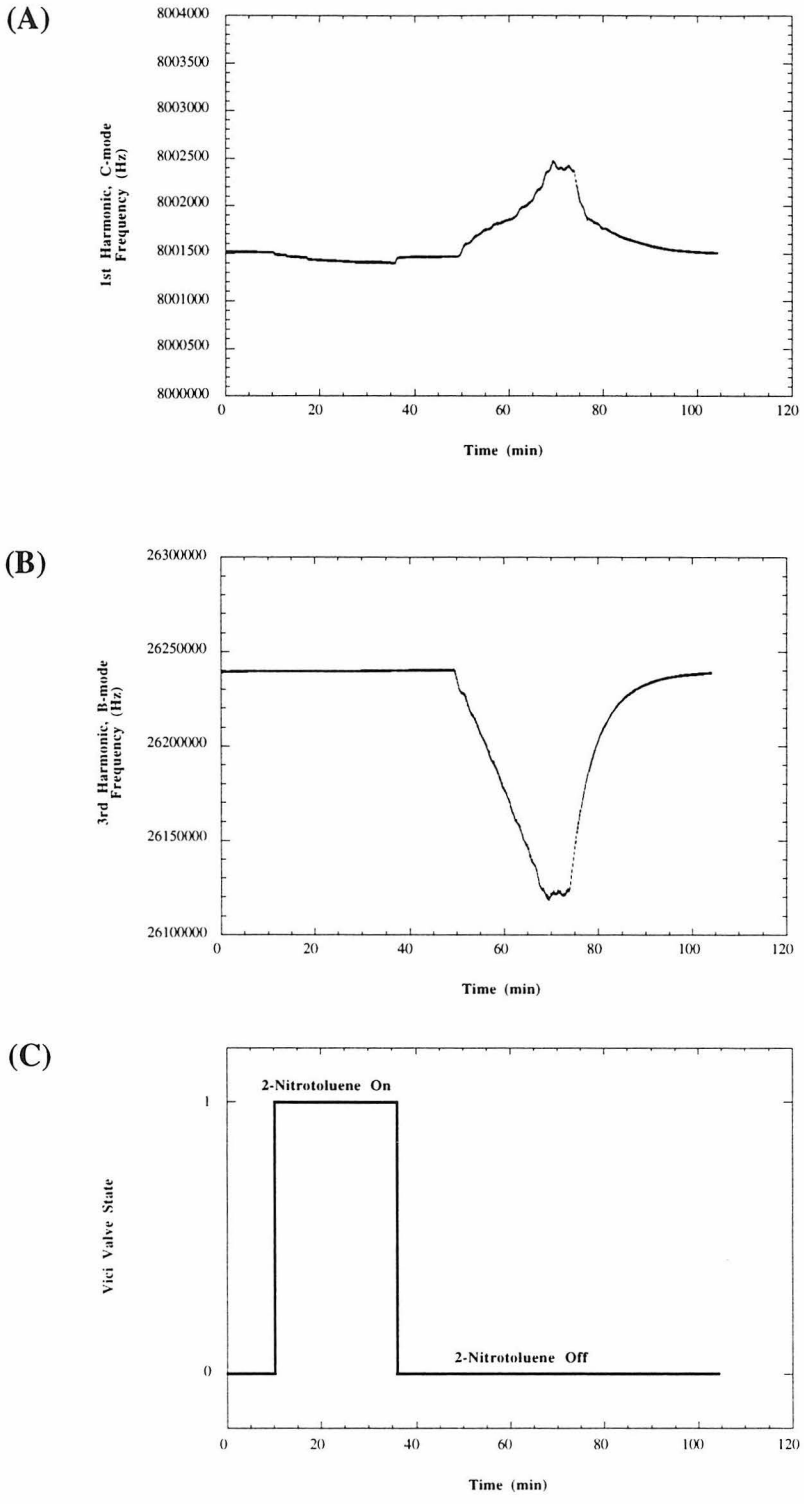


**Figure 6.11:** Results of a TPD experiment for sensing 2-Nitrotoluene on a 4-Poly(vinylpyridine) coated crystal.

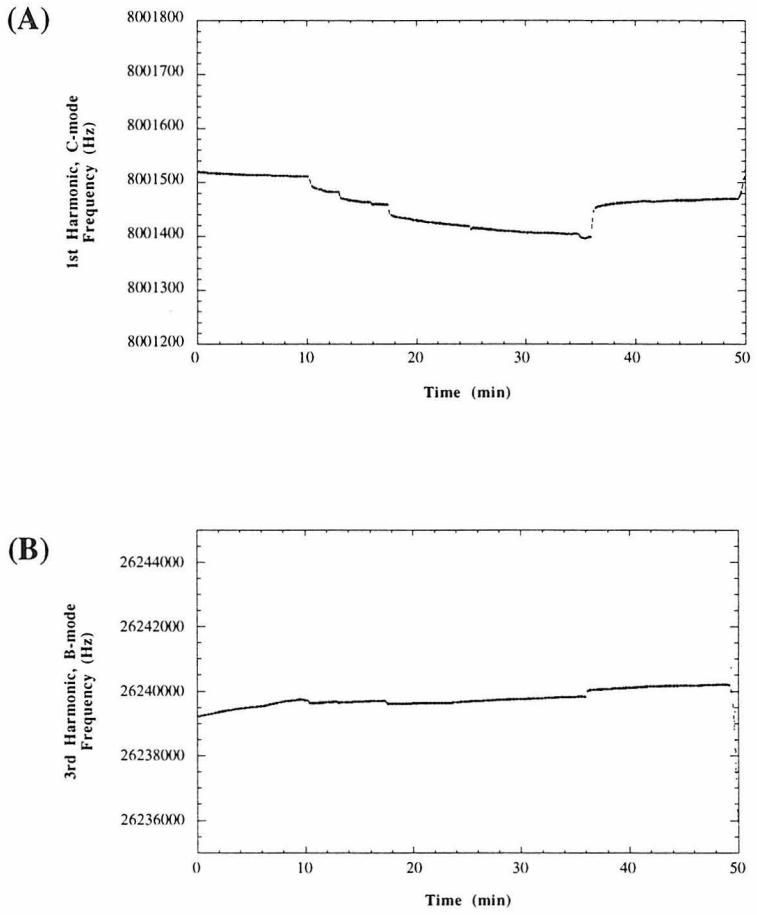


**Figure 6.12:** Adsorption period of a TPD experiment showing the adsorption of 2-nitrotoluene on a poly(4-vinylpyridine) coated crystal sensor.

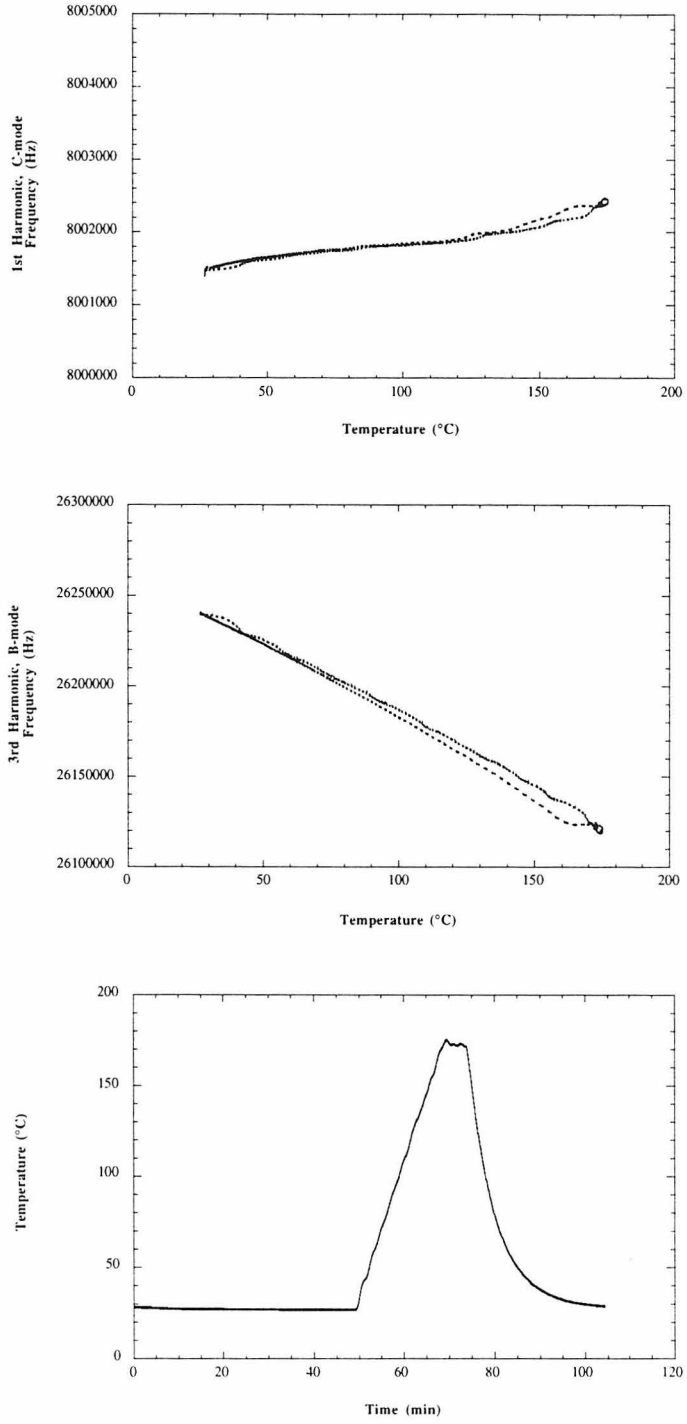


**Figure 6.13:** Results of a TPD experiment for sensing 2-Nitrotoluene on a 4-Poly(vinylpyridine) coated crystal showing the frequency response of the two modes as a function of time as well as the temperature profile of the experiment.

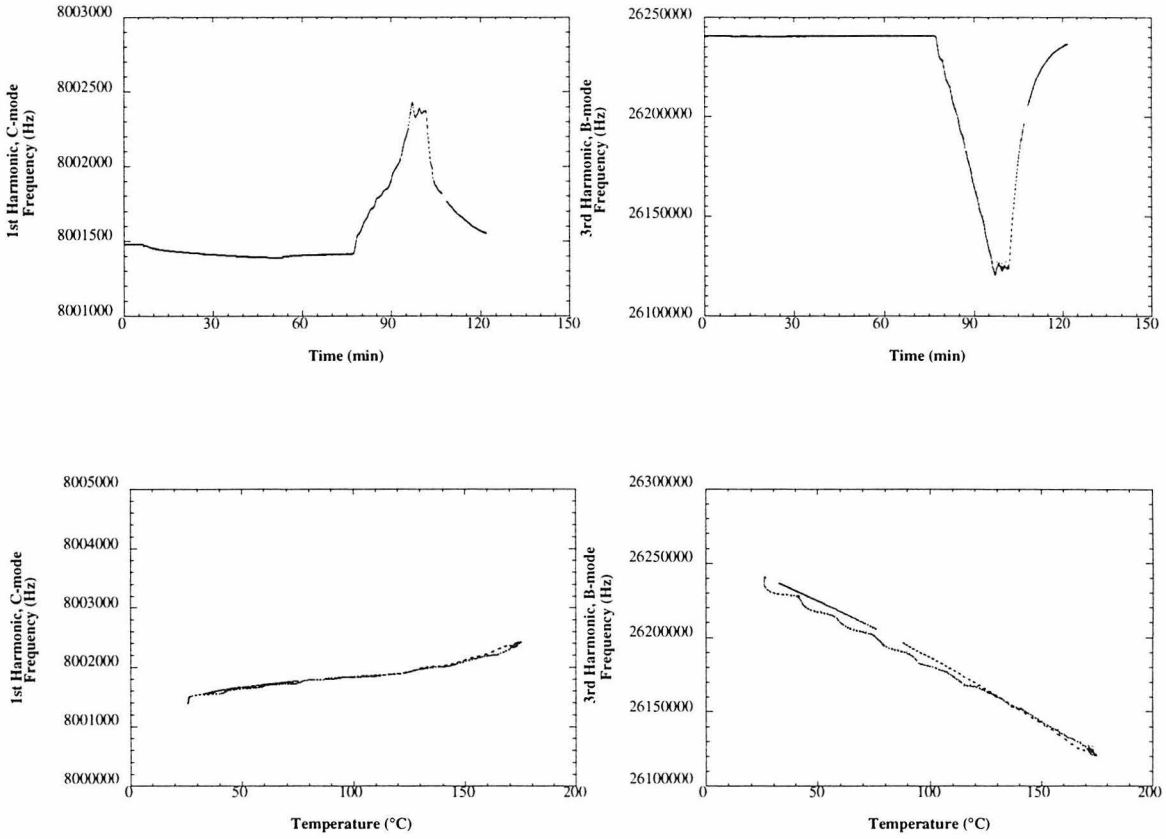


**Figure 6.14:** Results from a TPD experiment for sensing isopropanol on a poly(4-vinylpyridine) coated crystal showing the frequency responses for the two modes of interest as a function of time during the experiment and temperature during the desorption period of the experiment.

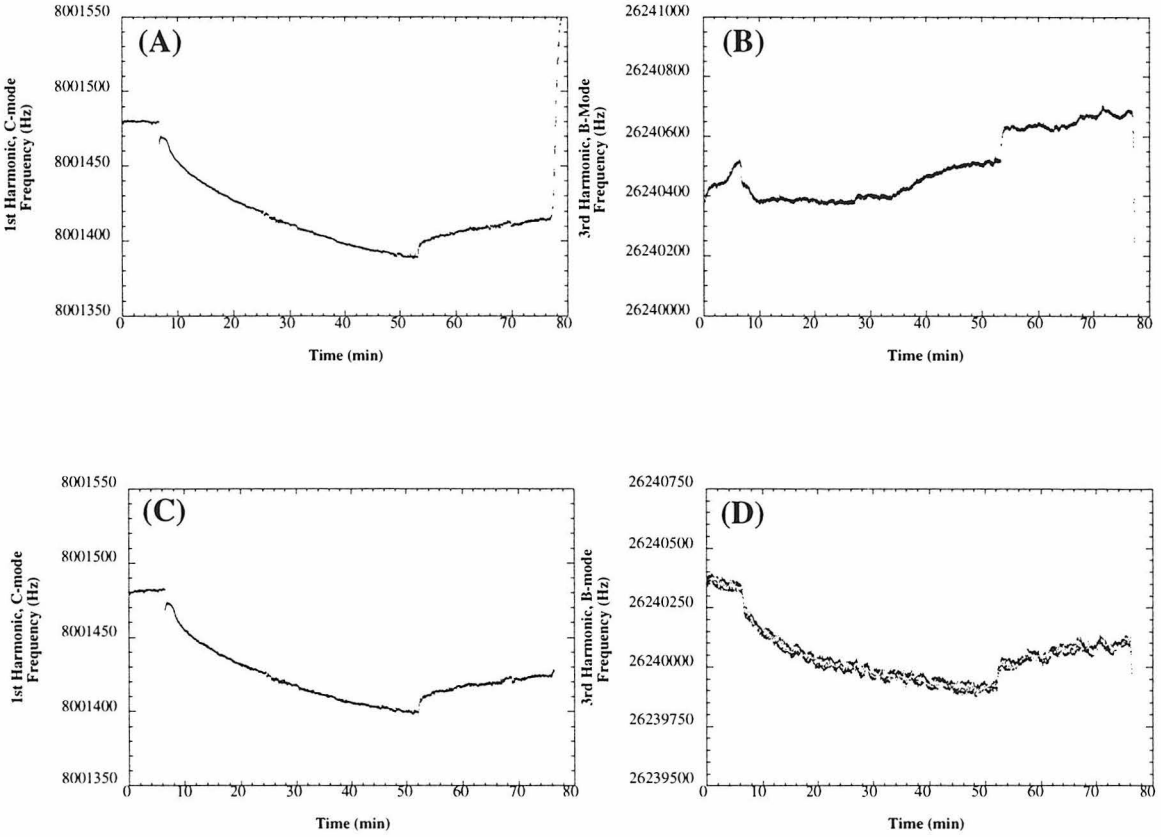


**Figure 6.15:** Results from a TPD experiment for sensing isopropanol on a poly(4-vinylpyridine) coated crystal. The top graphs, (A) and (B), show the responses of the two modes as they were recorded during the experiment. The bottom two graphs, (C) and (D), have had the temperature response of the two modes determined and eliminated from the graphs by the use of a dual mode analysis method, and thus show only the mass response during the adsorption period.

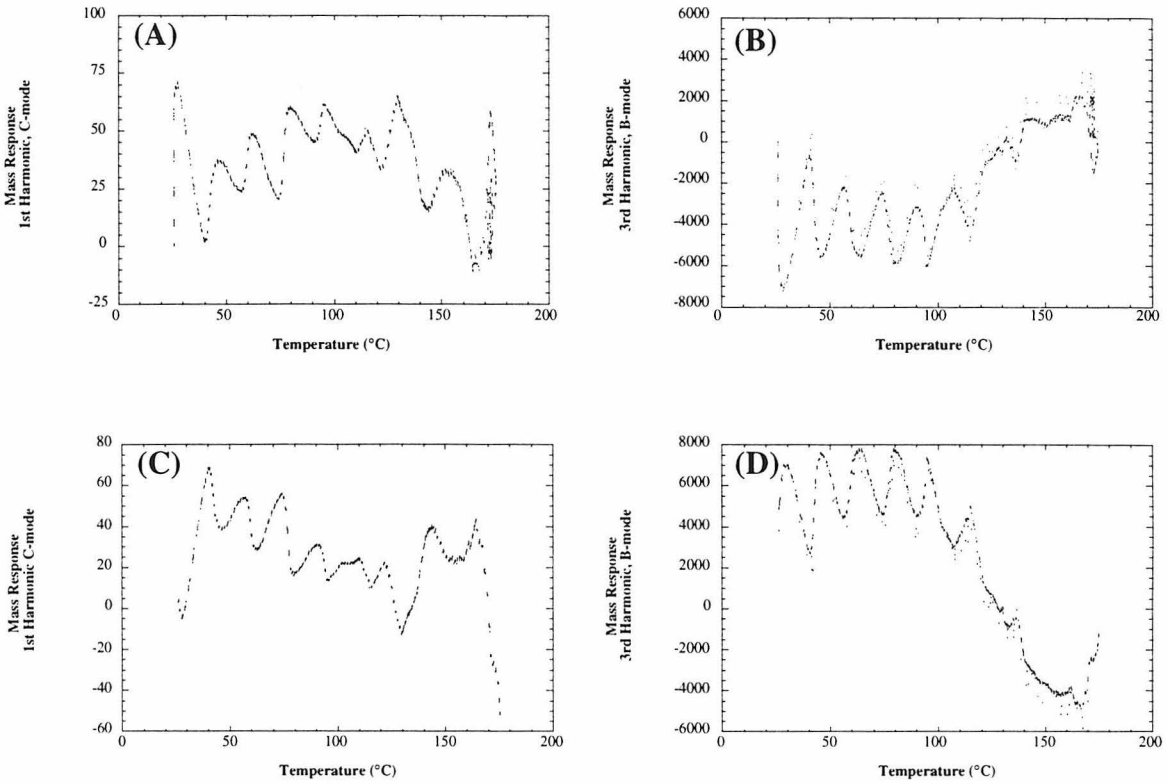


**Figure 6.16:** Deconvoluted mass responses for a TPD experiment for sensing isopropanol on a poly(4-vinylpyridine) coated crystal. The top graphs, (A) and (B), show the results from the use of a dual mode analysis. The bottom two graphs are generated by subtracting the frequency response curves for the heating part of the TPD experiment from the response curve for the cooling part of the experiment.

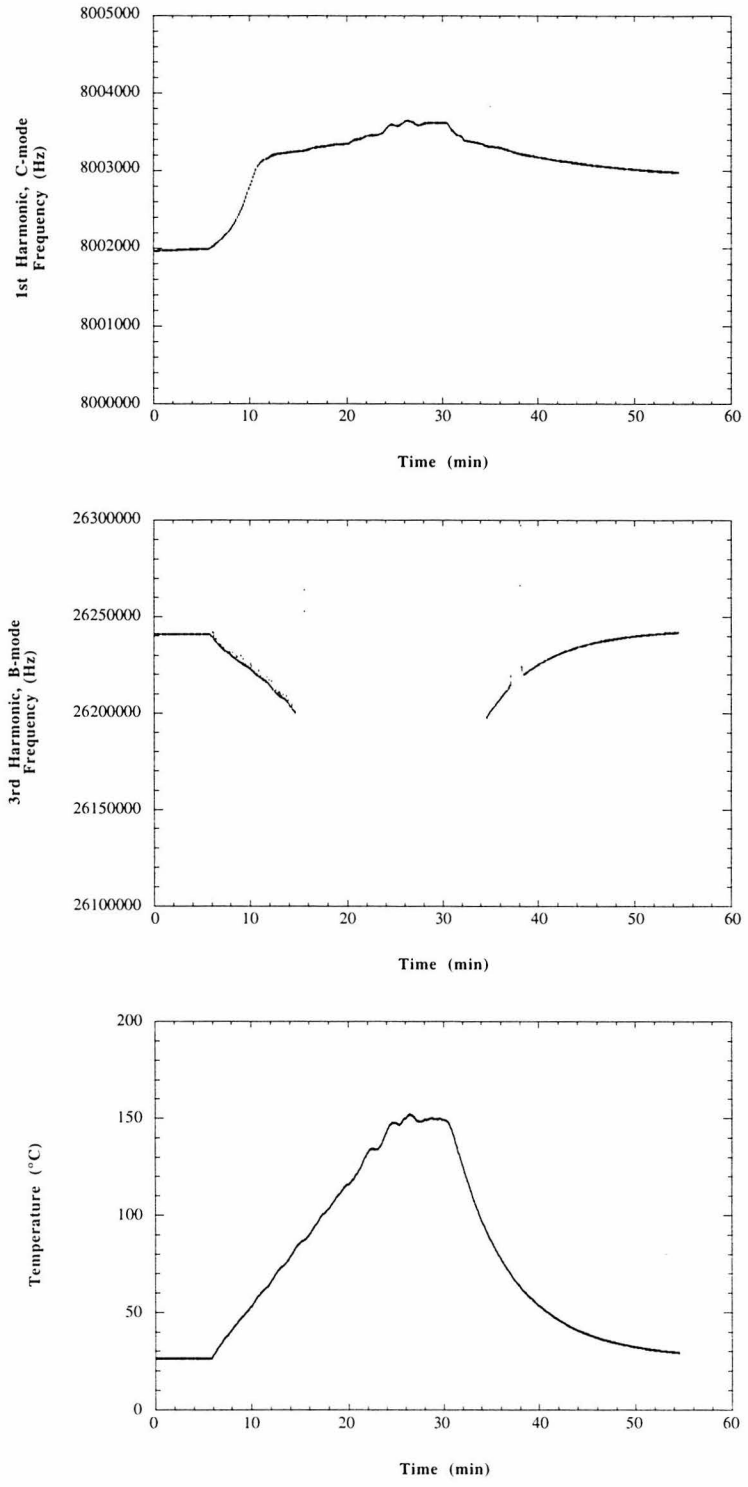


**Figure 6.17:** Results of a TPD experiment showing the desorption of water from a PEI coated sensor.

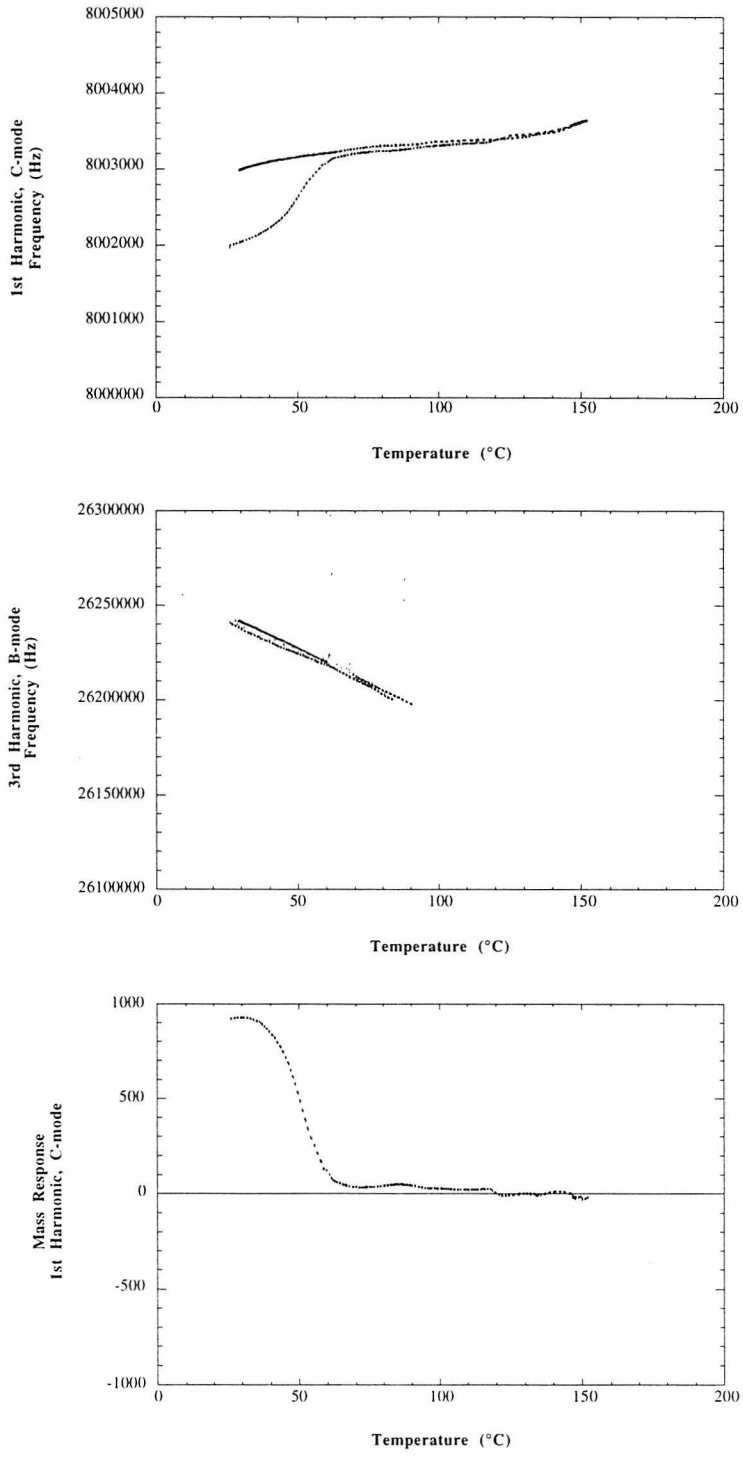


**Figure 6.18:** Results of a TPD experiment showing the desorption of water from a PEI coated sensor.

| Polyethyleneimine Coating on a Clean Quartz Oscillator | |
|---|---|
| 1st Harmonic, C-mode | $2.05 \times 10^{-8} \pm 0.4 \times 10^{-8}$ g/Hz |
| 3rd Harmonic, B-mode | $5.86 \times 10^{-9} \pm 1 \times 10^{-9}$ g/Hz |
| Water on a Polyethyleneimine Coated Oscillator | |
| 1st Harmonic, C-mode | $3.60 \times 10^{-8} \pm 0.5 \times 10^{-8}$ g/Hz |
| 3rd Harmonic, B-mode | $1.05 \times 10^{-8} \pm 0.2 \times 10^{-8}$ g/Hz |

**Table 6.2:** Relationships between mass change and frequency response for polyethlyeneimine on a clean oscillator and for water on a polyethyleneimine coated oscillator.

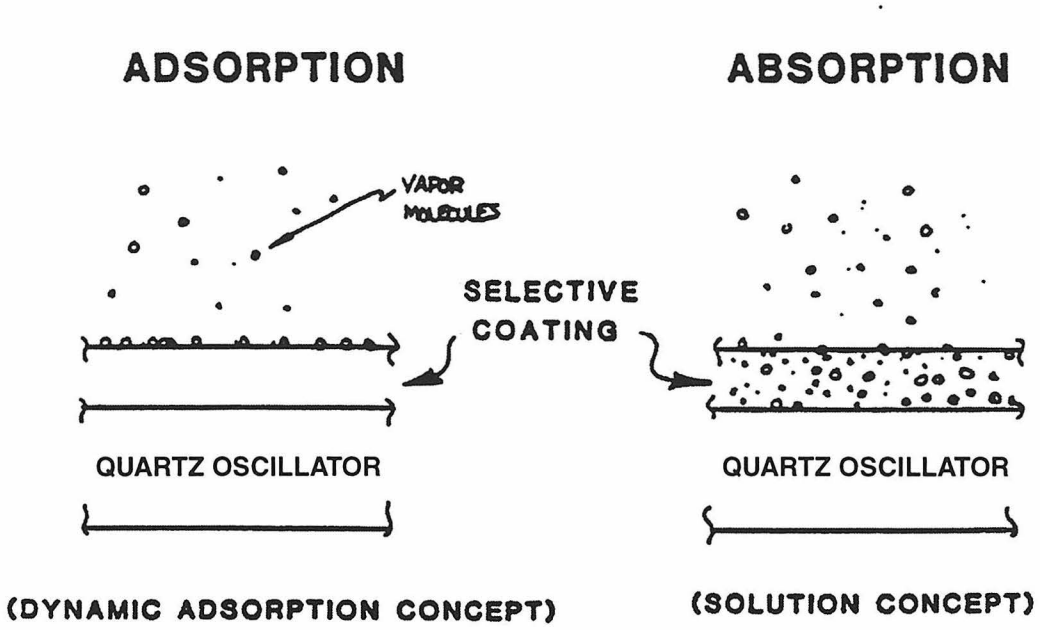


**Figure 6.19:** Schematic diagram showing the two conceptual approaches to describe sorption on a polymer coated oscillator. The *dynamic adsorption concept* (adsorption) relies on the kinetic theory of gaseous adsorption described by Langmuir in 1918[5] that models sorption as a surface phenomenon only. The *solution concept* (absorption) models the coating layer as solvent and the vapor analyte as solute.

# *Chapter 7:*

## *Conclusions*

## *7.1 Summary and Conclusions*

This thesis describes study from two different and unrelated projects. The first project, presented in Section I of this thesis, involved a family of materials called spherosiloxanes. These materials have a unique combination of molecular structure and properties that make them well suited for use as building blocks or precursors for the fabrication of engineered materials. The objective of this project was to use appropriately functionalized spherosiloxanes as molecular building blocks for the construction of ordered bulk materials and thin films.

The synthesis of the spherosiloxanes and the process used to convert them to a variety of reactive ligands is presented. Thorough characterization of these materials was accomplished by using an array of analytical spectroscopic techniques. The synthesis of two previously unsynthesized forms of the spherosiloxanes, $(C_2H_5O)_8Si_8O_{12}$ and $(n\text{-}C_3H_7O)_8Si_8O_{12}$, is described, as well as several unsuccessful alternative synthetic methods.

Attempts were made to use these spherosiloxane building units as precursors for the synthesis of bulk microporous material. A binary reaction scheme utilizing non-hydrolytic reaction conditions was proposed as a way to possibly control condensation and produce ordered microporous materials from spherosiloxane precursors. Experiments utilizing this reaction scheme between $(CH_3O)_8Si_8O_{12}$ and $Cl_8Si_8O_{12}$ failed to produce any condensed products. Attempts to aid the condensation process through the use of catalysts led to a loss of control of the condensation and resulted in amorphous materials. A multinuclear solution NMR study was performed using analogue compounds ($SiCl_4$ and

$Si(OCH_3)_4$) for the reactive components in order to fully understand the behavior of silicate species under non-hydrolytic condensation conditions. It is found that under the conditions of interest, the primary reaction taking place is a ligand exchange between the precursors; little or no condensation occurs. Based on these data, it appears that the spherosiloxanes are undergoing ligand exchange rather than condensation to bulk microporous materials.

A reaction scheme and growth mechanism using spherosiloxane precursors for the production of microporous thin films was developed and discussed. The first critical steps in this reaction scheme, namely the condensation behavior of spherosiloxanes on the Si (100) - (2x1) reconstructed surface, were studied with a variety of surface characterization techniques. Dosing experiments were performed on the reconstructed Si (100) surface. Low temperature STM studies suggest a very high degree of reactivity for the spherosiloxanes with the surface, as indicated by images of the surface revealing complete coverage by the adsorbates. An image of a single isolated $(CH_3O)_8Si_8O_{12}$ molecule adsorbed on the surface was recorded. The molecule was found to be aligned along the direction of the dimer rows on the surface and it appeared to be situated in a bridging position between two dimer rows. Linescans taken parallel and perpendicular to the dimer rows suggest that the molecule had fully condensed with the underlying surface. HREELS/TPD experiments of the spherosiloxanes on the same surface suggest that both $H_8Si_8O_{12}$ and $(CH_3O)_8Si_8O_{12}$ adsorb molecularly onto low temperature (90-120K) Si(100) surfaces without degradation of the $[Si_8O_{12}]$ core of the molecule and begin to desorb near room temperature. These two contradictory results were achieved in different laboratories utilizing different conditions for dosing the spherosiloxanes onto the surface

and this discrepancy will need to be addressed before future steps toward producing a microporous thin film can be taken.

The second project covered by this thesis, presented in Section II, was devoted to the development and evaluation of a new technique for chemical sensing. The motivation for this project was to address the need to develop new sensing techniques which are sensitive, selective, and cost effective for application to the rising threats of terrorism and pollution present today. To that end, we proposed a technique for chemical sensing based on a new type of quartz crystal oscillator (SC-Cut) that is used in combination with the analytical technique known as thermal programmed desorption (TPD). The objective of the work was to design and build a sensor system based on this TPD/quartz oscillator sensing technique and to evaluate its potential as a chemical sensor.

An introduction to microsensors that are based on quartz oscillators was presented. Included in this discussion was a review of the basic physics which govern these devices. The experimental design and construction of the system used for fabricating and testing this sensor device were described, including a description of the data acquisition and control program written to operate the sensor system.

Experiments to verify the theoretical behavior of the SC-cut quartz oscillator and obtain its frequency spectrum were performed using an impedance analyzer. The thermal response of the resonator was characterized with the C-mode and was shown to have a relatively flat thermal response up to 225°C, whereas the B-mode was shown to have a strong negative temperature response over the same temperature range. The behavior was qualitatively the same for both coated and uncoated crystals. Chemically selective coatings were applied to the resonators and it was found that the structure and morphology of

the coating can significantly impact the oscillatory behavior of the acoustic waves. Coatings which resulted in smooth, even layers on the surface could be deposited in large amounts, whereas coatings which resulted in rough or uneven coatings disrupted the acoustic waves after only a small amount of the coating was applied.

Experiments were performed to evaluate the performance of the SC-cut sensor. For some combinations of analytes and coatings, only physical adsorption was observed. For the cases where some chemical adsorption was observed, a thermal programmed desorption experiment was performed with the sensor. In nearly all cases, it was impossible to discern any desorption signal during the experiment. Data analysis, including the use of a dual mode analysis to deconvolute the temperature and mass responses of the vibrational modes, failed to yield any distinguishable desorption peaks. It was possible to distinguish a desorption peak for water from a polyethyleneimine coated sensor due to the extremely large amount of water which this polymer will adsorb. A TPD microbalance experiment was performed on a hydrated polyethyleneimine-coated crystal in order to correlate a mass change with the frequency changes observed in the TPD sensor experiments. The coated SC-cut sensor was shown to have a mass response of $2.05 \times 10^{-8} \pm 0.4 \times 10^{-8}$ g/Hz for the coating of PEI on a clean crystal, and $3.60 \times 10^{-8} \pm 0.5 \times 10^{-8}$ g/Hz for water desorbing from a PEI coated crystal. The water loading levels (43 wt%) indicated that sorption of water on PEI was occurring via bulk absorption rather than surface adsorption which provided a sufficiently high mass loading to be detectable in the TPD experiment. A mass loading more typical of adsorption, ~ 1 wt%, on the coated crystal would produce a frequency response of 2 Hz, below the minimum detection levels for this system. Based on these data, it was determined that the SC-cut based sensor fails to show the sensitivity

required to produce a practical sensor device.

# *Appendices*

## *Appendix A: List of Chemicals Used*

Ammonium hydroxide: 29.9%, Reagent Grade, JT Baker.

Benzaldehyde, 99+%, Aldrich.

Benzene-d6: 99.6%, Cambridge Isotope Lab.

2-Butanone: 99.5%, Malinckrodt.

Calcium Chloride: anhydrous, Aldrich.

Carbon dioxide: Liquid Air Corp.

Carbon Tetrachloride: 99+% anhydrous, Aldrich.

Chlorine Gas: High Purity, Matheson.

Chloroform-d1: 99.8%, Cambridge Isotope Lab.

Chromium (III) Acetylacetonate, Cr(acac)3: 97%, Aldrich.

2,3-Dinitrotoluene: 99%, Aldrich.

2,4-Dinitrotoluene: 97%, Aldrich.

2,3-Dimethyl-2-butene: 99+%, Aldrich.

Dimethyl Carbonate: 99%, Aldrich.

N,N-Dimethylmethyleneammonium chloride: Aldrich.

Ethanol: dehydrated, 100%, Quantum Chemical.

Germanium Tetrachloride: 99.9%, Gelest.

n-Hexane: 99% anhydrous, Omnisolv, EM S0cience.

Hydrochloric Acid: 36.5-38% reagent grade, Baker.

Hydrofluoric Acid: 49% electronics grade, EM Science.

Iron (III) chloride: 98% anhydrous, Aldrich.

Isopropanol: 99+%, Aldrich.

Lithium tert-butoxide: 97%, Aldrich.

Lithium isopropoxide: 95%, Aldrich.

2,6-Lutidine: 99+% redistilled, Aldrich.

Methanol: 99.9%, Fisher.

99+%, anhydrous, Aldrich

Nitromethane, 96+%, HPLC Grade, Sigma Aldrich.

2-Nitrotoluene: 99+%, Aldrich.

3-Nitrotoluene: 99%, Aldrich.

4-Nitrotoluene: 99%, Aldrich.

Pentane: 99% anhydrous, Aldrich.

Perfluorodecane: Fluorinert FC-40, 3M.

Poly(4-aminostyrene): Polysciences.

Polyaniline: Polysciences.

Polyethylene: Medium density, Aldrich.

Poly(ethyleneimine): 50 wt% solution in water, Aldrich.

Polystyrene: MW 280,000, Aldrich.

Poly(2-vinyl pyridine): MW 50,000, Polysciences.

Poly(4-vinyl pyridine): MW 50,000, Polysciences.

Potassium Carbonate: anhydrous, Malinckrodt.

2-Propanol: 99+% anhydrous, Aldrich.

Pyridine: 99+% anhydrous, Aldrich.

Silicon (IV) Bromide: 99+%, Aldrich.

Silicon (IV) Chloride: 99%, Aldrich.

Tetrabutyl orthosilicate: 97%, Aldrich.

Tetraethoxygermane: Gelest.

Tetraethyl orthosilicate: 98%, Aldrich.

Tetrahydrofuran: 99.9% anhydrous, Aldrich.

Tetraisopropoxygermane: Gelest.

Tetramethyl orthosilicate: 99+%, Aldrich.

Tetramethylsilane: 99.9+%, NMR Grade, Aldrich.

Tetrapropyl orthosilicate: 95%, Aldrich.

Toluene: 99% anhydrous, Aldrich.

Trichlorogermane: Gelest.

Trichlorosilane: 99%, Aldrich.

Triethylamine: 99+%, Aldrich.

Triethyl orthoformate: 98% anhydrous, Aldrich.

Trimethyl orthoformate: 99+% anhydrous, Aldrich.

Tripropylamine: 99+%, Aldrich.

Tripropyl orthoformate: 97% anhydrous, Aldrich.

Tris(triphenylphosphine)-rhodium(I) chloride: 99.99%, Aldrich.

Water: deionized and double distilled in the lab.

Zeolite NaY (Sodium Exchanged Y): Aldrich.

## *Appendix B: Simulation of Structure and X-ray Diffraction Data*

Simulation crystal structures and X-ray powder diffraction data was carried out using Cerius Software from Molecular Simulations running on a Silicon Graphics Personal Iris system. Optimization of the condensed spherosiloxane structure was performed using DLS-76, running on a Digital Instruments MicroVax 3100, and from within the Cerius software package

### *Appendix B.1: Simulated Powder X-ray Diffraction Pattern and List of Indexed Peaks for the Auf der Heyde Crystal Structure of $H_8Si_8O_{12}$ at 100K*[1].

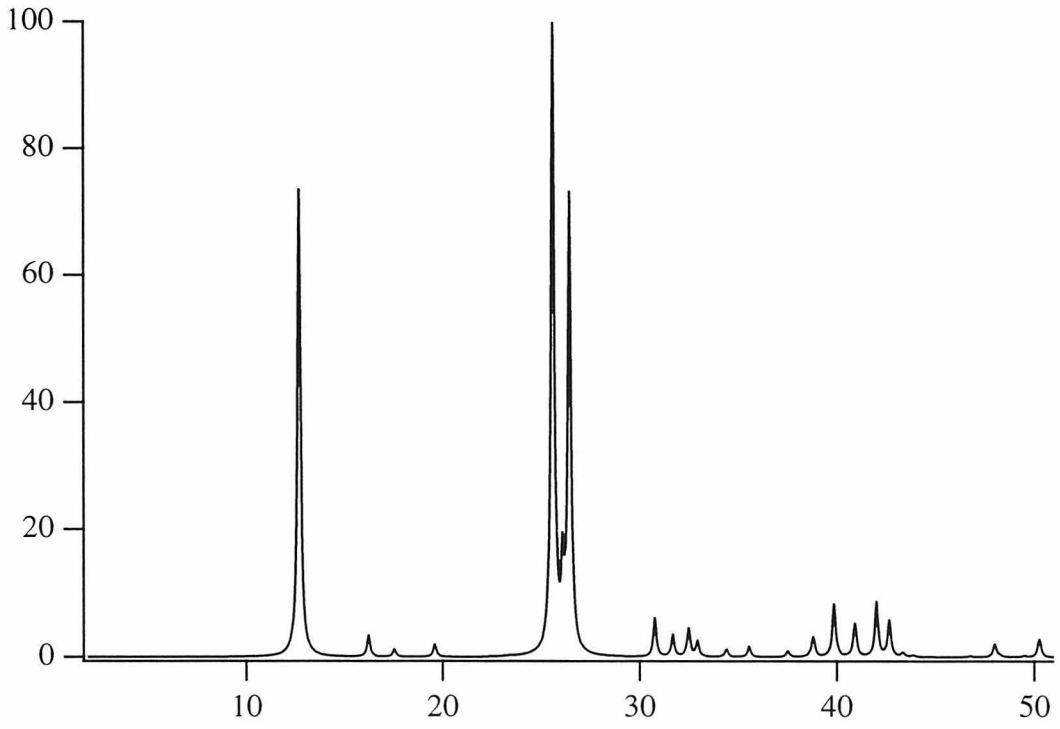


**Figure B.1:** Simulated Powder X-ray diffraction pattern for $H_8Si_8O_{12}$ based on Auf der Heyde[1] structure at 100K.

**List of Indexed Peaks:**

Powder diffraction data:

Radiation used = XRAY

Wavelength = 1.54178

| h | k | l | d-spacing | 2-theta | Integrated intensity | |
|---|---|---|---|---|---|---|
| 1 | 0 | 1 | 6.9605 | 12.717 | 0.345187E+07 | 73.14 % |
| 1 | 0 | 2 | 5.4481 | 16.269 | 161330. | 3.42 % |
| 0 | 0 | 3 | 5.0540 | 17.547 | 58897.7 | 1.25 % |
| 1 | 1 | 0 | 4.5235 | 19.624 | 96641.0 | 2.05 % |
| 2 | 0 | 1 | 3.7929 | 23.454 | 3426.17 | 0.07 % |
| 2 | 0 | 2 | 3.4803 | 25.595 | 0.471972E+07 | 100.00 % |
| 1 | 0 | 4 | 3.4122 | 26.115 | 574217. | 12.17 % |
| 1 | 1 | 3 | 3.3706 | 26.442 | 0.342080E+07 | 72.48 % |
| 2 | 1 | 1 | 2.9064 | 30.762 | 297094. | 6.29 % |
| 1 | 0 | 5 | 2.8280 | 31.637 | 170351. | 3.61 % |
| 2 | 1 | 2 | 2.7583 | 32.458 | 218420. | 4.63 % |
| 2 | 0 | 4 | 2.7241 | 32.878 | 119070. | 2.52 % |
| 3 | 0 | 0 | 2.6116 | 34.336 | 58649.4 | 1.24 % |
| 0 | 0 | 6 | 2.5270 | 35.524 | 84097.3 | 1.78 % |
| 2 | 0 | 5 | 2.3979 | 37.505 | 47214.8 | 1.00 % |
| 2 | 1 | 4 | 2.3336 | 38.579 | 10260.7 | 0.22 % |
| 3 | 0 | 3 | 2.3202 | 38.811 | 153955. | 3.26 % |
| 2 | 2 | 0 | 2.2617 | 39.856 | 413315. | 8.76 % |
| 1 | 1 | 6 | 2.2061 | 40.906 | 259465. | 5.50 % |
| 3 | 1 | 1 | 2.1510 | 42.002 | 429377. | 9.10 % |
| 2 | 1 | 5 | 2.1187 | 42.675 | 287101. | 6.08 % |
| 3 | 1 | 2 | 2.0889 | 43.313 | 3727.61 | 0.08 % |
| 1 | 0 | 7 | 2.0877 | 43.339 | 27737.6 | 0.59 % |
| 2 | 2 | 3 | 2.0645 | 43.852 | 12045.3 | 0.26 % |
| 4 | 0 | 1 | 1.9426 | 46.761 | 9675.86 | 0.21 % |
| 4 | 0 | 2 | 1.8965 | 47.969 | 7805.52 | 0.17 % |
| 2 | 0 | 7 | 1.8956 | 47.993 | 99914.1 | 2.12 % |
| 3 | 1 | 4 | 1.8852 | 48.274 | 12318.3 | 0.26 % |
| 1 | 0 | 8 | 1.8421 | 49.477 | 9374.54 | 0.20 % |
| 3 | 0 | 6 | 1.8160 | 50.237 | 144870. | 3.07 % |
| 3 | 2 | 1 | 1.7850 | 51.174 | 73278.5 | 1.55 % |
| 3 | 1 | 5 | 1.7663 | 51.754 | 909558. | 19.27 % |
| 3 | 2 | 2 | 1.7490 | 52.306 | 35100.7 | 0.74 % |
| 2 | 1 | 7 | 1.7483 | 52.329 | 79410.0 | 1.68 % |
| 4 | 0 | 4 | 1.7401 | 52.592 | 201191. | 4.26 % |
| 4 | 1 | 0 | 1.7097 | 53.601 | 20481.0 | 0.43 % |
| 2 | 0 | 8 | 1.7061 | 53.725 | 11651.6 | 0.25 % |
| 2 | 2 | 6 | 1.6853 | 54.441 | 29352.3 | 0.62 % |
| 0 | 0 | 9 | 1.6847 | 54.464 | 59482.4 | 1.26 % |
| 4 | 0 | 5 | 1.6453 | 55.878 | 28218.3 | 0.60 % |
| 3 | 2 | 4 | 1.6241 | 56.674 | 15648.0 | 0.33 % |

| | | | | | | |
|---|---|---|---|---|---|---|
| 4 | 1 | 3 | 1.6196 | 56.847 | 354485. | 7.51 % |
| 2 | 1 | 8 | 1.5963 | 57.752 | 164115. | 3.48 % |
| 1 | 1 | 9 | 1.5787 | 58.457 | 8430.23 | 0.18 % |
| 5 | 0 | 1 | 1.5587 | 59.284 | 20573.5 | 0.44 % |
| 3 | 2 | 5 | 1.5462 | 59.810 | 6768.37 | 0.14 % |
| 5 | 0 | 2 | 1.5345 | 60.312 | 95366.5 | 2.02 % |
| 3 | 1 | 7 | 1.5341 | 60.333 | 166087. | 3.52 % |
| 3 | 3 | 0 | 1.5078 | 61.495 | 1877.85 | 0.04 % |
| 1 | 0 | 10 | 1.4886 | 62.379 | 4640.08 | 0.10 % |
| 4 | 2 | 1 | 1.4737 | 63.083 | 22378.7 | 0.47 % |
| 4 | 2 | 2 | 1.4532 | 64.075 | 87894.5 | 1.86 % |
| 4 | 0 | 7 | 1.4528 | 64.095 | 21131.8 | 0.45 % |
| 5 | 0 | 4 | 1.4481 | 64.327 | 2303.37 | 0.05 % |
| 3 | 3 | 3 | 1.4449 | 64.488 | 397814. | 8.43 % |
| 3 | 1 | 8 | 1.4283 | 65.329 | 350746. | 7.43 % |
| 4 | 1 | 6 | 1.4161 | 65.966 | 206767. | 4.38 % |
| 3 | 0 | 9 | 1.4157 | 65.986 | 24928.3 | 0.53 % |
| 2 | 0 | 10 | 1.4140 | 66.075 | 1451.63 | 0.03 % |
| 5 | 1 | 1 | 1.4012 | 66.758 | 89610.5 | 1.90 % |
| 5 | 0 | 5 | 1.3921 | 67.251 | 1922.29 | 0.04 % |
| 5 | 1 | 2 | 1.3836 | 67.722 | 147.211 | 0.00 % |
| 3 | 2 | 7 | 1.3832 | 67.741 | 22236.1 | 0.47 % |
| 4 | 2 | 4 | 1.3792 | 67.966 | 546.471 | 0.01 % |
| 4 | 0 | 8 | 1.3620 | 68.941 | 220.304 | 0.00 % |
| 1 | 0 | 11 | 1.3575 | 69.203 | 6084.48 | 0.13 % |
| 2 | 2 | 9 | 1.3511 | 69.581 | 176637. | 3.74 % |
| 2 | 1 | 10 | 1.3496 | 69.668 | 48735.2 | 1.03 % |

*Appendix B.2: Simulated Powder X-ray Diffraction Pattern and List of Indexed Peaks for the Day Crystal Structure of $(CH_3O)_8Si_8O_{12}$[2].*

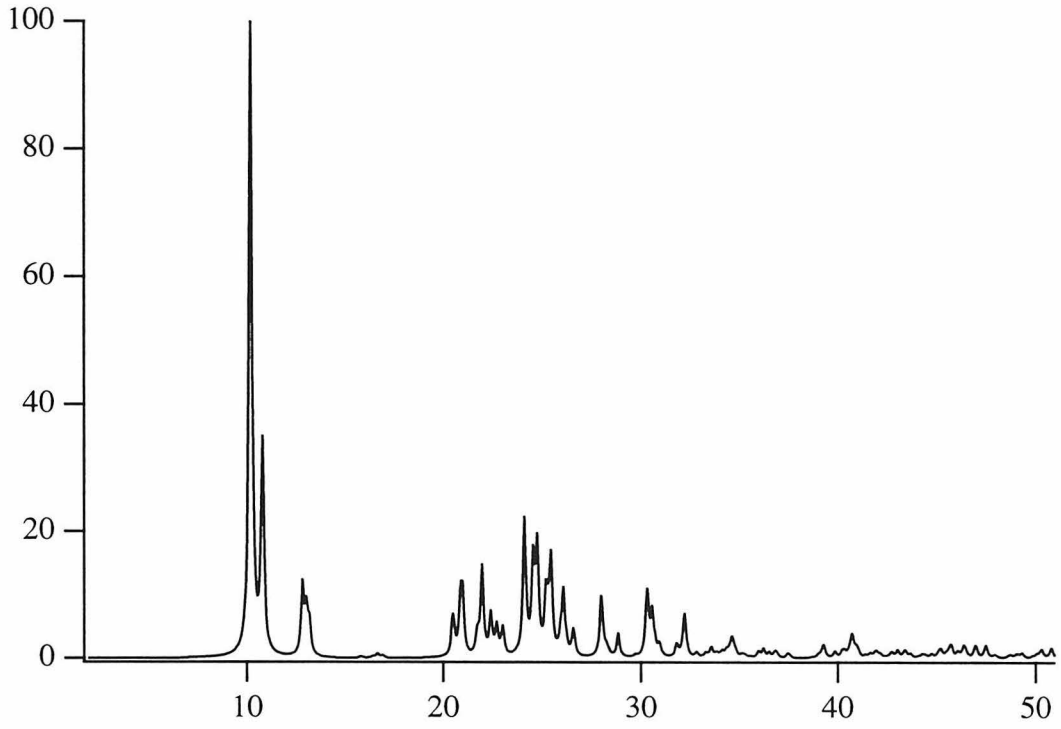


**Figure B.2:** Simulated powder X-ray diffraction pattern for $(CH_3O)_8Si_8O_{12}$ based on the structure solution by Day[2].

**List of Indexed Peaks:**

Powder diffraction data:
Radiation used = XRAY
Wavelength = 1.54178

| h | k | l | d-spacing | 2-theta | Integrated intensity | |
|---|---|---|---|---|---|---|
| 1 | 0 | 0 | 8.6855 | 10.184 | 634613. | 88.56 % |
| 0 | 1 | 0 | 8.6687 | 10.204 | 716565. | 100.00 % |
| 0 | 0 | 1 | 8.1930 | 10.798 | 448811. | 62.63 % |
| 1 | -1 | 0 | 6.8779 | 12.871 | 149224. | 20.82 % |
| 1 | 0 | -1 | 6.7885 | 13.041 | 91488.2 | 12.77 % |
| 0 | 1 | -1 | 6.7029 | 13.208 | 62420.5 | 8.71 % |
| 1 | 1 | 0 | 5.5913 | 15.850 | 2835.11 | 0.40 % |
| 0 | 1 | 1 | 5.4112 | 16.381 | 207.537 | 0.03 % |
| 1 | 1 | -1 | 5.3851 | 16.461 | 1597.63 | 0.22 % |
| 1 | 0 | 1 | 5.3755 | 16.490 | 1975.28 | 0.28 % |

| | | | | |
|---|---|---|---|---|
| 1 -1 -1 | 5.3052 | 16.710 | 9472.33 | 1.32 % |
| 1 -1 1 | 5.2311 | 16.949 | 5009.85 | 0.70 % |
| 2 0 0 | 4.3428 | 20.450 | 28223.2 | 3.94 % |
| 0 2 0 | 4.3344 | 20.490 | 64911.8 | 9.06 % |
| 2 0 -1 | 4.2635 | 20.834 | 78508.4 | 10.96 % |
| 2 -1 0 | 4.2454 | 20.924 | 16520.4 | 2.31 % |
| 1 -2 0 | 4.2396 | 20.953 | 112774. | 15.74 % |
| 0 2 -1 | 4.2170 | 21.066 | 19.6221 | 0.00 % |
| 1 1 1 | 4.1070 | 21.637 | 399.754 | 0.06 % |
| 0 0 2 | 4.0965 | 21.693 | 33580.8 | 4.69 % |
| 1 0 -2 | 4.0846 | 21.757 | 11919.0 | 1.66 % |
| 0 1 -2 | 4.0488 | 21.952 | 192054. | 26.80 % |
| 2 -1 -1 | 3.9709 | 22.388 | 88999.5 | 12.42 % |
| 1 -2 1 | 3.9195 | 22.686 | 63228.9 | 8.82 % |
| 1 1 -2 | 3.8698 | 22.981 | 59818.6 | 8.35 % |
| 2 1 -1 | 3.6956 | 24.080 | 289678. | 40.43 % |
| 1 2 -1 | 3.6790 | 24.191 | 12954.3 | 1.81 % |
| 1 -2 -1 | 3.6280 | 24.536 | 191633. | 26.74 % |
| 2 1 0 | 3.5996 | 24.733 | 119912. | 16.73 % |
| 1 2 0 | 3.5960 | 24.758 | 102135. | 14.25 % |
| 2 -1 1 | 3.5958 | 24.759 | 3859.40 | 0.54 % |
| 1 -1 -2 | 3.5418 | 25.142 | 377.675 | 0.05 % |
| 0 2 1 | 3.5351 | 25.191 | 114206. | 15.94 % |
| 2 0 1 | 3.5174 | 25.320 | 42593.4 | 5.94 % |
| 1 -1 2 | 3.4977 | 25.465 | 202332. | 28.24 % |
| 2 -2 0 | 3.4390 | 25.907 | 4717.59 | 0.66 % |
| 0 1 2 | 3.4342 | 25.944 | 37583.9 | 5.25 % |
| 1 0 2 | 3.4149 | 26.093 | 134375. | 18.75 % |
| 2 0 -2 | 3.3943 | 26.255 | 11969.8 | 1.67 % |
| 0 2 -2 | 3.3514 | 26.596 | 58389.1 | 8.15 % |
| 2 -2 -1 | 3.1872 | 27.994 | 125804. | 17.56 % |
| 2 1 -2 | 3.1773 | 28.083 | 20570.3 | 2.87 % |
| 1 2 -2 | 3.1587 | 28.252 | 7336.06 | 1.02 % |
| 2 -2 1 | 3.1549 | 28.286 | 7833.84 | 1.09 % |
| 2 -1 -2 | 3.1442 | 28.384 | 4347.55 | 0.61 % |
| 1 -2 2 | 3.0957 | 28.839 | 52741.7 | 7.36 % |
| 1 2 1 | 3.0072 | 29.707 | 3098.15 | 0.43 % |
| 2 1 1 | 3.0024 | 29.755 | 1145.60 | 0.16 % |
| 3 0 -1 | 2.9509 | 30.287 | 142171. | 19.84 % |
| 3 -1 0 | 2.9318 | 30.489 | 928.278 | 0.13 % |
| 1 1 2 | 2.9313 | 30.494 | 4361.60 | 0.61 % |
| 1 -3 0 | 2.9267 | 30.544 | 90335.5 | 12.61 % |
| 0 3 -1 | 2.9258 | 30.554 | 222.761 | 0.03 % |
| 3 -1 -1 | 2.9133 | 30.687 | 42.3009 | 0.01 % |
| 2 2 -1 | 2.9106 | 30.717 | 16961.3 | 2.37 % |
| 3 0 0 | 2.8952 | 30.884 | 13839.3 | 1.93 % |

| | | | | | |
|---|---|---|---|---|---|
| 0 | 3 | 0 | 2.8896 | 30.946 | 13427.4 | 1.87 % |
| 1 | -3 | 1 | 2.8836 | 31.011 | 1230.51 | 0.17 % |
| 1 | -2 | -2 | 2.8160 | 31.776 | 27697.9 | 3.87 % |
| 2 | 2 | 0 | 2.7956 | 32.013 | 448.922 | 0.06 % |
| 1 | 0 | -3 | 2.7954 | 32.016 | 2227.76 | 0.31 % |
| 1 | 1 | -3 | 2.7857 | 32.130 | 2462.03 | 0.34 % |
| 2 | -1 | 2 | 2.7843 | 32.147 | 20801.5 | 2.90 % |
| 0 | 1 | -3 | 2.7784 | 32.217 | 80198.9 | 11.19 % |
| 0 | 0 | 3 | 2.7310 | 32.792 | 11520.0 | 1.61 % |
| 0 | 2 | 2 | 2.7056 | 33.109 | 241.792 | 0.03 % |
| 2 | 2 | -2 | 2.6925 | 33.274 | 9292.83 | 1.30 % |
| 2 | 0 | 2 | 2.6877 | 33.335 | 1155.93 | 0.16 % |
| 3 | 1 | -1 | 2.6873 | 33.340 | 667.959 | 0.09 % |
| 1 | 3 | -1 | 2.6736 | 33.516 | 4875.75 | 0.68 % |
| 3 | -2 | 0 | 2.6727 | 33.528 | 6552.77 | 0.91 % |
| 3 | 0 | -2 | 2.6710 | 33.550 | 4478.18 | 0.62 % |
| 2 | -3 | 0 | 2.6703 | 33.559 | 7722.63 | 1.08 % |
| 2 | -2 | -2 | 2.6526 | 33.789 | 9030.38 | 1.26 % |
| 1 | -3 | -1 | 2.6441 | 33.901 | 1654.57 | 0.23 % |
| 0 | 3 | -2 | 2.6382 | 33.979 | 3782.45 | 0.53 % |
| 3 | -1 | 1 | 2.6293 | 34.098 | 10919.2 | 1.52 % |
| 2 | -2 | 2 | 2.6156 | 34.283 | 13116.4 | 1.83 % |
| 3 | -2 | -1 | 2.6045 | 34.433 | 11922.2 | 1.66 % |
| 2 | 0 | -3 | 2.5961 | 34.548 | 13116.8 | 1.83 % |
| 3 | 1 | 0 | 2.5917 | 34.609 | 22043.5 | 3.08 % |
| 3 | -1 | -2 | 2.5898 | 34.635 | 7083.87 | 0.99 % |
| 1 | 3 | 0 | 2.5881 | 34.658 | 5069.22 | 0.71 % |
| 2 | -3 | 1 | 2.5802 | 34.768 | 11277.1 | 1.57 % |
| 0 | 2 | -3 | 2.5681 | 34.936 | 344.969 | 0.05 % |
| 0 | 3 | 1 | 2.5607 | 35.041 | 4502.00 | 0.63 % |
| 3 | 0 | 1 | 2.5519 | 35.166 | 2376.03 | 0.33 % |
| 1 | -3 | 2 | 2.5519 | 35.166 | 363.151 | 0.05 % |
| 1 | -1 | -3 | 2.5508 | 35.182 | 3804.10 | 0.53 % |
| 2 | 1 | -3 | 2.5425 | 35.299 | 2371.67 | 0.33 % |
| 1 | 2 | -3 | 2.5289 | 35.496 | 2242.04 | 0.31 % |
| 1 | -1 | 3 | 2.5259 | 35.540 | 181.178 | 0.03 % |
| 3 | 1 | -2 | 2.5169 | 35.671 | 1071.06 | 0.15 % |
| 2 | -3 | -1 | 2.4994 | 35.929 | 8779.40 | 1.23 % |
| 1 | 3 | -2 | 2.4977 | 35.954 | 4962.14 | 0.69 % |
| 3 | -2 | 1 | 2.4818 | 36.192 | 20546.4 | 2.87 % |
| 0 | 1 | 3 | 2.4601 | 36.523 | 12192.6 | 1.70 % |
| 1 | 0 | 3 | 2.4493 | 36.690 | 306.028 | 0.04 % |
| 2 | 2 | 1 | 2.4423 | 36.799 | 13021.3 | 1.82 % |
| 2 | -1 | -3 | 2.4348 | 36.916 | 7320.85 | 1.02 % |
| 1 | -2 | 3 | 2.4015 | 37.447 | 2475.59 | 0.35 % |
| 1 | 2 | 2 | 2.3999 | 37.472 | 6268.95 | 0.87 % |

| | | | | | |
|---|---|---|---|---|---|
| 1 | 0 | -4 | 2.1045 | 42.977 | 13039.5 | 1.82 % |
| 2 | 0 | 3 | 2.1043 | 42.979 | 6.46311 | 0.00 % |
| 2 | -4 | 1 | 2.1009 | 43.053 | 4853.09 | 0.68 % |
| 0 | 1 | -4 | 2.0948 | 43.184 | 175.356 | 0.02 % |
| 1 | -4 | 2 | 2.0879 | 43.335 | 8280.68 | 1.16 % |
| 4 | 1 | -1 | 2.0841 | 43.418 | 10561.4 | 1.47 % |
| 1 | 4 | -1 | 2.0738 | 43.645 | 9129.79 | 1.27 % |
| 1 | -4 | -1 | 2.0554 | 44.056 | 2478.64 | 0.35 % |
| 2 | 2 | 2 | 2.0535 | 44.098 | 102.965 | 0.01 % |
| 0 | 0 | 4 | 2.0483 | 44.217 | 1275.44 | 0.18 % |
| 4 | -1 | 1 | 2.0478 | 44.228 | 6329.40 | 0.88 % |
| 2 | 0 | -4 | 2.0423 | 44.353 | 426.595 | 0.06 % |
| 2 | 1 | -4 | 2.0407 | 44.389 | 4954.21 | 0.69 % |
| 1 | 2 | -4 | 2.0315 | 44.601 | 255.033 | 0.04 % |
| 4 | 1 | -2 | 2.0279 | 44.684 | 7950.23 | 1.11 % |
| 0 | 2 | -4 | 2.0244 | 44.767 | 1130.05 | 0.16 % |
| 3 | 2 | -3 | 2.0187 | 44.899 | 471.322 | 0.07 % |
| 3 | -3 | -2 | 2.0129 | 45.035 | 1947.27 | 0.27 % |
| 1 | 4 | -2 | 2.0122 | 45.052 | 135.879 | 0.02 % |
| 4 | 1 | 0 | 2.0117 | 45.064 | 851.692 | 0.12 % |
| 2 | 3 | -3 | 2.0114 | 45.071 | 5522.54 | 0.77 % |
| 1 | 4 | 0 | 2.0086 | 45.138 | 6481.16 | 0.90 % |
| 2 | -4 | -1 | 2.0067 | 45.182 | 12366.5 | 1.73 % |
| 4 | -2 | 1 | 1.9970 | 45.414 | 675.387 | 0.09 % |
| 2 | 3 | 1 | 1.9961 | 45.437 | 2283.35 | 0.32 % |
| 3 | 2 | 1 | 1.9951 | 45.460 | 2650.57 | 0.37 % |
| 0 | 4 | 1 | 1.9936 | 45.496 | 1547.76 | 0.22 % |
| 3 | -2 | -3 | 1.9934 | 45.502 | 1619.83 | 0.23 % |
| 4 | 0 | 1 | 1.9889 | 45.611 | 6930.49 | 0.97 % |
| 3 | -3 | 2 | 1.9886 | 45.618 | 539.818 | 0.08 % |
| 4 | -2 | -2 | 1.9855 | 45.694 | 26293.5 | 3.67 % |
| 1 | -1 | -4 | 1.9708 | 46.054 | 8875.83 | 1.24 % |
| 1 | 3 | 2 | 1.9708 | 46.054 | 4174.79 | 0.58 % |
| 3 | 1 | 2 | 1.9646 | 46.207 | 187.705 | 0.03 % |
| 2 | -3 | 3 | 1.9630 | 46.247 | 2714.25 | 0.38 % |
| 2 | -4 | 2 | 1.9598 | 46.328 | 21428.0 | 2.99 % |
| 1 | -1 | 4 | 1.9554 | 46.436 | 11391.5 | 1.59 % |
| 3 | 3 | -1 | 1.9405 | 46.816 | 1180.21 | 0.16 % |
| 2 | -1 | -4 | 1.9389 | 46.855 | 135.806 | 0.02 % |
| 1 | 2 | 3 | 1.9373 | 46.897 | 345.586 | 0.05 % |
| 4 | -3 | 0 | 1.9361 | 46.927 | 1270.79 | 0.18 % |
| 2 | 2 | -4 | 1.9349 | 46.958 | 25605.7 | 3.57 % |
| 3 | -4 | 0 | 1.9348 | 46.960 | 195.326 | 0.03 % |
| 2 | 1 | 3 | 1.9323 | 47.025 | 1566.83 | 0.22 % |
| 4 | 0 | -3 | 1.9291 | 47.109 | 19.1101 | 0.00 % |
| 1 | -2 | 4 | 1.9166 | 47.434 | 29407.1 | 4.10 % |

| | | | | |
|---|---|---|---|---|
| 3 3 -2 | 1.9137 | 47.511 | 2.12860 | 0.00 % |
| 4 -3 -1 | 1.9115 | 47.569 | 668.919 | 0.09 % |
| 0 1 4 | 1.9054 | 47.731 | 933.932 | 0.13 % |
| 0 4 -3 | 1.9048 | 47.747 | 230.171 | 0.03 % |
| 1 0 4 | 1.8986 | 47.913 | 5519.90 | 0.77 % |
| 3 -4 1 | 1.8980 | 47.928 | 1177.68 | 0.16 % |
| 4 -1 -3 | 1.8960 | 47.981 | 1095.32 | 0.15 % |
| 3 0 -4 | 1.8891 | 48.168 | 405.450 | 0.06 % |
| 1 -3 -3 | 1.8732 | 48.602 | 3549.45 | 0.50 % |
| 4 1 -3 | 1.8703 | 48.684 | 2380.50 | 0.33 % |
| 4 2 -1 | 1.8702 | 48.685 | 1933.90 | 0.27 % |
| 3 1 -4 | 1.8699 | 48.695 | 977.873 | 0.14 % |
| 3 -4 -1 | 1.8684 | 48.735 | 106.656 | 0.01 % |
| 1 -4 3 | 1.8681 | 48.744 | 6.40876 | 0.00 % |
| 2 4 -1 | 1.8649 | 48.833 | 1669.04 | 0.23 % |
| 3 3 0 | 1.8638 | 48.865 | 18.3099 | 0.00 % |
| 2 -3 -3 | 1.8598 | 48.977 | 205.620 | 0.03 % |
| 4 -3 1 | 1.8581 | 49.023 | 4964.23 | 0.69 % |
| 1 3 -4 | 1.8554 | 49.098 | 15.6430 | 0.00 % |
| 3 -1 3 | 1.8549 | 49.115 | 4999.79 | 0.70 % |
| 1 4 -3 | 1.8531 | 49.166 | 148.010 | 0.02 % |
| 4 2 -2 | 1.8478 | 49.315 | 11508.9 | 1.61 % |
| 1 4 1 | 1.8474 | 49.327 | 76.6184 | 0.01 % |
| 3 -2 3 | 1.8366 | 49.636 | 162.981 | 0.02 % |
| 1 -4 -2 | 1.8296 | 49.839 | 3208.10 | 0.45 % |
| 3 -1 -4 | 1.8226 | 50.044 | 7732.80 | 1.08 % |
| 4 -1 2 | 1.8166 | 50.220 | 3061.94 | 0.43 % |
| 2 -4 -2 | 1.8140 | 50.297 | 18640.7 | 2.60 % |
| 5 -1 -1 | 1.8073 | 50.497 | 1078.81 | 0.15 % |
| 0 3 3 | 1.8037 | 50.604 | 8.79509 | 0.00 % |
| 4 2 0 | 1.7998 | 50.722 | 2.62903 | 0.00 % |
| 2 4 0 | 1.7980 | 50.777 | 18884.9 | 2.64 % |
| 4 -2 2 | 1.7979 | 50.779 | 1067.87 | 0.15 % |
| 1 -3 4 | 1.7973 | 50.796 | 51.9756 | 0.01 % |
| 3 3 -3 | 1.7950 | 50.866 | 2551.42 | 0.36 % |
| 4 -3 -2 | 1.7949 | 50.871 | 2850.63 | 0.40 % |
| 1 -5 1 | 1.7948 | 50.873 | 171.287 | 0.02 % |
| 3 0 3 | 1.7918 | 50.964 | 301.756 | 0.04 % |

*Appendix B.3: Structural Information and List of Indexed Peaks for the Condensed Spherosiloxane Structure Presented in Chapter 3.*

**Structural Information:**

Space Group: I m3m (Cubic), No. 229

Cell Parameters: $a = b = c = 9.8861$ Å; $\alpha = \beta = \gamma = 90°$

Atomic Positions:

| Atom | X | Y | Z | Special Positions |
|---|---|---|---|---|
| Si | 0.15676 | 0.15676 | 0.15676 | X, X, X |
| O(1) | 0.18786 | 0.00000 | 0.18786 | X, 0, X |
| O(2) | 0.25000 | 0.25000 | 0.25000 | 1/4, 1/4, 1/4 |

**Table B.1:** Atomic coordinates used for the simulated structure created from condensed spherosiloxanes.

**List of Indexed Peaks:**

Powder diffraction data:
Radiation used = XRAY
Wavelength = 1.54178

| h | k | l | d-spacing | 2-theta | Integrated intensity | |
|---|---|---|---|---|---|---|
| 1 | 1 | 0 | 6.9905 | 12.663 | 0.677675E+07 | 100.00 % |
| 2 | 0 | 0 | 4.9430 | 17.944 | 0.294708E+07 | 43.49 % |
| 2 | 1 | 1 | 4.0359 | 22.023 | 592446. | 8.74 % |
| 2 | 2 | 0 | 3.4952 | 25.483 | 109327. | 1.61 % |
| 3 | 1 | 0 | 3.1262 | 28.551 | 0.335806E+07 | 49.55 % |
| 2 | 2 | 2 | 2.8538 | 31.343 | 11500.2 | 0.17 % |
| 3 | 2 | 1 | 2.6421 | 33.928 | 303794. | 4.48 % |
| 4 | 0 | 0 | 2.4715 | 36.349 | 8109.83 | 0.12 % |
| 4 | 1 | 1 | 2.3302 | 38.639 | 61310.6 | 0.90 % |
| 3 | 3 | 0 | 2.3302 | 38.639 | 492859. | 7.27 % |
| 4 | 2 | 0 | 2.2106 | 40.819 | 78766.2 | 1.16 % |
| 3 | 3 | 2 | 2.1077 | 42.907 | 76419.1 | 1.13 % |
| 4 | 2 | 2 | 2.0180 | 44.917 | 122286. | 1.80 % |
| 5 | 1 | 0 | 1.9388 | 46.858 | 375431. | 5.54 % |

| | | | | | | |
|---|---|---|---|---|---|---|
| 4 | 3 | 1 | 1.9388 | 46.858 | 191975. | 2.83 % |
| 5 | 2 | 1 | 1.8049 | 50.568 | 71580.9 | 1.06 % |
| 4 | 4 | 0 | 1.7476 | 52.349 | 237113. | 3.50 % |
| 5 | 3 | 0 | 1.6954 | 54.089 | 135791. | 2.00 % |
| 4 | 3 | 3 | 1.6954 | 54.089 | 166734. | 2.46 % |
| 6 | 0 | 0 | 1.6477 | 55.792 | 285076. | 4.21 % |
| 4 | 4 | 2 | 1.6477 | 55.792 | 135304. | 2.00 % |
| 6 | 1 | 1 | 1.6037 | 57.461 | 129150. | 1.91 % |
| 5 | 3 | 2 | 1.6037 | 57.461 | 21180.7 | 0.31 % |
| 6 | 2 | 0 | 1.5631 | 59.099 | 35069.5 | 0.52 % |
| 5 | 4 | 1 | 1.5254 | 60.710 | 25.1462 | 0.00 % |
| 6 | 2 | 2 | 1.4904 | 62.296 | 21143.6 | 0.31 % |
| 6 | 3 | 1 | 1.4576 | 63.859 | 422074. | 6.23 % |
| 4 | 4 | 4 | 1.4269 | 65.401 | 1860.97 | 0.03 % |
| 7 | 1 | 0 | 1.3981 | 66.924 | 69878.7 | 1.03 % |
| 5 | 5 | 0 | 1.3981 | 66.924 | 86285.4 | 1.27 % |
| 5 | 4 | 3 | 1.3981 | 66.924 | 1763.99 | 0.03 % |
| 6 | 4 | 0 | 1.3709 | 68.431 | 193302. | 2.85 % |
| 7 | 2 | 1 | 1.3453 | 69.922 | 30391.7 | 0.45 % |
| 6 | 3 | 3 | 1.3453 | 69.922 | 230568. | 3.40 % |
| 5 | 5 | 2 | 1.3453 | 69.922 | 4892.64 | 0.07 % |

## *Literature Cited*

(1) Auf der Heyde, T. P. E.; Bürgi, H. B.; Bürgy, H.; Törnroos, K. W. *Chimia* **1991**, *45*, 38-40.

(2) Day, V. W.; Klemperer, W. G.; Mainz, V. V.; Millar, D. M. *J. Am. Chem. Soc.* **1985**, *107*, 8262-8264.